Volume: 19 Number: 3 June 2024, (Issue 84)

Volume: 19 Number: 3 June 2024

RPS

2022 IF by Clarivate Analytics 2.1 and Q1

Research in Pharmaceutical Sciences

Indexed by: ISI (WOS), PubMed, Scopus

The Official Publication of the School of Pharmacy & Pharmaceutical Sciences
Isfahan University of Medical Sciences
Isfahan, I.R.Iran

ISSN: 1735-5362

Research in Pharmaceutical Sciences (84)

Research in Pharmaceutical Sciences

A bimonthly publication of School of Pharmacy and Pharmaceutical Sciences, Isfahan University of Medical Sciences, Isfahan, I.R. Iran

Volume 19, Number 3 June 2024
ISSN: Print 1735-5362, Online 1735-9414

Abstracting and Indexing: Research in Pharmaceutical Sciences (RPS) is included in Thomson Reuters ESCI Web of Science (searchable at WoS master journal list), indexed with PubMed and PubMed Central and abstracted in the Elsevier Bibliographic Databases. Databases include Scopus, EMBASE, EMCare, EMBiology and Elsevier BIOBASE. It is also indexed in several specialized databases including Scientific Information Database (SID), Google Scholar, Iran Medex, Magiran, Index Copernicus (IC) and Islamic World Science Citation Center (ISC).

Publisher: Medknow as part of Wolters Kluwer (Philadelphia, PA), Wolters Kluwer India Pvt. Ltd. Mumbai, Maharashtra, INDIA
Website: www.medknow.com

Editorial Office: RPS, School of Pharmacy and Pharmaceutical Sciences, Isfahan University of Medical Sciences, Isfahan, P.O. Box 81746-73461, Iran.

Homepage: www.journalonweb.com/jrps
www.rps.mui.ac.ir

Tel. 0098 31 37927038
Fax. 0098 31 36680011

Email: rps@pharm.mui.ac.ir

Research in Pharmaceutical Sciences
Volume 19, Number 3, June 2024

Original Articles

Research in Pharmaceutical Sciences, June 2024; 19(3): 251-266
Received: 09-10-2023
Peer Reviewed: 30-10-2023
Revised: 29-01-2024
Accepted: 11-03-2024
Published: 01-07-2024

School of Pharmacy & Pharmaceutical Sciences
Isfahan University of Medical Sciences

Original Article

Pharmacological evaluation of anti-inflammatory, antipyretic, analgesic, and antioxidant activities of *Castanopsis costata* leaf fractions (water, ethyl acetate, and *n*-hexane fractions): the potential medicinal plants from North Sumatra, Indonesia

Maulana Yusuf Alkandahri[1,*], Asman Sadino[2], Barolym Tri Pamungkas[3], Zulpakor Oktoba[4], Maya Arfania[1], Nia Yuniarsih[5], Eko Sri Wahyuningsih[6], and Dea Eka Putri[7]

[1]*Department of Pharmacology and Clinical Pharmacy, Faculty of Pharmacy, Universitas Buana Perjuangan Karawang, Karawang, West Java, Indonesia.*
[2]*Department of Pharmacy, Faculty of Mathematics and Natural Science, Universitas Garut, Garut, West Java, Indonesia.*
[3]*Department of Pharmaceutical Biology, Faculty of Pharmacy, Universitas Mulawarman, Samarinda, East Kalimantan, Indonesia.*
[4]*Department of Pharmacy, Faculty of Medicine, Universitas Lampung, Bandar Lampung, Indonesia.*
[5]*Department of Pharmaceutical Technology, Faculty of Pharmacy, Universitas Buana Perjuangan Karawang, Karawang, West Java, Indonesia.*
[6]*Department of Pharmaceutical Biology, Faculty of Pharmacy, Universitas Buana Perjuangan Karawang, Karawang, West Java, Indonesia.*
[7]*Student of Pharmacy, Faculty of Pharmacy, Universitas Buana Perjuangan Karawang, Karawang, West Java, Indonesia.*

Abstract

Background and purpose: Inflammation, fever, and pain can be associated with several diseases, and the synthetic drugs used in the treatment of these conditions often have severe side effects. As a result, there is a need for effective, economical, and safe alternative drugs, such as those derived from medicinal plants. Therefore, this study aimed to evaluate the anti-inflammatory, antipyretic, analgesic, and antioxidant activities of *Castanopsis costata* leaf fractions (CcLF), as well as its acute toxicity.
Experimental approach: For anti-inflammatory, antipyretic, and analgesic tests, rats were given CcLF (WFCC, EAFCC, and *n*-HFCC) at 50 and 100 mg/kg, diclofenac sodium (10 mg/kg), paracetamol (150 mg/kg), aspirin (100 mg/kg), and tramadol (20 mg/kg). For the antioxidant activity test, various concentrations of CcLF were used ranging from 25 to 200 µg/mL. This study also looked into whether there could be any acute toxicity and histopathology of the liver, stomach, and kidneys in experimental animals.
Findings/Results: The administration of CcLF significantly inhibited the increase in foot edema volume, and CcLF (EAFCC at 100 mg/kg) considerably decreased rectal temperature and was proportional to the standard drug paracetamol, and significantly inhibited pain sensation in various models. Additionally, CcLF showed strong antioxidant activity, and its administration at a dose limit of 5000 mg/kg/day did not show any toxic effects or death in test animals.
Conclusions and implications: The results of the current confirmed that CcLF has demonstrated anti-inflammatory, antipyretic, analgesic, and antioxidant properties in experimental models, and is practically non-toxic.

Keywords*:* Acute toxicity; Analgesic; Anti-inflammatory; Antioxidant; Antipyretic; *Castanopsis costata*.

INTRODUCTION

Inflammation is a protective tissue response against endogenous and exogenous antigens through activation of the immune system (1,2). This inflammatory response leads to the release of several proinflammatory mediators such as tumor necrosis factor-alpha (TNF-α), interleukins (IL-1, IL-6, and IL-8), bradykinin (BK), and histamine (3).

*Corresponding author: M.Y. Alkandahri
Tel: +62-82167757738, Fax: +02678403140
Email: alkandahri@gmail.com

Access this article online

Website: http://rps.mui.ac.ir

DOI: 10.4103/RPS.RPS_201_23

Meanwhile, some other pro-inflammatory mediators such as prostaglandins (PGs) and prostacyclins (PGI_2) are also produced during inflammation through the release and conversion of arachidonic acid from damaged cellular phospholipid membranes using cyclooxygenase enzymes (COX-1 and COX-2) (4).

PG (especially PGE_2) produced in this inflammatory response can directly affect the increase in thermoregulation setpoint in the hypothalamus and cause an increase in body temperature/fever (5). This response can also have harmful side effects such as excessive free radical production and a decrease in natural antioxidants in the body (1). Meanwhile, some other pro-inflammatory mediators, especially PGs, can also cause an increase in nociceptor sensitivity, causing pain and discomfort (6). Nonsteroidal anti-inflammatory drugs (NSAIDs) are one of the treatments that have long been used in the treatment of inflammation, fever, and pain because of their ability to inhibit COX-1 and/or COX-2 activities involved in PG production (7). However, long-term use of NSAIDs can increase the risk of gastrointestinal, liver, kidney, and cardiovascular disorders (8). Additionally, NSAIDs cannot neutralize the side effects of inflammation, such as excessive production of free radicals. Therefore, there is a need for alternative drugs with stronger anti-inflammatory, antipyretic, analgesic, and antioxidant effects as well as fewer side effects.

Castanopsis costata is one of the medicinal plants widely used in traditional medicine in North Sumatra. Leaf extract of this plant has been used empirically for the treatment of fever, digestive disorders, inflammation, wound healing, and pain relief (9). Meanwhile, several previous studies reported that *C. costata* leaf extract has pharmacological activity such as antimalarial (10), antidiabetic (11), anti-hypercholesterolemia (12), antioxidant (7), and antidiarrheal (13). Although there is an existing report on the traditional and scientific use of *C. costata* leaf extract, there are no reports in the literature on the anti-inflammatory, antipyretic, analgesic, and antioxidant activities of *C. costata* leaf fractions (CcLF). Therefore, this study aimed to phytochemical investigations, pharmacognostical evaluation, and investigate anti-inflammatory, antipyretic, analgesic, and antioxidant activities as well as the acute toxicity of CcLF.

MATERIALS AND METHODS

Chemicals and drugs

Sodium diclofenac (PT. Indofarma Tbk, Indonesia), paracetamol (Sigma Chemical Company, USA), aspirin (Bayer, Germany), tramadol (PT. Sanbe Farma Tbk, Indonesia), ascorbic acid (Sigma Chemical Company, USA), 0.9% sodium chloride (Otsuka®), diethyl ether (PT. Brataco, Indonesia), paraffin (PT. Kirana Mitra Abadi, Indonesia), 10% formalin solution (PT. Arjuna Utama Kimia, Indonesia), xylene (PT. Anugrah Putra Kencana, Indonesia), hematoxylin-eosin stains (H&E; HiMedia, USA), 1,1, dipheny-2-picrylhydrazyl (DPPH), acetic acid, 70% ethanol, 1% ferric chloride, 1% gelatin, hydrogen chloride, zink, magnesium, mercury (II) chloride, potassium iodide, bismuth subnitrate, acetic acid anhydride, sulfuric acid, aquadest, ethyl acetate, *n*-hexane, methanol, pulvis gummi arabicum, carrageenans, and peptone (EMSURE® ACS Merck, Darmstadt, Germany) of analytical grade.

Sample collection, determination, and fractionation of plants

About 15 kg of fresh *C. costata* leaves were obtained from the traditional market in Pancur Batu, North Sumatra, Indonesia in February 2022. *C. costata* was then identified at the Herbarium Medanense, Universitas Sumatera Utara, Indonesia (Voucher No. 183/MEDA/2022). Furthermore, the cleaned leaf was taken to the Pharmacognosy Laboratory, Universitas Buana Perjuangan Karawang for the fractionation process. About 5.0 kg of *C. costata* powder was macerated using 70% ethanol 3 times, 24 h each. The liquid extract was then collected and concentrated using a rotary evaporator (Eyela OSB-2100) at 50 °C (14). Subsequently, 100 g of dried *C. costata* extract was dissolved in a mixture of ethanol-water (1:3) and then fractionated using the liquid-liquid partition method with *n*-hexane (4 × 150 mL) and ethyl acetate (4 × 150 mL) as solvents. This procedure resulted in 3 fractions including *n*-hexane (*n*-HFCC; 20 g, 20%), ethyl acetate (EAFCC; 45 g, 45%), and water (WFCC; 30 g, 30%) fractions.

Preliminary phytochemical investigations

The phytochemical investigations of CcLF were performed to determine the presence of secondary metabolites such as polyphenols, saponins, flavonoids, tannins, alkaloids, triterpenoids, and steroids.

Determination of loss on drying

About 2 g of the CcLF powder was weighed and placed in a previously tared porcelain. The powder was spread into an even layer and put in an oven. The lid was opened and dried at 105 °C for 60 min until the constant weight. Before each drying, the closed crucible was left to reach room temperature in a desiccator (15). The percent of loss on drying (LOD) was calculated using equation (1):

$$\text{LOD (\%)} = \frac{\text{Initial weight of CcLF} - \text{Weight of CcLF after drying}}{\text{Initial weight of CcLF}} \times 100 \quad (1)$$

Determination of total ash

Three grams of the CcLF powder was accurately weighed in previously tared porcelain and then ignited with a meker burner for about 1 h. The ignition was completed by keeping it in a muffle furnace at 600 °C until grey ash and cooled into a desiccator, then weighed without delay (15). The percent of total ash (TA) was calculated using equation (2):

$$\text{TA (\%)} = \frac{\text{Ash weight}}{\text{Weight of CcLF}} \times 100 \quad (2)$$

Determination of acid-insoluble ash

TA was boiled with 25 mL 4 N hydrogen chloride for 5 min, covering the dish with a watch glass to prevent spattering; filtered through paper or previously ignited and weighed crucible and washed with hot water until a negative chloride test was obtained with silver NO_3 solution. Paper and content were returned to the crucible, dried at 100-102 °C, ignited for 30 min at 600 °C, covered with a watch glass, cooled in the desiccator, and weighed as soon as room temperature was attained (15). The percent of acid-insoluble ash (AIA) was calculated using equation (3):

$$\text{AIA (\%)} = \frac{\text{AIA weight}}{\text{Weight of CcLF}} \times 100 \quad (3)$$

Experimental animals

In this study, a total of 128 healthy male Wistar strain rats weighing 150 to 250 g were used for anti-inflammatory, antipyretic, and analgesic tests. The rats were collected from the Animal House, CV. Mitra Putra Animal, Bandung, Indonesia, and were well-maintained in the Pharmacology Laboratory, Universitas Buana Perjuangan Karawang under a 12/12-h light/dark cycle along with *ad libitum* access to standard pellets and water. The rats were kept in plastic cages with softwood shavings.

Treatment groups

CcLF (WFCC, EAFCC, and *n*-HFCC) was tested for anti-inflammatory (carrageenan-induced paw edema model) (16), antipyretic (peptone-induced pyrexia model) (17), analgesic (acetic acid-induced writhing test and hot plate model) (18,19), and antioxidant (DPPH method) (20) activities. This study also examined the potential for acute toxicity and histopathology of the liver, stomach, and kidneys in experimental animals. For anti-inflammatory, antipyretic, and analgesic tests, rats were given CcLF (WFCC, EAFCC, and *n*-HFCC) at 50 and 100 mg/kg orally, respectively. Meanwhile, for the antioxidant activity test, various concentrations of CcLF (WFCC, EAFCC, and *n*-HFCC) were used ranging from 25 to 200 µg/mL, and the acute toxicity test rats were given CcLF (WFCC, EAFCC, and *n*-HFCC) at 500, 1000, 2000, and 5000 mg/kg/day orally, respectively. The protocol and study design are presented in Fig. 1.

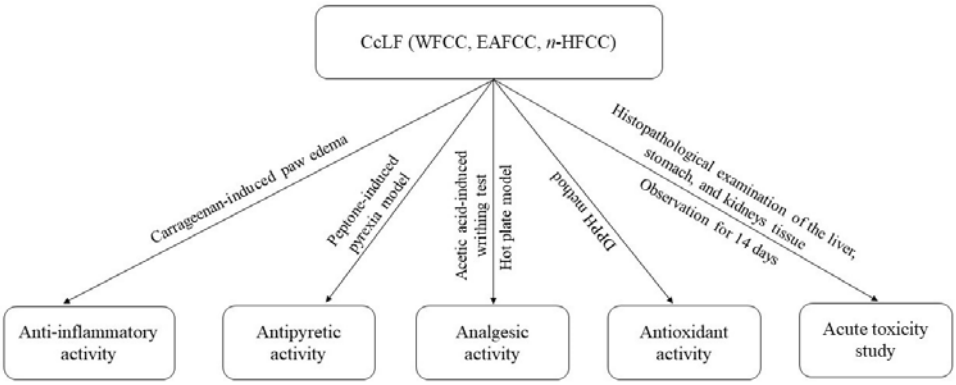

Fig. 1. Graphic schematic of the protocol and study design.

Anti-inflammatory activity

The anti-inflammatory activity test in this experiment was conducted using the carrageenan-induced paw edema model. The rats were divided into eight groups, 4 each. Subsequently, group I acted as a negative control and received a 1% w/v pulvis gummi arabicum (PGA) suspension, and group II acted as a positive control and received the standard drug (diclofenac sodium) at 10 mg/kg orally. Furthermore, groups III-VIII received WFCC, EAFCC, and *n*-HFCC at 50 and 100 mg/kg orally, respectively. After 30 min of therapy, 0.1 mL of carrageenan (1% w/v) in 0.9% sodium chloride was injected intradermally into the right hind paws of the rats. The edema volume was measured using a digital plethysmometer at 1, 3, and 6 h after the carrageenan injection, respectively (16). The paw edema volume of the rats and the percentage inhibition of edema were calculated using equations (4 and 5):

$$\text{Edema volume} = \text{PVAI} - \text{PVBI} \quad (4)$$

where PVBI stands for paw volume before carrageenan injection and PVAI for paw volume after carrageenan injection;

$$\text{Inhibition (\%)} = \frac{\text{EVNC} - \text{EVTD}}{\text{EVNC}} \times 100 \quad (5)$$

where EVNC stands for edema volume of negative control and EVTD for edema volume of test drugs.

Antipyretic activity (peptone-induced pyrexia model)

In this study, the antipyretic activity test was performed using a peptone-induced pyrexia model. The rats were randomly divided into eight groups, 4 each. Group I acted as a negative control and received a 1% w/v PGA suspension, while group II acted as a positive control and received the standard drug (paracetamol) at 150 mg/kg, orally. Furthermore, groups III-VIII were treated with WFCC, EAFCC, and *n*-HFCC at 50 and 100 mg/kg, orally, respectively. Before the experiment, the initial rectal temperature was measured using a rectal thermometer at a depth of 1.5 cm in the rectum of each rat. Furthermore, 0.5 mL of peptone (5% w/v) in aqua pro injection was injected into each experimental rat intraperitoneally. The fever induction was confirmed by an increase in rat temperature of more than 0.5 ℃ (17). Moreover, the rectal temperature of the rats was measured regularly at 1, 2, 3, and 4 h after the therapy administration. The % of fever reduction was calculated using equation (6):

$$\text{Inhibition (\%)} = \frac{\text{D} - \text{Xn}}{\text{D} - \text{E}} \times 100 \quad (6)$$

where, D stands for rats' rectal temperature after fever induction, Xn for rats' rectal temperature at 1, 2, 3, and 4 h after administration of therapy, and E for rats' rectal temperature before fever induction (normal temperature).

Analgesic activity

Acetic acid-induced writhing test

The peripheral analgesic effect in this experiment was evaluated by counting the acetic acid-induced torsional response in rats (18). About 10 mL/kg of 1% v/v acetic acid solution was injected intraperitoneally into each experimental rat, thereby inducing writhing (a condition where there is abdominal muscle contraction along with hind limb stretching) and the number of writhes was recorded. To evaluate analgesic activity in this model, rats were randomly divided into eight groups, each consisting of four rats. Group I received a negative control treatment of a 1% w/v PGA suspension, while group II received a positive control treatment of a standard drug (aspirin) at 100 mg/kg, orally. Meanwhile, groups III-VIII received treatment using WFCC, EAFCC, and *n*-HFCC at 50 and 100 mg/kg, orally, respectively, 30 min before acetic acid injection. The % of inhibition of writhing movement in rats was calculated using equation (7):

$$\text{Analgesia (\%)} = \frac{\text{WNC} - \text{WTD}}{\text{WNC}} \times 100 \quad (7)$$

where, WNC stands for the number of writhing in the negative control and WTD for the number of writhing in test drugs.

Hot plate model

In this model, the central analgesic effect was tested using the hot plate analgesia meter (PT. Andaru Analitika Sains, Bogor, Indonesia) (19). Before the experiment, the rats were pre-

tested by being placed on a hot plate maintained at a temperature of 55.00 ± 0.10 °C. Subsequently, rats with a lag time (the time the rats remained on the hot plate without licking their hind feet or kicking or jumping) during the pretest greater than 15 s were excluded from the experiment. Furthermore, the rats were randomly divided into eight groups, 4 each. Group I acted as a negative control and received a suspension of 1% w/v PGA, while group II acted as a positive control and received the standard drug (tramadol) at 20 mg/kg, orally. Meanwhile, groups III-VIII were treated with WFCC, EAFCC, and *n*-HFCC at 50 and 100 mg/kg, orally, respectively. After 30 min of therapy, the experimental rats were placed on a hot plate cylinder, and the latency time was recorded in seconds. A cut-off time of 30 s was set for all treatment groups to prevent tissue damage. For each treatment group, latency-time recordings were performed at 0, 30, 60, 90, and 120 min after drug administration. The analgesia percentage was calculated using equation (8):

$$\text{Analgesia (\%)} = \frac{\text{LT} - \text{CL}}{\text{COT} - \text{CL}} \times 100 \quad (8)$$

where, LT stands for latency test, CL for control latency, and COT for cut-off time.

Antioxidant activity

In this experiment, antioxidant activity was tested using the DPPH method (20). Furthermore, 5 mg of DPPH was dissolved in 100 mL of methanol to obtain a stock solution with a concentration of 50 µg/mL. About 250 mg of WFCC, EAFCC, and *n*-HFCC were dissolved in 25 mL of methanol, followed by dilution to obtain various test concentrations including 25, 50, 100, and 200 µg/mL. Subsequently, 2 mL of each solution was mixed with 2 mL of the DPPH stock solution until homogeneous and incubated at 30 °C for 30 min. The determination of antioxidant activity was performed using a UV-Vis spectrophotometer at a wavelength of 515.50 nm and repeated four times. Meanwhile, 1 mL of the DPPH solution was dissolved in 10 mL of methanol to obtain a blank solution, which was then measured at the same time and wavelength (Db). In this experiment, ascorbic acid with various concentrations (25, 50, 100, and 200 µg/mL) was used as the standard drug. The percent of DPPH radical scavenging activity was calculated using equation (9):

$$\text{Inhibition rate (\%)} = \frac{\text{Db}-\text{Ds}}{\text{Db}} \times 100 \quad (9)$$

where Db stands for absorbance of the blank and Ds for absorbance of the sample.

Acute toxicity study

In this experiment, an acute toxicity test was performed to evaluate the potential toxicity after administration of CcLF. The acute toxicity test was performed on Wistar strain rats of both sexes according to the guidelines of the OECD. The rats were divided into four treatment groups, each consisting of 10 rats. Each rat received WFCC, EAFCC, and *n*-HFCC at various doses including 500, 1000, 2000, and 5000 mg/kg, orally. Meanwhile, the control group rats were treated with the vehicle only (1% w/v PGA), and all treatment groups were monitored for 14 days. Any changes in behavior and signs of distress experienced by the test animals were carefully recorded (21).

Specimen collection

At the end of the 14-day experiment, on day 15, the rats in each treatment group were anesthetized with diethyl ether. Subsequently, all rats were euthanized by cervical dislocation. The abdominal cavity was opened to remove the liver, stomach, and kidneys from each rat, which were immediately wrapped in filter paper. The organs were rinsed with normal saline, and relevant parts of each organ were collected and placed in sample bottles for histopathological examination.

Histopathological examination

During the autopsy, tissue samples were collected and sent to the Histology Laboratory at the Department of Biology, Universitas Padjadjaran in Indonesia for histopathological examination. The liver, stomach, and kidney tissue samples were further processed through ethanol dehydration, followed by xylene clearing and paraffin infiltration. Subsequently, the paraffin blocks were cut into 3-4 µm thick sections, and the slides were deparaffinized in xylene and stained with H&E. The slides were observed using a light microscope (Olympus BX-51) equipped with a camera (Olympus Q

Color-5) connected to a computer. For further analysis, micrographs of liver, stomach, and kidney tissue were taken with a 100× objective. The micrographs from the treatment groups were compared to the control group. Changes were recorded using a standard nonlinear semiquantitative scoring system on a scale of 0-5 (22). The scoring criteria for tissue damage can be seen in Table 1.

Ethical approval

This study protocol was approved by the Research Ethics Commission, Universitas Padjadjaran, Indonesia, with the following numbers: 358/UN6.KEP/EC/2021 (for anti-inflammatory, antipyretic, and analgesic activity test) and 409/UN6.KEP/EC/2022 (for acute toxicity study).

Statistical analysis

In this study, all data obtained are expressed as mean ± SEM, and differences in the mean of the measured parameters were compared using a one-way analysis of variance (ANOVA) followed by Tukey's post hoc test using GraphPad Prism version 8. *P*-values < 0.05 were considered statistically significant.

RESULTS

Phytochemical investigations

The phytochemical investigations of WFCC revealed the presence of chemical constituents such as polyphenols, saponins, flavonoids, and tannins, whereas the EAFCC contained polyphenols, saponins, flavonoids, tannins, and triterpenoids and steroids triterpenoids. Meanwhile, *n*-HFCC showed the presence of alkaloids, triterpenoids, and steroids. A summary of the phytochemical investigations of CcLF is presented in Table 2.

Table 1. Description of tissue damage scoring.

Scoring	Description
0	No change, with the usual morphology
1	< 10% of the affected tissue
2	< 20% of the affected tissue
3	More widespread changes that might be expected to be associated with changes in organ function or weight
4	Almost 75% of the affected tissue
5	The entire tissue being impacted by changes that might be functionally relevant

Table 2. Phytochemical investigations of *C. costata* leaf fractions.

Phytochemical compounds	Reagents	Results		
		WFCC	EAFCC	*n*-HFCC
Polyphenols	1% Ferric chloride	√	√	–
Saponins	Hot water + hydrogen chloride	√	√	–
Flavonoids	Zn + hydrogen chloride (p)	√	√	–
	Mg + hydrogen chloride (p)	√	√	
Tannins	1% Gelatin	√	√	–
Alkaloids	Mayer Dragendorff Bouchardat	–	–	√
Triterpenoids and steroids	Liebermann-Burchard	–	√	√

√, Contained; –, not contained; *C. costata, Castanopsis costata;* WFCC, water fraction of the *C. costata* leaves; EAFCC, ethyl acetate fraction of the *C. costata* leaves; *n*-HFCC, *n*-hexane fraction of the *C. costata* leaves.

Table 3. Phytochemical properties of *C. costata* leaf fractions. Data are presented as mean ± SEM of four replicates in each group.

C. costata leaf fractions	Loss on drying (%)	Total ash (%)	Acid-insoluble ash (%)
WFCC	8.11 ± 0.15[#]	7.44 ± 0.21[#]	0.58 ± 0.13[#]
EAFCC	7.65 ± 0.12[#]	8.66 ± 0.35[#]	0.77 ± 0.21[#]
***n*-HFCC**	9.52 ± 0.18[#]	8.71 ± 0.42[#]	1.37 ± 0.16[#]

[#], Meet the quality standards according to the Indonesian Herbal Pharmacopoeia-II; *C. costata, Castanopsis costata;* WFCC, water fraction of the *C. costata* leaves; EAFCC, ethyl acetate fraction of the *C. costata* leaves; *n*-HFCC, *n*-hexane fraction of the *C. costata* leaves.

Determination of LOD, TA, and AIA

LOD is residual substances after drying at 105 °C for 30 min or until the constant weight. LOD describes loss of water and volatile compounds (15). High water content in the CcLF will become a microbial growth medium during the storage as well as hydrolysis media which can cause decomposition of chemical compounds (23). Meanwhile, all CcLF in this study met the requirements of LOD (< 10%) (15,24). TA is designed to measure the total amount of material remaining after ignition. This includes both "physiological ash", which is derived from the plant tissue itself, and "non-physiological ash", which is the residue of the extraneous matter (*e.g.* sand and soil) adhering to the plant surface. Meanwhile, AIA is the residue obtained after boiling the TA with dilute hydrogen chloride and igniting the remaining insoluble matter. This measures the amount of silica present, especially sand and siliceous earth. The results showed that all CcLF in this study met the requirements of TA (< 10%) and AIA (< 3.4%) (15,24). LOD, TA, and AIA of WFCC, EAFCC, and *n*-HFCC are presented in Table 3.

Anti-inflammatory activity

Anti-inflammatory activity was assessed using a carrageenan-induced rat paw edema model. Based on the results obtained, administration of WFCC, *n*-HFCC, and EAFCC at 50 and 100 mg/kg, as well as the standard drug diclofenac sodium, significantly inhibited the increase in paw edema volume induced by carrageenan at 3 and 6 h. The highest percentage inhibition of edema was observed with EAFCC at 100 mg/kg after 6 h, which was 62.28%. This anti-inflammatory activity was not significantly different from the diclofenac sodium, which had an anti-edema effect of 63.40% (Table 4). These findings indicated that administration of WFCC, EAFCC, and *n*-HFCC can reduce carrageenan-induced paw edema in a dose and time-dependent manner.

Antipyretic activity

In this study, a model of peptone-induced fever in rats was used to determine antipyretic activity. The rectal temperature of the rats was measured using a digital thermometer immediately after 0 h (when the rats had reached a fever state). After the administration of the therapy, the rectal temperature of the rats was measured again after 1, 2, 3, and 4 h. Based on the results, EAFCC at 100 mg/kg and paracetamol significantly reduced the rectal temperature in a time-dependent manner (Table 5). Meanwhile, the maximum percentage of fever inhibition was shown with EAFCC at 100 mg/kg at 3 h and 4 h, as well as the standard drug paracetamol at 2, 3, and 4 h. Antipyretic activity of WFCC, EAFCC, and *n*-HFCC is presented in Fig. 2.

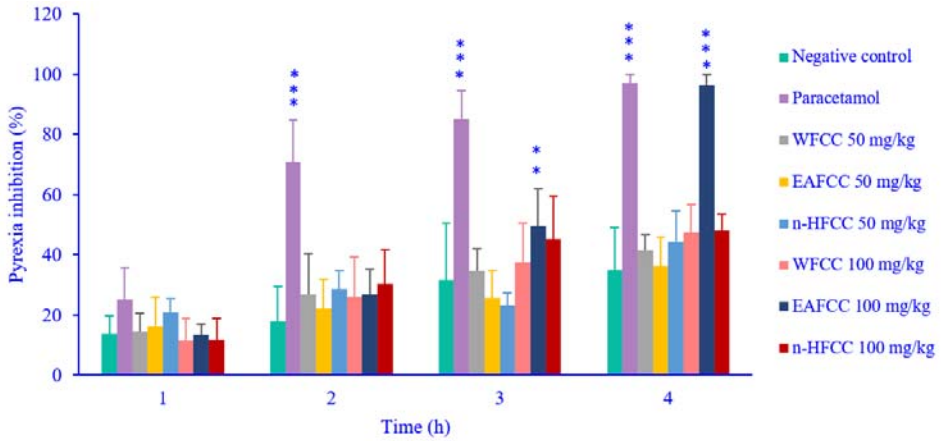

Fig. 2. Antipyretic activity of WFCC, EAFCC, and *n*-HFCC in rat model. rats were treated with for 1, 2, 3, and 4 h with paracetamol (150 mg/kg), WFCC, EAFCC, or *n*-HFCC. Data are presented as mean ± SEM of four animals in each group. $^{**}P < 0.01$ and $^{***}P < 0.001$ indicate significant differences compared to the respective negative control. WFCC, Water fraction of the *Castanopsis costata* leaves; EAFCC, ethyl acetate fraction of the *C. costata* leaves; *n*-HFCC, *n*-hexane fraction of the *C. costata* leaves.

Table 4. Anti-inflammatory activity of WFCC, EAFCC, and *n*-HFCC on carrageenan-induced paw edema in rats. Data are presented as mean ± SEM of four replicates in each group. *$P < 0.05$ and **$P < 0.01$ indicate significant differences compared to the negative control.

Treatments	Dose (mg/kg)	PV (mL) before carrageenan injection	EV (mL)			% Inhibition		
			1 h	3 h	6 h	1 h	3 h	6 h
Negative control	1% PGA	1.01 ± 0.03	2.94 ± 0.02	3.51 ± 0.13	2.98 ± 0.05	-	-	-
Diclofenac sodium	10	1.05 ± 0.03	2.26 ± 0.07	1.44 ± 0.04**	1.09 ± 0.04**	23.11 ± 2.96	58.83 ± 1.25	63.40 ± 1.53
WFCC	50	1.09 ± 0.08	2.62 ± 0.06	2.01 ± 0.02*	1.52 ± 0.07**	10.98 ± 1.67	42.34 ± 2.34	49.08 ± 2.15
EAFCC	50	1.18 ± 0.05	2.61 ± 0.08	1.94 ± 0.04*	1.48 ± 0.06**	11.24 ± 2.29	44.42 ± 2.43	50.26 ± 1.94
***n*-HFCC**	50	1.14 ± 0.03	2.74 ± 0.06	2.14 ± 0.02*	1.56 ± 0.06**	6.98 ± 1.77	38.83 ± 1.93	44.07 ± 1.75
WFCC	100	1.12 ± 0.02	2.53 ± 0.08	1.88 ± 0.07*	1.36 ± 0.04**	14.04 ± 2.46	46.04 ± 3.10	54.29 ± 0.96
EAFCC	100	1.09 ± 0.02	2.37 ± 0.07	1.59 ± 0.06**	1.12 ± 0.01**	19.33 ± 2.81	54.64 ± 0.94	62.28 ± 0.70
***n*-HFCC**	100	1.12 ± 0.03	2.68 ± 0.06	1.98 ± 0.04*	1.43 ± 0.04**	8.77 ± 1.59	43.22 ± 2.90	52.19 ± 1.04

PV, Paw volume; EV, edema volume; PGA, pulvis gummi arabicum; WFCC, water fraction of the *Castanopsis costata* leaves; EAFCC, ethyl acetate fraction of the *C. costata* leaves; *n*-HFCC, *n*-hexane fraction of the *C. costata* leaves.

Table 5. Changes in rectal temperature after administration of WFCC, EAFCC, and *n*-HFCC. Data are presented as mean ± SEM of four replicates in each group. *$P < 0.05$ Indicates significant differences compared to the negative control.

Treatments	Dose (mg/kg)	Rectal temperature (°C)					
		Control (E)	0 h (D)	1 h (X1)	2 h (X2)	3 h (X3)	4 h (X4)
Negative control	1% PGA	36.68 ± 0.12	38.15 ± 0.16	37.95 ± 0.12	37.97 ± 0.27	37.82 ± 0.33	37.70 ± 0.31
Paracetamol	150	36.30 ± 0.10	38.00 ± 0.16	37.60 ± 0.10	36.80 ± 0.18*	36.57 ± 0.13*	36.37 ± 0.10*
WFCC	50	36.66 ± 0.11	38.00 ± 0.12	37.85 ± 0.10	37.70 ± 0.09	37.57 ± 0.13	37.47 ± 0.10
EAFCC	50	36.40 ± 0.10	37.97 ± 0.11	37.70 ± 0.11	37.60 ± 0.10	37.52 ± 0.10	37.35 ± 0.12
***n*-HFCC**	50	36.70 ± 0.20	38.00 ± 0.11	37.77 ± 0.11	37.70 ± 0.11	37.70 ± 0.10	37.50 ± 0.10
WFCC	100	36.30 ± 0.30	38.00 ± 0.10	37.85 ± 0.14	37.65 ± 0.15	37.45 ± 0.16	37.25 ± 0.15
EAFCC	100	36.30 ± 0.10	38.12 ± 0.12	37.90 ± 0.12	37.62 ± 0.11	37.22 ± 0.13	36.35 ± 0.12*
***n*-HFCC**	100	36.67 ± 0.11	37.97 ± 0.12	37.85 ± 0.14	37.60 ± 0.15	37.40 ± 0.13	37.37 ± 0.11

PGA, Pulvis gummi arabicum; WFCC, water fraction of the *Castanopsis costata* leaves; EAFCC, ethyl acetate fraction of the *C. costata* leaves; *n*-HFCC, *n*-hexane fraction of the *C. costata* leaves.

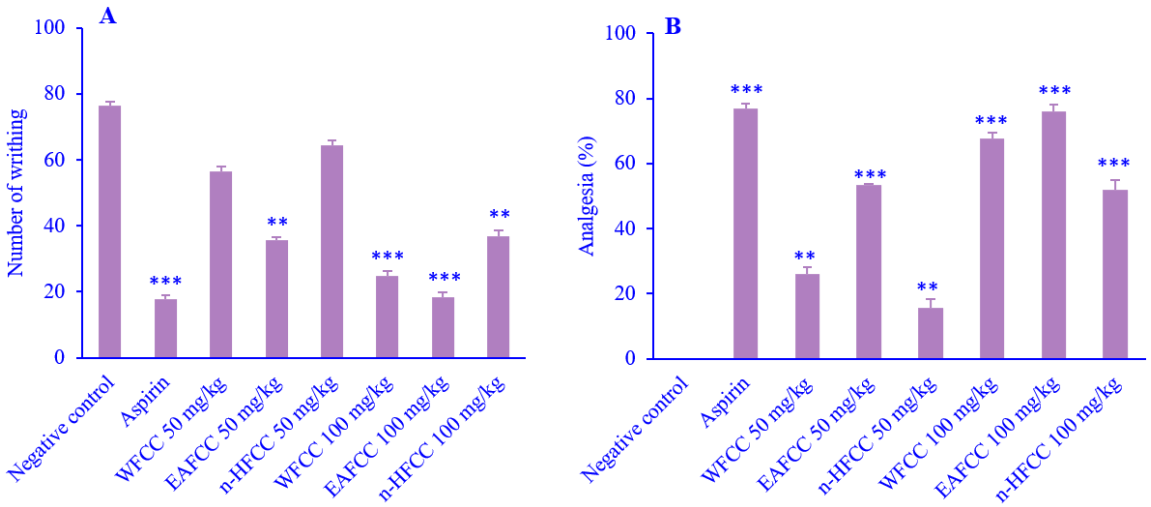

Fig. 3. Analgesic effect of WFCC, EAFCC, and *n*-HFCC on acetic acid-induced writhing test. (A) number of writhing and (B) % analgesia after the treatment with aspirin (100 mg/kg), WFCC, EAFCC, and *n*-HFCC. Data are presented as mean ± SEM of four animals in each group. $^{**}P < 0.01$ and $^{***}P < 0.001$ indicate significant differences compared to the negative control. WFCC, Water fraction of the *Castanopsis costata* leaves; EAFCC, ethyl acetate fraction of the *C. costata* leaves; *n*-HFCC, *n*-hexane fraction of the *C. costata* leaves.

Analgesic activity

Acetic acid-induced writhing test (peripheral analgesic effect)

In this study, the evaluation of the peripheral analgesic effect was performed using the acetic acid-induced writhing model. The calculation of abdominal constrictions or writhing in rats was performed for 60 s for all treatment groups after 20 min-injection of 1% acetic acid injection. Based on the study, it can be observed that EAFCC at 50 and 100 mg/kg, as well as WFCC and *n*-HFCC at 100 mg/kg significantly reduced the number of abdominal constrictions or writhing in rats (Fig. 3A). The highest peripheral analgesic effect was observed with EAFCC at 100 mg/kg, which was 76.14%. This analgesic effect was not significantly different from the standard aspirin group, which had an analgesic effect of 76.79% (Fig. 3B). These findings indicated that the administration of WFCC, EAFCC, and *n*-HFCC can reduce the number of abdominal constrictions or writhing induced by acetic acid in a dose-dependent manner.

Hot plate model (central analgesic effect)

In this study, the central analgesic effect was evaluated using the hot-plate model. The calculation of latency time was performed for each rat in all treatment groups at 0, 30, 60, and 120 min. Based on the results obtained, WFCC, EAFCC, and *n*-HFCC at 50 and 100 mg/kg, significantly increased the latency time in the hot plate model compared to the negative control (Fig. 4A). The highest central analgesic effect was observed with EAFCC at 100 mg/kg, which was 76.04%. However, this analgesic effect was still below the standard drug tramadol, which had an analgesic effect of 85.42% (Fig. 4B). These findings indicated that the administration of WFCC, EAFCC, and *n*-HFCC can increase the latency time in the hot plate model in a dose and time-dependent manner.

Antioxidant activity

Antioxidant activity is quantitatively determined by testing with the DPPH method, with the results expressed as IC_{50}, which is the concentration required to inhibit 50% of DPPH free radicals (20). Various concentrations ranged from 25 to 200 µg/mL of each CcLF to test their antioxidant activity in the DPPH model. Based on the results obtained, WFCC, EAFCC, and *n*-HFCC were able to scavenge DPPH radicals in a concentration-dependent manner, and their respective IC_{50} values were 40.22, 39.46, and 44.20 mg/mL. These results indicated that WFCC, EAFCC, and *n*-HFCC possess strong antioxidant activity *in vitro*. Meanwhile, the ascorbic acid used as the standard drug had an IC_{50} of 20.88 µg/mL (Table 6).

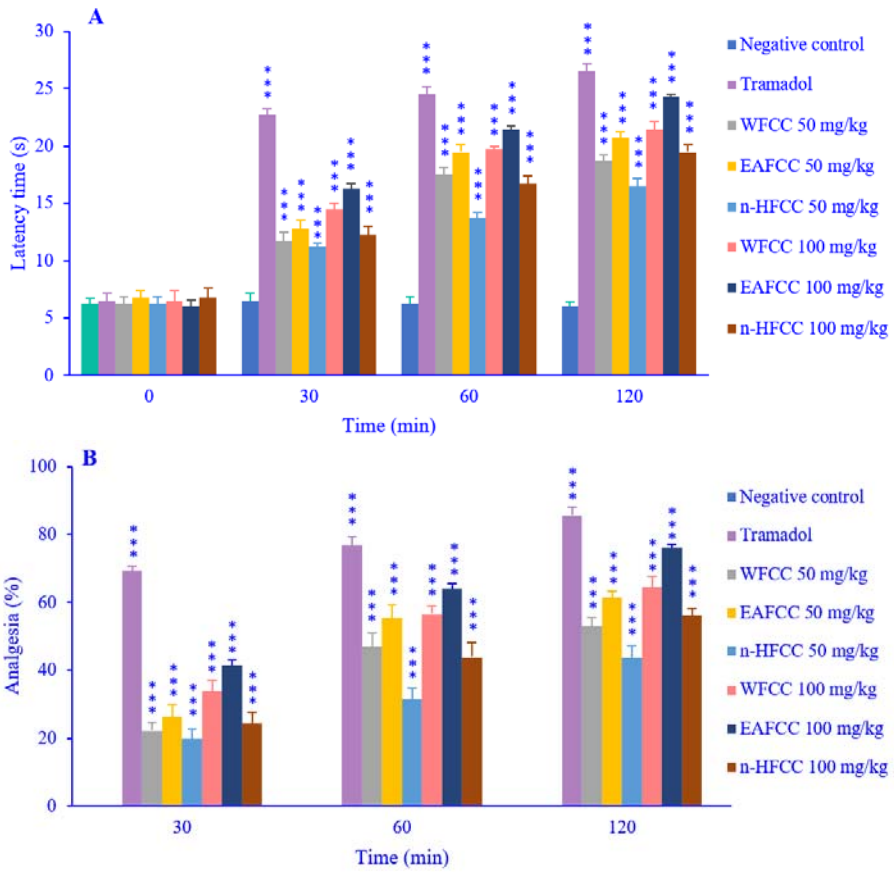

Fig. 4. Analgesic effect of WFCC, EAFCC, and *n*-HFCC in hot plate test. (A) Latency time and (B) percentage of analgesia after 30, 60, and 120 minutes of the treatment with tramadol (20 mg/kg) and WFCC, EAFCC, and *n*-HFCC (50 and 100 mg/kg). Data are presented as mean ± SEM of four animals in each group. ***$P < 0.001$ Indicates significant differences compared to the negative control. WFCC, Water fraction of the *Castanopsis costata* leaves; EAFCC, ethyl acetate fraction of the *C. costata* leaves; *n*-HFCC, *n*-hexane fraction of the *C. costata* leaves.

Table 6. IC_{50} value of ascorbic acid and WFCC, EAFCC, and *n*-HFCC. Data are presented as mean ± SEM of four replicates in each group.

Samples	IC_{50} (µg/mL)	Antioxidant activity (25)
Ascorbic acid	20.88 ± 1.58	Very strong
WFCC	40.22 ± 1.18	Very strong
EAFCC	39.46 ± 1.08	Very strong
***n*-HFCC**	44.20 ± 1.04	Very strong

WFCC, Water fraction of the *Castanopsis costata* leaves; EAFCC, ethyl acetate fraction of the *C. costata* leaves; *n*-HFCC, *n*-hexane fraction of the *C. costata* leaves.

Acute toxicity study

Based on the results of the acute toxicity test, p.o administration of WFCC, EAFCC, and *n*-HFCC in a limiting dose of 5000 mg/kg in rats showed normal behavior and no death or lethargy as well as any signs of toxic effects on any behavior pattern for up to 14 days. Meanwhile, the LD_{50} of WFCC, EAFCC, and *n*-HFCC was greater than 5000 mg/kg orally and appeared to be safe and non-toxic.

Histopathological examination

The effect of the administration of WFCC, EAFCC, and *n*-HFCC on the liver, stomach, and kidney organs of rats was determined by examining the histopathological changes of these organs compared to the control group. Based on the histopathological observations, the administration of WFCC, EAFCC, and *n*-HFCC up to a dose limit of 5000 mg/kg was reported to cause no damage to these organs (with a tissue damage score of 0 for each). The liver histopathological results showed polygonal-shaped hepatocyte plates with several nuclei. Additionally, the sinusoids between the hepatocyte plates and the portal/triad portal area (central vein, artery, bile duct) were visible and wide/large (Fig. 5).

Histopathological findings from the stomach revealed a clear histological structure characterized by mucosal, submucosa, and muscularis mucosa layers. In the area of the mucosa layer, gastric pits or foveolar gastrica were observed with single-layered cylindrical epithelial cells and small mucosal glands, and the gastric glands were visible in the lamina propria (Fig. 6).

Furthermore, the kidney histopathological results showed a clear histological structure of its parts. There were three renal corpuscles located in the glomerulus and Bowman's capsule. The proximal tubules appeared to be more abundant with relatively small, uneven, and darker lumens (brush border) as well as comprised of cuboidal-shaped cells. The distal tubules appeared in fewer numbers with larger and more regular lumens, and their cells were smaller and cuboidal and appeared brighter in color (Fig. 7).

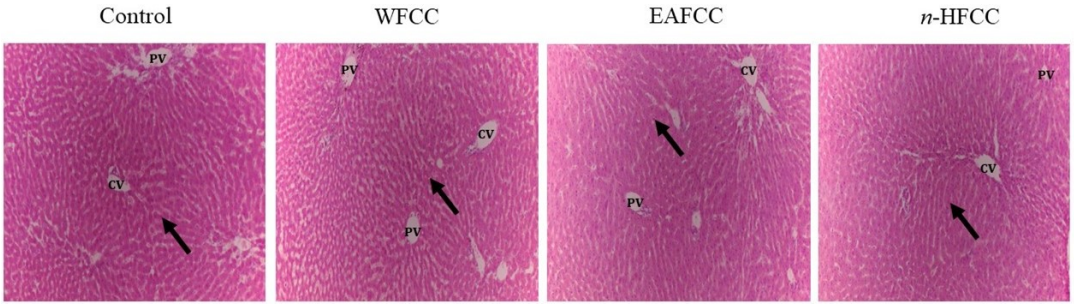

Fig. 5. The effect of WFCC, EAFCC, and *n*-HFCC on liver histopathology resealed using hematoxylin and eosin staining method; magnification of 100 ×. Black arrows show normal hepatocyte. WFCC, Water fraction of the *Castanopsis costata* leaves; EAFCC, ethyl acetate fraction of the *C. costata* leaves; *n*-HFCC, *n*-hexane fraction of the *C. costata* leaves; PV, portal vein; CV, central vein.

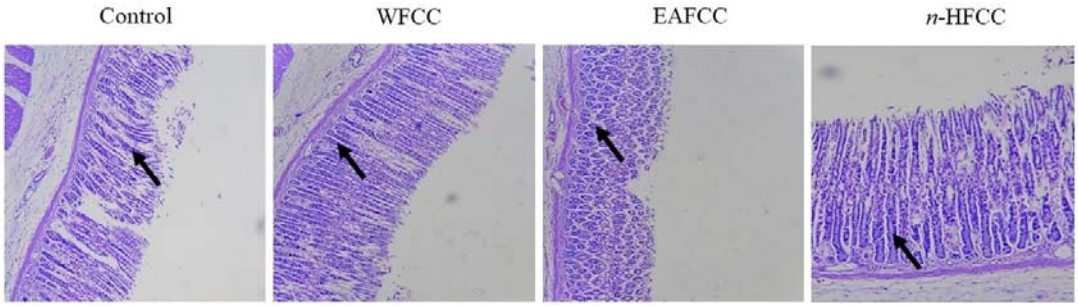

Fig. 6. The effect of WFCC, EAFCC, and *n*-HFCC on stomach histopathology revealed using hematoxylin and eosin staining method; magnification of 100 ×. Black arrows show normal cells with a basic structure of columnar epithelium. WFCC, Water fraction of the *Castanopsis costata* leaves; EAFCC, ethyl acetate fraction of the *C. costata* leaves; *n*-HFCC, *n*-hexane fraction of the *C. costata* leaves.

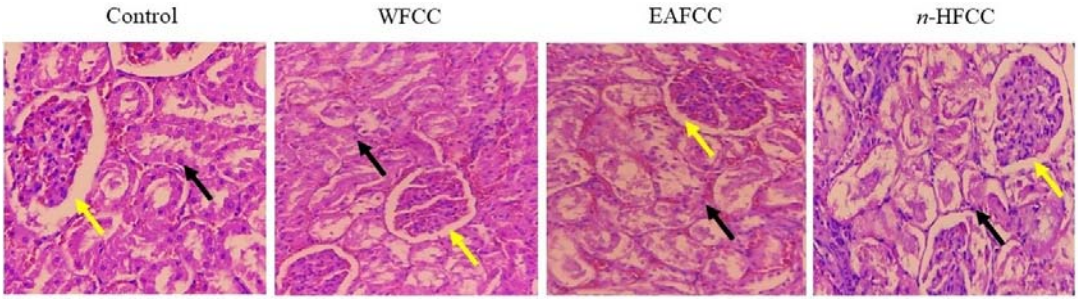

Fig. 7. Effect of WFCC, EAFCC, and *n*-HFCC on kidney histopathology revealed using hematoxylin and eosin staining method; magnification of 100 ×. Yellow arrows show the glomerulus; black arrows show normal cells. WFCC, Water fraction of the *Castanopsis costata* leaves; EAFCC, ethyl acetate fraction of the *C. costata* leaves; *n*-HFCC, *n*-hexane fraction of the *C. costata* leaves.

DISCUSSION

Generally, inflammation is known as the body's defensive response to various physiological conditions such as infection and thermal or physical injury (26). Inflammation aims to eliminate danger, induce tissue repair, and restore tissue homeostasis (27). Conceptually, the inflammation process is divided into 4 stages, consisting of the trigger system (danger), sensor mechanism (danger receptor), signal transmission, as well as mediator production, and cellular effector activation (28). Additionally, there are five major signs of inflammation such as pain, redness, heat, swelling, and loss of function (18). During inflammation, there is a significant increase in prostanoid biosynthesis in inflamed tissue. Several major prostanoids formed, such as PGE2 and PGI2, can increase vascular permeability, local blood flow, and leukocyte infiltration through activation of their respective receptors, namely IP and EP-2 (29). In this study, an anti-inflammatory activity test was performed using the carrageenan-induced paw edema model. Injecting carrageenan can lead to the release of many inflammatory mediators such as BK, PGs, serotonin, and histamine. Carrageenan-induced rat paw edema is a biphasic event in which the initial phase involves the release of histamine and serotonin, while the second phase involves the release of BK and PGs (30). The paw size is used as a parameter to measure inflammation in this model where the increase in rat paw size produced is directly proportional to edema. The results showed that the administration of EAFCC significantly inhibits the increase in paw edema volume induced by carrageenan at 3 and 6 h. Meanwhile, the administration of WFCC and n-HFCC significantly inhibited the increase in paw edema volume induced by carrageenan only at 6 h. Moreover, the results also revealed that the anti-inflammatory effect of EAFCC is not significantly different from the standard drug group diclofenac sodium.

Inflammation can also cause the release of IL-1β, IL-2, IL-6, IL-8, TNF-α, and interferon, whose role is to recruit inflammatory cells to the site of tissue injury (31). Additionally, the formation of these cytokines also increases the set point of thermoregulation in the hypothalamus. In the early phase, the thermoregulatory response to these cytokines is believed to be mediated by the release of ceramide in the preoptic area of the anterior hypothalamus (32). Meanwhile, in the slow response, the formation of PGE2 mediated by COX-2 and microsomal PGE synthase-1 (mPGES-1) occurs in the endothelium of blood vessels in the preoptic hypothalamus area (33). PGE2 can cross the blood-brain barrier and act on EP-1 and three receptors of temperature-sensitive neurons, causing the hypothalamus to increase body temperature by promoting heat production and reducing heat loss (34). In this study, an antipyretic activity test was carried out using peptone-induced fever rat models. Injection of peptone intraperitoneally can induce fever by increasing PG production (especially PGE2) (35). Previous studies have reported that *C. costata* extract has antipyretic activity in peptone-induced fever rats (7). Meanwhile, in this study, we evaluated the antipyretic activity of various fractions of *C. costata* leaves. The results showed that administration of EAFCC significantly reduces rectal temperature time-dependently. Meanwhile, the antipyretic effect of EAFCC is nearly equivalent to the standard drug paracetamol after 4 h of therapy.

Several inflammatory mediators such as histamine, BK, serotonin, PGs, and LTs released from non-neuronal cells during tissue injury cause an increase in the sensitivity of nociceptors (peripheral terminals of primary afferent fibers that sense pain) and improve pain perception (36). The pain response consists of two phases: in the first phase, there is nociceptor stimulation caused by the release of BK and substance P. In the second phase, there is inflammation caused by the production of serotonin, histamine, and PGs (37). Conversely, centrally active PGs can contribute to central sensitization by increasing stimulation of dorsal horn neurons in the spinal cord, leading to hyperalgesia (38). In this study, an analgesic activity test was conducted in 2 models, namely the acetic acid-induced writhing test (peripheral analgesic effect) and the hot plate model (central analgesic effect). The results indicated that the administration of

WFCC, EAFCC, and n-HFCC significantly reduces the number of writhing in rats and EAFCC has a peripheral analgesic effect almost equal to that of the standard drug aspirin. Meanwhile, based on the central analgesic effect test results, the administration of WFCC, EAFCC, and n-HFCC remarkably increased latency time. However, the central analgesic effect of these fractions is still below the standard drug tramadol.

In the case of inflammation, the immune cells consume a lot of oxygen for energy production, leading to an excess of free radicals produced by mitochondria (1,39). These free radical products are usually reactive oxygen species (ROS) and reactive nitrogen species, which are generated by cellular redox processes. At high concentrations, these free radicals can cause oxidative stress, which can damage all cell structures and lead to more severe diseases such as cancer, cardiovascular disease, aging, neurodegenerative disorders, and autoimmune disorders (39). Meanwhile, the human body is known to have several mechanisms to counteract oxidative stress by producing antioxidants (free radical scavengers), but during inflammation, the body's natural antioxidant production decreases (1), thereby requiring antioxidants from outside the body, such as those derived from food or herbal plants (40). In this study, a quantitative antioxidant activity test is conducted using the DPPH method. The results show that WFCC, EAFCC, and n-HFCC have a very strong *in-vitro* antioxidant activity. The results of this study are in line with the results of previous research, which reported that *C. costata* extract had a very strong antioxidant activity using the DPPH method (7).

It is believed that the anti-inflammatory, antipyretic, analgesic, and antioxidant effects of CcLF are due to the active ingredients it contains. Previous studies reported that the leaf of *C. costata* contains quercetin (12), which has anti-inflammatory, antipyretic, and analgesic activities by inhibiting the production of pro-inflammatory mediators such as NF-κB, TNF-α, AP-1, IL-1β, IL-6, IL-8, and COX, then stopping PGs synthesis (41-43). Furthermore, quercetin can reduce inflammatory hyperalgesia associated with hyperexcitability of nociceptive SpVc neurons by inhibiting peripheral COX-2 signaling cascades and voltage-gated ion channels (44). Meanwhile, quercetin can increase total GSH levels and reduce ROS levels, thereby reducing the excessive production of free radicals during inflammation (45).

Although natural, some studies have reported that phytoconstituents in plants may cause unexpected toxicity targeting certain organs such as the liver, stomach, and kidneys, and hence, a proper dose is needed for their use (46). Subsequently, as a preventive measure to avoid toxicity, further studies are needed to determine the effects of herbal administration on behavioral changes, signs of toxic effects, death of experimental animals, and histopathological changes in toxicity studies (47). The results of the current study indicated that the administration of WFCC, EAFCC, and n-HFCC at a single oral dose of about 5000 mg/kg does not show any signs of toxic effects and death in experimental rats. The administration of WFCC, EAFCC, and n-HFCC could also prevent histopathological changes in the liver, stomach, and kidneys. The findings of this study indicated that the oral administration of CcLF is safe and virtually non-toxic at doses of up to 5000 mg/kg/day. This suggests that CcLF could potentially be used as a safe treatment option for various conditions. Further research and clinical trials are needed to explore the full potential of CcLF as a therapeutic agent.

CONCLUSIONS

According to this study, CcLF exhibited anti-inflammatory, antipyretic, analgesic, and antioxidant activities. Additionally, the administration of CcLF up to 5000 mg/kg orally showed no signs of toxic effects and death in the experimental animals for 14 days. Histological observations indicated that there is no damage to the liver, stomach, and kidneys after the administration of CcLF. Based on these findings, it can be inferred that the traditional use of *C. costata* leaf for treating inflammation, fever, and pain is safe and poses minimal risk of toxicity.

Acknowledgments

This research was funded by the Institute of Research and Community Service, Universitas Buana Perjuangan Karawang with Grant No. 32/P-PkM/LPPM/II/2023.

Conflict of interest statement

The authors declared no conflict of interest in this study.

Authors' contributions

M.Y. Alkandahri and A. Sadino conceptualized the study. B.T. Pamungkas and Z. Oktoba contributed to the methodology. M. Arfania and N. Yuniarsih conducted the experiments. E.S. Wahyuningsih and D.E. Putri contributed to the data collection and analysis. All authors read and approved the finalized article.

REFERENCES

1. Khansari N, Shakiba Y, Mahmoudi M. Chronic inflammation and oxidative stress as a major cause of age-related diseases and cancer. Recent Pat Inflamm Allergy Drug Discov. 2009;3(1):73-80. DOI: 10.2174/187221309787158371.
2. Athamena S, Laroui S, Bouzid W, Meziti A. The antioxidant, anti-inflammatory, analgesic and antipyretic activities of *Juniperu thurifera*. J Herbs Spices Med Plants. 2019;25(3):271-286. DOI: 10.1080/10496475.2019.1608886.
3. Zampronio AR, Soares DM, Souza GE. Central mediators involved in the febrile response: effects of antipyretic drugs. Temperature (Austin). 2015;2(4):506-521. DOI: 10.1080/23328940.2015.1102802.
4. Purssell E, While AE. Does the use of antipyretics in children who have acute infections prolong febrile illness? A systematic review and meta-analysis. J Pediatr. 2013;163(3):822-827. DOI: 10.1016/j.jpeds.2013.03.069.
5. Rakib A, Ahmed S, Islam MA, Haye A, Uddin SMN, Uddin MMN, *et al*. Antipyretic and hepatoprotective potential of *Tinospora crispa* and investigation of possible lead compounds through *in silico* approaches. Food Sci Nutr. 2019;8(1):547-556. DOI: 10.1002/fsn3.1339.
6. Jang Y, Kim M, Hwang SW. Molecular mechanisms underlying the actions of arachidonic acid-derived prostaglandins on peripheral nociception. J Neuroinflammation. 2020;17(1):30,1-27. DOI: 10.1186/s12974-020-1703-1.
7. Alkandahri MY, Arfania M, Abriyani E, Ridwanuloh D, Farhamzah F, Fikayuniar L, *et al*. Evaluation of antioxidant and antipyretic effects of ethanolic extract of Cep-cepan leaves (*Castanopsis costata* (Blume) A.DC). J Adv Pharm Educ Res. 2022;12(3):107-112. DOI: 10.51847/twcOIyzqTM.
8. Walker C, Biasucci LM. Cardiovascular safety of non-steroidal anti-inflammatory drugs revisited. Postgrad Med. 2018;130(1):55-71. DOI: 10.1080/00325481.2018.1412799.
9. Salim E, Fatimah C, Fanny DY. Analgetic activity of Cep-cepan (*Saurauia cauliflora* Dc.) leaves extract. J Nat. 2017;17(1):31-38. DOI: 10.24815/jn.v17i1.6856.
10. Alkandahri MY, Berbudi A, Utami NV, Subarnas A. Antimalarial activity of extract and fractions of *Castanopsis costata* (Blume) A.DC. Avicenna J Phytomed. 2019;9(5):474-481. DOI: 10.22038/AJP.2019.13188.
11. Alkandahri MY, Sujana D, Hasyim DM, Shafirany MZ, Sulastri L, Arfania M, *et al*. Antidiabetic activity of extract and fractions *of Castanopsis costata* leaves on alloxan-induced diabetic mice. Pharmacogn J. 2021;13(6)Suppl:1589-1593. DOI: 10.5530/pj.2021.13.204.
12. Alkandahri MY, Kusumiyati K, Renggana H, Arfania M, Frianto D, Wahyuningsih ES, *et al*. Antihyperlipidemic activity of extract and fractions of *Castanopsis costata* leaves on rats fed with high cholesterol diet. Rasayan J Chem. 2022;15(4):2350-2358. DOI: 10.31788/RJC.2022.1547015.
13. Alkandahri MY, Sholih MG, Fadilah NN, Arfania M, Amal S, Frianto D, *et al*. Evaluation of antidiarrheal, antispasmodic, and antisecretory activities of extract and fractions of *Castanopsis costata* leaves in animal. Pharmacogn J. 2023;15(1):31-37. DOI: 10.5530/pj.2023.15.5.
14. Hidayah H, Amal S, Yuniarsih N, Farhamzah F, Kusumawati AH, Gunarti NS, *et al*. Sun protection factor activity of Jamblang leaves serum extract (*Syzygium cumini*). Pharmacogn J. 2023;15(1):134-140. DOI: 10.5530/pj.2023.15.18.
15. Kartini K, Jayani NIE, Octaviyanti ND, Krisnawan AH, Avanti C. Standardization of some Indonesian medicinal plants used in "Scientific Jamu". IOP Conf. Ser.: Earth Environ Sci. 2019;391:1-8. DOI: 10.1088/1755-1315/391/1/012042.
16. Sharma VC, Kaushik A, Dey YN, Srivastava B, Wanjari M, Jaiswal B. Analgesic, anti-inflammatory and antipyretic activities of ethanolic extract of stem bark of *Anogeissus latifolia* Roxb. Clin Phytosci. 2020;6(22):1-9. DOI: 10.1186/s40816-020-00171-2.
17. Kang JY, Khan MN, Park NH, Cho JY, Lee MC, Fujii H, *et al*. Antipyretic, analgesic, and anti-inflammatory activities of the seaweed *Sargassum fulvellum* and *Sargassum thunbergii* in mice. J Ethnopharmacol. 2008;116(1):187-190. DOI: 10.1016/j.jep.2007.10.032.
18. Ghauri MA, Iqbal L, Raza A, Hayat U, Atif N, Javeed A. *In vivo* anti-inflammatory, antipyretic, analgesic activity and *in vitro* anti-proliferative activity of aqueous methanolic extract of *Euphorbia granulata* Forssk. Future J Pharm Sci. 2021; 7(34):1-10. DOI: 10.1186/s43094-021-00184-9.

19. Afsar T, Khan MR, Razak S, Ullah S, Mirza B. Antipyretic, anti-inflammatory and analgesic activity of *Acacia hydaspica* R. Parker and its phytochemical analysis. BMC Complement Altern Med. 2015;15(136):1-12. DOI: 10.1186/s12906-015-0658-8.
20. Kusumawati AH, Farhamzah F, Alkandahri MY, Sadino A, Agustina LS, Apriana SD. Antioxidant activity and sun protection factor of black glutinous rice (*Oryza sativa* var. glutinosa). Trop J Nat Prod Res. 2021;5(11):1958-1961. DOI: 10.26538/tjnpr/v5i11.11.
21. Organization for Economic Cooperation and Development (OECD). Guideline for the testing of chemicals, 2001. Revised draft guideline 423. Document on acute oral toxicity and acute toxicity class method. Available from: http://www.oecd.org. Cited: 2022 Jun 30.
22. Khairani S, Fauziah N, Wiraswati HL, Panigoro R, Setyowati EY, Berbudi A. Oral administration of piperine as curative and prophylaxis reduces parasitaemia in *Plasmodium berghei* ANKA-infected mice. J Trop Med. 2022;2022:1-11. DOI: 10.1155/2022/5721449.
23. Pertiwi DI, Naufalin R, Arsil P, Erminawati, Wicaksono R, Auliya T. Quality of simplician bioactive components and liquid extract of *Kecombrang flower* powder from temperature and time optimization results. IOP Conf. Ser.: Earth Environ Sci. 2019;406:1-14. DOI: 10.1088/1755-1315/406/1/012008.
24. Ministry of Health Republic of Indonesia. Indonesian Herbal Pharmacopoeia 2nd Edition. Jakarta: Ministry of Health Republic of Indonesia. 2017.
25. Jun M, Fu HY, Hong J, Wan X, Yang CS, Ho CT. Comparison of antioxidant activities of isoflavones from kadzu root (*Puerari lobata* ohwi). J Food Sci. 2003;68(6):2117-2122. DOI: 10.1111/j.1365-2621.2003.tb07029.x.
26. Kuropakornpong P, Itharat A, Panthong S, Sireeratawong S, Ooraikul B. *In vitro* and *in vivo* anti-inflammatory activities of *Benjakul*: a potential medicinal product from Thai traditional medicine. Evid Based Complement Alternat Med. 2020;2020:9760948,1-8. DOI: 10.1155/2020/9760948.
27. Okin D, Medzhitov R. Evolution of inflammatory diseases. Curr Biol. 2012;22(17):R733-740. DOI: 10.1016/j.cub.2012.07.029.
28. Medzhitov R. Origin and physiological roles of inflammation. Nature. 2008;454(7203):428-435. DOI: 10.1038/nature07201.
29. Lugrin J, Rosenblatt-Velin N, Parapanov R, Liaudet L. The role of oxidative stress during inflammatory processes. Biol Chem. 2014;395(2):203-230. DOI: 10.1515/hsz-2013-0241.
30. Singh A, Malhotra S, Subban R. Anti-inflammatory and analgesic agents from Indian medicinal plants. Int J Integr Biol. 2008;3(1):57-72.
31. Nathan C. Points of control in inflammation. Nature. 2002;420(6917):846-852. DOI: 10.1038/nature01320.
32. Sanchez-Alavez M, Tabarean IV, Behrens MM, Bartfai T. Ceramide mediates the rapid phase of febrile response to IL-1beta. Proc Natl Acad Sci U S A. 2006;103(8):2904-2908. DOI: 10.1073/pnas.0510960103.
33. Engblom D, Saha S, Engström L, Westman M, Audoly LP, Jakobsson PJ, *et al*. Microsomal prostaglandin E synthase-1 is the central switch during immune-induced pyresis. Nat Neurosci. 2003;6(11):1137-1138. DOI: 10.1038/nn1137.
34. Blomqvist A, Engblom D. Neural mechanisms of inflammation-induced fever. Neuroscientist. 2018;24(4):381-399. DOI: 10.1177/1073858418760481.
35. Muhammad N, Saeed M, Khan H. Antipyretic, analgesic and anti-inflammatory activity of *Viola betonicifolia* whole plant. BMC Complement Altern Med. 2012;12:59,1-8. DOI: 10.1186/1472-6882-12-59.
36. Pulichino AM, Rowland S, Wu T, Clark P, Xu D, Mathieu MC, *et al*. Prostacyclin antagonism reduces pain and inflammation in rodent models of hyperalgesia and chronic arthritis. J Pharmacol Exp Ther. 2006;319(3):1043-1050. DOI: 10.1124/jpet.106.110387.
37. Sandrini G, Ruiz L, Capararo M, Garofoli F, Beretta A, Nappi G. Central analgesic activity of ibuprofen. A neurophysiological study in humans. Int J Clin Pharmacol Res. 1992;12(4):197-204. PMID: 1297643.
38. Reinold H, Ahmadi S, Depner UB, Layh B, Heindl C, Hamza M, *et al*. Spinal inflammatory hyperalgesia is mediated by prostaglandin E receptors of the EP2 subtype. J Clin Invest. 2005;115(3):673-679. DOI: 10.1172/JCI23618.
39. Pham-Huy LA, He H, Pham-Huy C. Free radicals, antioxidants in disease and health. Int J Biomed Sci. 2008;4(2):89-96. PMCID: PMC3614697.
40. Xu DP, Li Y, Meng X, Zhou T, Zhou Y, Zheng J, *et al*. Natural antioxidants in foods and medicinal plants: extraction, assessment and resources. Int J Mol Sci. 2017;18(1):1-32. DOI: 10.3390/ijms18010096.
41. Li Y, Yao J, Han C, Yang J, Chaudhry MT, Wang S, *et al*. Quercetin, inflammation and immunity. Nutrients. 2016;8(3):1-14. DOI: 10.3390/nu8030167.
42. Al-Khayri JM, Sahana GR, Nagella P, Joseph BV, Alessa FM, Al-Mssallem MQ. Flavonoids as potential anti-inflammatory molecules: a review. Molecules. 2022;27(9):2901,1-24. DOI: 10.3390/molecules27092901.
43. Farhamzah, Kusumawati AH, Alkandahri MY, Hidayah H, Sujana D, Gunarti NS, *et al*. Sun protection factor activity of black glutinous rice emulgel extract (*Oryza sativa* var glutinosa). Indian J Pharm Educ Res. 2022;56(1):302-310. DOI: 10.5530/ijper.56.1.36.
44. Itou H, Toyota R, Takeda M. Phytochemical quercetin alleviates hyperexcitability of trigeminal

nociceptive neurons associated with inflammatory hyperalgesia comparable to NSAIDs. Mol Pain. 2022;18:17448069221108971,1-11.
DOI: 10.1177/17448069221108971.

45. Xu D, Hu MJ, Wang YQ, Cui YL. Antioxidant activities of quercetin and its complexes for medicinal application. Molecules. 2019;24(6):1123,1-15.
DOI: 10.3390/molecules24061123.

46. Bhowmik D, Chiranjib, Dubay P, Chandira M, Kumar KPS. Herbal drug toxicity and safety evaluation of traditional medicines. Arch Appl Sci Res. 2009;1(2):32-56.

47. Sudira IW, Merdana IM, Budiasa K. Gastric histopathology of white rats after administration of *Kedondong* leaves extract. Adv Trop Biodivers Environ Sci. 2018;2(1):18-21.
DOI: 10.24843/ATBES.2018.v02.i01.p05.

Research in Pharmaceutical Sciences, June 2024; 19(3): 267-275
Received: 06-05-2023
Peer Reviewed: 14-07-2023
Revised: 13-08-2023
Accepted: 25-11-2023
Published: 01-07-2024

School of Pharmacy & Pharmaceutical Sciences
Isfahan University of Medical Sciences

Original Article

Spiroconjugated 1,2,3-triazolo[5,1-*b*]1,3,4-thiadiazine stimulates functional activity of fibroblasts under skin injury regeneration

Irina M Petrova[1], Sofya Iu Chebanova[1], Sergey L Khatsko[1,2,*], Tatyana A Kalinina[1], Dmitry V Zaitsev[1,3], and Tatyana V Glukhareva[1]

[1]Ural Federal University named after the first President of Russia B. N. Yeltsin, Yekaterinburg, 620026, Russia
[2]Federal State Budgetary Scientific Institution "Ural Federal Agrarian Scientific Research Centre, Ural Branch of Russian Academy of Sciences", Yekaterinburg, 620142, Russia.
[3]Ural State Mining University, Yekaterinburg, 620144, Russia.

Abstract

Background and purpose: One of the most important mechanisms of tissue regeneration is the high functional activity of cells, including proliferation. Currently, there are practically no effective skin cell activators on the pharmaceutical market. The purpose of this work was to demonstrate the stimulating effect of spiroconjugated 1,2,3-triazolo[5,1-*b*]1,3,4-thiadiazine (STT) on the functional activity of fibroblasts.
Experimental approach: STT containing ointment for dermal application was made. To assess *in vivo* effect of the STT a linear wound model in rats was tested. A combination of histological techniques and mechanical testing was employed to estimate the stimulating effect of STT on the functional activity of fibroblasts.
Findings/Results: The STT significantly increased the number of fibroblasts as well as the density and order of produced collagen fibers in the dermis during the wound healing process. As a result, a tissue was formed at the site of damage with the structure corresponding to normal skin. In addition, skin functions were restored, in particular mechanically.
Conclusion and implications: The results suggested the stimulating effect of the STT on fibroblast activity and demonstrated its potential for skin regeneration.

Keywords*:* Collagen; Fibroblasts, Ki-67; Mast cells; Skin wound; 1,2,3-Triazolo-1,3,4-thiadiazine; Vimentin.

INTRODUCTION

Skin injury is an acute issue in modern medicine. Damage skin is characterized by changes in morphology and loss of functionality. Successful cutaneous wound repair requires a series of tightly coordinated steps including inflammation, tissue formation, and remodeling (1-3). Increasingly, some studies reveal the role of different tissue elements' interaction in regeneration. It is known that fibroblasts are the most important element of granulation tissue. These cells determine the processes of formation and remodeling of new tissue. Fibroblasts are also significant because they coordinate the activities of other cells in different phases of regeneration. The fibroblasts' involvement in recovery processes is determined by the level of their proliferative and synthetic activity (1,2,4). Restoration of the skin fibrous component is also crucial because it provides the mechanical characteristics of the skin and maintains dermis architectonics (5).

Because of the regeneration complexity a failure of wound healing takes place. The repair process mainly becomes recurrently deficient due to extended trauma, infections, and inflammation (6). Despite advances in skin wound treatment, a therapeutic effect is not always achieved. In this line, extensive research is underway, focused on searching for regeneration stimulators, so far, the number of effective substances is limited to a few examples. Standard wound healing therapy relies mainly on proliferation activators of natural origin. For example, to accelerate the regeneration Solcoseryl® is widely used (7).

*Corresponding author: S.L. Khatsko
Tel: +7-9097048774, Fax: +7-3433899703
Email: sergey.khatsko@urfu.ru

Access this article online

Website: http://rps.mui.ac.ir

DOI: 10.4103/RPS.RPS_74_23

Chitosan-based products showed reduced inflammation, improved angiogenesis, and accelerated epithelialization (8). The popular substance methyluracil also has a stimulating effect on cell proliferation and microcirculation (9).

Previously, compounds that selectively accelerate the proliferation of human skin fibroblasts *in vitro* were discovered (10). It was found that ethyl 5-(4-ethoxybenzoyl)-5,7- dihydrospiro[[1,2,3] triazolo[5,1-*b*][1,3,4] thiadiazine-6, 1'-cyclopentane]-3-carboxylate (STT) stimulates skin regeneration (5,11). However, the way to achieve this effect is still unclear. In this paper, we evaluated regenerative process parameters that can indicate a possible mechanism of STT action and help determine further approaches to its study.

MATERIALS AND METHODS

Animals

The experiment utilized 63 male outbred laboratory rats (434.7 ± 8.8 g) and complied with the Principles of Laboratory Animal Care. All the experiments were permitted by the Ethics Committee of the Institute of Natural Sciences and Mathematics, UrFU, Russia (Ethic No. 2/2022).

Animals were randomly divided into 4 groups, including 5 (morphological studies) or 4 (mechanical studies) individuals: (1) intact rats (INT); (2) untreated rats as the control group (CONTR); (3) rats exposed to vaseline (VAS); and (4) rats exposed to STT (STT).

Chemicals

Vaseline and Analgin were obtained from Samaramedprom JSC (Russia) and Pharmstandard-UfaVITA JSC (Russia), respectively. The synthesis of STT was carried out at the Institute of Chemical Engineering (UrFU, Russia) (12).

Ointment preparing

Ointment for skin application was prepared by dissolving 208 mg of the 1,2,3-triazolo-1,3,4-thiadiazine in 100 µL of dimethyl sulfoxide, adding this solution to 50 g of Vaseline, and stirring to a homogeneous consistency. To avoid the effects of ointment base, a group of animals (VAS) were exposed to it. Vaseline was chosen due to its beneficial properties for wound healing (13,14).

Experimental procedures

The study included linear wound modeling. The skin from the back was prepared by hair plucking and rinsed with ethanol 96%. A linear wound of 50 ± 2 mm long was created using a surgical scalpel. Before the wound was applied, rats were injected intramuscularly with 0.2 mL Analgin 50%.

After wound modeling, animals were exposed to an experimental ointment (0.4% of STT) or Vaseline. Ointments were applied epicutaneously at the dose of 0.2 g once a day for 14 days. Animals were taken out of the experiment on the 14th and 21st days by an overdose of diethyl ether.

Histological and immunohistochemical analysis

A strip of skin tissue was obtained and fixed in 10% neutral formalin. Tissue specimens were embedded in paraffin wax, sectioned (4 µm), and stained with hematoxylin-eosin (H&E), picrofuchsin (Van Gieson's), and Azure B, to visualize the neotissue formation, collagen deposition, and mast cells number, respectively.

To estimate the cell proliferation intensity and fibroblast synthetic activity, immunohistochemical staining with antibodies against Ki-67 (SP6, rabbit monoclonal antibody, Cell Marque, USA) and vimentin (V9, mouse monoclonal antibody, Cell Marque, USA) was performed according to manufacturer's protocols. Briefly, 4-µm-thick sections were placed on poly-L-lysine-coated adhesive microscope slides (Thermo Scientific-Menzel, Germany) and then dewaxed in xylene and rehydrated in graded alcohols. Sections were incubated in Trilogy™ (Cell Marque, USA) to antigens unmasking for 20 min at 92 °C and in H_2O_2 solution for 10 min at room temperature. After that, sections were washed in tris buffered saline (TBS) immunohistochemistry wash buffer + Tween® 20 (Cell Marque, USA) for 1 min and incubated with primary antibodies for 60 min at 30 °C.

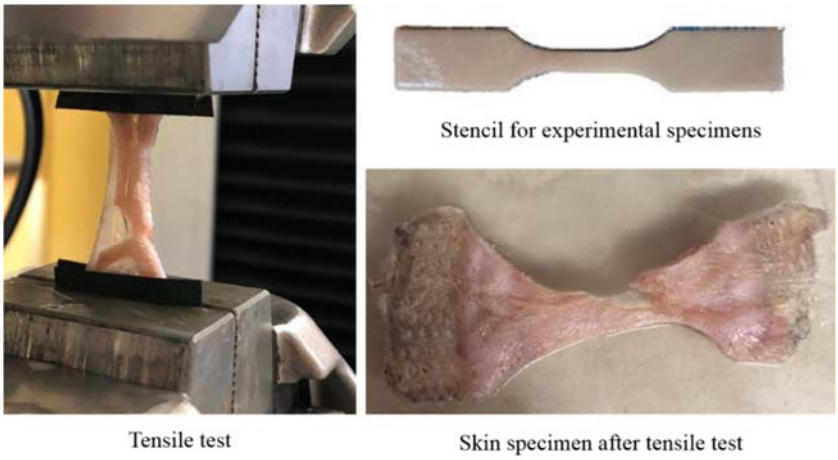

Fig. 1. Mechanical test.

Sections were washed three times with TBS before incubation with secondary antibodies (N-Histofine® Simple Stain MAX PO (MULTI), Nichirei Biosciences INC, Japan) for 30 min at 30 °C. Sections were washed three extra times in TBS and coated with DAB chromogen (DAB Substrate Kit, Cell Marque, USA), and incubated for approximately 30-60 s. After that sections were washed in distilled water and stained with hematoxylin.

Zeiss Primostar provided histological analysis. The average vessels and cell number (fibroblasts, mast cells, Ki-67- and vimentin-positive cells), collagen fibers thickness, and vessel area were analyzed by TopView software according to 10 randomly selected fields with conversion to 1 mm^2. Mast cells were defined as dark purple cells with granular cytoplasm (stained with Azur B). Fibroblasts were defined as cells with a branched basophilic cytoplasm surrounding an elliptical nucleus (stained with H&E). Cells with a brown-stained nucleus and yellow-stained cytoplasm were considered Ki-67 positive and vimentin-positive, respectively.

Mechanical tests

Mechanical tests were conducted on a Shimadzu AGX 50kN tensile testing machine (Japan). The analysis of the sample's mechanical strength was carried out using the method for assessing the deformation behavior of the material under uniaxial compression (15,16). According to a special cardboard stencil, skin samples were cut out. The sample edges were rigidly fixed in the grips of the testing machine (7). After that, a uniaxial tensile load was applied to the sample (Fig. 1). The time of one test was on average 71.342 ± 4.211 s. Upon reaching the point of maximum mechanical stress and the onset of irreversible deformation (ruptures), the tests were stopped.

Statistical analysis

All data were expressed as the mean ± SEM. Statistical analysis was performed using Statistica 12.0 software by Kruskal-Wallis test with Dunn's post-hoc analysis. *P*-values < 0.05 were considered statistically significant. Mathematica software (Wolfram language) was used to visualize the received data.

RESULTS

H&E and Azure B staining

The study aimed to evaluate the effect of the chemical compound STT on the fibroblast's functional activity under linear skin wound regeneration. The points of the experiment were chosen to assess the skin condition at the final stages of regeneration.

On the 14th day, intense fibroblast proliferation was observed in the STT group. Acanthoses were detected, but on the 21st day, the epidermis acquired a uniform thickness. The dermis was divided into papillary and reticular layers. Numerous hair follicles as well as glandular structures were found. The scar was characterized by maturity with a fibrous component predominance (Fig. 2A).

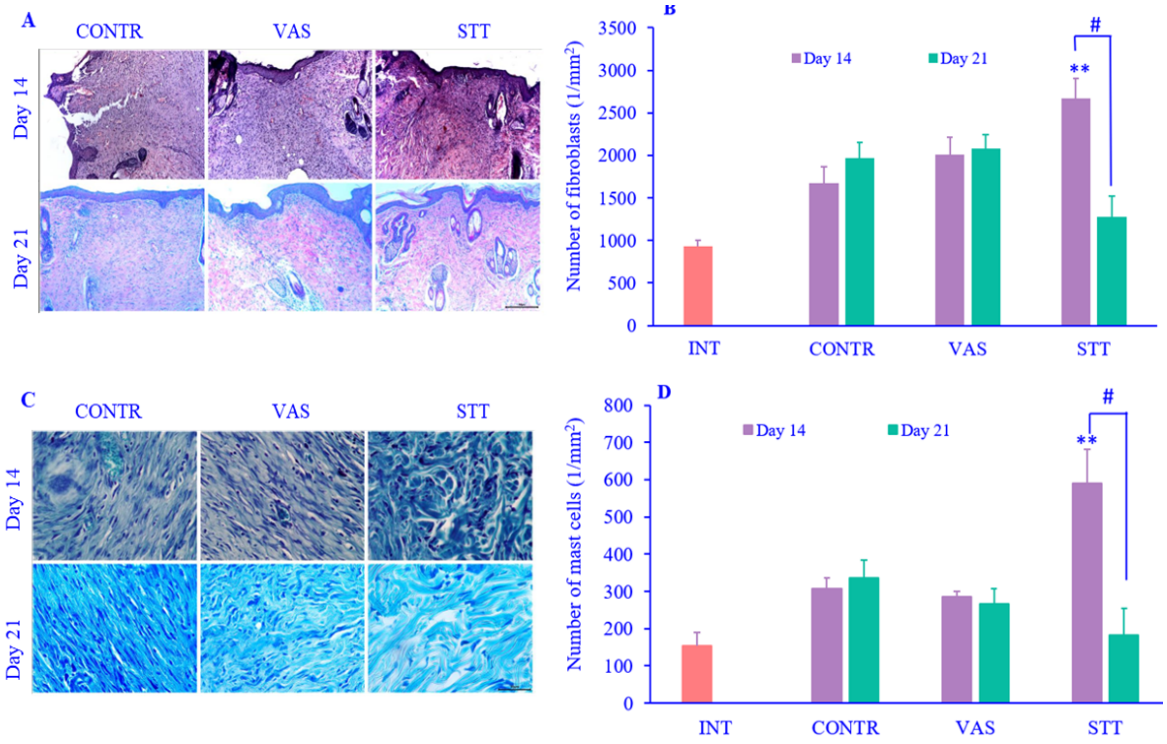

Fig. 2. (A) Hematoxylin and eosin staining, magnification: 100 ×; (B) the number of fibroblasts; (C) Azure B staining, magnification: 400 ×; (D) the number of mast cells. Data are presented mean ± SEM, n = 5. $^{**}P < 0.01$ Indicates significant differences in comparison with the INT group; and $^{\#}P < 0.05$ between the indicated groups. INT, Intact; CONTR, control; VAS, vaseline; STT, spiroconjugated 1,2,3-triazolo[5,1-b]1,3,4-thiadiazine.

The fibroblast number increased in STT groups by the 14th day relative to the CONTR and VAS groups (Fig. 2B). The high content of cells persisted by the 21st day. Changes were noted in the mast cell population (Fig. 2C). On the 14th day, the number of mast cells significantly increased in the STT group comparing other groups (Fig. 2D).

Immunohistochemical staining

The cell implication in regeneration is determined mainly by their proliferative activity (4,5). To assess the intensity of cell proliferation, the Ki-67 marker was used (17). Ki-67 positive cells were determined in the epidermis germ layer, and most of the cells were observed in the STT group on the 14th day (Fig. 3A), which was significantly higher than the values of the CONTR and VAS groups. It was typical that in the earlier period of regeneration, there were more dividing cells (Fig. 3B). However, in the STT group, the number of cells remained significantly high even by the 21st day and it also applied to the dermis (Fig. 3D).

Fibroblasts are an important link that unites various processes during regeneration (5). *Via* vimentin production, fibroblasts coordinate cell proliferation, collagen accumulation, keratinocyte transdifferentiation, and re-epithelialization (4,18-20). The number of vimentin-positive dermal cells on the 14th day of the experiment was high (Fig. 4A and B), which correlated with the fibroblasts number (Fig. 2B). By the 21st day, the number of vimentin-positive cells sharply decreased in the CONTR and VAS groups, so it was significantly less than the values of the STT group on the 14th day. The microvasculature normalization served as reliable marker of successful regeneration. Here, on the 21th day of the experiment we observe normal indicators of vessels number and area (Fig. 4C and D).

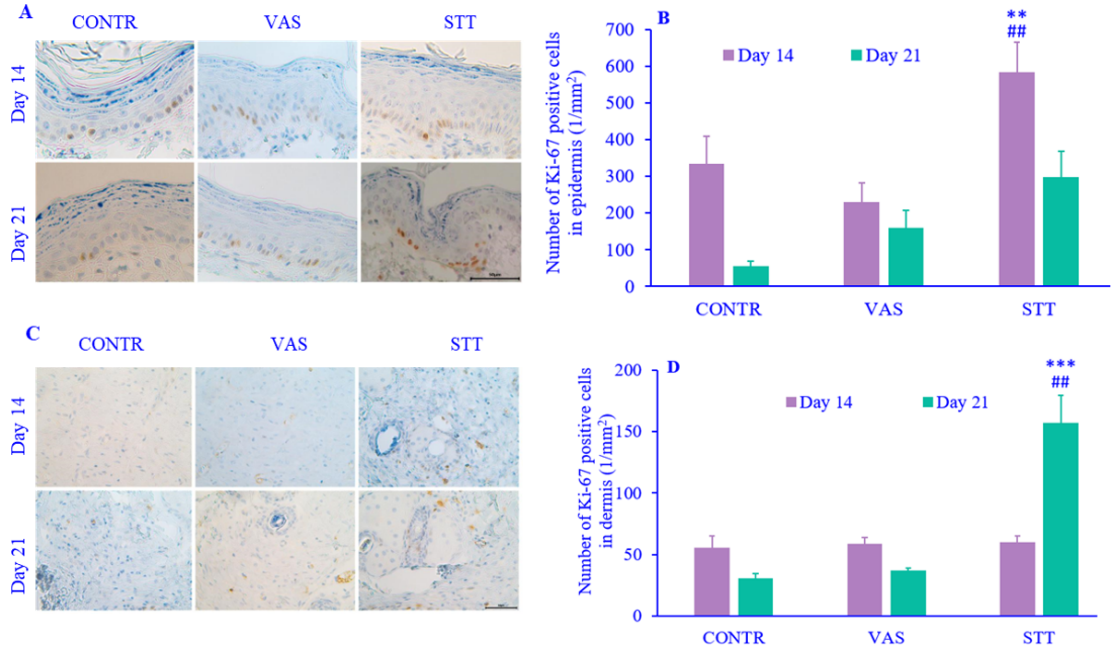

Fig. 3. (A) Immunohistochemical staining of Ki-67 in the epidermis, magnification: 400 ×; (B) number of Ki-67 positive cells in the epidermis; (C) immunohistochemical staining of Ki67 in the dermis, magnification: 400 ×; (D) number of Ki-67 positive cells in the dermis. Data are presented mean ± SEM, n = 5. $^{**}P < 0.01$ and $^{***}P < 0.001$ indicate significant differences in comparison with the control group; $^{\#\#}P < 0.01$ versus VAS group. INT, Intact; CONTR, control; VAS, vaseline; STT, spiroconjugated 1,2,3-triazolo[5,1-b]1,3,4-thiadiazine.

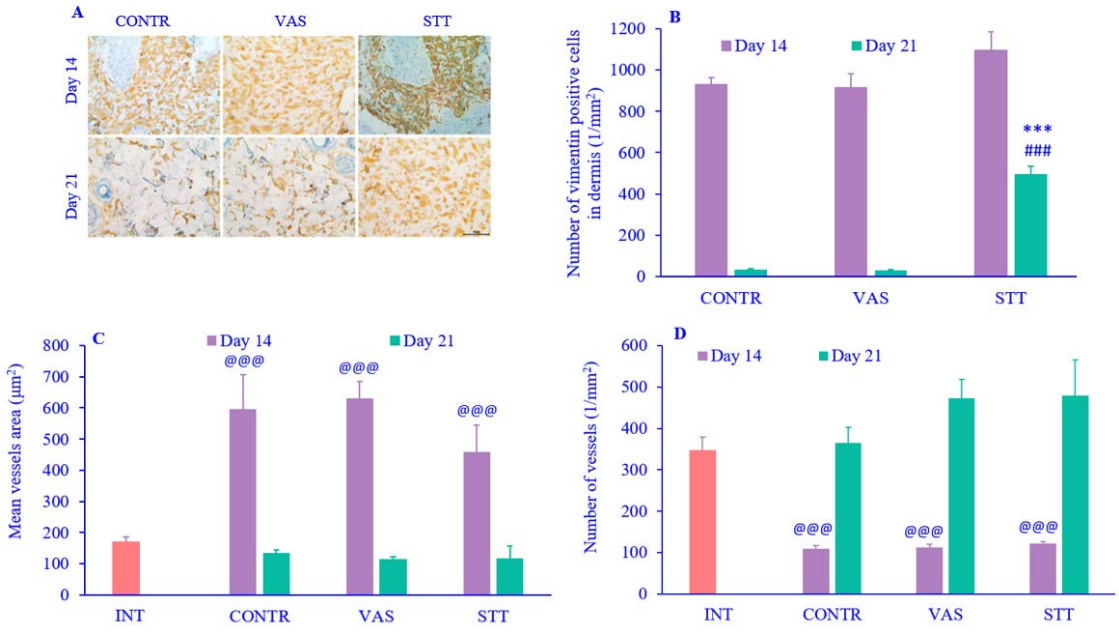

Fig. 4. (A) Immunohistochemical staining of vimentin in the dermis, magnification: 400 ×; (B) the number of vimentin-positive cells in the dermis; (C) mean vessels area; and (D) vessels number. Data are presented mean ± SEM, n = 5. $^{***}P < 0.001$ indicates a significant difference in comparison with the respective control group; $^{\#\#\#}P < 0.001$ versus VAS group; $^{@@@}P < 0.001$ against INT group. INT, Intact; CONTR, control; VAS, vaseline; STT, spiroconjugated 1,2,3-triazolo[5,1-b]1,3,4-thiadiazine.

Van Gieson's staining

Assessment of the skin's fibrous component state can serve as a marker of both the successful restoration of the skin's mechanical functions and the normal scar formation. Collagen deposition became more abundant with prolongation of the time after injury. By the 21st day in the STT group, most of the dermis was occupied by collagen fibers. The papillary region was composed of thin fibers collected in loose bundles. The reticular dermis represented by thick and crimped fibers formed certain direction bundles. The fiber dye was more intense in the CONTR and VAS groups. The morphology and distribution of collagen fibers approximated those in the normal dermis (Fig. 5A). The collagen fiber thickness showed no significant differences between the INT and STT groups on the 14th day. By the 21st day in the STT group fiber bundles were significantly thicker in comparison with the CONTR group (Fig. 5B).

Mechanical tests

Skin characteristics such as resistance to deformation or failure under applied loads can be determined from mechanical tests (16,21). Mechanical tests revealed a general trend in the dependence of the collagen fiber thickness on the skin strength properties. Therefore, on the 14th day, all samples had weak mechanical characteristics that were significantly different from the intact value (Fig. 5C). By the 21st day, the mechanical properties of the skin samples improved. STT group had the highest strength characteristics: at a maximum load of 4.903 ± 1.554 MPa, skin stretched by 34.874 ± 4.829%, which significantly differed from the values of the CONTR group (at 3.772 ± 0.640 MPa, samples stretched by 49.673 ± 14.06%) and approached the INT values (at 4.844 ± 0.206 MPa the percentage of stretch was 33.36 ± 4.92) (Fig. 5D).

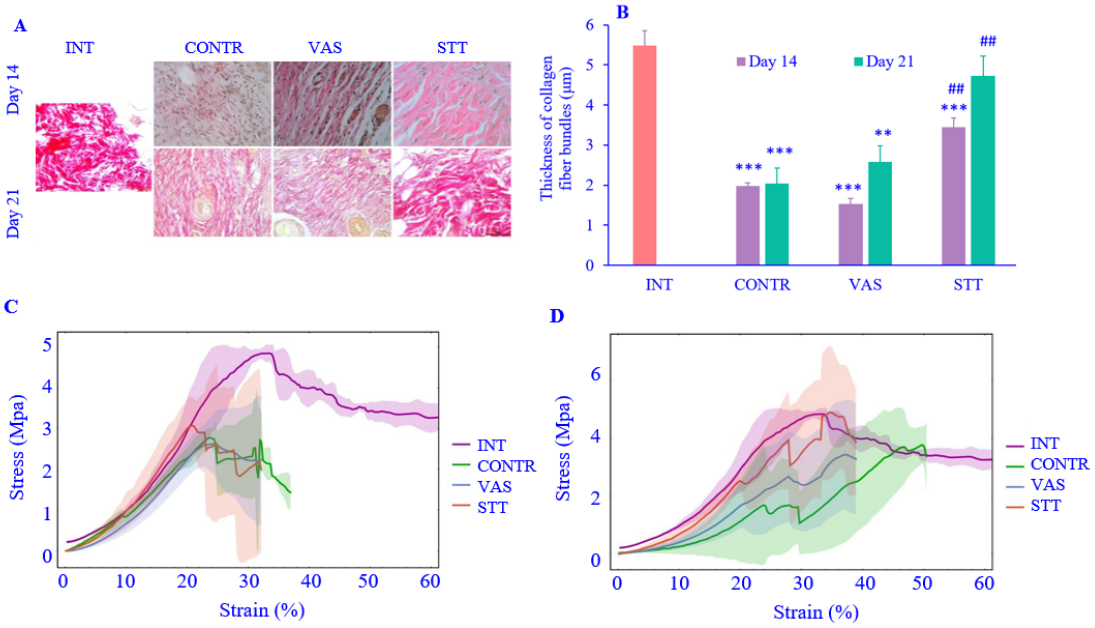

Fig. 5. (A) Van Gieson's staining, magnification: 400 ×; (B) thickness of collagen fiber bundles; (C) mechanical tests on the 14th day of the experiment; (D) mechanical tests on the 21st day of the experiment. Data are presented mean ± SEM, n = 4. $^{**}P < 0.01$ and $^{***}P < 0.001$ indicates significant difference in comparison with the INT group; $^{\#\#}P < 0.01$ versus control group. INT, Intact; CONTR, control; VAS, vaseline; STT, spiroconjugated 1,2,3-triazolo[5,1-b]1,3,4-thiadiazine.

DISCUSSION

The results of this study were consistent with the previously described effect of STT associated with the activation of fibroblasts and scar formation with a developed fibrous component (11). Here, additional parameters were evaluated that can more fully describe the state of the tissue during the regeneration and indicate the possible mechanisms of STT action. On the 14th day, the epidermis in the STT group was characterized by acanthoses, which were associated with epithelium remodeling. Upon injury, keratinocytes at the wound edges form epithelial tongues that move and interact with the dermal cells and matrix to re-establish coverage of the wound bed (3,22). In the STT group, this process was probably more intense, which was confirmed by the high content of Ki-67-positive cells in the epidermis. In addition, a more intensive recovery was observed by the skin derivatives restoration, which could also be associated with increased proliferation of keratinocytes.

In comparison with the previous study, it was found that the fibroblasts number decreased only by the 21st day of the experiment, which may indicate an active restructuring of the scar. The presence of a large number of proliferating cells was correlated with the number of Ki-67-positive cells. Furthermore, a high number of vimentin-positive cells in the STT group may indicate a high functional activity of cells, in particular synthetic. Vimentin participates in numerous processes as an integrator, with functions in cell adhesion, migration, and differentiation (16-18,23-27). Thus, in the dermis, by the 21st day, an increase in the number of Ki-67 positive cells was found in the STT group. Activated fibroblasts through vimentin may coordinate the migratory and proliferative activity of other cells, for example, progenitor cells involved in scar restructuring. This correlates with studies where activated fibroblasts have been shown to facilitate cell migration and tissue reconstruction (3,22,24).

Except for vimentin, synthetic activity is certainly associated with collagens. By the 21st day, the structure of the fibrous component approached the norm. It is worth mentioning that no sclerotic changes were detected, and microcirculation indicators on the 21st day significantly corresponded to intact ones (Fig. 4C and D). Fibrosis may occur due to intense collagenases, but this did not occur in the STT group, which was probably due to the accelerated scar restructuring. Thus, it is known that rapid scar maturation and remodeling prevent the formation of hypertrophic or keloid scars.

In addition, possible interactions between fibroblasts and mast cells played a certain role here. Mast cells are known to be involved in scar remodeling processes. Thus, it is reported that mast cells are responsible for fibroblast proliferation inhibition, which prevents keloid scar formation (28). Considering our results, possibly a large number of activated-STT fibroblasts was a kind of trigger for mast cells to increase their functional activity. As a result, a better-quality scar with better mechanical characteristics was formed. As long as about 60% of the skin is collagen, it is primarily responsible for mechanical properties (29). The structure of collagen fibers in the scar differs from normal skin, which leads to functional disorders. The fibers in the scar are less differentiated, sharply thickened, and randomly located. In keloid scars, an abundance of collagen is noted not only in the reticular but also in the papillary layer (30). In our work, it was demonstrated for CONTR and VAS groups, which presented weak mechanical characteristics. However, in the STT group, the mechanical properties of the skin improved. Probably, due to the STT stimulation of fibroblasts, a mature scar with a predominance of the fibrous component was formed. Considering the described trends, it seems relevant in future studies to study key biomarkers of fibroblast to reveal the mechanisms of their activation under STT treatment. The mechanism of STT action can be clarified by gene expression analyses (such as matrix metallopeptidase 9 and matrix remodeling associated 7 genes) or protein quantification (vimentin, collagens, and fibroblast activation protein α), which play an important role in fibroblast activation during regeneration (1,31).

CONCLUSION

The results of the current study revealed the beneficial effect of STT on skin wound regeneration. Morphological studies indicated that STT was responsible for scar formation with a structure similar to normal skin. An increase in the fibroblasts number, high levels of vimentin, and an intensification of collagenogenesis point to the stimulating effect of STT on the functional activity of fibroblasts. However, detailed mechanisms remain to be explored in future studies.

Acknowledgments

The work was supported by the Ural Federal University named after the first President of Russia B.N. Yeltsin as part of the Enhancement Program Competitiveness, Decree 211 of the Government of the Russian Federation (Contract No. 02.A03.21.0006).

Conflict of interest statement

The authors declared no conflicts of interest in this study.

Authors' contributions

I.M. Petrova performed all histological analyses, data acquisition and analysis, statistical analysis, literature search, and wrote the first draft of the manuscript; S.I. Chebanova assisted in microscopic studies; S.L. Khatsko performed all experimental studies with the animals and provided close supervision and helpful discussions about the project direction; T.A. Kalinina synthesized STT and prepared the skin ointment; D.V. Zaitsev assisted with mechanical testing and interpretation of results; and T.V. Glukhareva participated in the concept, design, and coordination of the study and also provided proofreading of the manuscript. All authors read and approved the finalized article.

REFERENCES

1. Shen Y, Ning J, Zhao L, Liu W, Wang T, Yu J, *et al*. Matrix remodeling associated 7 proteins promote cutaneous wound healing through vimentin in coordinating fibroblast functions. Inflamm Regen. 2023;43(5):1-11. DOI: 10.1186/s41232-023-00256-8.
2. Gurtner GC, Werner S, Barrandon Y, Longaker MT. Wound repair and regeneration. Nature. 2008;453(7193):314-321. DOI: 10.1038/nature07039.
3. Reinke JM, Sorg H. Wound repair and regeneration. Eur Surg Res. 2012;49(1):35-43. DOI: 10.1159/000339613.
4. Cheng F, Shen Y, Mohanasundaram P, Lindstrom M, Ivaska J, Ny T, *et al*. Vimentin coordinates fibroblast proliferation and keratinocyte differentiation in wound healing via TGF-beta-Slug signaling. Proc Natl Acad Sci USA. 2016;113(30):4320-4327. DOI: 10.1073/pnas.1519197113.
5. Petrova IM, Zaitsev DV, Zhdanova AV, Khatsko SL, Vysokova OA, Kalinina TA, *et al*. The assessment 1,2,3-triazolo- [5,1-b]-1,3,4-thiadiazine derivative influence on restoration of the fibrous skin component during regeneration caused by burn injury. Russ J of Biomech. 2022;26(2):31-41. DOI: 10.15593/RJBiomech/2022.2.03.
6. Otterco AN, Andrade AL, Brassolatti P, Pinto KNZ, Araujo HSS, Parizotto NA. Photobiomodulation mechanisms in the kinetics of the wound healing process in rats. J Photochem Photobiol B. 2018;183:22-29. DOI: 10.1016/j.jphotobiol.2018.04.010.
7. Eissa AE, Zaki MM. Saeid S, Abdelsalam M, Ali HM, Moustafa AA, *et al*. *In vitro* evaluation of the efficacy of hemodialysate (Solcoseryl®) as a wound healing agent in *Nile tilapia* (*Oreochromis niloticus*). Int J Vet Sci. 2013;1(2):57-64. DOI: 10.1016/j.ijvsm.2013.09.003.
8. Yuan J, Hou Q, Chen D, Zhong L, Dai X, Zhu Z, *et al*. Chitosan/LiCl composite scaffolds promote skin regeneration in full-thickness loss. Sci China Life Sci. 2020;63(4):552-562. DOI: 10.1007/s11427-018-9389-6.
9. Nozdrin VI, Belousova TA, Iatskovskii AN. Morphological aspects of dermatotrophic action of methyluracil applied epicutaneously. Morfologiia. 2002;122(5):74-78. PMID: 12530313.
10. Kalinina TA, Bystrykh OA, Pozdina VA, Glukhareva TV, Ulitko MV, Morzherin YY. Synthesis of spiro derivatives of 1,2,3-triazolo[5,1-b][1,3,4]thiadiazines and biological activity thereof. Chem Heterocycl. 2015;51(6):589-592. DOI: 10.1007/s10593-015-1742-1.
11. Vysokova OA, Zhdanova AV, Petrova IM, Medvedeva SY, Kalinina TA, Khatsko S, *et al*. Wound-healing effect of spiroconjugated [1,2,3]triazolo[5,1-b][1,3,4] thiadiazine on a linear skin wound model. Pharm Chem J. 2019;53(6):642-645. DOI: 10.1007/s11094-019-02054-4.
12. Kalinina TA, Bystrykh OA, Glukhareva TV, Morzherin YY. Transformation of 1,2,3-thiadiazolyl hydrazones as method for preparation of 1,2,3-triazolo[5,1-b][1,3,4]thiadiazines. J Heterocycl Chem. 2015;54(1):137-146. DOI: 10.1002/jhet.2554.

13. Morales-Burgos A, Loosemore MP, Goldberg LH. Postoperative wound care after dermatologic procedures: a comparison of 2 commonly used petrolatum-based ointments. J Drugs Dermatol. 2013;12(2):163-164.
PMID: 23377388.
14. Fang QQ, Wang XF, Zhao WY, Shi BH, Lou D, Chen CY, *et al*. Development of a chitosan-vaseline gauze dressing with wound-healing properties in murine models. Am J Trop Med Hyg. 2020;102(2):468-475.
DOI: 10.4269/ajtmh.19-0387.
15. Bai H, Kyu-Cheol N, Wang Z, Cui Y, Liu H, Liu H, *et al*. Regulation of inflammatory microenvironment using a self-healing hydrogel loaded with BM-MSCs for advanced wound healing in rat diabetic foot ulcers. J Tissue Eng. 2020;11:1-13.
DOI: 10.1177/2041731420947242.
16. Rogel MR, Soni PN, Troken JR, Sitikov A, Trejo HE, Ridge KM. Vimentin is sufficient and required for wound repair and remodeling in alveolar epithelial cells. FASEB J. 2011; 25(11): 3873-3883.
DOI: 10.1096/fj.10-170795.
17. Bleaken BM, Menko AS, Walker JL. Cells activated for wound repair have the potential to direct collective invasion of an epithelium. Mol. Biol. Cell. 2016;27(3):451-465.
DOI: 10.1091/mbc.E15-09-0615.
18. Walker JL, Bleaken BM, Romisher AR, Alnwibit AA, Menko AS. In wound repair vimentin mediates the transition of mesenchymal leader cells to a myofibroblast phenotype. Mol Biol Cell. 2018;29(13):1555-1570.
DOI: 10.1091/mbc.E17-06-0364.
19. Karimi A, Rahmati SM, Navidbakhsh M. Mechanical characterization of the rat and mice skin tissues using histostructural and uniaxial data. Bioengineered, 2015;6(3):153-160.
DOI: 10.1080/21655979.2015.1036202.
20. Chao CYL, Ng GYF, Cheung KK, Zheng YP, Wang LK, Cheing GLY. *In vivo* and *ex vivo* approaches to studying the biomechanical properties of healing wounds in rat skin. J Biomech Eng. 2013;135(10):101009,1-8.
DOI: 10.1115/1.4025109.
21. Hudson LG, Newkirk KM, Chandler HL, Choi C, Fossey SL, Parent AE, *et al*. Cutaneous wound reepithelialization is compromised in mice lacking functional Slug (Snai2). J Dermatol Sci. 2009; 56(1):19-26.
DOI: 10.1016/j.jdermsci.2009.06.009.
22. Boehnke K, Mirancea N, Pavesio A, Fusenig NE, Boukamp P, Stark HJ. Effects of fibroblasts and microenvironment on epidermal regeneration and tissue function in long-term skin equivalents. Eur J Cell Biol. 2007;86(11-12):731-346.
DOI: 10.1016/j.ejcb.2006.12.005.
23. Ivaska J, Pallari HM, Nevo J, Eriksson JE. Novel functions of vimentin in cell adhesion, migration, and signaling. Exp Cell Res. 2007;313(10):2050-2062.
DOI: 10.1016/j.yexcr.2007.03.040.
24 Mendez MG, Kojima SI, Goldman RD. Vimentin induces changes in cell shape, motility, and adhesion during the epithelial to mesenchymal transition. FASEB J. 2010;24(6):1838-1851.
DOI: 10.1096/fj.09-151639.
25. Dave JM, Bayless KJ. Vimentin as an integral regulator of cell adhesion and endothelial sprouting. Microcirculation. 2014;21(4):333-344.
DOI: 10.1111/micc.12111.
26. Battaglia RA, Delic S, Herrmann H, Snider NT. Vimentin on the move: new developments in cell migration. F1000Res. 2018;7:F1000,1-10.
DOI: 10.12688/f1000research.15967.1.
27. Meenakshi J, Jayaraman V, Ramakrishnan KM, Babu M. Keloids and hypertrophic scars: a review. Indian J Plast Surg. 2005;38(2):175-179.
DOI: 10.1097/00006534-198911000-00021.
28. Yang W, Sherman VR, Gludovatz B, Schaible E, Stewart P, Ritchie RO, *et al*. On the tear resistance of skin. Nat Commun. 2015;6(1): 1-10.
DOI: 0.1038/ncomms7649.
29. Haydont V, Bernard BA, Fortunel NO. Age-related evolutions of the dermis: clinical signs, fibroblast and extracellular matrix dynamics. Mech Ageing Dev. 2019;177:150-156.
DOI: 10.1016/j.mad.2018.03.006.
30. Stunova A, Vistejnova L. Dermal fibroblasts- a heterogeneous population with regulatory function in wound healing. Cytokine Growth Factor Rev. 2018;39:137-150.
DOI: 10.1016/j.cytogfr.2018.01.003.
31. Boink MA, Roffel S, Breetveld M, Thon M, Haasjes MSP, Waaijman T, *et al*. Comparison of advanced therapy medicinal product gingiva and skin substitutes and their *in vitro* wound healing potentials. J Tissue Eng Regen Med. 2018;12(2):e1088–e1097.
DOI: 10.1002/term.2438.

ONLINE SUBMISSION

https://review.jow.medknow.com/rps

Research in Pharmaceutical Sciences, June 2024; 19(3): 276-286
Received: 17-07-2023
Peer Reviewed: 08-08-2023
Revised: 20-08-2023
Accepted: 16-12-2023
Published: 01-07-2024

School of Pharmacy & Pharmaceutical Sciences
Isfahan University of Medical Sciences

Original Article

Effect of *Tamarindus indica* L. fruit pulp and seed extracts on experimental ulcerative colitis in rats

Mohsen Minaiyan[1,*], Sepehr Abolhasani[2], Setareh Sima[3], and Afsaneh Yegdaneh[4]

[1]*Department of Pharmacology and Toxicology and Isfahan Pharmaceutical Sciences Research Centre, School of Pharmacy and Pharmaceutical Sciences, Isfahan University of Medical Sciences, Isfahan, Iran.*
[2]*School of Pharmacy and Pharmaceutical Sciences, Isfahan University of Medical Sciences, Isfahan, Iran.*
[3]*Department of Pharmaceutical Biotechnology, School of Pharmacy and Pharmaceutical Sciences, Isfahan University of Medical Sciences, Isfahan, Iran.*
[4]*Department of Pharmacognosy, School of Pharmacy and Pharmaceutical Sciences, Isfahan University of Medical Sciences, Isfahan, Iran.*

Abstract

Background and purpose: *Tamarindus indica* L. which has anti-inflammatory, radical scavenging, and ulcer healing effects can be useful for the alleviation of inflammatory bowel disease (IBD). Therefore, the effects of *T. indica* fruit pulp (TIPE) and seed extracts (TISE) were investigated on experimental colitis.
Experimental approach: TIPE and TISE (125, 250, and 500 mg/kg) were made by maceration (ethanol/water: 80/30) and administered to male Wistar rats with acetic acid-induced colitis. Prednisolone (4 mg/kg) and mesalazine (100 mg/kg) were used as reference drugs. The colon tissues were examined for macroscopic and pathologic parameters and myeloperoxidase (MPO) and malondialdehyde (MDA) values.
Findings/Results: The total phenols were 45.7 ± 1.1 and 453.0 ± 3.3 mg/g in terms of gallic acid for TIPE and TISE, respectively. Both of the extracts significantly improved most of the investigated parameters including body weight loss, the weight of colons, indices of ulcers, and total colitis. MPO activity and MDA in the treatment groups (except for TIPE at 125 mg/Kg) significantly decreased compared to the control.
Conclusion and implications: Both TIPE and TISE were effective in the treatment of colitis however it seems that the effective ingredients were more concentrated in seeds rather than pulp extract so the highest dose of seed extract had a competitive effect with reference drugs. More studies are needed to introduce *T. indica* as a suitable complementary medicine or food for patients with IBD.

Keywords: Acetic acid; Animal model; Colitis; *Tamarindus indica*; Plant extracts.

INTRODUCTION

Inflammatory bowel disease (IBD) is a common inflammatory disease of the gastrointestinal tract which is difficult to diagnose and treat. IBD comes in two forms: Crohn's disease and ulcerative colitis. The exact cause of IBD is unknown, but the most likely explanation involves a combination of one or more of the following: immune system disorders (caused by environmental or genetic factors), abnormal gastrointestinal factors (such as changes in the normal gut flora), and oxidative stress (1,2). IBD is associated with disorders in the gut mucosal barrier that allow luminal factors such as leukotriene B4, nuclear factor-κB (NF-κB), nitric oxide, and abnormal activity of cyclooxygenase-2 (COX-2) to penetrate the mucosa (3).

Corticosteroids, immunomodulatory drugs, including methotrexate, 6-mercaptopurine, and azathioprine, as well as anti-tumor necrosis factor alpha (TNF-α) drugs such as infliximab and adalimumab, are commonly used to treat IBD.

*Corresponding author: M. Minaiyan
Tel: +98-3137927088, Fax: +98-3136680011
Email: minaiyan@pharm.mui.ac.ir

Access this article online

Website: http://rps.mui.ac.ir

DOI: 10.4103/RPS.RPS_131_23

Allergic reactions, bone loss, kidney disease, and bone marrow suppression are possible side effects of these drugs. So, despite being one of the most effective anti-inflammatory drugs, the use of corticosteroids is limited. Only about 60-70% of resistant cases respond to azathioprine and 6-mercaptopurine, and adverse effects such as severe liver damage, bone marrow depression, and pancreatitis might occur (4). Although non-steroidal anti-inflammatory drugs (NSAIDs) are among the drugs most often prescribed to treat various types of inflammation, they are rarely used to treat IBD due to their negative effects on leukotriene synthesis, sometimes even increasing it, which leads to gastrointestinal mucosal damage and aggravation of IBD (5).

The insufficient efficacy and safety of current drugs, as well as side effects and patient complaints, have created a strong motivation to use new and effective treatments including probiotics and herbal medicine, especially during the last 30 years. These drugs have attracted the curiosity of the public and researchers for a long time due to their potent and diverse compounds, low side effects, affordable price, and potential for long-term use (6,7).

The Indian tamarind (*Tamarindus indica* L.) is an evergreen tree of the Fabaceae family that is widely grown in India, Sri Lanka, Thailand, the South of Iran, and tropical parts of Asia (8). Pharmacological studies have shown the presence of abundant active ingredients including polyphenols, tannins, flavonoids, cardiac glycosides, organic acids, mucilage, pectin, and sugars (arabinose, xylose, galactose, fructose, and glucose) in this plant (8,9). Besides it has been proven that tamarind ethanolic extract contains fatty acids and several essential and trace elements including cadmium, calcium, magnesium, arsenic, copper, iron, sodium, manganese, potassium, phosphorus, and zinc (10).

Tamarind fruit pulp contains pyrazines (trans-2-hexanal), thiazoles (2-ethylthiazole, 2-methylthiazole), amino acids, inverted sugar (25-30%), pectin, protein, fat, and various organic acids including tartaric acid, acetic acid, citric acid, formic acid, malic acid, and benzoic acid for which antibacterial, anti-inflammatory, anti-diarrheal, anti-diabetic, spasmolytic, vasodilator, ulcer healing, antioxidant, and anticancer properties have demonstrated (10,11). In traditional Indian medicine (Ayurveda), the leaf decoction of tamarind is used for washing indolent and resistant ulcers and promotes healthy action (12). In addition, fruit seeds of *T. indica* contain protein, fatty acids, lipids with xylose (alpha-1,6), and specific keto acids (13).

Tamarind has traditionally been used to alleviate diarrhea and dysentery, parasitic infections, jaundice, and nausea during pregnancy (14). The beneficial effect of the drug on bloody diarrhea, which is usually caused by an intestinal infection, also indicates the antiseptic effect of this natural product (15). It is worth noting that according to toxicity studies, tamarind extract is considered almost non-toxic due to its lethal dose of 50% (LD50) of more than 5000 mg/kg in mice (16).

Considering the beneficial pharmacological effects (anti-ulcer, anti-diarrheal, anti-infective, and anti-inflammatory), ease of access, relatively reasonable price, and wide use as a seasoning and flavoring agent, this plant seems to have a good potential for treating and/or preventing the recurrence of the colitis. Therefore, this study was conducted to demonstrate the possible healing and therapeutic effects of *T. indica* fruit pulp (TIPE) and seed extract (TISE) in experimental colitis.

MATERIALS AND METHODS

Preparation of plant and its extracts

Indian tamarind with the brand Alfa® Food and Product Co. (Thailand) was procured from a trusted local market in Isfahan. It was approved by a botanist from Isfahan University. Fruit pulp (1 Kg) and seeds (422 g) were thoroughly and separately pulverized after drying. To make a hydroalcoholic extract, the crude materials were separately mixed with EtOH: water (80:20), and the mixture was shaken and filtered three times over three days. The result of each step was pooled and finally, it was dried in a rotary evaporator after that it was freeze-dried to produce a fully dried extract (17).

Measurement of yield values

When the final extract was achieved, the weight of each was freshly measured, and the overall yield value was measured for TIPE and TISE based on the primary crude material (18).

Determination of total phenol contents of plant extracts

The Folin-Ciocalteu method was conducted to measure the phenolic ingredients of TIPE and TISE overall (18). In this method, phenolic ingredients react with a color-making reagent, whose absorbance is measurable at 765 nm. In this method, gallic acid (0-500 mg/mL) was used for depicting of standard curve and biophenols were evaluated as gallic acid equivalents for each extract.

Drugs and chemicals

We bought powders of mesalazine and prednisolone from Iran Hormone Co. (Tehran, Iran). Ortodianisidine dihydrochloride and hexadecyl trimethyl ammonium bromide were also purchased from Sigma Co. (St. Louis, USA). All of the organic solvents and chemicals were procured from Merck Co. (Darmstadt, Germany).

Animals

Sixty male Wistar rats were purchased from the animal house of the School of Pharmacy, which was dedicated to the maintenance and breeding of laboratory animals. They were given a week to acclimatize to the laboratory conditions. They were housed in standard-sized polycarbonate cages with controlled light/dark photoperiods, temperature (21-23 °C), and humidity (20-50%), and provided with chow pellets and free access to drinking water. The study was conducted according to the national guidelines for animal experiments provided by the Ethics Committee of Isfahan University of Medical Sciences under Ethic No. IR.MUI.RESEARCH.REC.1399.025.

Animal grouping

The rats were randomly assigned to the following ten groups (6 each): (1) normal group (vehicle): normal saline, 2 mL/kg was administered orally (p.o.); (2) control group: colitis was induced and normal saline was administered (2 mL/kg, p.o.); (3-5, fruit pulp extract): rats with colitis were treated with TIPE (125, 250, 500 mg/kg, p.o.); (6-8, fruit seed extract): rats with colitis were treated with TISE (125, 250, 500 mg/kg, p.o.) (19,20); (9 and 10, reference): rats with colitis were treated with prednisolone (4 mg/kg, p.o.) or mesalazine (100 mg/kg, p.o.).

Administration of drugs and extracts was conducted by gavage starting 2 h before induction of colitis and repeated daily for 5 days thereafter.

Experimental protocol

Plant extracts and drugs were freshly made as suspensions or solutions, respectively. Rats were fasted for 24 h with free access to drinking water before colitis induction. Two mL of acetic acid (3%) was administered intra-rectally to induce acute colitis (21). Midazolam (5 mg/kg) was used to give the rats a favorable sedation, while a suitable tube with an inner diameter of 2 mm and a length of 8 cm was inserted into the anus. On the sixth day, the animals were weighed and euthanized by CO_2 inhalation, then their abdominal cavity was opened and the colon tissue was assessed both macroscopically and microscopically. In the end, myeloperoxidase (MPO) activity and malondialdehyde (MDA) levels were measured in the colon tissue and compared with the control group (22).

Evaluation of colon macroscopic damage

The distal colon was cleaned with normal saline, cut longitudinally, and its wet weight was measured. After mounting on a light and transparent sheet, macroscopic features of colitis were recorded. To measure ulcerated areas, pictures of colon sections were taken with a camera, downloaded to a computer, and analyzed using Fiji Win 32 software (22). Moreover, the following values were used to determine ulcer severity: 0, no wound; 1, inflammation and thickness; 2, hemorrhagic spots and bleeding; 3, necrosis and/or perforation. Ulcer score and ulcer area were added together and the ulcer index was obtained for each tissue sample. Tissue samples were cut lengthwise into three equal parts for further analysis. Two sections were immediately frozen (-20 °C) for analysis of biomarkers (MPO and MDA), while the other section was deposited in formalin (10%) for further evaluation (22).

Evaluation of colon histological damage

Fixed colon tissue was subjected to the following steps: dehydration, clearing, paraffin embedding, blocking, processing, cutting into 4-µm thick slices, and staining with hematoxylin and eosin (H&E). A valid scoring method provided by Dieleman *et al*. (23) and modified by Motavallian-Naeini *et al*. (24) was used to evaluate the intensity, extent, crypt damage, and leukocyte infiltration on H&E-stained tissue. Finally, for each sample, the total index for colitis; the sum of the four above-mentioned sub-scores was obtained. Digital photography and imaging were conducted by using a modern camera and optic microscope while pathological examination and scoring were performed by a blind pathologist.

Evaluation of colonic MPO activity

A previously published method was set up in this laboratory and MPO activity, a marker of polymorphonuclear aggregation, was assessed (25). Colon tissues were thawed and a part (0.1 g) was crushed in 5 mL of potassium phosphate buffer (pH 6) containing 0.5% w/v hexadecyl trimethyl ammonium bromide, transferred to a tube, and homogenized three times for 45 s with one-minute intervals. The homogenate was centrifuged at 4000 rpm for 10 min. Then, 0.1 mL of the solution was mixed with 2.9 mL of potassium buffer (pH 6) containing 0.167 mg/mL ortho-dianisidine dihydrochloride and 0.005% H_2O_2. Then, MPO activity was measured at 450 nm using a UV-VIS spectrophotometer (Unico, USA). MPO activity was measured in units (U) per 100 mg of wet colon and was defined as the amount of enzyme degrading 1 µmol H_2O_2 per minute at 25 °C (25).

Evaluation of MDA level

Evaluation of MDA (a lipid peroxidation marker) was done by adding KCl (1 mL, 1.15% w/v) to 10 mg of colon tissue. The homogenized mixture was centrifuged (7500 rpm for 10 min) and its absorbance was measured at 532 nm. The experiments were performed using its specific kit (Navand-Salam, Urmia) based on the instructions of the company (26).

Statistical analysis

The statistical software SPSS 16.0 was used to conduct the statistical analysis. Using Student's t. paired test and parametric one-way analysis of variance (ANOVA) followed by Turkey's HSD as a post hoc test, differences between groups were investigated. The Mann-Whitney U test was used to assess non-parametric (scoring) data. The mean ± SEM/SD or median (range) was used to express the data. The *P*-values < 0.05 were considered statistically significant.

RESULTS

Yield values and total phenolic contents of extracts

The yield values were 34.4% and 13.8% for TIPE and TISE, respectively. Also, the average percentage of dry material determined was 80.1 % and 92.3% for TIPE and TISE, respectively. The amount of total phenol in the extract in terms of gallic acid equivalent after thrice repeats equals 45.7 ± 1.1 and 453.0 ± 3.3 mg/g of dried TIPE and TISE, respectively.

Effect of T. indica extracts on body weight of rats

As shown in Table 1, the rats in the normal group gained weight in a significant manner. On the contrary, the rats in the control group had a significant weight loss, which indicates the induction of the disease condition. The results of other groups showed that treatment with different doses of extracts could stop the process of weight loss, although the weight gain that occurred was not significant. Administration of prednisolone was associated with weight loss in rats; however, it was not significant.

Effect of T. indica extracts on macroscopic parameters

As shown in Table 2 and Fig. 1, TIPE at 250 and 500 mg/kg and TISE at all examined doses (125, 250, and 500 mg/kg) significantly reduced the weight of colon tissue and related macroscopic colitis features like ulcer area, severity and index in overall in comparison with the control group. Similar and more clear results were obtained with reference drugs (prednisolone and mesalazine). No signs of inflammation, edema, ulcer, or necrosis were observed in the normal colon tissue, while the most extreme intensity of these parameters occurred in the tissue of the control group (Fig. 1).

Table 1. Weight changes of rats in experimental groups. Data are presented as mean ± SD, n = 6. Normal and control (colitis-induced) groups were treated with normal saline. *P < 0.05 and **P < 0.01 represent significant differences before and after treatment.

Groups	Before	After	*P*-value
Normal	207.5 ± 7.9	218.5 ± 10.3	*
Control	222.0 ±7.4	198.3 ± 6.8	**
TIPE (125 mg/kg)	205.6 ± 8.4	212.0 ± 8.5	NS
TIPE (250 mg/kg)	189.3 ± 5.3	198.3 ± 4.8	NS
TIPE (500 mg/kg)	222.3 ± 13.3	236.1 ± 10.1	NS
TISE (125 mg/kg)	220.5 ± 11.7	223.5 ± 6.2	NS
TISE (250 mg/kg)	214.3 ± 11.5	219.3 ± 13.8	NS
TISE (500 mg/kg)	220.8 ± 10.1	236.8 ± 11.9	NS
Prednisolone (4 mg/kg)	196.8 ± 8.8	187.5 ± 11.8	NS
Mesalazine (100 mg/kg)	198.5 ± 3.4	203.5 ± 3.0	NS

TIPE, *Tamarindus indica* pulp extract; TISE, *Tamarindus indica* seed extract; NS, non-significant.

Table 2. Macroscopic parameters of colitis in experimental groups of rats. Data are presented as mean ± SD, n = 6. Normal and control (colitis-induced) groups were treated with normal saline. *P < 0.05, **P < 0.01, and ***P < 0.001 represent significant differences compared to the control group, $^{###}P$ < 0.001 versus the normal group.

Groups	Ulcer area (cm^2)	Ulcer score (0-3)	Ulcer index (0-11)	Colon (mg/8 cm)
Normal	0.00 ± 0.00	0.0 (0-0)	0.0 ± 0.0	110.3 ± 15.0
Control	6.5 ± 0.4$^{###}$	3.0 (3-3)$^{###}$	9.5 ± 0.4$^{###}$	380.4 ± 18.0$^{###}$
TIPE (125 mg/kg)	5.3 ± 0.5	2 (2-3)	7.6 ± 0.6	368.6 ± 28
TIPE (250 mg/kg)	3.9 ± 0.4***	1.5 (1-3)*	5.6 ± 0.6***	254.4 ± 20***
TIPE (500 mg/kg)	2.6 ± 1.0***	2.0 (1-3)*	5.6 ± 1.4**	217.1 ± 30***
TISE (125 mg/kg)	2.9 ± 0.7***	1.5 (0-3)*	4.4 ± 1.0**	310.5 ± 30*
TISE (250 mg/kg)	1.1 ± 0.5***	1.0 (0-3)**	2.3 ± 0.9***	257.7 ± 10***
TISE (500 mg/kg)	0.5 ± 0.2***	1.5 (0-2)*	2.0 ± 0.5***	160.2 ± 10***
Prednisolone (4 mg/kg)	1.5 ± 0.6***	1.0 (0-3)***	2.6 ± 1.0***	127.2 ± 20***
Mesalazine (100 mg/kg)	1.6 ± 0.1***	1.0 (1-2)***	2.9 ± 0.3***	150.0 ± 17***

TIPE, *Tamarindus indica* pulp extract; TISE, *Tamarindus indica* seed extract.

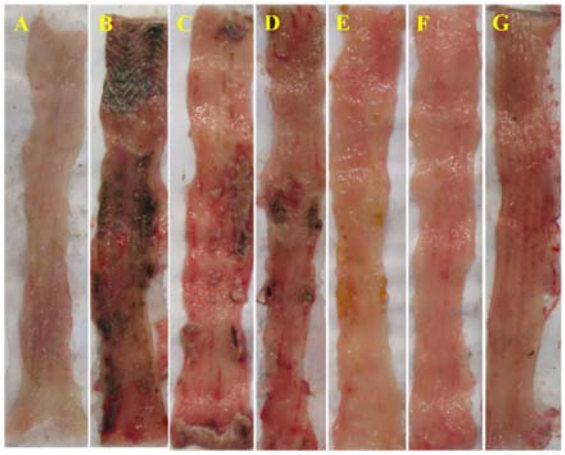

Fig. 1. Photos of colon tissue, 6 days after acetic acid-induced colitis in rats. (A) Normal colon treated with normal saline (5 mL/kg); (B) control colitis treated with normal saline (5 mL/kg); (C and D) colitis rats treated with TIPE at 125 and 500 mg/kg, respectively; (E) colitis rats treated with TISE at 500 mg/kg; (F and G) colitis rats treated with prednisolone at 4 mg/kg and mesalazine at 100 mg/kg, respectively. TIPE, *Tamarindus indica* pulp extract; TISE, *Tamarindus indica* seed extract.

Effect of T. indica extracts on microscopic parameters

As shown in Table 3 and Fig. 2, TIPE at 250 and 500 mg/kg and TISE at all examined doses (125, 250, and 500 mg/kg) decreased the total colitis index and involved pathologic features like inflammatory extent and severity, crypt damage, and leukocyte infiltration compared to the control group. Similar results were obtained with approved drugs. No signs of inflammation, infiltration of leukocytes, and crypt damage were occurred in the normal colon tissue, while the most obvious intensity of these parameters observed in the tissue of the control colitis group (Fig. 2).

Effect of T. indica extracts on MPO activity

MPO activity significantly decreased in the groups treated with TIPE (250, 500 mg/kg) and TISE (125, 250, 500 mg/kg) compared to the control. As expected, prednisolone and mesalazine were successful in decreasing MPO activity (Fig. 3A). MPO activity in normal tissue was negligible while it was exponentially increased (about 10 folds) after inducing colitis (Fig. 3).

Table 3. Pathologic parameters of colitis in experimental groups of rats. Data are presented as median (range). n = 6. Normal and control (colitis-induced) groups were treated with normal saline. *$P < 0.05$, **$P < 0.01$, and ***$P < 0.001$ represent significant differences compared to the control group, $^{###}P < 0.001$ versus the normal group.

Groups	Inflammatory severity (0-3)	Inflammatory extent (0-3)	Leukocyte infiltration (0-3)	Crypt damage (0-4)	Total colitis index (0-12)
Normal	0.0 (0-0)	0.0 (0-0)	0.0 (0-0)	0.0 (0-0)	0.0 (0-0)
Control	3.0 (3-3)###	3.0 (2-3)###	2.0 (2-3)###	4.0 (3-4)###	12.0 (11-13)###
TIPE (125 mg/kg)	2.0 (2-3)	2.0 (2-3)	2.0 (1-3)	3.0 (3-4)	9.0 (8-13)
TIPE (250 mg/kg)	2.0 (1-3)	1.5 (1-2)*	1.5 (1-2)	2.0 (2-4)*	7.0 (5-11)*
TIPE (500 mg/kg)	1.5 (0-3)*	1.5 (1-2)	1.5 (1-3)	2.0 (2-3)**	6.5 (4-11)**
TISE (125 mg/kg)	1.5 (1-3)*	1.5 (1-2)*	1.0 (1-2)**	1.5 (1-2)**	5.5 (4-9)***
TISE (250 mg/kg)	1.0 (1-1)**	0.5 (1-2)***	1.0 (0-1)***	2.0 (1-3)*	4.5 (3-7)***
TISE (500 mg/kg)	0.5 (1-2)***	1.0 (1-1)***	1.0 (0-2)**	1.5 (0-2)***	4.0 (2-7)***
Prednisolone (4 mg/kg)	0.5 (0-1)***	0.5 (0-1)***	1.0 (1-1)***	1.0 (1-2)***	3.0 (2-5)***
Mesalazine (100 mg/kg)	1.0 (0-1)**	1.0 (1-2)***	1.0 (1-2)**	1.5 (1-2)***	4.5 (3-6)***

TIPE, *Tamarindus indica* pulp extract; TISE, *Tamarindus indica* seed extract.

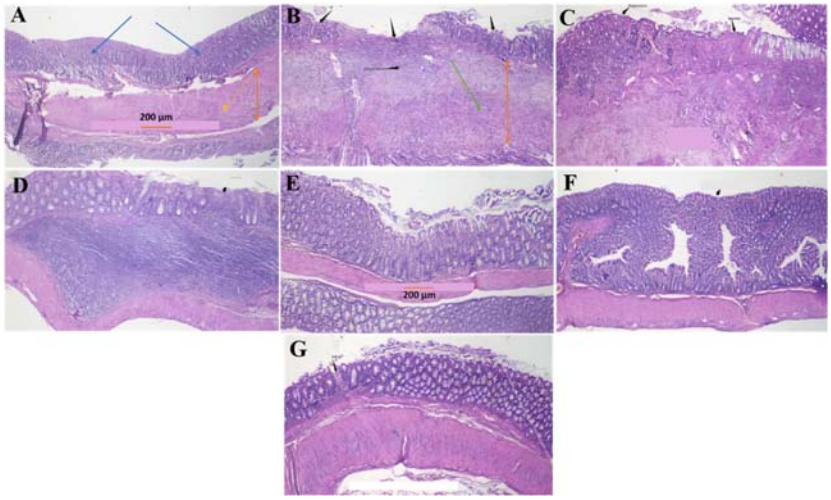

Fig. 2. Microscopic illustration of colonic tissue in rats by applying hematoxylin and eosin staining method. (A) Normal tissue treated with normal saline (5 mL/kg), the mucosal layer and the submucosa were intact and there was no sign of an ulcer or crypt damage (blue arrow); (B) control colitis treated with normal saline (5 mL/kg), the mucosal layer was completely damaged (black arrow) and the submucosa layer was severely swollen and inflamed (orange arrow). Crypts were severely damaged (black arrow) and leukocytes accumulated (green arrow); (C and D) colitis rats treated with TIPE at 125 and 500 mg/kg; (E) colitis rats treated with TISE at 500 mg/kg; (F and G) colitis rats treated with prednisolone (4 mg/kg) and mesalazine (100 mg/kg), respectively. Magnification: ×40. TIPE, *Tamarindus indica* pulp extract; TISE, *Tamarindus indica* seed extract.

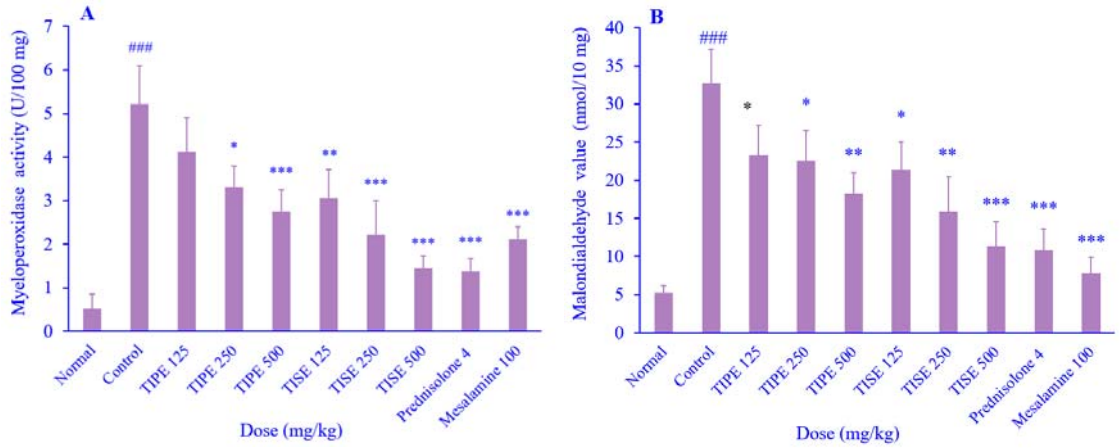

Fig. 3. (A) Myeloperoxidase activity and (B) malondialdehyde value in colonic tissue of rats treated with normal saline (control group, 5 mL/kg), TIPE and TISE, prednisolone, and mesalamine. Data are presented as mean ± SEM, n = 6. *$P < 0.05$, **$P < 0.01$, ***$P < 0.001$ represent significant differences compared to the control group; $^{###}P < 0.001$ versus the normal group. TIPE, *Tamarindus indica* pulp extract; TISE, *Tamarindus indica* seed extract.

Effect of T. indica extracts on MDA value

MDA significantly decreased in all groups treated with TIPE (125, 250, 500 mg/kg) or TISE (125, 250, 500 mg/kg) compared to the control group. As expected, reference agents were successful in decreasing MDA activity (Fig. 3B). The amount of MDA in normal tissue was negligible while it exponentially increased (about 7 folds) after inducing colitis (Fig. 3B).

DISCUSSION

In this study, based on the general results and various evaluations at the tissue level and inflammatory biomarkers, it has been shown that tamarind hydroalcoholic seed and pulp extracts had a healing effect on experimental colitis.

Our results demonstrated obvious destruction of colon tissue in the control untreated group following the inoculation of acetic acid as an approved model of experimental colitis (27).

Weight loss in animals is one of the clinical symptoms of colitis, which can be caused by frequent bloody or watery diarrhea and anorexia caused by the disease condition (28). At the end of this study, animals in the control group showed significant weight loss compared to day one of the study, which could be caused by the complications of colitis. On the other hand, the cessation of weight loss and an increase in body weight, even though insignificant, in the treatment groups indicated the improvement of the disease (28). The only exception was the group treated with prednisolone, which showed weight loss despite the improvement of the disease features, and this can be attributed to its catabolic effects as a corticosteroid (29). In the current study, all the treatments were made by oral intake, so it can be concluded that there was a good bioavailability of the active ingredients. However, the active ingredients that were not absorbed probably reached the site of their action, the colon, through the bowel (30).

In addition, our results showed that the content of MPO and MDA of the colon tissue increased exponentially in the untreated colitis group indicating the activation and migration of macrophages and neutrophils, which leads to an increase in oxidative stress (26,27). In our study, almost all the doses of TIPE and TISE (except 125 mg/kg of TIPE) diminished MPO and MDA activity, which is due to the antioxidant and anti-inflammatory effects of the extracts. Interestingly, the least examined dose of TIPE (125 mg/kg) which did not affect most parameters of colitis, reduced MDA levels in colon tissue, indicating a significant antioxidant effect. This is a reason suggesting that the antioxidant effect alone is not enough for the treatment of acute colitis (31). The weight of the colon indicates the severity and level of inflammation and immune system response in the colon area. The higher the weight of the

colon, the more the accumulation of interstitial fluid indicates which is an important measure of edema and aggravation of colitis (32). The results of this study showed that TISE at all test doses and TISE at two larger doses were effective in reducing this parameter and this effect was directly related to the reduction of MPO level in the colon tissue. This result emphasizes the importance of MPO activity in evaluating the severity and extent of the disease in this model of colitis (27,32).

Also, the ineffectiveness of the low dose of pulp extract (125 mg/kg) can probably be due to the low content of effective substances or their low availability by oral intake. Therefore, other routes of administration including parenteral or rectal for the pulp extract should be tried (33). Also, the highest examined dose of TISE (500 mg/kg) had clear anti-inflammatory and anti-ulcer effects, which in some cases was well comparable with the effect of reference drugs.

The difference in the effectiveness of the two parts of the *T. indica* (TISE and TIPE) could be attributed to the existence of different effective substances. The phenolic and flavonoid compounds obtained from the seed cover extract of this plant reduced nitric oxide production induced by lipopolysaccharide and interferon-gamma in RAW 264.7 mouse macrophage cells by 68% compared to the control group, and this effect was dose-related (20).

In another study carried out by Kalra *et al*. tamarind seed methanolic extract (100-200 mg/kg) has been shown to have dose-related protective effects on three models of experimental gastric ulcers including ibuprofen, alcohol, and pylorus-ligation-induced methods. This protective effect has been attributed to its polyphenolic compounds, mainly procyanidin, epicatechin, and seed polymer tannins, which have antioxidant and cytoprotective properties against free radicals. It seems tannins prevent ulcer formation through protein accumulation and stimulating the synthesis of antibodies (19).

Previous studies have reported that *T. indica* contains polyphenolic compounds mainly including polymeric tannins and pro-anthocyanidins in various forms such as apigenin, catechin, procyanidin derivatives, epicatechin, and taxifolinol (9). Procyanidin and its derivatives, which are abundantly found in tamarind seed and its coating, have great power in trapping oxygen free radicals and reducing oxidative stress in the target tissue (9,10). The same protective effect has been reported for apigenin and catechin to inhibit nitric oxide, TNF-α, NF-κB, interleukin (IL)-4, and COX-2 production. These substances have been shown to have cytoprotective properties and are associated with anti-ulcer activity (34-36). In many studies, the anti-ulcer and anti-inflammatory effects of polyphenolic compounds are attributed to their antioxidant properties. However, the antioxidant effect has many different components and cannot be fully evaluated by measuring one parameter such as MDA (31,37). In one study carried out by L. Roja *et al*., it was demonstrated that ethanol extract of tamarind leaves (200 and 400 mg/kg/d) caused protection against three models of gastric ulcer including cold and restraint, indomethacin-induced, and pylorus ligation and the effect was dose-related. They concluded that these effects were due to antioxidant properties, neutralization of free radicals, and prostaglandin mobilization in the gastric tissue. They also showed that the examined tamarind extract was quite safe up to 4000 mg/kg/day for two weeks and had no serious toxic effects on the main activities and vital organs of the animals (38). In another study conducted on xyloglucan (mucoadhesive abundant hemicellulose) isolated from tamarind seeds (100-300 mg/kg/day) on dextran sulfate sodium-induced colitis in mice, the authors found that this fraction could reduce the level of cytokines, especially IL-1β, IL-6, and NF-κB in the intestinal mucosa (39). In the previous study, no clinical, macroscopic, and pathologic evaluation was done on the affected tissue, and the study was limited to a polysaccharide fraction of the tamarind seeds. There are reports that flavonoids inhibit COX-2 activity. COX-2 catalyzes the synthesis of prostaglandin E2 playing an important role in inflammation and related diseases (40). Flavonoids inhibit inflammatory cytokines such as IL-6, IL-7, and TNF-α (38,41). Some flavonoids inhibit the NF-κB pathway, which

leads to a decrease in the production of TNF-α and IL-1β as one of the key enzymes in activating inflammatory cells. The reduction of IL-1β production by this group of compounds leads to the reduction of IL-2 and TNF-α production (41). Among the polyphenolic compounds, especially tannins, they are astringent and have a strong anti-diarrheal effect. This effect was well observed in the experimental groups and it was more evident in those who were treated with TISE. Intriguingly, the phenolic content of the TISE was much higher than that of the TIPE, which is consistent with the above-mentioned results. The astringent action can help deposit microproteins at the ulcerated area, thereby forming an impermeable layer on the lining that prevents intestinal secretions and protects the underlying mucosa from toxins and other irritants (19,38,41).

According to the pathology results (total colitis index), it is obvious that TISE and TIPE had a protective effect on colitis in rats, while the result of seed extract was better than pulp, especially at higher doses. It seems that seed extract can provide more impact on oxidative stress and inflammatory factors in colitis tissue.

CONCLUSION

Our results suggested that TIPE and TISE are effective in the colitis murine model. It seems the seeds of *T. indica* are more beneficial candidates due to better results obtained however, more complementary studies at analytical, toxicological, and clinical levels are required to explore the exact mechanism of *T. indica* action and its usefulness in IBD therapy.

Acknowledgments

The research was financially supported by the Vice-Chanceller of Research of Isfahan University of Medical Sciences through Grant No. 3400140. The authors would like to thank Dr. Ardeshir Talebi for his sincere cooperation in preparation and the evaluation of pathological samples.

Conflict of interest statement

The authors declared conflicts of interest in this study.

Authors' contribution

M. Minaiyan presented the idea of research, designed, and supervised all of the parts related to the grouping of animals, determining the doses of drugs, arrangement of interventions, induction of colitis, and statistical analysis of data; S. Abolhasani carried out the experiments and interventions; S. Sima cooperated in the experiments related to MPO and MDA measurements, preparing pathology samples, drawing diagrams, and writing the manuscript; A. Yegdaneh designed and supervised all of the experiments related to the identification, preparation, and evaluation of herbal materials and extracts. All authors contributed to the writing, reviewing, and preparation of the manuscript. The finalized article was read and approved by all authors.

REFERENCES

1. Podolsky DK. The current future understanding of inflammatory bowel disease. Best Pract Res Clin Gastroenterol. 2002;1:16(6):933-943. DOI: 10.1053/bega.2002.0354.
2. Loftus Jr EV. Clinical epidemiology of inflammatory bowel disease: incidence, prevalence, and environmental influences. Gastroenterology. 2004;126(6):1504-1517. DOI: 10.1053/j.gastro.2004.01.063.
3. Guan Q. A Comprehensive review and update on the pathogenesis of inflammatory bowel disease. J Immunol Res. 2019;2019:1-17. DOI: 10.1155/2019/7247238.
4. Summers RW. Novel and future medical management of inflammatory bowel disease. Surg Clin North Am. 2007;87(3):727-741. DOI: 10.1016/j.suc.2007.03.004.
5. Klein A, Eliakim R. Non-steroidal anti-inflammatory drugs and inflammatory bowel disease. Pharmaceuticals. 2010;3(4):1084-1092. DOI: 10.3390/ph3041084.
6. Rahimi R, Mozaffari S, Abdollahi M. On the use of herbal medicines in management of inflammatory bowel diseases: a systematic review of animal and human studies. Dig Dis Sci. 2009;54(3):471-480. DOI: 10.1007/s10620-008-0368-x.
7. Rahimi R, Shams-Ardekani MR, Abdollahi M. A review of the efficacy of traditional Iranian medicine for inflammatory bowel disease. World J Gastroenterol. 2010;16(36):4504-5014. DOI: 10.3748/wjg.v16.i36.4504.
8. Rao YS, Mathew MK, Potty SN. Tamarindus indica. Ind J Arecanut Spices Med Plants.1999;1:127-145. DOI: 10.4103/0973-7847.79102.
9. Ibrahim NA, El-Gengaihi S, El-Hamidi A, Bashandy SAE. Chemical and biological evaluation of

Tamarindus indica L. growing in Sudan. Acta Hortic. 1995;390:51-57.
DOI: 10.17660/ActaHortic.1995.390.6.
10. Kabir Khanzada, Shaikh W, Shahzadi S, Kazi T, Usmanghani K, Kabir A, *et al*. Chemical constituents of *Tamarindus indica*. Medicinal plant in Sindh. Pak J Bot. 2008;40(6):2553-2559.
DOI: 4435/443543720011.
11. Wong Kc, Tan CP, Chow CH, Chee SG. Volatile constituents of the fruit of *Tamarindus indica L*. J Essent Oil Res. 1998;10:219-221.
DOI: 10.1080/10412905.1998.9700886.
12. Nadkarni KM. Indian Materia Medica, 1st ed. Mumbai: Bombay Popular Prakashan; 1976. pp. 1191-1193.
DOI: 10.4236/cm.2011.24024.
13. Kuru P. Tamarindus indica and its health related effects. Asian Pac J Trop Biomed. 2014;4(9):676-681.
DOI: 10.12980/APJTB.4.2014APJTB-2014-0173.
14. Havinga RM, Hartl A, Putscher J, Prehsler S, Buchmann C, Vogl CR. Tamarindus indica patterns of use in traditional African medicine. J Ethnopharmacol. 2010;127(3):573-588.
DOI: 10.1016/j.jep.2009.11.028.
15. Chhabra SC, Mahunnah RL, Mshiu EN. Plants used in traditional medicine in Eastern Tanzania, pteridophytes and angiosperms (Acanthaceae to Canellaceae). J Ethnopharmacol. 1987;21:253-277.
DOI: 10.1016/0378-8741(87)90103-6.
16. Abubakar M, Yerima M, Zahriya AG, Ukwuani AN. Acute toxicity and antifungal studies of ethanolic leaves, stem and pulp extract of *Tamarindus indica*. Res J Pharm Biol Chem Sci. 2010;4:104-111.
17. Handa SS, Khanuja SPS, Longo G, Rakesh DD. Extraction technologies for medicinal and aromatic plants. 1st ed. Trieste: ISC-UNDO Publication; 2008. pp. 131-150.
18. Chandra S, Khan S, Avula B, Lata H, Yang MH, El-Sohly MA, *et al*. Assessment of total phenolic and flavonoid content, antioxidant properties, and yield of aeroponically and conventionally grown leafy vegetables and fruit crops: a comparative study. Evid Based Complement Alternat Med. 2014; 2014:1-10.
DOI: 10.1155/2014/253875.
19. Kalra P, Sharma S, Suman, Kumar S. Antiulcer effect of the methanolic extract of *Tamarindus indica* seeds in different experimental models. J Pharm Bioallied Sci. 2011;3(2):236-241.
DOI: 10.4103/0975-7406.80778.
20. Kumutarin T, Azadi S, Butterworth L, Keil D, Chitsomboon B, Suttajit M, *et al*. Extract of the seed coat of *Tamarindus indica* inhibits nitric oxide production by murine macrophages *in-vitro* and *in-vivo*. Food Chem Toxicol. 2004;42(4):649-658.
DOI: 10.1016/j.fct.2003.12.001.
21. Minaiyan M, Ghannadi A, Mahzouni P, Nabi-Meibodi M. Anti-ulcerogenic effect of ginger (rhizome of *Zingiber officinale* Roscoe) hydroalcoholic extract on acetic acid-induced acute colitis in rats. Res Pharm Sci. 2008;3(2):79-86.
22. Niknami E, Sajjadi SE, Talebi A, Minaiyan M. Protective effect of *Vitis vinifera* (black grape) seed extract and oil on acetic acid-induced colitis in rats. Int J Prev Med. 2020;11:102,1-7.
DOI: 10.4103/ijpvm.IJPVM_362_19.
23. Dieleman LA, Palmen MJ, Akol H, Bloemena E, Pena AS, Meuwissen SG, *et al*. Chronic experimental colitis induced by dextran sulfate sodium (DSS) is characterized by Th1 and Th2 cytokines. Clin Exp Immunol. 1998;114(3):385-391.
DOI: 10.1046/j.1365-2249.1998.00728.x.
24. Motavallian-Naeini A, Minaiyan M, Rabbani M, Mahzuni P. Anti-inflammatory effect of ondansetron through 5-HT3 receptors on TNBS-induced colitis in rat. EXCLI J. 2012;11:30-44.
PMCID: PMC4919924.
25. Mahdavi NS, Talebi A, Minaiyan M. Ameliorative effect of galantamine on acetic acid induced colitis in rats. Res Pharm Sci. 2019;14(5):391-399.
DOI: 10.4103/1735-5362.268199.
26. Khoramian L, Sajjadi SE, Minaiyan M. Anti-inflammatory effect of *Adiantum capillus-veneris* hydroalcoholic and aqueous extracts on acetic acid-induced colitis in rats. Avicenna J Phytomed. 2020;10(5):492-503.
PMCID: PMC7508316.
27. Tahan G, Aytac E, Aytekin H, Gunduz F, Dogusoy G, Aydin S, *et al*. Vitamin E has a dual effect of anti-inflammatory and antioxidant activities in acetic acid-induced ulcerative colitis in rats. Can J Surg. 2011;54(5):333-338.
DOI: 10.1503/cjs.013610.
28. Owusu G, Obiri DD, Ainooson GK, Osafo N, Antwi AO, Duduyemi BM, *et al*. Acetic acid-induced ulcerative colitis in Sprague Dawley rats is suppressed by hydroethanolic extract of *Cordia vignei* leaves through reduced serum levels of TNF-α and IL-6. Int J Chronic Dis. 2020;8785497:1-11.
DOI: 10.1155/2020/8785497.
29. Keyvanara AH, Yegdaneh A, Talebi A, Minaiyan M. Evaluating anti-inflammatory effect of hydroalcoholic extracts of *Citrus medica L*. pulp and peel on rat model of acute colitis. Res J Pharmacognosy. 2023:10(2):29-38.
DOI: 10.22127/RJP.2023.377466.2027.
30. Minaiyan M. Sajjadi SE, Naderi N, Taheri D. Anti-inflammatory effect of *Kelussia odoratissima* Mozaff. hydroalcoholic extract on acetic acid-induced acute colitis in rats. J Reports Pharm Sci. 2014;3(1):28-35.
31. Frankel EN, Meyer AS. The problems of using one-dimensional methods to evaluate multifunctional food and biological antioxidants. J Sci Food Agr. 2000;80(13):1925-1941.
DOI: 10.1002/1097-0010(200010)80:13<1925::AID-JSFA714>3.0.CO;2-4.
32. Yamada Y, Marshall S, Specian RD, Grisham MB. A comparative analysis of two model of colitis in rats. Gastroentrology. 1992;102(5):1524-1534.
DOI: 10.1016/0016-5085(92)91710-l.
33. Naini MA, Zargari-Samadnejad A, Mehrvarz S, Tanideh R, Ghorbani M, Dehghanian A, *et al*.

Anti-inflammatory, antioxidant, and healing-promoting effects of *Aloe vera* extract in the experimental colitis in rats. Evid Based Complement Alternat Med. 2021;2021.
DOI: 10.1155/2021/9945244.

34. Karaoglan ES, Bayir Y, Albayrak A, Toktay E, Ozgen U, Kazaz C, *et al*. Isolation of major compounds and gastroprotective activity of *Alchemilla caucasica* on indomethacin induced gastric ulcers in rats. Eurasian J Med. 2020;52(3):249-253.
DOI: 10.5152/eurasianjmed.2020.19243.
35. Sadraei H, Asghari G, Khanabadi M, Minaiyan M. Anti inflammatory effect of apigenin and hydroalcoholic extract of *Dracocephalum kotschyi* on acetic acid induced colitis in rats. Res Pharm Sci. 2017;12(4):322-329.
DOI: 10.4103/1735-5362.212050.
36. Kim JW, Kim CY, Kim JH, Jeong JS, Lim JO, Ko JW, *et al*. Prophylactic catechin-rich green tea extract treatment ameliorates pathogenic enterotoxic *Escherichia coli*-induced colitis. Pathogens. 2021;10(12):1573,1-12.
DOI: 10.3390/pathogens10121573.
37. Dangles O. Antioxidant activity of plant phenols: chemical mechanisms and biological significance. Curr Organ Chem. 2012;16(6):692-714.
DOI: 10.2174/138527212799957995.
38. Roja L, Jahan N, Wesley J. Antiulcerogenic activity of alcoholic extract of the leaves of *Tamarindus indica L*. on experimental ulcer models. Pharmacologyonline. 2008;3:85-92.
39. Periasamy S, Lin CH, Nagarajan B, Sankaranarayanan NV, Desai UR, Liu MY. Mucoadhesive role of tamarind xyloglucan on inflammation attenuates ulcerative colitis. J Funct Foods. 2018;47:1-10.
DOI: 10.1016/j.jff.2018.05.035.
40. O'Leary KA, de Pascual-Tereasa S, Needs PW, Bao YP, O'Brien NM, Williamson G. Effect of flavonoids and vitamin E on cyclooxygenase-2 (COX-2) transcription. Mutat Res. 2004;551(1-2):245-254.
DOI: 10.1016/j.mrfmmm.2004.01.015.
41. Gupta M, Mishra V, Gulati M, Kapoor B, Kaur A, Gupta R, *et al*. Natural compounds as safe therapeutic options for ulcerative colitis. Inflammopharmacol. 2022;30(2):397-434.
DOI: 10.1007/s10787-022-00931-1.

ONLINE SUBMISSION

https://review.jow.medknow.com/rps

Research in Pharmaceutical Sciences, June 2024; 19(3): 287-302
Received: 22-08-2023
Peer Reviewed: 20-09-2023
Revised: 14-10-2023
Accepted: 13-11-2023
Published: 01-07-2024

School of Pharmacy & Pharmaceutical Sciences
Isfahan University of Medical Sciences

Original Article

A bioinformatics approach of specificity protein transcription factors in head and neck squamous cell carcinoma

Adel Rezvani Sichani[1], Ziba Rezvani Sichani[2], Behnaz Yazdani[3], Mehdi Azizmohammad Looha[4], and Hajar Sirous[5,*]

[1]Department of Food Science and Technology, Shahreza Branch, Islamic Azad University, Shahreza. I.R. Iran.
[2]Department of Biochemistry, Islamic Azad University, Falavarjan Branch, I.R. Iran.
[3]Bioscience Department, Faculty of Science and Technology (FCT), Universitat de Vic—Universitat Central de Catalunya (Uvic-UCC), 08500 Vic, Spain.
[4]Basic and Molecular Epidemiology of Gastrointestinal Disorders Research Center, Research Institute for Gastroenterology and Liver Diseases, Shahid Beheshti University of Medical Sciences, Tehran, Iran.
[5]Bioinformatics Research Center, School of Pharmacy and Pharmaceutical Sciences, Isfahan University of Medical Sciences, Isfahan, I.R. Iran.

Abstract

Background and purpose: The seventh most common type of cancer with increasing diagnosis rates around the world is head and neck squamous cell carcinoma (HNSCC). Specificity proteins (SPs) have been known for their role in the regulation of cellular division, growth, and apoptotic pathways in various cancers. In this work, we analyzed the expression levels of SPs in HNSCC to assess their diagnostic and prognostic biomarker potential.
Experimental approach: Differential gene expression and correlation analysis methods were used to determine the top dysregulated genes in HNSCC. Functional enrichment and protein-protein interaction analyses were done with the DAVID database and Cytoscape software to understand their function and biological processes. Receiver operating test, logistic regression, and Cox regression analyses were performed to check SP genes' diagnostic and prognostic potential.
Findings/Results: SP1 (LogFC = -0.27, P = 0.0013) and SP2 (LogFC = -0.20, P = 0.0019) genes were upregulated in HNSCC samples, while SP8 (LogFC = 2.57, $P < 0.001$) and SP9 (LogFC = 2.57, $P < 0.001$) genes were downregulated in cancer samples. A moderate positive correlation was observed among the expression levels of SP1, SP2, and SP3 genes. The SP8 and SP9 genes with AUC values of 0.79 and 0.75 demonstrated diagnostic potential which increased to 0.84 when both genes were assessed by logistic regression test. Also, the SP1 gene held a marginally significant prognostic potential.
Conclusion and implications: Our findings clarify the potential of SP transcription factors as candidate diagnostic and prognostic biomarkers for early screening and treatment of HNSCC.

Keywords: Head and neck squamous cell carcinoma; Specificity protein; SP1; TCGA.

INTRODUCTION

Head and neck cancers are a type of malignancy the cellular origin of most of them lies in the mucosal epithelium layer of the larynx, pharynx, and oral cavity. Around 900,000 new cases are diagnosed each year with this type of cancer, but a great percentage of them face short survival periods (1,2). The high diagnosis rates of head and neck cancers have made this cancer known as the seventh most common form of cancer worldwide (1). The incidence of head and neck cancers has been predicted to elevate up to 30% each year by 2030 (3). There is an increasing need for the identification of biomarkers in the prediction of head and neck squamous cell carcinoma (HNSCC) that could help with better diagnosis and prediction of survival period in patients.

*Corresponding author: H. Sirous
Tel: +98-3137927065, Fax: +98-3136680011
Email: h_sirous@pharm.mui.ac.ir

Access this article online	
	Website: http://rps.mui.ac.ir
	DOI: 10.4103/RPS.RPS_171_23

The genes coding specificity proteins (SP) are transcription factors (TFs) holding a common zinc-binding domain that aids with DNA-binding and the regulation of genes that participate in specific cellular pathways including cell cycle regulation and cellular differentiation (4). SP transcription factors consist of several members and their altered expression level has been associated with the regulator pathways involved in varying biological processes of cancer cells (5). SP TFs have a high binding affinity for GC/GT-rich sequences within the promoter regions of genes. Multiple studies have linked multiple correlations between cellular growth and the metastatic potential of SP TFs in a variety of cancer cells, while their function and expression profile in HNSCC are poorly investigated.

SP factors have been noticed to play a notable role in the regulation of cellular division, growth, and induction of anti-apoptotic signals (6). However, it appears that the tumor suppressor or oncogenic activities of these factors vary across different types of cancer types (7). Most of the previous investigations on SPs have been focused on the molecular functions of SP1 and SP3 genes more than the other members of the SP transcription family. This gap in knowledge about SPs could be due to the higher DNA-binding affinity of these factors with GC-rich promoter regions (8). The regulatory function of SPs in expression levels of pro-apoptotic or anti-apoptotic genes has made these factors an ideal target for the design of new therapeutic opportunities for the treatment of cancers (9). Due to the lack of enough information about the molecular function and expression patterns of SPs in HNSCC, more investigations should be carried out before using these genes as biomarkers in clinical trials.

In the current research, we aimed to investigate the expression patterns of 9 different members of SP TFs in the expression matrix of HNSCC with the use of comprehensive bioinformatic tools. We suggested ideal biomarkers with notable prognostic and diagnostic capability that could serve better approaches in early screening and prediction of survival period with patients with different expression profiles of SPs in HNSCC.

METHODS AND MATERIAL

Data processing and gene expression analysis

The Cancer Genome Atlas (TCGA) program is a highly practical online dataset (Available at the Cancer Genome Atlas Program (TCGA) - NCI) that allows free access usage of RNA-seq count data of more than 13 different types of cancers with normal adjacent tissue samples under the principles organized in the declaration of Helsinki statements. The genome expression matrix of 502 HNSC cancer samples along with 44 normal tissue samples in the format of count data was downloaded and normalized with the help of TCGAbiolinks, Limma, and edgeR packages (Fig. 1).

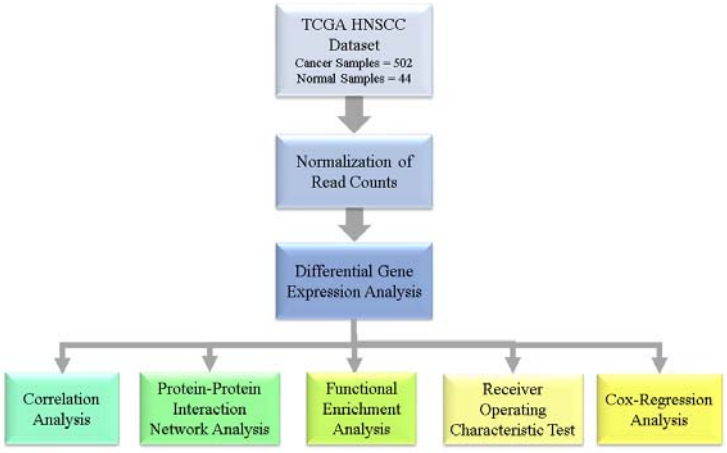

Fig. 1. The flowchart of the study.

The clinical information of the patients has been summarized in Table S1. The count data was converted into a log2 ratio after normalization by the Voom package. The differentially expressed genes (DEGs) were calculated and reordered based on adjusted *P*-values and the top 100 DEGs with the smallest adjusted *P*-values were selected genes in HNSCC samples concerning normal tissue samples for further analysis and *P*-values smaller or equal to 0.01 were considered as statistically significant (10-14).

Correlation analysis

To better understand the interaction and molecular relationships between the SP TFs and the top DEGs in HNSCC, correlation analysis can be used as a useful method to explore this relationship. Accordingly, correlation analysis was performed using the normalized expression data of the SP TFs and top 10 DEGs in HNSCC samples. The metan package in R programming was used for this analysis and the Pearson statistical method was selected for the estimation of *P*-values and correlation coefficient values.

Functional enrichment analysis

To better understand the important biological pathways that are involved in the progression and development of HNSCC, functional enrichment analysis was performed with the help of the DAVID database (version 6.8, available at https://david-d.ncifcrf.gov/), which is an online platform that gives free access opportunities to practical functions and algorithms that can estimate the enrichment of genes in different biological pathways and predict their cellular function and localization. One of the practical analyses that can be done using the DAVID database, is the gene ontology (GO) analysis that was used for the top 200 DEGs in HNSCC to achieve a better perspective of their functions and associated biological pathways (15-17).

Protein-protein interaction analysis

Protein-protein interaction (PPI) network analysis is a practical method that aids with the understanding of the interaction and interplay of a large number of genes that are significantly dysregulated and the function of a majority of them is still unexplored. For this analysis, the STRING online platform (version 10, available at http://www.string.db.org) (18,19) was used from Cytoscape software (version: 3.2.0, available at http://www.cytoscape.org/) (20,21). The PPI network was constructed in Cytoscape using the list of SP TFs with the top 100 DEGs in HNSCC and was analyzed with the CytoNCA tool (available at https://apps.cytoscape.org/apps/cytonca) (22) in Cytoscape software.

Receiver operating characteristic test

A practical statistical method for estimation of the diagnostic potential of genes based on their expression levels in two defined phenotypes of interest is the receiver operating characteristic (ROC) test which can be easily accessed using the GraphPad Prism software (version 9.1.0). Through this analysis, ROC plots are generated based on the sensitivity and specificity of the data, respectively (23). With the help of this method, the diagnostic potential of SP transcription factors in HNSC and normal groups was calculated and ROC plots were generated. To test the potential of the combination of SP genes with moderate AUC values in the diagnosis of HNSCC, the logistic regression statistical test was applied using the R software (version 4.3.1) and *P*-values ≤ 0.05 were considered statistically significant.

Cox-regression analysis

OncoLnc is a highly practical online database (available at http://www.oncolnc.org/) (24) that utilizes specific statistical methods for the estimation of the survival period based on the expression data from the TCGA database. To explore the association between the expression levels of SP genes in HNSCC with the time of survival in patients, the OncoLnc database was used which utilizes the Cox-regression statistical method for survival analysis concerning the clinical data of the patients. It also uses the samples with expression values according to the upper quartile or lower quartile criteria and reports Logrank *P*-values as well, which is a hypothesis test that compares the difference in the survival distributions and Logrank *P*-values smaller than 0.01 would be considered statistically significant (25).

RESULTS

Expression analysis of SP TFs in HNSCC

The gene expression analysis of HNSC cancer samples about normal samples was performed and the top 100 genes with the most statistically significant adjusted *P*-values were identified and reported in Table S2. Differential gene expression analysis of SP TFs in HNSC cancer demonstrated an uneven pattern between the expression levels of these genes, indicating that the expression level of each SP factor contributes differently to the progression of HNSCC. As demonstrated in Fig. 2, among all 9 members of the SP transcription family, SP1 ($P = 0.002$) and SP2 ($P = 0.01$) showed notable decreased expression levels in HNSCC tissue samples, while SP8 ($P < 0.0001$) and SP9 ($P < 0.0001$) genes revealed very significant increased expression levels in HNSCC samples and their high expression ratio might be associated with the biological pathways in HNSCC. The expression levels of SP3 ($P = 0.02$), and SP7 ($P = 0.03$) genes were also notably higher in cancer samples, while the expression levels of SP4 ($P = 0.98$), SP5 ($P = 0.07$), and SP6 ($P = 0.21$) were not statistically significantly different between HNSCC cancer and normal samples.

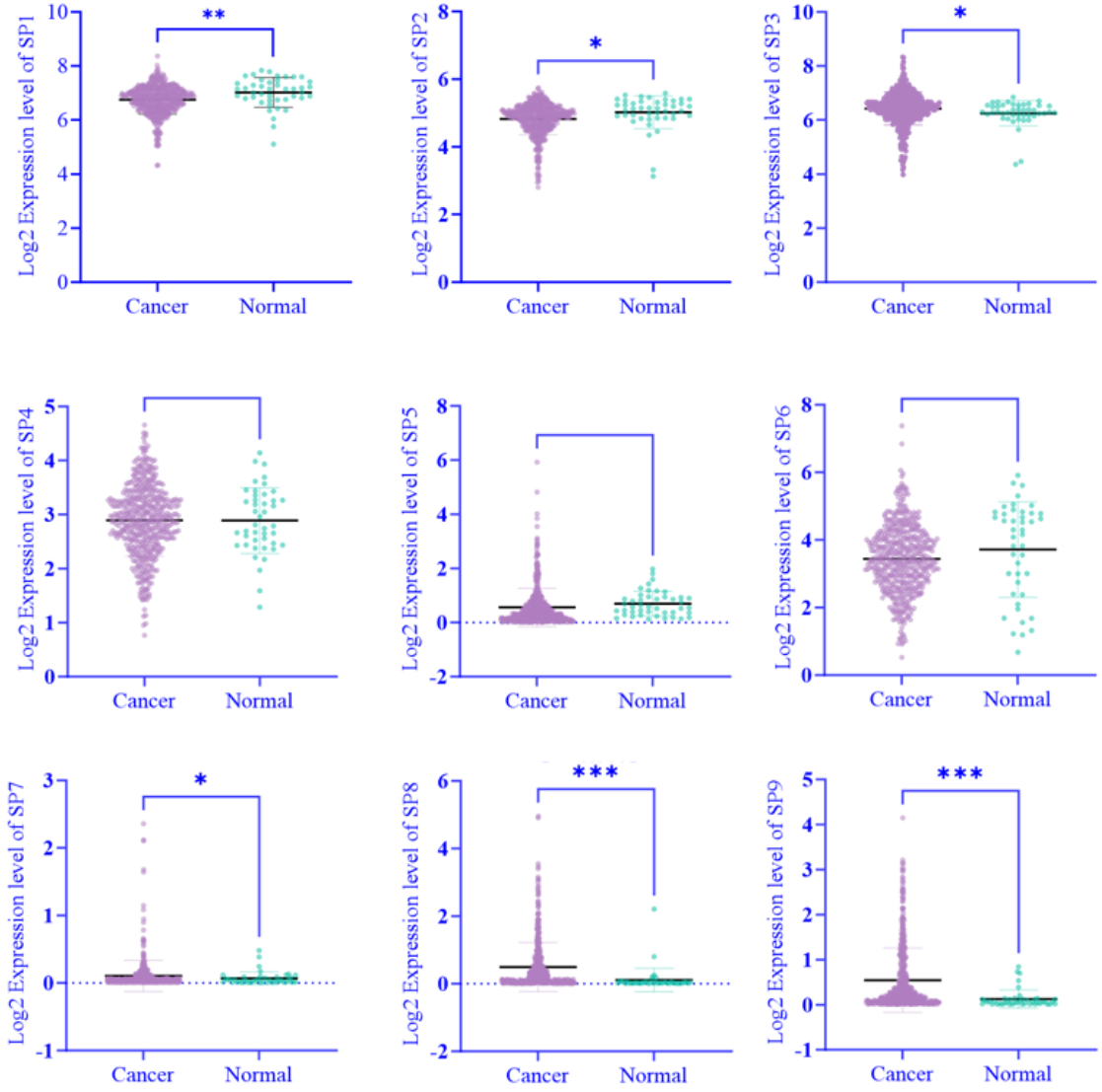

Fig. 2. Differential gene expression analysis of SP transcription factors in HNSCC. The RNA-seq count data of TCGA HNSC cancer and normal tissue samples were normalized and analyzed to identify the top differentially expressed genes. *$P \leq 0.05$, **$P \leq 0.01$, and ***$P \leq 0.001$ indicate statistically significant differences between groups. SP, Specificity protein; HNSCC, head and neck squamous cell carcinoma.

Correlation analysis between top DEGs and expression levels of SP genes

A practical method for the prediction of possible interactions at a molecular level is correlation analysis. This technique was applied using the normalized expression data of SP genes and the top 10 DEGs in HNSCC. As shown in Fig. 3, there was a moderate positive correlation between SP1 with SP3 (correlation coefficient = 0.63, $P \leq 0.001$), and SP1 with SP2 (correlation coefficient = 0.66, $P \leq 0.001$) gene. From the top 10 DEGs in HNSCC, the expression level of the ADIPOQ gene also had a significant positive correlation with the PLIN1 gene (correlation coefficient = 0.94, $P \leq 0.001$).

GO analysis of top DEGs

As depicted in Fig.4, most of the genes were predicted by the GO tool of the DAVID database to be involved in cell division (GO: 00051301) and mitotic cell cycle (GO: 0000278). The molecular function of a majority of the DEGs in HNSCC was associated with protein binding (GO: 0005515), DNA binding (GO: 0003677), and ATP binding (GO: 0005524). The majority of these genes were also estimated to localize in the cytosol (GO: 0005829) and the nucleus (GO: 0005634). The KEGG database also predicted that a large count of the DEGs were involved in the cell cycle (hsa04110) and peroxisome proliferator-activated receptors signaling pathway (hsa03320).

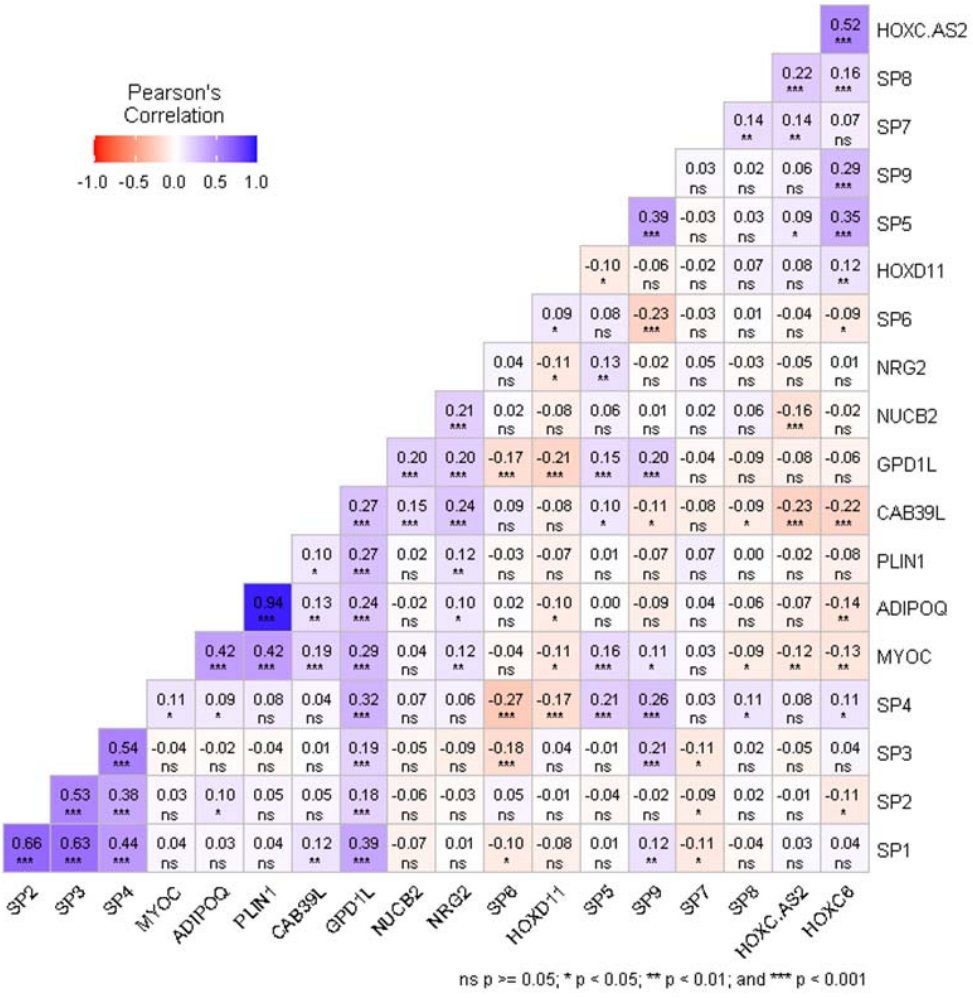

Fig. 3. Correlation analysis between SP transcription factors and top DEGs in HNSCC. The correlation analysis was performed using the Pearson method between the normalized expression levels of SP genes and the top 10 DEGs in the HNSCC. SP, Specificity protein; HNSCC, head and neck squamous cell carcinoma; DEGs, differentially expressed genes.

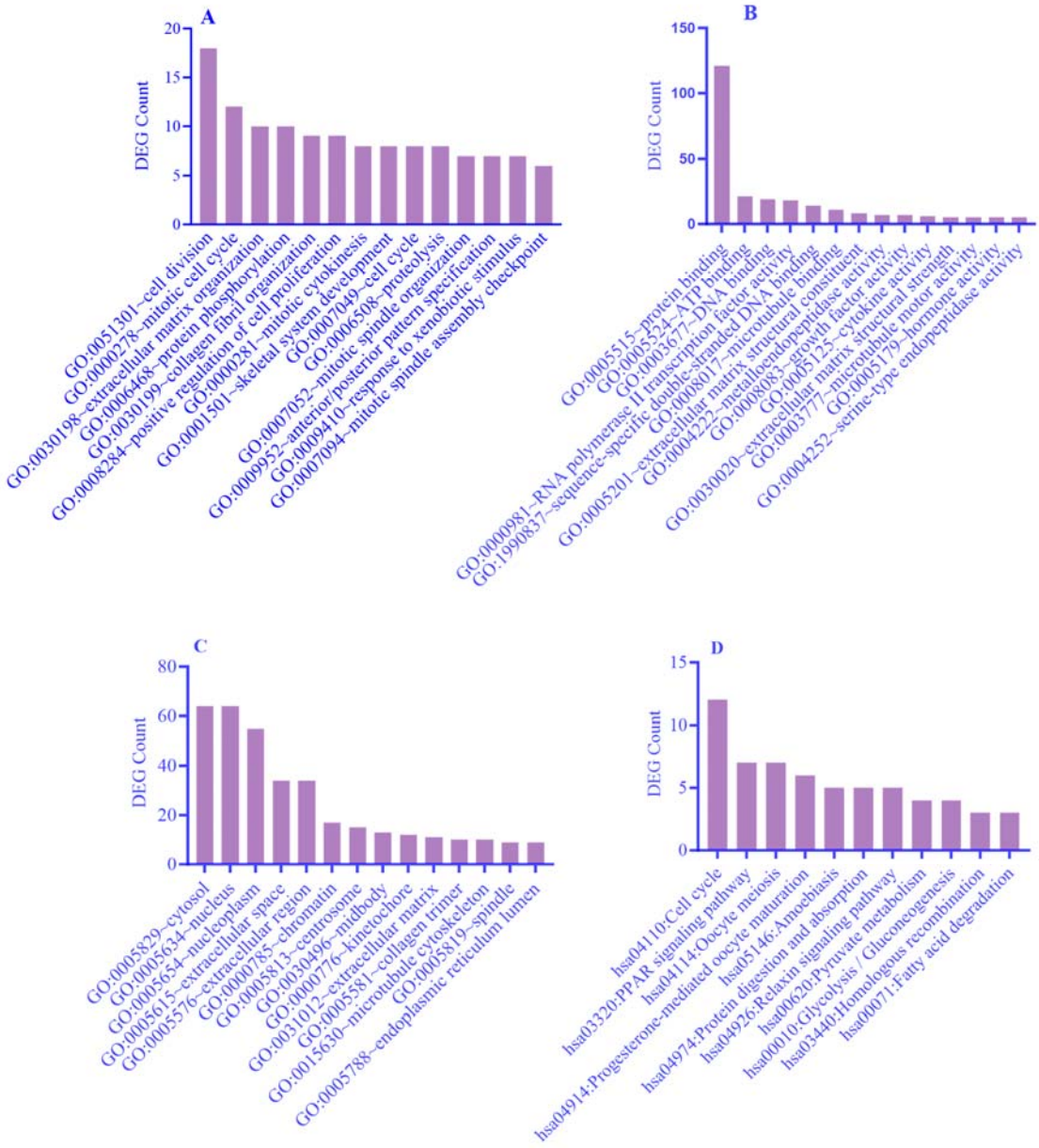

Fig. 4. GO and KEGG pathway analysis of top DEGs in HNSCC. (A) Functional enrichment analysis of top DEGs in the HNSC cancer showed that most of the dysregulated genes were involved in biological pathways such as cell division; (B) molecular functions of most DEGs were associated with protein binding and ATP binding; (C) most of the DEGs were predicted to be localized mostly in the cytosol or nucleus regions; (D) the KEGG pathway also predicted that most of the genes were involved in the regulation of cellular division. GO, Gene Ontology; DEG, differentially expressed gene; HNSCC, head and neck squamous cell carcinoma.

PPI network analysis

HNSCC is a poorly investigated cancer in which the function of the majority of the high DEGs is still under investigation. Therefore, to gain a better insight into the biological processes and molecular interplay between the genes in HNSCC, a PPI network was constructed in Cytoscape and the hub genes in the network were employed with the CytoNCA tool that allows easier measurement of cluster coefficient and node degree in a set of gene list converted into an interactive network. The threshold for the PPI score was set to 0.4, which resulted in the calculation of the

medium-confidence network generated in Cytoscape software. The CytoNCA tool can help with the estimation of the topological parameters of the PPI network and its calculations were performed by excluding the weight, so it can better predict and identify the highly interacting proteins in the network.

The interconnectivity between the DEGs in HNSCC has been shown in Fig. 5, in which each gene in the network has been grouped with other genes that are involved in similar biological processes that were previously predicted using the DAVID database. As it can be understood from the network, intense connectivity exists between the gene sets from the mitotic cell cycle, cell division, centrosome complex assembly, microtubule-based movement, and regulation of cell cycle pathways. The SP1, SP2, and SP7 genes were predicted to interact with genes from the cell division pathway and the SP1 gene also interacted with genes in the regulation of the cell cycle pathway. The top genes with degree scores above 46 from the network topology analysis results by the CytoNCA tool have been summarized in Table 1, in which between the top 19 genes with highest degree, subgraph, betweenness, and closeness scores, the Forkhead box M1, aurora A kinase, RAD51 recombinase, MYB proto-oncogene like 2, baculoviral IAP repeat containing 5, and kinesin family member 14 genes had the highest node degree scores within the PPI network. The Forkhead box M1, aurora A kinase, RAD51 recombinase, and kinesin family member 14 genes had the highest betweenness and closeness scores, which indicates the quicker reach and higher control of these genes to other nodes in the PPI network.

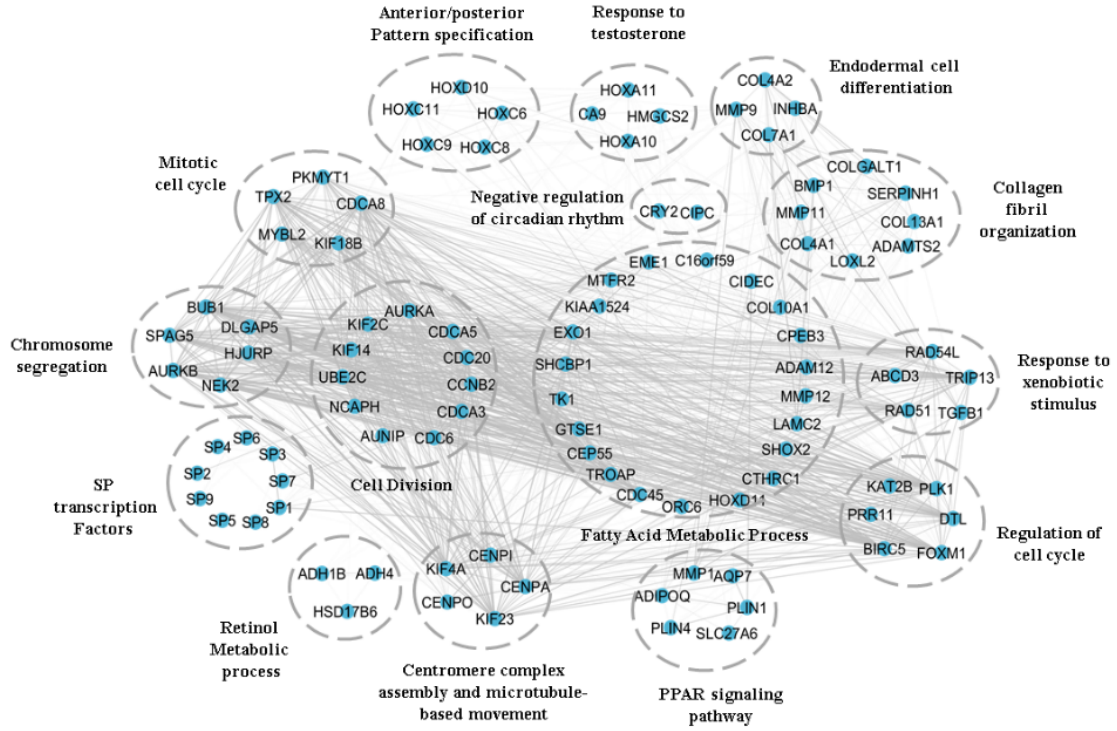

Fig. 5. Protein-protein interaction network of top DEGs in head and neck squamous cell carcinoma. Network analysis of the top DEGs with the help of the STRING database and CytoNCA plugin in the Cytoscape software revealed a notable connection among important cellular pathways that most of the genes were predicted previously by GO analysis to be enriched and involved in. SP factors also showed to interact with other proteins and pathways shown in the network. GO, Gene Ontology; DEG, differentially expressed gene; SP, specificity protein.

Table 1. Top 19 genes from the top 200 differentially expressed genes in head and neck squamous cell carcinoma cancer with the highest degrees in protein-protein interaction network analyzed by CYTOCNA application in Cytoscape.

Ensemble protein ID	Gene ID	Description	Degree	Betweenness	Closeness
ENSP00000342307	FOXM1	Forkhead box M1	53	840.25543	0.2820513
ENSP00000216911	AURKA	Aurora kinase A	51	403.89383	0.27576602
ENSP00000372088	RAD51	RAD51 recombinase	51	420.04904	0.27423823
ENSP00000217026	MYBL2	MYB proto-oncogene like 2	51	270.12604	0.27348065
ENSP00000301633	BIRC5	Baculoviral IAP repeat containing 5	50	362.1902	0.27348065
ENSP00000356319	KIF14	Kinesin family member 14	50	224.12881	0.27272728
ENSP00000300403	TPX2	TPX2 microtubule nucleation factor	49	258.1087	0.27272728
ENSP00000336868	CENPA	Centromere protein A	48	132.00188	0.27123287
ENSP00000405726	CDC45	Cell division cycle 45	48	90.10279	0.26902175
ENSP00000300093	PLK1	Polo-like kinase 1	48	60.806026	0.2682927
ENSP00000361540	CDC20	Cell division cycle 20	47	200.96227	0.26756757
ENSP00000313950	AURKB	Aurora kinase B	47	63.645523	0.26612905
ENSP00000302530	BUB1	BUB1 mitotic checkpoint	47	66.95278	0.26190478
ENSP00000363524	KIF4A	Kinesin family member 4A	47	15.906779	0.26121372
ENSP00000362146	CDCA8	Cell division cycle associated 8	47	15.906779	0.26121372
ENSP00000260363	KIF23	Kinesin family member 23	47	15.906779	0.26121372
ENSP00000275517	CDCA5	Cell division cycle associated 5	47	70.41854	0.26121372
ENSP00000355506	EXO1	Exonuclease 1	47	49.754776	0.26121372
ENSP00000288207	CCNB2	Cyclin B2	47	110.61793	0.26052633

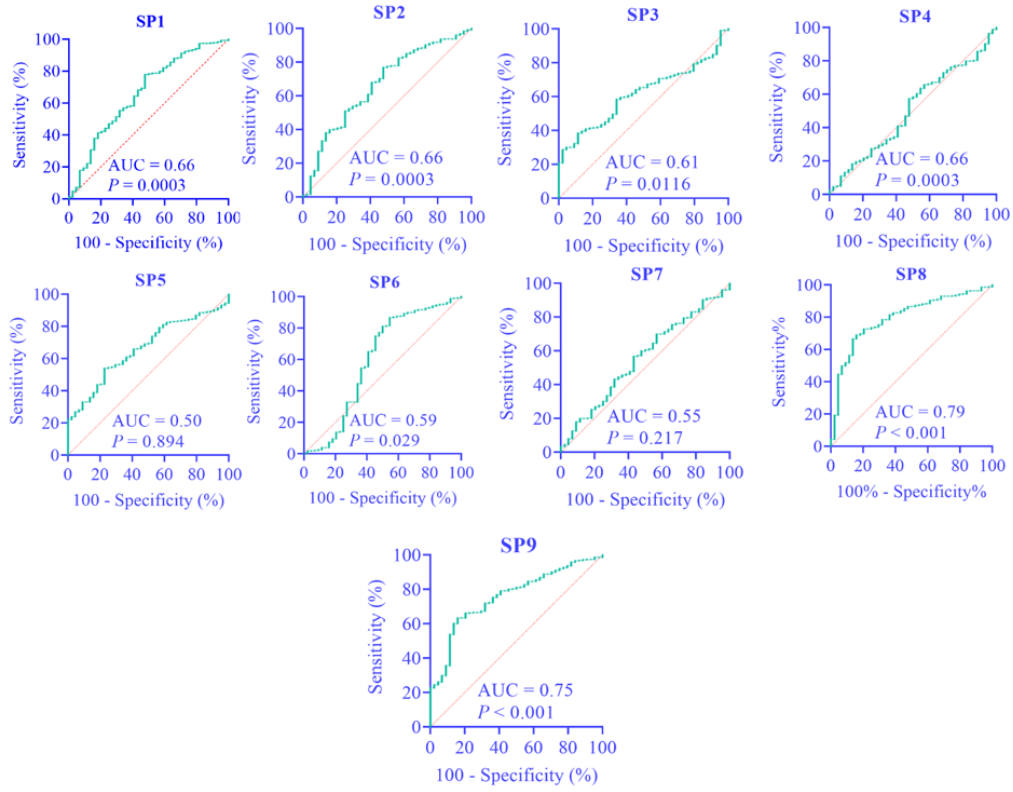

Fig. 6. Receiver operating characteristic test of SP transcription factors in HNSCC. The receiver operating characteristic test was used to assess and clarify the potential of SP transcription factors as diagnostic biomarkers in HNSCC and the results revealed that only SP8 and SP9 genes could hold a diagnostic potential for HNSCC. Logistic regression analysis was performed for the prediction of the diagnostic power of the combination of SP8 and SP9 genes in HNSCC. The AUC values below 0.70 were considered weak diagnostic capability and $P \leq 0.01$ are considered statistically significant. SP, Specificity protein; HNSCC, head and neck squamous cell carcinoma; AUC, the area under the curve.

Diagnostic potential of SP genes in HNSCC

The diagnostic capability of SP transcription factors was assessed using GraphPad Prism software based on the normalized expression matrix of HNSCC and normal samples. As demonstrated in Fig. 6, two genes revealed significant diagnostic potential including the SP8 and SP9 genes compared to the rest of the members of the SP TF family, whose AUC values did not meet the satisfactory statistical criteria. While the diagnostic potential of SP genes in HNSCC was not statistically significant, SP8 and SP9 genes demonstrated better diagnostic capability compared to the other SP genes. The analysis of the logistic regression test for estimation of diagnostic capability for the combination of SP8 and SP9 genes predicted an AUC value of 0.84, which indicates better diagnostic potential of these two genes together in the HNSCC.

Analysis of prognostic biomarker capability of SP genes

Based on the Cox-regression analysis results presented in Fig. 7, only SP1 (Logrank $P = 0.05$) and SP5 (Logrank $P = 0.01$) genes demonstrated marginally significant statistical prognostic potential compared to the rest of the SP members, while the prognostic potential of other SP genes in HNSCC was statistically poor and not significant. Also, it can be seen that SP1 and SP5 expression levels correlated with better survival periods in HNSCC patients. It should be mentioned that the OncoLnc database did not provide any Cox-regression results over the SP7 gene as the expression level of SP7 did not meet the expression cutoff demanded for this analysis. Overall, SP1 and SP5 transcription factors revealed better prognostic potential compared to other SP genes in HNSCC.

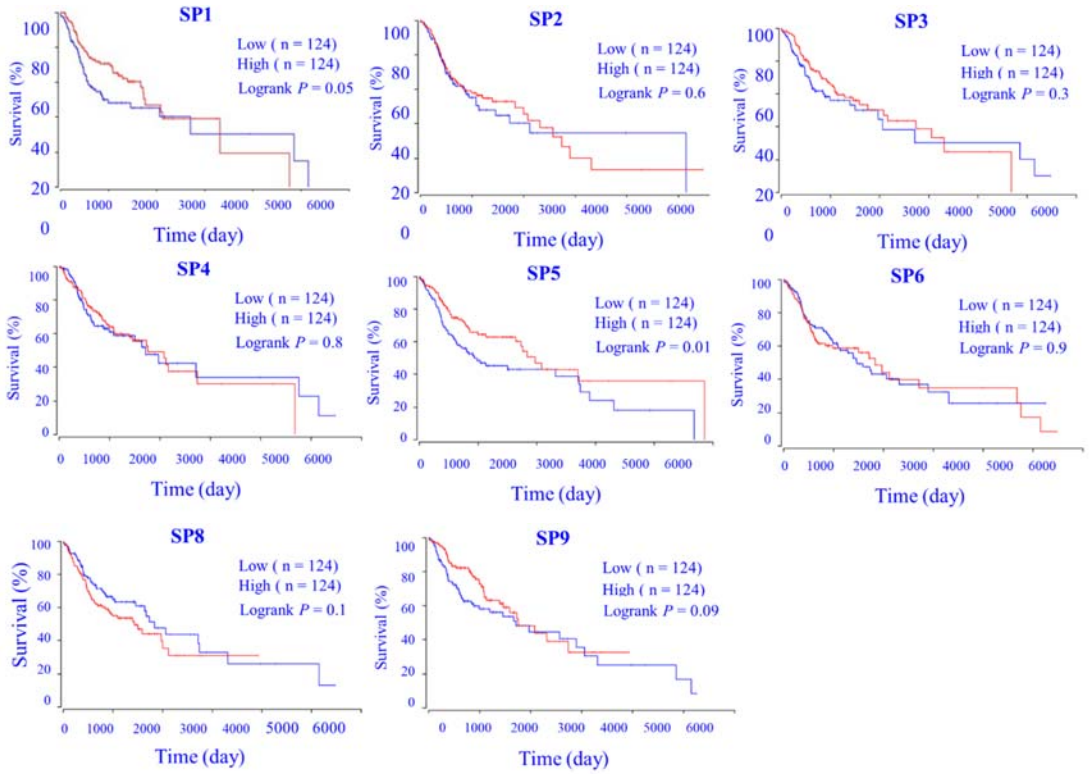

Fig. 7. Cox-regression analysis of SP transcription factors in HNSCC. Survival analysis was performed with the help of the Cox-regression analysis tool provided by the OncoLnc database, which utilized the mRNA expression data from the TCGA database along with the clinical data of the patients. The OncoLnc database calculates the Cox-regression analysis for interest genes using the samples with expression values above the upper quartile ('high' group) and lower quartile ('low' group). This test was done to check the prognostic potential of SP transcription factors in HNSCC, and only SP1 and SP5 genes revealed better prognostic potential compared to other members of the SP family. However, the prognostic values of SP genes were statistically not significant in the HNSCC. The last graph shows the result of the Logistic regression test performed on the combination of SP8 and SP9 genes for the prediction of their diagnostic potential in HNSCC. The Logrank $P \leq 0.01$ was considered statistically significant. SP, Specificity protein; HNSCC, head and neck squamous cell carcinoma; AUC, the area under the curve.

DISCUSSION

One of the common malignancies that affect the head and neck regions of the human body is the HNSCC. The unstable genomic nature and the high metastatic potential of this cancer have increased the need for further investigations on more specific molecular therapies and the identification of better biomarkers for early detection and prevention in HNSCC patients (9,26).

TFs are important and attractive molecular targets for the design of specific therapeutic approaches for the treatment of different types of cancer in humans (27,28). Previous studies that analyzed the expression spectrum of HNSCC identified varying common mutations in the genomic regions of proteins in about 30% of the patients with HNSCC. Specific genes such as tumor protein p63, cyclin-dependent kinase inhibitor A2, and phosphatase and tensin homolog genes were found to be mutated in HNSCC, but their tumor suppressor or oncogenic activities were reported to vary among different types of cancers (29,30).

SPs are a class of TFs with DNA-binding activity and multiple cellular functions that help with the maintenance of cellular homeostasis such as regulation of cellular division, apoptotic pathway, and metastasis that have been reported previously by multiple investigations on different cancers. Multiple members of SP TFs such as SP1, SP3, and SP4 genes have been reported to regulate important pathways that involve cellular growth, division, survival, and inflammatory pathways of different types of cancer cells. The SP1 gene has been reported as a pro-oncogenic factor due to its role in the regulation of survival and metastasis of cancer cells and has been suggested as a molecular target for the design of new anticancer drugs and chemotherapies(31,32).

In this study, we performed genome expression analysis using RNA-seq count data of HNSCC samples from the TCGA database and clarified the expression pattern of 9 members of the SP TF family. The Differential gene expression analysis revealed a notable decrease in the expression levels of SP1 and SP2 genes along with a significant increase in the expression levels of SP8 and SP9 genes in HNSCC samples. This indicates that each SP gene has a unique role and expression pattern in the HNSCC. Previous studies have investigated on SP1 gene far more than the other SP members in multiple types of human cancer cell lines, such as pancreatic ductal adenocarcinoma, colorectal cancer, and glioma cancer (33-36).

Differential gene expression and correlation analysis results of the HNSCC expression matrix revealed that there is a moderate positive correlation among the expression levels of SP1, SP2, and SP3 genes. This indicates that a co-expression regulation mechanism might exist among these SP genes. There was also a notable positive correlation between the ADIPOQ gene with PLIN1 and SP4 genes. While the expression levels and biological roles of the ADIPOQ gene in HNSCC are poorly investigated, a study has reported an association between different genetic variants of this gene and with risk of breast cancer (37). Other studies also found an association between the human papillomavirus (HPV) with the risk of oropharyngeal squamous cancer cells and HNSCC (38-40).

To achieve a better vision of the common biological pathways in HNSCC, functional enrichment analysis was done and most of the DEGs were shown to participate in major biological pathways in cancer, such as cell division and mitotic cell cycle pathways. Also, their molecular functions were associated with DNA-binding, ATP-binding, and protein-binding activities and most of them were found to localize in the cytosol and nucleus regions of the cells. PPI network analysis revealed extensive connectivity between the genes that are predicted to be involved in the regulation of the cell cycle and the assembly of the chromosome complex. Genes such as SP1, SP2, and SP3 were shown to interact with pathways associated with cellular growth and division as well.

To clarify the diagnostic and prognostic capabilities of SP TFs in HNSCC, ROC test and Cox-regression survival analysis were used and we found that most of the SP genes have very weak diagnostic potential in HNSCC except for SP8 and SP9 genes, which demonstrated better sensitivity in the detection of cancer phenotype

from normal tissue samples. Also, the combination of SP8 and SP9 genes revealed a better diagnostic capability in the detection of HNSCC. The Cox-regression analysis also showed that only the SP1 gene showed a marginally significant potential for the prognosis of HNSCC and the estimation of survival period in patients with HNSCC. Previous studies have also noted that the SP1 gene can be a great prognostic biomarker in human gastric cancer (40-43).

Currently, there are no trials that have experimentally investigated the molecular role and expression patterns of all 9 SP genes in HNSCC, and our study has clarified their expression pattern along with their prognostic and diagnostic capabilities for the first time. A recent study reviewed the role of SP1, SP3, and SP4 genes in cancer, while the data on the role of other members of the SP TF family in HNSCC is poorly understood (44). Other studies had also used microarray and RNAseq data of head and neck cancer samples to investigate the expression dysregulation of TFs or microRNA-mRNA interactions of high DEGs in head and neck cancer samples, while in this study we analyzed the expression dysregulation and biomarker capability of 9 different SP TFs in the HNSC samples as their importance in the HNSC was still poorly understood (45-47). Some drugs were reported to be capable of decreasing the expression levels of the SP1 gene in cancer cells indirectly (32,43), such as anti-inflammatory and chemo-preventive agents (32). Further investigations are demanded to clarify the molecular functions and importance of the SP TF expression levels in the progression of HNSCC. These genes can have the potential to be used and investigated as diagnostic and prognostic biomarkers for the development of advanced and specific targeted therapies in HNSC cancer.

CONCLUSION

HNSCC is a type of cancer affecting the regions in the head and neck area and its origin site can be from the epithelium cells located in the oral cavity and pharynx regions. The increasing rates of HNSCC around the world have increased the need for the identification of practical biomarkers for early prediction of HNSCC. In this work, we analyzed the expression matrix of HNSCC tissue samples with adjacent control tissues and we found a significant dysregulation in the expression levels of SP1, SP2, SP8, and SP9 genes from the 9 members of specificity proteins. The correlation analysis results also revealed a positive correlation among the expression levels of SP1, SP2, and SP3 genes, which indicates the presence of a co-expression regulation interaction among these SP genes. A notable correlation was also estimated among SP4, ADIPOQ, and PLIN1 genes in HNSCC samples as well. We suggested that SP8 and SP9 genes can be potential diagnostic biomarkers while the SP1 gene can serve as prognostic biomarkers in faster detection of HNSCC and the survival period in patients with different expression levels of SP genes. Therefore, further experimental investigations are highly needed to examine and validate the real diagnostic and prognostic potential of the SP genes on HNSCC tissue samples.

Acknowledgments

The authors would like to thank the Bioinformatics Research Center at Isfahan University of Medical Sciences, Isfahan, I.R. Iran.

Conflict of interest statement

All authors declared no conflict of interest in this study.

Authors' contribution

The study design was performed by A. Rezvani Sichani, Z. Rezvani Sichani, B. Yazdani, and H. Sirous; data analysis was done by B. Yazdani and M.A. Looha; interpretations of the data and bioinformatics analysis were performed by B. Yazdani, A. Rezvani Sichani, Z. Rezvani Sichani, M.A. Looha, and H. Sirous; the manuscript was written by B. Yazdani, A. Rezvani Sichani, Z. Rezvani Sichani, M.A. Looha, and H. Sirous. The finalized article was read and approved by all authors.

REFERENCES

1. Johnson DE, Burtness B, Leemans CR, Lui VWY, Bauman JE, Grandis JR. Head and neck squamous cell carcinoma. Nat Rev Dis Primers. 2020;6(1): 92,1-49. DOI: 10.1038/s41572-020-00224-3.
2. Sung H, Ferlay J, Siegel RL, Laversanne M, Soerjomataram I, Jemal A, *et al*. Global cancer statistics 2020: GLOBOCAN estimates of incidence and mortality worldwide for 36 cancers in 185 countries. CA Cancer J Clin. 2021;71(3):209-249. DOI: 10.3322/caac.21660.
3. Gormley M, Creaney G, Schache A, Ingarfield K, Conway DI. Reviewing the epidemiology of head and neck cancer: definitions, trends and risk factors. Br Dent J. 2022;233(9):780-786. DOI: 10.1038/s41415-022-5166-x.
4. Safe S, Abdelrahim M. SP transcription factor family and its role in cancer. Eur J Cancer. 2005;41(16):2438-2448. DOI: 10.1016/j.ejca.2005.08.006.
5. Bouwman P, Philipsen S. Regulation of the activity of Sp1-related transcription factors. Mol Cell Endocrinol. 2002;195(1-2):27-38. DOI: 10.1016/s0303-7207(02)00221-6.
6. Black AR, Black JD, Azizkhan-Clifford J. Sp1 and krüppel-like factor family of transcription factors in cell growth regulation and cancer. J Cell Physiol. 2001;188(2):143-160. DOI: 10.1002/jcp.1111.
7. Beishline K, Azizkhan-Clifford J. Sp1 and the 'hallmarks of cancer'. FEBS J. 2015;282(2):224-258. DOI: 10.1111/febs.13148.
8. Liu Y, Zhong X, Li W, Brattain MG, Banerji SS. The role of Sp1 in the differential expression of transforming growth factor-β receptor type II in human breast adenocarcinoma MCF-7 cells. J Biol Chem. 2000;275(16):12231-12236. DOI: 10.1074/jbc.275.16.12231.
9. Marur S, Forastiere AA. Head and neck squamous cell carcinoma: update on epidemiology, diagnosis, and treatment. Mayo Clin Proc. 2016;91(3): 386-396. DOI: 10.1016/j.mayocp.2015.12.017.
10. Colaprico A, Silva TC, Olsen C, Garofano L, Cava C, Garolini D, *et al*. TCGAbiolinks: an R/bioconductor package for integrative analysis of TCGA data. Nucleic Acids Res. 2016;44(8):e71,1-11. DOI: 10.1093/nar/gkv1507.
11. Robinson MD, McCarthy DJ, Smyth GK. edgeR: a Bioconductor package for differential expression analysis of digital gene expression data. Bioinformatics. 2010;26(1):139-140. DOI: 10.1093/bioinformatics/btp616.
12. Subramanian A, Tamayo P, Mootha VK, Mukherjee S, Ebert BL, Gillette MA, *et al*. Gene set enrichment analysis: a knowledge-based approach for interpreting genome-wide expression profiles. Proc Natl Acad Sci USA. 2005;102(43):15545-15550. DOI: 10.1073/pnas.0506580102.
13. Yazdani B, Sirous H. Expression analysis of HIF-3α as a potent prognostic biomarker in various types of human cancers: a case of meta-analysis. Res Pharm Sci. 2022;17(5):508-526. DOI: 10.4103/1735-5362.355210.
14. Parsazad E, Esrafili F, Yazdani B, Ghafarzadeh S, Razmavar N, Sirous H. Integrative bioinformatics analysis of ACS enzymes as candidate prognostic and diagnostic biomarkers in colon adenocarcinoma. Res Pharm Sci. 2023;18(4):413-429. DOI: 10.4103/1735-5362.378088.
15. Harris MA, Clark J, Ireland A, Lomax L, Ashburner M, Foulger R, *et al*. The gene ontology (GO) database and informatics resource. Nucleic Acids Res. 2004;32:D258-D261. DOI: 10.1093/nar/gkh036.
16. Touzet H, Perriquet O. CARNAC: folding families of related RNAs. Nucleic Acids Res. 2004;32(suppl_2):W142-W145. DOI: 10.1093/nar/gkh415.
17. Huang DW, Sherman BT, Tan Q, Kir J, Liu D, Bryant D, *et al*. DAVID bioinformatics resources: expanded annotation database and novel algorithms to better extract biology from large gene lists. Nucleic Acids Res. 2007;35:W169-W175. DOI: 10.1093/nar/gkm415.
18. Mering Cv, Huynen M, Jaeggi D, Schmidt S, Bork P, Snel B. STRING: a database of predicted functional associations between proteins. Nucleic Acids Res. 2003;31(1):258-261. DOI: 10.1093/nar/gkg034.
19. Szklarczyk D, Gable AL, Nastou KC, Lyon D, Kirsch R, Pyysalo S, *et al*. The STRING database in 2021: customizable protein-protein networks, and functional characterization of user-uploaded gene/measurement sets. Nucleic Acids Res. 2021;49(D1):D605-D612. DOI: 10.1093/nar/gkaa1074.
20. Shannon P, Markiel A, Ozier O, Baliga NS, Wang JT, Ramage D, *et al*. Cytoscape: a software environment for integrated models of biomolecular interaction networks. Genome Res. 2003;13(11):2498-2504. DOI: 10.1101/gr.1239303.
21. Cline MS, Smoot M, Cerami E, Kuchinsky A, Landys N, Workman C, *et al*. Integration of biological networks and gene expression data using Cytoscape. Nat Protoc. 2007;2(10):2366-2382. DOI: 10.1038/nprot.2007.324.
22. Tang Y, Li M, Wang J, Pan Y, Wu FX. CytoNCA: a cytoscape plugin for centrality analysis and evaluation of protein interaction networks. Biosystems. 2015;127:67-72. DOI: 10.1016/j.biosystems.2014.11.005.
23. Metz CE. Receiver operating characteristic analysis: a tool for the quantitative evaluation of observer performance and imaging systems. J Am Coll Radiol. 2006;3(6):413-422. DOI: 10.1016/j.jacr.2006.02.021.
24. Anaya J. OncoLnc: linking TCGA survival data to mRNAs, miRNAs, and lncRNAs. Peer J Comput Sci. 2016;2:e67,1-20. DOI: 10.7717/peerj-cs.67.

25. Benítez-Parejo N, del Águila MMR, Pérez-Vicente S. Survival analysis and Cox regression. Allergol Immunopathol. 2011;39(6):362-373. DOI: 10.1016/j.aller.2011.07.007.
26. Stransky N, Egloff AM, Tward AD, Kostic AD, Cibulskis K, Sivachenko A, *et al*. The mutational landscape of head and neck squamous cell carcinoma. Science. 2011;333(6046):1157-1160. DOI: 10.1126/science.1208130.
27. Bhagwat AS, Vakoc CR. Targeting transcription factors in cancer. Trends Cancer. 2015;1(1):53-65. DOI: 10.1016/j.trecan.2015.07.001.
28. Lambert M, Jambon S, Depauw S, David-Cordonnier MH. Targeting transcription factors for cancer treatment. Molecules. 2018;23(6):1479,1-51. DOI: 10.3390/molecules23061479.
29. Argiris A, Karamouzis MV, Raben D, Ferris RL. Head and neck cancer. Lancet. 2008;371(9625):1695-1709. DOI: 10.1016/S0140-6736(08)60728-X.
30. Lee C, Kim JS, Waldman T. PTEN gene targeting reveals a radiation-induced size checkpoint in human cancer cells. Cancer Res. 2004;64(19):6906-6914. DOI: 10.1158/0008-5472.CAN-04-1767.
31. Suske G, Bruford E, Philipsen S. Mammalian SP/KLF transcription factors: bring in the family. Genomics. 2005;85(5):551-556. DOI: 10.1016/j.ygeno.2005.01.005.
32. Safe S, Abbruzzese J, Abdelrahim M, Hedrick E. Specificity protein transcription factors and cancer: opportunities for drug development. Cancer Prev Res. 2018;11(7):371-382. DOI: 10.1158/1940-6207.CAPR-17-0407.
33. Jiang NY, Woda BA, Banner BF, Whalen GF, Dresser KA, Lu D. Sp1, a new biomarker that identifies a subset of aggressive pancreatic ductal adenocarcinoma. Cancer Epidemiol Biomarkers Prev. 2008;17(7):1648-1652. DOI: 10.1158/1055-9965.EPI-07-2791.
34. Gao Y, Gan K, Liu K, Xu B, Chen M. SP1 expression and the clinicopathological features of tumors: a meta-analysis and bioinformatics analysis. Pathol Oncol Res. 2021;27:581998,1-12. DOI: 10.3389/pore.2021.581998.
35. Dong Q, Cai N, Tao T, Zhang R, Yan W, Li R, *et al*. An axis involving SNAI1, microRNA-128 and SP1 modulates glioma progression. PLoS One. 2014;9(6):e98651,1-11. DOI: 10.1371/journal.pone.0098651.
36. Maurer GD, Leupold JH, Schewe DM, Biller T, Kates RE, Hornung HM, *et al*. Analysis of specific transcriptional regulators as early predictors of independent prognostic relevance in resected colorectal cancer. Clin Cancer Res. 2007;13(4): 1123-1132. DOI: 10.1158/1078-0432.CCR-06-1668.
37. Hu X, Cui C, Sun T, Wang W. Associations between ADIPOQ rs2241766 SNP and breast cancer risk: a systematic review and a meta-analysis. Genes Environ. 2021;43:48,1-9. DOI: 10.1186/s41021-021-00221-2.
38. Morris LGT, Sikora AG, Patel SG, Hayes RB, Ganly I. Second primary cancers after an index head and neck cancer: subsite-specific trends in the era of human papillomavirus-associated oropharyngeal cancer. J Clin Oncol. 2011;29(6):739-746. DOI: 10.1200/JCO.2010.31.8311.
39. Westra WH. The changing face of head and neck cancer in the 21st century: the impact of HPV on the epidemiology and pathology of oral cancer. Head Neck Pathol. 2009;3(1):78-81. DOI: 10.1007/s12105-009-0100-y.
40. Wang L, Wei D, Huang S, Peng Z, Le X, Wu TT, *et al*. Transcription factor Sp1 expression is a significant predictor of survival in human gastric cancer. Clin Cancer Res. 2003;9(17):6371-6380. PMID: 14695137.
41. Yao JC, Wang L, Wei D, Gong W, Hassan M, Wu TT, *et al*. Association between expression of transcription factor Sp1 and increased vascular endothelial growth factor expression, advanced stage, and poor survival in patients with resected gastric cancer. Clin Cancer Res. 2004;10(12): 4109-4117. DOI: 10.1158/1078-0432.CCR-03-0628.
42. Wang LW, Li Q, Hua ZL, Zhou F, Keping X, Daoyan W, *et al*. Expression of transcription factor Sp1 in human gastric cancer tissue and its correlation with prognosis. Zhonghua Zhong Liu Za Zhi. 2007;29(2):107-111. PMID: 17645844.
43. Jutooru I, Guthrie AS, Chadalapaka G, Pathi S, Kim K, Burghardt R, *et al*. Mechanism of action of phenethylisothiocyanate and other reactive oxygen species-inducing anticancer agents. Mol Cell Biol. 2014;34(13):2382-2395. DOI: 10.1128/MCB.01602-13.
44. Safe S. Specificity proteins (Sp) and cancer. Int J Mol Sci. 2023;24(6):5164,1-22. DOI: 10.3390/ijms24065164.
45. Zhang B, Wang H, Guo Z, Zhang X. A panel of transcription factors identified by data mining can predict the prognosis of head and neck squamous cell carcinoma. Cancer Cell Int. 2019;19:297,1-10. DOI: 10.1186/s12935-019-1024-6.
46. Jin Y, Qin X. Comprehensive analysis of transcriptome data for identifying biomarkers and therapeutic targets in head and neck squamous cell carcinoma. Ann Transl Med. 2020;8(6): 282,1-17. DOI: 10.21037/atm.2020.03.30.
47. Yan L, Zhan C, Wu J, Wang S. Expression profile analysis of head and neck squamous cell carcinomas using data from The Cancer Genome Atlas. Mol Med Rep. 2016;13(5):4259-4265. DOI: 10.3892/mmr.2016.5054.

Supplementary Materials

Table S1. Summary statistics and distribution of variables in the study population. Descriptive statistics were elucidated in terms of the median with its corresponding interquartile range for numeric variables, while categorical variables were conveyed by their respective frequencies and associated percentages.

Variables	Levels	Mean ± SD / Frequency (%)
Days to last follow-up	-----	616.15 (171.75, 847.25)
Days to death	-----	747.85 (215.50, 800.25)
Tobacco smoking history	-----	2.46 (2.00, 4.00)
Year of tobacco smoking onset	-----	1967.31 (1959.00, 1975.00)
Stopped smoking year	-----	1997.25 (1989.75, 2009.00)
Number of pack years smoked	-----	45.75 (25.00, 60.00)
Amount of alcohol consumption per day	-----	3.24 (0.00, 5.00)
Anatomic neoplasm subdivision	Alveolar ridge	18 (3.41)
	Base of tongue	27 (5.11)
	Buccal mucosa	23 (4.36)
	Floor of mouth	63 (11.93)
	Hard palate	7 (1.33)
	Hypopharynx	10 (1.89)
	Larynx	117 (22.16)
	Lip	3 (0.57)
	Oral cavity	73 (13.83)
	Oral tongue	133 (25.19)
	Oropharynx	9 (1.70)
	Tonsil	45 (8.52)
Gender	Male	386 (73.11)
	Female	142 (26.89)
Vital status	Alive	358 (67.80)
	Dead	170 (32.20)
Clinical stage	Stage I	21 (3.98)
	Stage II	99 (18.75)
	Stage III	107 (20.27)
	Stage IVA	269 (50.95)
	Stage IVB	11 (2.08)
	Stage IVC	7 (1.33)
	NA	14 (2.65)
	Not evaluated	114 (21.59)
	Unknown	8 (1.52)
HPV status	Negative	74 (14.02)
	Positive	41 (7.77)
	NA	291 (55.11)
Alcohol history documented	No	165 (31.25)
	Yes	352 (66.67)
	NA	11 (2.08)

Table S2. The list of the top 100 differentially expressed genes in head and neck squamous cell carcinoma samples has been shown and ordered according to adjusted *P*-value numbers.

Ensemble ID	Gene symbol	Log 2 of fold change	Average expression	*P*-value	Adjusted *P*-value
ENSG00000250133	HOXC-AS2	4.067035229	-1.148967402	2.67E-61	6.77E-57
ENSG00000102547	CAB39L	-2.250606008	2.62578651	1.72E-60	1.45E-56
ENSG00000181092	ADIPOQ	-7.297369413	-4.67972223	1.72E-60	1.45E-56
ENSG00000034971	MYOC	-6.497505799	-4.397185746	6.03E-60	3.82E-56
ENSG00000197757	HOXC6	4.410758803	0.438512566	3.12E-59	1.58E-55
ENSG00000152642	GPD1L	-2.643818057	3.928493656	4.92E-55	1.79E-51
ENSG00000166819	PLIN1	-4.967671556	-2.462249755	4.95E-55	1.79E-51
ENSG00000070081	NUCB2	-1.87934893	5.407735058	1.36E-54	4.29E-51
ENSG00000128713	HOXD11	6.052475249	1.296197492	3.95E-54	1.11E-50
ENSG00000158458	NRG2	-4.18405847	-1.928509504	6.35E-54	1.61E-50
ENSG00000167588	GPD1	-4.703472835	-0.454576838	8.04E-54	1.85E-50
ENSG00000278966	AL031602.1	4.247129426	-0.571218843	1.06E-53	2.22E-50
ENSG00000130309	COLGALT1	1.4236552	7.359154411	5.94E-53	1.16E-49
ENSG00000106351	AGFG2	-1.96785504	4.122153348	8.87E-51	1.60E-47
ENSG00000169258	GPRIN1	2.329497338	4.031573369	1.28E-50	2.16E-47
ENSG00000248554	AC114956.2	3.715658571	-0.008766588	1.48E-50	2.34E-47
ENSG00000150672	DLG2	-3.486651401	-0.589088001	2.16E-50	3.21E-47
ENSG00000237424	FOXD2-AS1	2.30376284	1.254237311	9.66E-50	1.36E-46
ENSG00000146670	CDCA5	2.045166234	5.378767931	1.29E-49	1.72E-46
ENSG00000180806	HOXC9	4.350482873	-0.038974379	2.52E-49	3.19E-46
ENSG00000101057	MYBL2	2.272679251	6.162260408	9.00E-49	1.08E-45
ENSG00000198478	SH3BGRL2	-4.130054038	3.194610672	2.46E-48	2.83E-45
ENSG00000025423	HSD17B6	2.301960774	1.051372234	4.00E-48	4.39E-45
ENSG00000184811	TUSC5	-4.658747805	-4.506695231	4.80E-48	5.06E-45
ENSG00000115163	CENPA	2.128467882	3.25318077	5.85E-48	5.92E-45
ENSG00000214544	GTF2IRD2P1	3.506956725	1.203269492	1.55E-47	1.50E-44
ENSG00000253293	HOXA10	4.176252692	1.161212768	1.88E-47	1.76E-44
ENSG00000139800	ZIC5	5.618903803	0.489738233	3.26E-47	2.95E-44
ENSG00000142945	KIF2C	1.991255599	5.252019293	3.70E-47	3.23E-44
ENSG00000043355	ZIC2	4.629791385	1.849227644	3.85E-47	3.24E-44
ENSG00000258711	AL358334.2	4.171140883	0.311740722	4.64E-47	3.79E-44
ENSG00000198099	ADH4	-4.040719663	-4.611534004	5.47E-47	4.32E-44
ENSG00000187288	CIDEC	-4.903313148	-4.018593361	7.27E-47	5.57E-44
ENSG00000122042	UBL3	-1.63484831	4.967289285	1.09E-46	8.08E-44
ENSG00000171503	ETFDH	-1.469479003	4.073134182	1.67E-46	1.20E-43
ENSG00000248240	AC114956.1	3.378352012	-1.495142579	7.85E-46	5.51E-43
ENSG00000267123	LINC02081	4.565860478	-0.451339804	1.27E-45	8.69E-43
ENSG00000165795	NDRG2	-2.905073821	5.929488402	2.78E-45	1.85E-42
ENSG00000187498	COL4A1	2.800204983	8.231112588	5.42E-45	3.51E-42
ENSG00000171201	SMR3B	-6.332001777	-5.553446752	1.03E-44	6.50E-42
ENSG00000096006	CRISP3	-8.652918707	-1.05688244	1.12E-44	6.94E-42
ENSG00000117122	MFAP2	3.070259914	5.281036959	1.45E-44	8.72E-42
ENSG00000088325	TPX2	2.000500763	6.551291145	2.18E-44	1.28E-41
ENSG00000168309	FAM107A	-3.813698518	1.134875309	2.88E-44	1.66E-41
ENSG00000037965	HOXC8	4.311335319	-0.549416927	4.06E-44	2.28E-41
ENSG00000154920	EME1	1.947067143	2.037572083	4.56E-44	2.51E-41
ENSG00000166851	PLK1	1.956518538	5.633233912	9.19E-44	4.95E-41
ENSG00000179528	LBX2	2.475528163	-0.702628111	1.12E-43	5.90E-41
ENSG00000196616	ADH1B	-6.687233254	-2.394052899	1.31E-43	6.75E-41
ENSG00000234041	AL512326.3	4.596160242	-1.284915057	2.31E-43	1.17E-40
ENSG00000164283	ESM1	3.397047925	1.900907484	4.36E-43	2.16E-40
ENSG00000000005	TNMD	-3.598553987	-5.596754377	4.59E-43	2.23E-40
ENSG00000095752	IL11	3.998145151	1.931565032	4.82E-43	2.30E-40

Table S2. Continued

Ensemble ID	Gene symbol	Log 2 of fold change	Average expression	*P*-value	Adjusted *P*-value
ENSG00000172340	SUCLG2	-1.193031896	5.037065521	7.10E-43	3.33E-40
ENSG00000090889	KIF4A	1.89933935	4.741108111	1.13E-42	5.21E-40
ENSG00000134871	COL4A2	2.534128298	8.525642026	1.62E-42	7.34E-40
ENSG00000138180	CEP55	2.06542102	5.296787324	2.59E-42	1.15E-39
ENSG00000127564	PKMYT1	2.086465524	4.943314123	2.81E-42	1.22E-39
ENSG00000060762	MPC1	-1.477814284	4.013536801	4.14E-42	1.78E-39
ENSG00000134013	LOXL2	3.069342726	5.643654837	5.91E-42	2.49E-39
ENSG00000108381	ASPA	-3.739067205	-2.388581691	8.85E-42	3.67E-39
ENSG00000099953	MMP11	4.564027571	5.426080692	1.40E-41	5.72E-39
ENSG00000134240	HMGCS2	-6.101300197	-3.47146165	1.72E-41	6.82E-39
ENSG00000281386	AP003500.1	-4.308213832	-4.281470987	1.72E-41	6.82E-39
ENSG00000100985	MMP9	4.002109105	6.202632834	1.77E-41	6.87E-39
ENSG00000186185	KIF18B	1.983342292	4.239610824	2.22E-41	8.53E-39
ENSG00000175063	UBE2C	1.998033406	5.452722034	2.91E-41	1.10E-38
ENSG00000094804	CDC6	1.853484263	4.840907474	3.22E-41	1.20E-38
ENSG00000174371	EXO1	1.919035726	3.627558953	3.29E-41	1.21E-38
ENSG00000039537	C6	-4.910536017	-4.57173203	3.92E-41	1.42E-38
ENSG00000124205	EDN3	-5.719837546	-3.797732365	5.27E-41	1.88E-38
ENSG00000171208	NETO2	1.997386805	4.852666648	6.39E-41	2.25E-38
ENSG00000089685	BIRC5	1.921936762	5.913256413	6.82E-41	2.36E-38
ENSG00000008441	NFIX	-1.899657175	6.047103492	1.02E-40	3.49E-38
ENSG00000235097	LINC00330	-4.849489969	-4.192716077	1.30E-40	4.37E-38
ENSG00000127423	AUNIP	1.760474148	2.413044437	1.32E-40	4.41E-38
ENSG00000167676	PLIN4	-4.141935223	1.045125369	1.66E-40	5.47E-38
ENSG00000093009	CDC45	1.956367959	4.269708117	1.82E-40	5.92E-38
ENSG00000123485	HJURP	1.995317333	4.061303218	2.68E-40	8.60E-38
ENSG00000197467	COL13A1	2.398246455	2.115312569	4.20E-40	1.33E-37
ENSG00000272549	LINC02538	-4.380681114	-4.147392374	4.51E-40	1.41E-37
ENSG00000168779	SHOX2	3.210264394	1.719294643	9.26E-40	2.86E-37
ENSG00000163815	CLEC3B	-3.017723679	0.960674494	1.48E-39	4.52E-37
ENSG00000118193	KIF14	2.15364894	3.721370764	1.58E-39	4.76E-37
ENSG00000075218	GTSE1	1.815903525	3.949201309	1.80E-39	5.34E-37
ENSG00000111713	GYS2	-4.635748285	-3.991607189	1.98E-39	5.81E-37
ENSG00000148848	ADAM12	3.712593833	4.722028621	2.22E-39	6.44E-37
ENSG00000107159	CA9	5.470416088	3.343690927	2.83E-39	8.06E-37
ENSG00000165269	AQP7	-4.018186501	-2.308894216	2.84E-39	8.06E-37
ENSG00000133466	C1QTNF6	2.799040555	4.867511201	3.90E-39	1.10E-36
ENSG00000111206	FOXM1	2.055018305	5.935424143	4.42E-39	1.23E-36
ENSG00000111665	CDCA3	1.81237011	4.049239803	4.94E-39	1.36E-36
ENSG00000204889	KRT40	-4.599123136	-4.369657322	5.32E-39	1.45E-36
ENSG00000164932	CTHRC1	3.372348783	4.641354086	7.70E-39	2.07E-36
ENSG00000087586	AURKA	1.745079635	4.74469077	1.09E-38	2.90E-36
ENSG00000113739	STC2	3.088138131	3.966544387	1.53E-38	4.03E-36
ENSG00000181234	TMEM132C	-4.677230557	-3.297734314	1.58E-38	4.11E-36
ENSG00000123388	HOXC11	5.270887041	0.245222717	1.75E-38	4.51E-36
ENSG00000091651	ORC6	1.802906347	3.3609245	3.40E-38	8.68E-36
ENSG00000076382	SPAG5	1.668663738	5.013816972	3.92E-38	9.92E-36

Research in Pharmaceutical Sciences, June 2024; 19(3): 303-318
Received: 13-05-2023
Peer Reviewed: 23-06-2023
Revised: 21-11-2023
Accepted: 25-11-2023
Published: 01-07-2024

School of Pharmacy & Pharmaceutical Sciences
Isfahan University of Medical Sciences

Original Article

Isolation of a novel quercetin derivative from *Terminalia chebula* and RT-PCR-assisted probing to investigate its DNA repair in hepatoma cells

Kallyadan Soumya, Karickal Raman Haridas, Jesna James, and Sudhakaran Sudheesh*

School of Chemical Sciences, Kannur University, Payyanur Campus, Edat P.O., Payyanur, Kannur, Kerala, India - 670327

Abstract

Background and purpose: DNA damage can lead to carcinogenesis if replication proceeds without proper repair. This study focused on the purification of a novel quercetin derivative present in *Terminalia chebula* fruit and studied its protective role in hepatoma cells due to H_2O_2-DNA damage.
Experimental approach: The pure compound obtained from the silica gel column was subjected to structural characterization using spectroscopic techniques. MTT assay was employed to select a non-toxic concentration of the isolated compounds on HepG2 and Chang liver cells. The antigenotoxic property of the compound on HepG2 and Chang liver cells was carried out by alkaline comet assay. Analyses of expression levels of mRNA for two DNA repair enzymes, OGG1 and NEIL1, in HepG2 and Chang liver cells, were carried out using the RT-PCR method.
Findings/Results: The pure compound obtained from the fraction-5 of diethyl ether extract was identified as a novel quercetin derivative and named 7-(but-2-en-1-yloxy)-2-(4(but-2-en-1-yloxy)-3-hydroxyphenyl)-3-(hexa-2,4-dien-1-yloxy)-6-hydroxy-4H-chromen-4-one. This compound recorded modest toxicity at the highest concentration tested (percentage cell viability at 100 µg/mL was 64.71 ± 0.38 for HepG2 and 45.32 ± 0.07 for Chang liver cells). The compound has demonstrated noteworthy protection against H_2O_2-induced DNA damage in both cell lines. Analyses of mRNA expression levels for enzymes OGG1 and NEIL1 enzymes in HepG2 and Chang liver cells asserted the protective role of the isolated compound against H_2O_2-induced DNA damage.
Conclusion and implication: The protective effect of a novel quercetin derivative isolated from *T. chebula* in the hepatoma cells is reported here for the first time.

Keywords: Antigenotoxicity; Chang liver cell; HepG2 cell; NEIL1, OGG1; Quercetin derivative; *T. chebula.*

INTRODUCTION

An insight into the formation of reactive oxygen species (ROS) is vital to establishing and improving an effective antioxidant defense system against the toxic oxidants that cause devastating effects within the body. ROS are mainly produced in living organisms as a by-product of normal metabolic processes and are also generated by environmental factors like exposure to electromagnetic radiation, chemical oxidants, chemotherapeutic drugs, etc. (1). Since it is especially stable and freely diffusible, among the ROS, hydrogen peroxide may cause damage to almost every component of a living cell. Thus, it could reach the nucleus and then intermingle with cellular components like DNA. ROS is a prime cause of a variety of DNA damage, namely oxidation of bases, abasic sites, and single-strand and double-strand breaks. Inefficient remediation of oxidative DNA base damage by DNA repair mechanisms leads to mutation, the initiation and progression of cancer (2).

*Corresponding author: S. Sudheesh
Tel: +91-9847421467
Email: sudheeshs@kannuruniv.ac.in

Access this article online

Website: http://rps.mui.ac.ir

DOI: 10.4103/RPS.RPS_56_23

Due to the lower redox potential, guanine is easily susceptible to base lesions. Over 100 types of DNA lesions have been identified, 7,8-dihydro-8-oxoguanine (8-oxoG) is one of the significantly studied and common DNA base lesions created by ROS (3,4). It has been assumed that approximately 180 guanine bases are oxidized to 8-oxoG per cell each day. It acts as a mutagenic miscoding lesion that preferentially mispairs with adenosine and leads to G: C to A: T transversion mutations. Since there exists a strong relationship between ROS generation and 8-oxoG formation, the level of 8-oxoG is often considered a biomarker of oxidative stress (5). After oxidative stress, other lesions like formamidopyrimidine, 2,6-diamino-4-hydroxy-5-formamidopyrimidine (FapyG), and 4,6-diamino-5-formamido-pyrimidine (FapyA) are also forged at equal or higher levels than 8-oxoG. These lesions are caused by the hydroxyl radical attack on the bases of guanine and adenine (6).

Oxidative DNA damage is mainly repaired by the base excision repair (BER) pathway. The BER pathway involves several genes; the primary step acts as DNA glycosylases. They remove the N-glycosylase bond between the base and the sugar, thus releasing the damaged base and forming an abasic site called an AP site (apurinic/apyrimidinic site). Several glycosylases recognize more than one type of cleavage. 8-Oxoguanine DNA glycosylase (OGG1) protein was found to exhibit strong specificity for 8-oxoG and FapyG, with no significant specificity for FapyA. While the endonuclease VIII-like 1 (NEIL1) protein efficiently excises FapyG and FapyA, it has not been shown to have specificity for 8-oxoG (1,6).

Terminalia chebula, commonly known as black myrobalan and belonging to the Combretaceae family, is a popular folk medicine prevalently cultivated in India and Southeast Asia (7). It has been studied for its homeostatic, antitussive, laxative, diuretic, and cardiotonic activities (8). *T. chebula* is widely used as a traditional medicine to cure several ailments, such as digestive and coronary disorders, coughs, and skin disorders (9). The *T. chebula* fruits are reported to have complex phytochemicals that can be used for managing a variety of diseases like cancer, cardiovascular, digestive problems, *etc*. The extracts obtained from this plant are also reported to have significant antibacterial activity against several bacterial species (10). Moreover, it is deemed an effective measure in inhibiting *Helicobacter pylori*, *Xanthomonas campestris,* and *Salmonella typhi.* Furthermore, significant antifungal activity against numerous dermatophytes and yeasts was also reported by the aqueous extract of *T. chebula* fruit (11).

The current study zeroed in on the antigenotoxic activity of a novel flavonoid purified from *T. chebula* on H_2O_2-caused DNA damage in the hepatocarcinoma (HepG2) and Chang liver cell lines. Additionally, the effect of the isolated compound on the expression levels of mRNA for the DNA repair enzymes encoding OGG1 and NEIL1 in HepG2 and Chang liver cells was measured employing the real-time polymerase chain reaction (RT-PCR) technique.

MATERIALS AND METHODS

Chemicals and reagents

The chemicals and solvents used for extraction and purification were of the highest purity and procured from Merck, India.

Preparation of T. chebula fruit extracts

Fresh fruits of *T. chebula* were purchased from the herbal medicine supplier in Kannur district, Kerala, India. The sample was authenticated by Dr. Sujanapal P, Scientist, Kerala Forest Research Institute (KFRI), Thrissur, Kerala, India and deposited in KFRI. The collected seeds were initially cleansed with pure water, shade-dried, and ground into a powder form. The soxhlet extraction method was used to prepare 80% of the methanolic extracts. The extracts were washed with petroleum ether to remove fatty matter. The filtrate was then partitioned with diethyl ether and ethyl acetate. Both the ethyl acetate and diethyl ether extracts were dried in a fume hood and thus obtained solid residues were stored in a desiccator.

Isolation and purification of flavonoids from T. chebula extracts

The extracts (diethyl ether and ethyl acetate) obtained from *T. chebula* fruit were subjected

to column chromatography to isolate the active components. A clean and dry glass column was filled with a slurry of silica gel (60-120 mesh size) using hexane. Each extract weighing 15 g was thoroughly mixed with a small amount of silica gel and loaded onto the top of the respective column. Once the sample was loaded, the column was eluted with varying ratios of hexane: ethyl acetate and ethyl acetate: methanol (12). Fractions of 20 mL from each solvent system were collected and further analyzed with thin-layer chromatography (TLC). To isolate the active principles, the fractions with similar R_f values were combined and concentrated with the aid of a rota vacuum flash evaporator. The entire pooled fractions were investigated for the presence of flavonoids and further subjected to *in vitro* antioxidant activity studies. Fraction 5 was obtained from the diethyl ether extract which yielded a pure compound. This compound recorded significant antioxidant properties and thus was selected for a thorough structural elucidation process.

Structural characterization of the compound

UV-visible spectroscopy, Fourier transform infrared spectroscopy (FT-IR), proton nuclear magnetic resonance spectroscopy (^{1}H NMR), and mass spectroscopy were used to determine the chemical structure of the isolated compound from fraction 5. From 200 to 600 nm, the UV-visible spectrum was recorded on a Shimadzu UV Pharmaspec-1700 spectrophotometer (Japan) with spectroscopic-grade methanol as the solvent. FT-IR spectrum of the compound was recorded in transmission mode with a Shimadzu FT-IR spectrometer-8400S, in the wave number range of 400-4000 cm^{-1} using potassium bromide (KBr) pellets. A Bruker Ascend 500 MHz spectrometer (Germany) was used to collect ^{1}H NMR spectra with CD3COCD3 (deuterated acetone) as the solvent and TMS tetramethyl silane as the internal standard. The purified compound's mass spectrum was recorded using a Thermo Fisher Scientific high-resolution mass spectrometer (USA; HR-MS).

Cytotoxicity of the isolated pure compound towards HepG2 and Chang liver cell lines

MTT assay was used to assess the cytotoxicity of the isolated novel compound from the diethyl ether extract of *T. chebula* fruit against HepG2 and Chang liver cells. The cell lines were initially obtained from the NCCS in Pune, India, and were kept in DMEM (Sigma Aldrich, USA) supplemented with L-glutamine, 10% fetal bovine serum (FBS), sodium bicarbonate, penicillin (100 U/mL), streptomycin (100 µg/mL), and amphotericin B (2.5 µg/mL). Cells were cultured in 25 cm^2 tissue culture flasks in a humidified 5% CO_2 incubator (NBS Eppendorf, Germany) at 37 °C. Trypsinization was used to subculture the cells, and the cells were kept in Dulbecco's modified eagle medium (DMEM). The experiment was carried out three times in triplicate.

A 96-well plate was seeded with a total of 2×10^3 cells. After a 24-h incubation period, the cells were treated with the compound at various concentrations (0.78-100 µg/mL). Negative control cells were untreated cells. The cells were treated and incubated for 24 h at 37 ℃ and 5% CO_2. After the chosen incubation time, 10 µL MTT (5 mg/mL) was added to each well and the plates were incubated for 4 h. The formazan crystals were dissolved in 100 µL of DMSO after the supernatants were removed. Using a microwell plate reader, the extent of MTT reduction was measured at 590 nm with a reference wavelength of 620 nm. Percentage cell viability was calculated by the following equation (13,14). All absorbance values have been adjusted against blank wells that only included growth media. The average absorbance of cells grown without the test compound was taken as 100% cell survival. Ascorbic acid was used as a positive control in this research.

$$\text{Cell viability (\%)} = \frac{Absorbance\ of\ sample}{Absorbance\ of\ control} \times 100$$

Antigenotoxic effects of the isolated compound by Comet assay on HepG2 and Chang liver cells

HepG2 and Chang liver cells were cultured at 37 °C in an atmosphere of 5% CO_2-95% air humidity. DMEM (Sigma Aldrich, USA) was used as the culture medium, which was supplemented with L-glutamine, 10% FBS, sodium bicarbonate, penicillin (100 U/mL), streptomycin (100 µg/mL), and amphotericin B (2.5 µg/mL). The cells were then seeded at a density of 3×10^4 cells per well in a 6-well

plate for testing. The isolated compound was applied to the cells for 1 h at 37 °C. The compound concentration was chosen from a range of non-toxic concentrations determined by the MTT assay on both cell lines. DNA damage was induced for 15 min with 50 µM H_2O_2 and then incubated for 24 h. The adherent cells were then trypsinized, centrifuged, and resuspended in ice-cold phosphate-buffered saline (PBS) before being thoroughly mixed with 50 µL of 0.5% low melting point agarose at pH 7.4 at 40 ℃. Microscopic slides were cleared in flame after being rinsed with alcohol. The slides were frosted and then coated with 1% normal melting point agarose before being stored at 40 °C. A 1.6 mL sample was pipetted onto a frosted glass slide that had been pre-coated with a layer of 1% normal melting point agarose prepared in PBS and covered with a glass coverslip. The agarose was immediately chilled for 5 min to allow for complete agarose solidification. After removing the coverslip, the slides were immersed in a lysis solution (2.5 M NaCl, 100 mM Na_2EDTA, 10 mM Tris, NaOH to pH 10, and 1% Triton X-100) at 4 ℃ for 1 h. DNA was allowed to unwind for 20 min in freshly prepared alkaline electrophoresis buffer (1 mM Na_2EDTA, 0.3 N NaOH, pH 13). The slides were then placed in a horizontal electrophoresis tank and electrophoresis was performed at 12 V/cm for 20 min at a temperature of 40 ℃. The slides were then washed three times with 1× Tris for 5 min with neutralizing buffer (0.4 M Tris-HCl buffer, pH 7.4) before staining with 20 µL ethidium bromide (20 µg/mL) (15,16).

Gene expression study

Culturing of cell lines

Initially, the cell lines (HepG2 and Chang) procured from NCCS, Pune, India were maintained in DMEM (Sigma Aldrich, USA) supplemented with L-glutamine, 10% FBS, sodium bicarbonate, penicillin (100 U/mL), streptomycin (100 µg/mL), amphotericin B (2.5 µg/mL). The cells were continuously cultured in 25 cm^2 tissue culture flasks and kept at 37 ℃ in a humidified 5% CO_2 incubator (NBS Eppendorf, Germany).

RNA isolation

After attaining 70% confluency, the cells (4 × 10^5cells) were treated with the test compound for 1 h in a 6-well plate. Succeeding the incubation, all the samples were treated with H_2O_2 for 15 min and the cells were subsequently incubated for 24 h. A set of untreated control cells was also kept synchronous with the treated cells. After the 24-h incubation, the media were removed aseptically and RNA was isolated. Total RNA was isolated using an RNA isolation kit according to the manufacturer's instructions (Invitrogen, USA; Product Code: 10296010). The disruption of cells and extraction of RNA were made with 200 µL of TRIzol solution followed by 200 µL of chloroform. The cells were vigorously shaken and incubated at room temperature for 3-5 min. After centrifugation at 14000 rpm for 15 min at 4 ℃, 500 µL of 100% isopropanol was added and incubated for 10 min at room temperature. Thereon, the mixture was centrifuged again at 14000 rpm for 15 min at 4 ℃. The supernatant was discarded, and the RNA was precipitated as a white pellet on the lower side of the tube. The resultant RNA pellet was washed with 200 µL of 70% ethanol (Merck, India) and centrifuged at 14000 rpm for 5 min at 4 ℃. Ultimately, the pellets were dried and suspended in Tris-EDTA (TE) buffer. The purity and quantity of the total RNA were determined by RNA assay using Qubit version-3 (Thermo Scientific, USA).

cDNA synthesis and amplification

The cDNA was synthesized using the Thermo Scientific Verso cDNA synthesis kit (Product Code: AB-1453/A). To an RNase-free tube, add about 4 µL of 5× cDNA synthesis buffer, 2 µL of deoxynucleotide triphosphate (dNTP) mix, 1 µL of anchored oligo dT, 1 µL of RT enhancer, 1 µL of verso enzyme mix, and 5 µL of RNA template (1 ng of total RNA), then the total reaction volume was made up to 20 µL with the addition of sterile distilled water and mixed gently. The cDNA synthesis was executed in the thermal cycler (Eppendorf master cycler). The following cycling conditions were employed for 30 min at 42 ℃ and 2 min at 95 ℃. Temperature conditions of cDNA synthesis are given in Table 1.

Table 1. Temperature conditions of cDNA synthesis.

Steps	Temperature (℃)	Time (min)	Number of cycles
cDNA synthesis	42	30	1
Inactivation	95	2	1

Table 2. Primers and their annealing temperatures.

Gene	Forward		Reverse	
	Sequence (5' > 3')	**Tm (℃)**	**Sequence (5' > 3')**	**Tm (℃)**
NEIL1	GCAGAATAACTGTGTGCCGCT	59.82	ACCCTGCTAGATGTCCAACTGATT	61.01
OGG1	GTGCCCGTTACGTGAGTGTGCCAGTGC	69.54	AGAGAAGTGGGGAATGGAGGGGAAGGTG	69.51
B-Actin	TCACCCACACTGTGCCCATCTACGA(25)	66.3	CAGCGGAACCGCTCATTGCCAATGG(25)	67.9

NEIL1, Endonuclease VIII-like 1; OGG1, 8-oxoguanine DNA glycosylase; Tm, melting temperature.

Table 3. Steps of polymerase chain reaction amplification.

Step	Temperature (℃)	Time	Number of cycles
Initial denaturation	95	3 s	1
Denaturation	95	30 s	
Annealing	50-65	30 s	25-40
Extension	72	1 min/kb	
Final extension	72	15 min	1

The amplification was performed by utilizing a Thermo Scientific amplification kit. The components from the kit were added to each PCR vial. The 50 µL reaction mixture consisted of 25 µL of PCR master mix, 2 µL of forward and reverse primers and 5 µL of template DNA. The components were made up to 50 µL with nuclease-free sterile distilled water. The PCR was programmed after standardization, and after amplification, the PCR products were segregated using agarose gel electrophoresis. Table 2 outlines the details of primers and their annealing temperatures. However, Table 3 shows the steps of PCR amplification.

A gel was prepared using 1.5% agarose in 1× TE buffer by adding 6 µL of 10 mg/mL ethidium bromide. Then, the gel was loaded with samples and accomplished the electrophoresis procedure at 50V for 30 min. The stained gel was then viewed under the gel documentation system (E gel imager, Invitrogen, USA), and the intensity of the band and the level of expression were calculated using the software Image J.

Statistical analyses

Statistical analysis of the data was performed by SPSS version 20.0 (SPSS Inc, Chicago, IL, USA). The outcome of the investigations is expressed as the mean ± SD of three independent experimentations. The student t-test and one-way ANOVA test followed by Tukey test were used to find out the statistical significance. Differences were considered statistically significant at $P < 0.05$.

RESULTS

Structural elucidation of the novel isolated compound

Various fractions collected from the column chromatography were pooled based on the TLC profile. All pooled fractions were tested for the occurrence of flavonoids. Afterward, the fractions were subjected to *in vitro* antioxidant studies (data not shown). Fraction 5, which yielded a pure compound and recorded significant antioxidant activity, was subjected to detailed structural elucidation. The pure compound yielded in fraction 5 appeared as a yellow solid, and its melting point was observed at 235 ℃. The UV-visible spectrum of the compound with λ_{max} at 254 and 365 is shown in Fig. 1. Absorption bands at 254 and 365 nm indicated the presence of an aromatic ring and carbonyl group, respectively. The higher value of the carbonyl group may be due to the

interaction of lone pairs of oxygen in the carbonyl and ester groups.

The FT-IR spectrum of the compound is depicted in Fig. 2A. The details of IR bands observed in the spectrum along with the structural details are given in Table 4.

^{1}H NMR spectra of the isolated compound are depicted in Fig. 2B. Phenolic O-H appeared at 9.3 ppm estimating the presence of two phenolic groups in the compound. The peaks detected between 7.0 and 7.4 ppm have marked the presence of five aromatic hydrogen atoms present in two rings. Peaks at 6.8-6.9 ppm indicated the presence of unsaturated moieties in aliphatic chains connected to the core structure. NMR peaks from 0.84-2.1 ppm pointed out the presence of aliphatic saturated hydrogens in the chain.

Based on UV-Vis, FT-IR, and NMR spectra, the following information was derived:

The core structure contained polyaromatic rings; the aromatic rings were substituted with the functional groups at various positions; at least, two phenolic hydrogens were present in the core; the presence of a C=O group was confirmed; unsaturation of the alkyl chain was also observed; and the presence of ether linkage connected between aliphatic and aromatic moieties was confirmed.

Given the obtained data, the mass spectra (as shown in Fig. 2C) have been interpreted as a confirmatory analysis for the elucidation of the compound. The structural elucidation was supported by the data for this family, available in the literature (17).

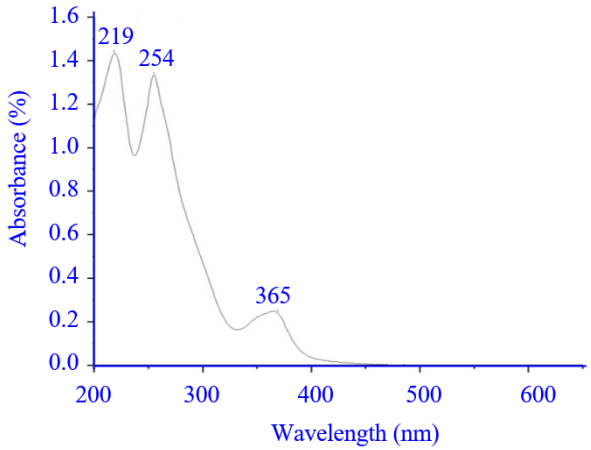

Fig. 1. UV-visible spectrum of the pure compound isolated from *Terminalia chebula* fruit.

Table 4. Description of the spectrum of compound isolated from *Terminalia chebula* fruit obtained by Fourier transform infrared spectroscopy.

No	Band frequency (cm^{-1})	Description
1	3247	C-H stretching vibrations of alkene
2	2933	C-H stretching vibrations of CH_3
3	2881	C-H stretching vibrations of CH_2
4	2837	C-H stretching vibrations of CH
5	1712	C=O stretching
6	1614	C=C stretching
7	1512-1448	C-C stretching of the aromatic ring
8	1340	C-O-C stretching band
9	1213	Aromatic C-O of the phenyl group
10	1114	Aliphatic C-O of the phenyl group
11	761	Poly substitution on aromatic rings

A

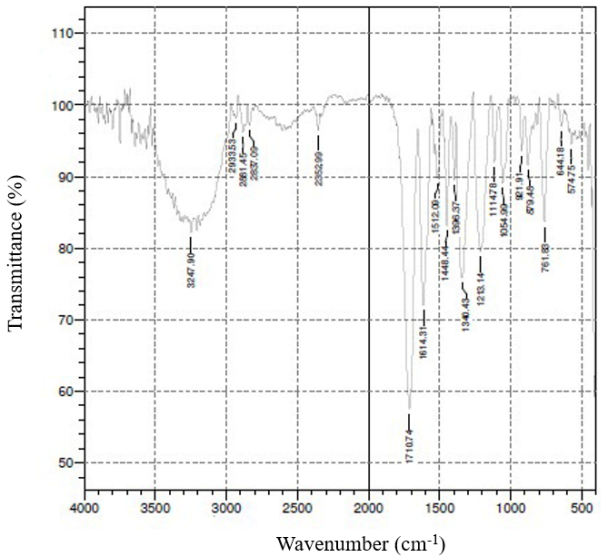
Transmittance (%)
Wavenumber (cm-1)
3247.90
2933.53
2851.45
2837.09
2358.99
1710.74
1614.31
1512.08
1448.44
1396.37
1340.43
1215.14
1114.78
1054.99
921.91
879.42
761.88
644.18
574.75

B

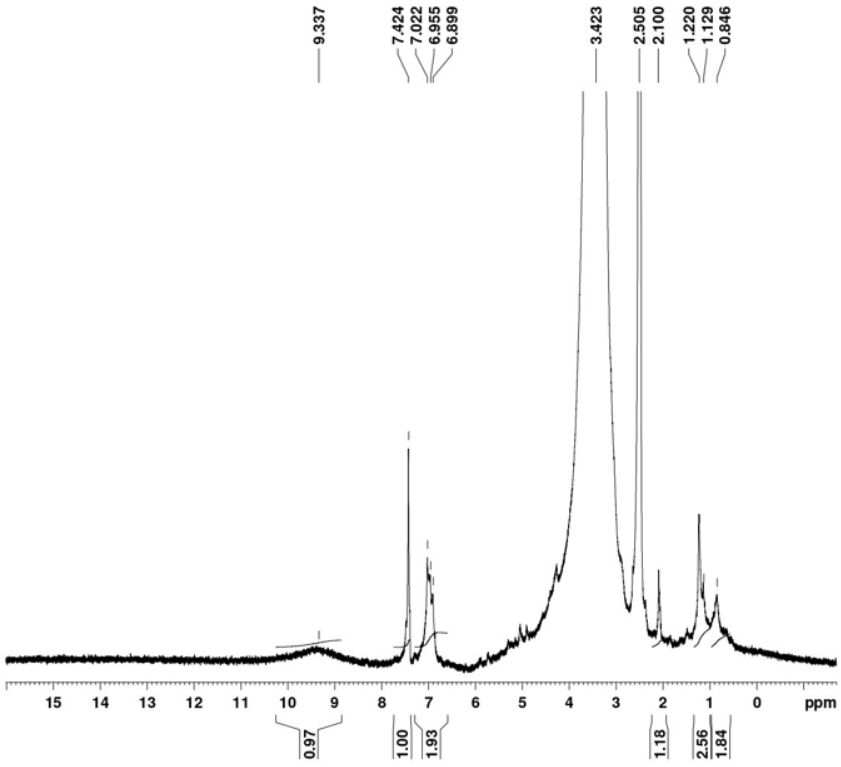
9.337
7.424
7.022
6.955
6.899
3.423
2.505
2.100
1.220
1.129
0.846
ppm
0.97
1.00
1.93
1.18
2.56
1.84

C

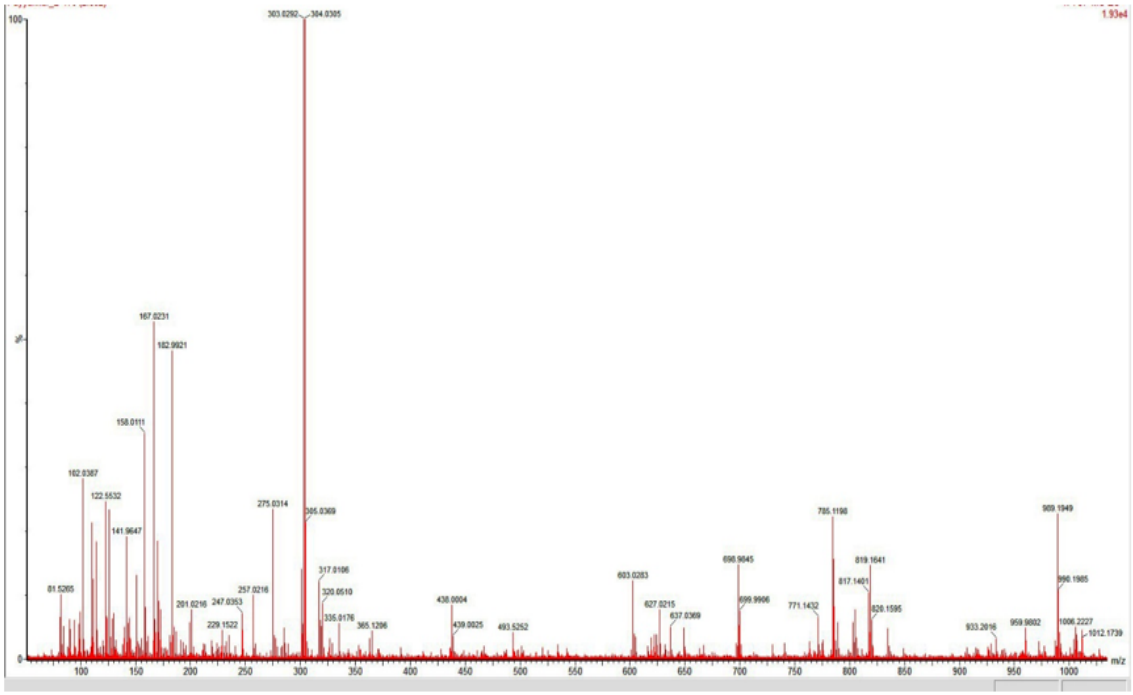

Fig. 2. (A) Fourier transform infrared spectroscopy, (B) proton nuclear magnetic resonance spectroscopy, and (C) mass spectra of the compound isolated from *Terminalia chebula* fruit.

The base peak at 303 shows the core structure of the compound, which consists of quercetin. The mass spectra were explained on this basis and elucidated for other substitutions of quercetin. This was confirmed by the fractions of 229 (fragmentation of the second benzene ring (B) from the parent compound) and 73 for the fragmented part. From the mass spectra values, it was observed that the compound existed sometimes as a dimer. The fragmentation pattern is shown in Table 5.

The substituents were placed preferably at positions 7, and 4' having the shortest substituent, and 3' having the longest substituent. This might be due to avoiding the steric hindrance. Figure 3 depicts the chemical structure of the isolated compound, a novel quercetin derivative known as 7-(hydroxyl alkyl substituted)-2-(4(hydroxyl alkyl substituted)-3-hydroxyphenyl)-3-(hydroxyl alkyl substituted)-6-hydroxy-4H-chromen-4-one.

Cytotoxic effects of novel quercetin derivative on HepG2 and Chang liver cells

The cytotoxic activity of isolated flavonoid on HepG2 cells after 24-h incubation was evaluated by MTT assay. The cell viability (%) was calculated in each concentration and the outcomes are depicted in Table 6. The cytotoxicity study aimed to determine the concentration that could elicit minimum cytotoxicity towards the cell line to be further used for antigenotoxic and expression studies. However, there was no cytotoxicity observed for the compound at their lower concentrations. The compound showed a moderate cytotoxic effect even at the high concentration (100 µg/mL). The compound showed a cell viability of 90% at the concentration of 1.56 µg/mL for HepG2 and 3.12 µg/mL for Chang liver cells, and this concentration was selected for the compound for antigenotoxic and expression studies.

Table 5. Description of mass spectra of pure compound isolated from *Terminalia chebula* fruit.

Sl. No.	Peak value	Structure	Existing peaks
1.	438	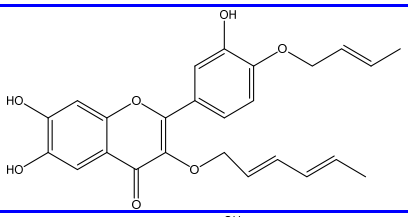	(303 + 95 - 15 + 55)
2.	317	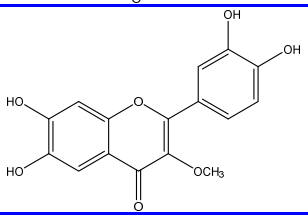	(303 + 15)
3.	493	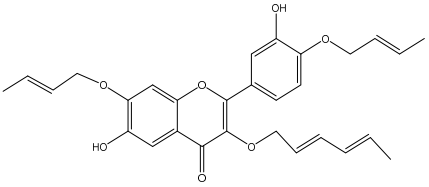	(303 + 95 – 15 + 55 + 55)
4.	603	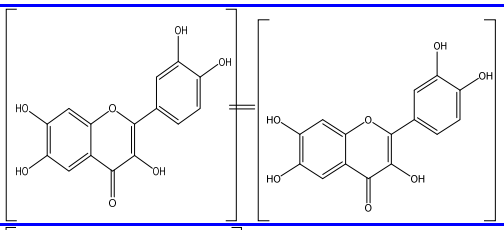	(303 × 2 = 606)
5.	698	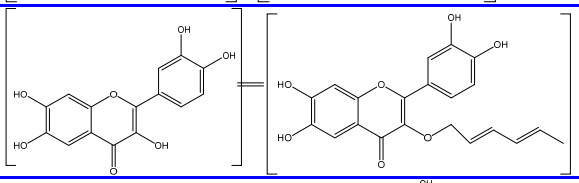	(606 + 95)
6.	785	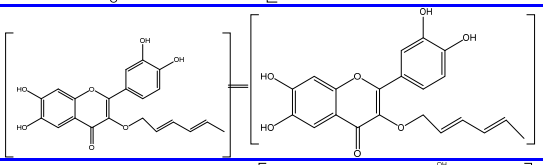	(606 + 95 + 95)
7.	933	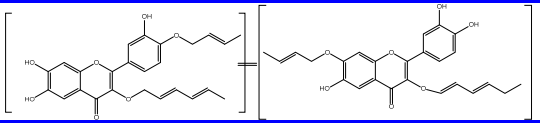	(438 + 438 + 55)
		Loss of side groups from parent compound	
8.	303	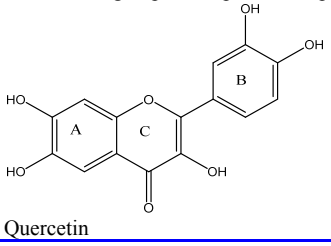 Quercetin	303
9.	285	Loss of OH from quercetin	303 - 17

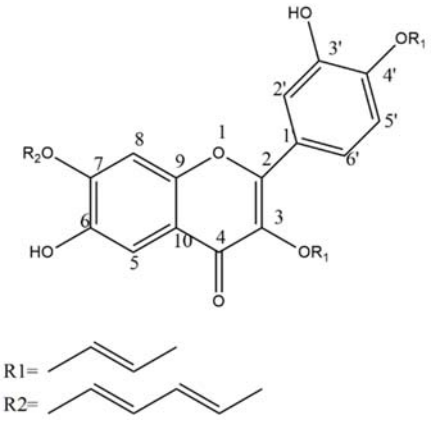

Fig. 3. Chemical structure of novel quercetin derivative isolated from *Terminalia chebula* fruit.

Table 6. The effect of flavonoid compound isolated from the fruit of *Terminalia chebula* on the viability of HepG2 and Chang liver cell by MTT assay. Results are expressed as mean ± SEM of six experiments. **P* < 0.05 Indicates statistically significant differences between two cell lines in each concentration.

Concentration (µg/mL)	Cell viability (%)	
	HepG2 cells	Chang liver
100	64.71 ± 0.38	45.32 ± 0.07
50	65.70 ± 0.87	57.00 ± 0.07
25	70.96 ± 0.33	60.12 ± 0.14
12.5	75.96 ± 0.86	73.00 ± 0.07
6.25	85.74 ± 0.86	81.79 ± 0.12
3.12	89.91 ± 0.99	92.48 ± 0.11*
1.56	92.35 ± 1.27*	95.44 ± 0.16*
0.78	94.37 ± 1.47*	97.68 ± 0.87*

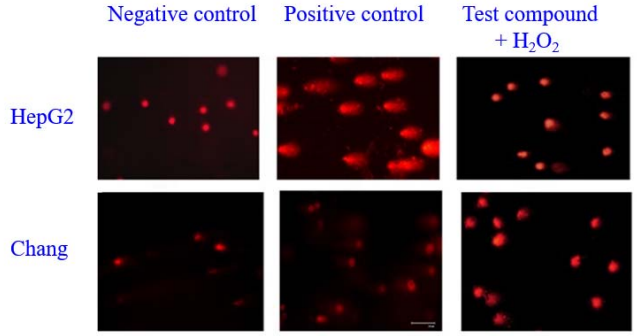

Fig. 4. The extent of DNA damage in HepG2 and Chang liver cells treated with the novel quercetin derivative isolated from *Terminalia chebula*. The untreated cells were designated as the negative control group while those treated with H_2O_2 were considered the positive control group.

Antigenotoxic effects of novel quercetin derivative on HepG2 and Chang liver cells

The antigenotoxic effect of the isolated compound on HepG2 and Chang liver cells was evaluated using an alkaline Comet assay (Fig. 4). The level of DNA damage was measured by comet length, tail length, and tail DNA percentage. The isolated quercetin compound recorded significant DNA damage in HepG2 and Chang liver cells. Table 7 shows the data for the antigenotoxicity calculation. Just before being exposed to H_2O_2, the cells were incubated for 1 h with a non-toxic concentration of the isolated compound. The cells were subsequently subjected to various concentrations of H_2O_2 and incubated for varying lengths of time. Because H_2O_2 at 50 µM for 15 min was found to be an adequate amount to induce a high level of DNA impairment, it was chosen for further research. Comet length, tail length, and tail DNA percentage were all measured in 100 cells per sample.

When the cells were exposed to H_2O_2, the comet length, tail length, and tail DNA percentage increased in comparison with the untreated cells. When the cells were pre-treated with the isolated compound, these parameters were found to decrease. Overall, the compound demonstrated significant protection against H_2O_2-induced DNA damage in both cells at the non-toxic concentration tested.

Table 7. Level of DNA damage in normal, control, and the isolated phenolic compound on HepG2 and Chang liver cells. Results are expressed as mean ± SEM, n = 6. *P < 0.05 Indicates significant differences compared to untreated cells as negative control.

Cell lines	Group	Comet length	Tail length	Tail DNA (%)
HepG2	Negative control	24.83 ± 5.8	1.66 ± 0.05	1.23 ± 0.03
	Positive control (H_2O_2)	94 ± 1.8*	27 ± 2.2*	20.6 ± 3.1*
	Test compound+ H_2O_2	70.86 ± 4.6*	4.66 ± 0.2*	4.4 ± 0.8*
Chang liver	Normal	23.12 ± 4.2	1.21 ± 0.0	1.5 ± 0.02
	H_2O_2	92.45 ± 3.5*	28.86 ± 2.1*	27.34 ± 2.3*
	Compound	56.97 ± 4.1*	4.2 ± 0.2*	4.2 ± 0.08*

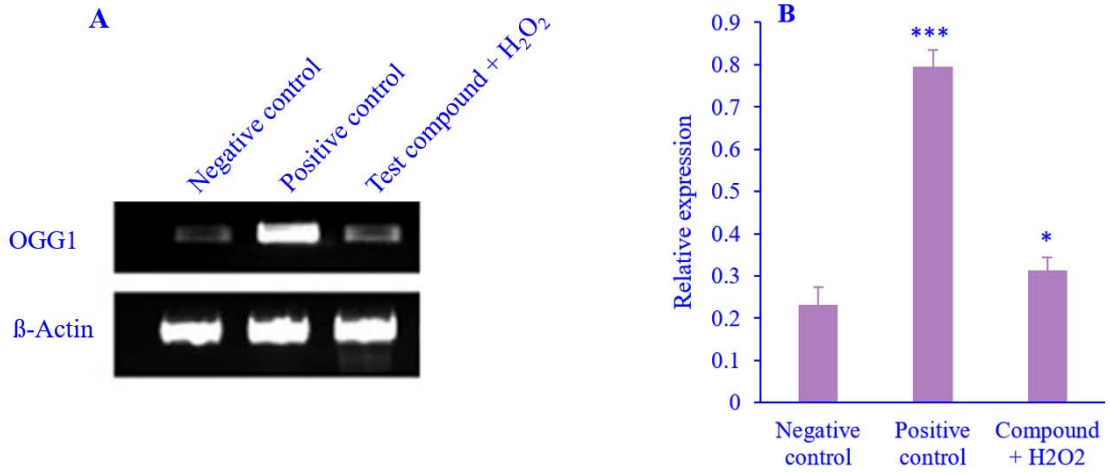

Fig. 5. The effect of H_2O_2 and test compound (novel quercetin derivative) isolated from *Terminalia chebula* on the relative expression of OGG1 in HepG2 cells. (A) Gel electrophoresis image OGG1 and β actin mRNA expression and (B) graphical representation of the relative expression of OGG1. The untreated cells were designated as the negative control group while those treated with H_2O_2 were considered the positive control group. Results are expressed as mean ± SEM; n = 6. *P < 0.05 and ***P < 0.001 indicate significant differences relative to negative control.

Effect of novel quercetin derivative on gene expression level in HepG2 and Chang liver cells

A gene expression study of an isolated phenolic compound in HepG2 and in Chang liver cells was performed by RT-PCR. The expression levels of OGG1 and NEIL1 in HepG2 cells (Figs. 5 and 6) were observed to be the highest under the H_2O_2 stress condition (0.796 and 1.002, respectively), indicating that these genes have an activating effect under these conditions. As shown in the figures, after treatment with the isolated compound, the expression level of OGG1 and NEIL1 was found to significantly decrease when compared to the H_2O_2-treated group. The isolated compound reduced OGG1 and NEIL1 levels in the HepG2 cell by 60.5% and 70.25% of those of the positive control groups, respectively.

In the case of untreated Chang liver cells, the expression levels of OGG1 and NEIL1 were found to be 0.994 and 0.323, respectively. Treating the cells with H_2O_2 at 50 M for 15 min resulted in high levels of OGG1 and NEIL1 expression. The pre-treatment with the isolated compound reduced the OGG1 and NEIL1 gene expression levels to 44.5% and 69.7% of that of the positive control groups, respectively (Figs. 7 and 8).

Overall results of the expression studies demonstrated that the isolated flavonoid compound can normalize the expression level of OGG1 and NEILl.

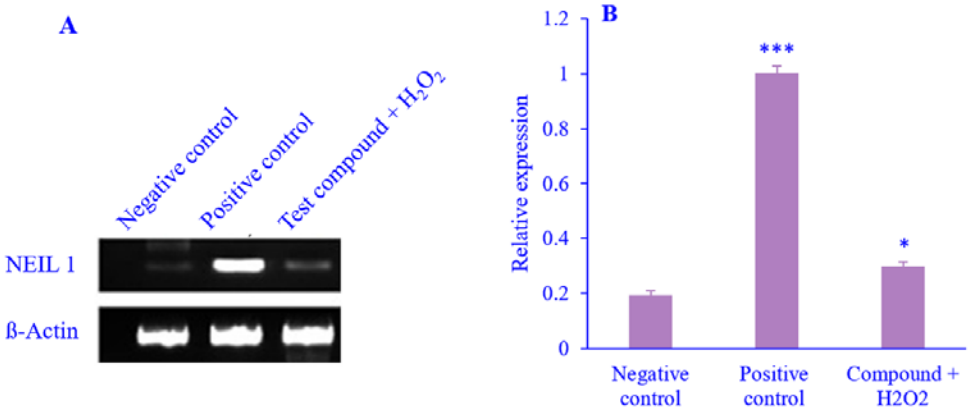

Fig. 6. The effect of H_2O_2 and test compound (novel quercetin derivative) isolated from *Terminalia chebula* on the relative expression of NEIL1 in HepG2 cells. (A]) Gel electrophoresis image for NEIL1 and β actin mRNA expression levels and (B) graphical representation of the relative expression of NEIL1 The untreated cells were designated as the negative control group while those treated with H_2O_2 were considered the positive control group. Results are expressed as mean ± SEM; n = 6. *$P < 0.05$ and ***$P < 0.001$ indicate significant differences relative to the negative control.

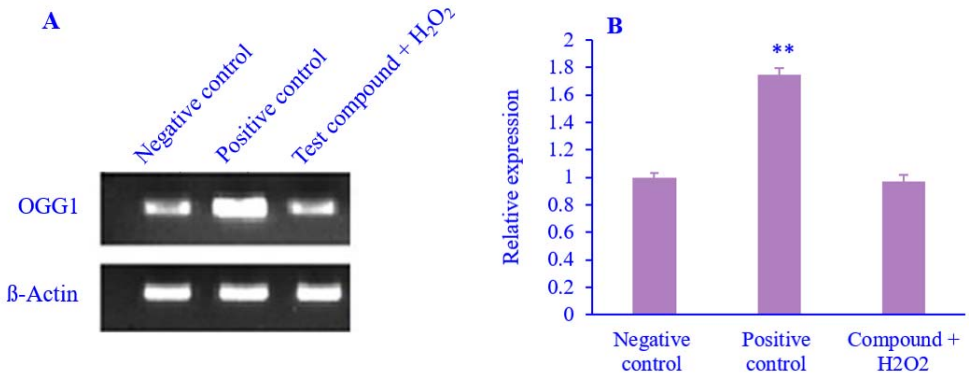

Fig. 7. The effect of H_2O_2 and test compound (novel quercetin derivative) isolated from *Terminalia chebula* on the relative expression of OGG1 in Chang liver cells. (A) Gel electrophoresis image for OGG1 and β actin mRNA expression levels and (B) graphical representation of the relative expression of OGG1 The untreated cells were designated as the negative control group while those treated with H_2O_2 were considered the positive control group. Results are expressed as mean ± SEM; n = 6. **$P < 0.01$ indicates significant differences relative to negative control.

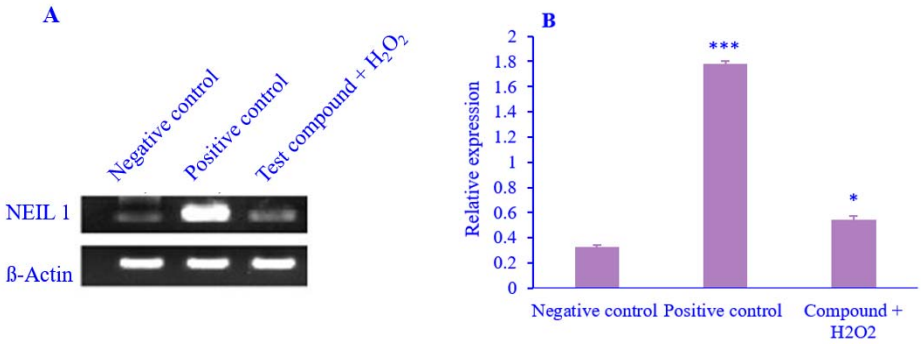

Fig. 8. The effect of H_2O_2 and test compound (novel quercetin derivative) isolated from *Terminalia chebula* on the relative expression of NEIL1 in Chang liver cells. (A) Gel electrophoresis image for NEIL1 and β actin mRNA expression levels and (B) graphical representation of the relative expression of NEIL1. The untreated cells were designated as the negative control group while those treated with H_2O_2 were considered the positive control group. Results are expressed as mean ± SEM; n = 6. *$P < 0.05$ and ***$P < 0.001$ indicate significant differences relative to negative control.

DISCUSSION

Oxidative damage to DNA due to ROS/reactive nitrogen species has been described to have a deleterious effect on the human body. A remarkable level of DNA damage has been widely accepted as the major cause of many maladies like cancer, neurodegenerative diseases, diabetes, and premature aging. Hence, the protection of DNA from the harmful effect of ROS has significant implications for the prevention of the above-mentioned diseases (18). An efficient antioxidative system can scavenge or detoxify the excess ROS; they comprise enzymatic (superoxide dismutase, catalase) and non-enzymatic components (glutathione) (19). Additionally, the cells have a network of DNA repair pathways to recognize and repair different types of lesions, and in this way, the equilibrium between DNA damage and repair is attained. However, erratically, the equilibrium can be disrupted; those systems would not be enough to counteract ROS action (20).

The liver is the chief organ attacked by ROS (21,22). The liver functions as one of the most indispensable organs in the body, playing a fundamental role in the regulation of diverse processes such as metabolism, secretion, storage, and detoxification of endogenous and exogenous substances (23,24). Considering these major functions, liver diseases account for a principal threat to public health. Moreover, it has been reported that the currently available synthetic drugs for hepatic diseases also cause supplementary damage to DNA (25,26). The present study delved into the promising DNA protective activity of a novel flavonoid isolated from *T. chebula* fruit on hepatic cells.

In this work, a novel flavonoid, (quercetin derivative) 7-(but-2-en-1-yloxy)-2-(4(but-2-en-1- yloxy)-3- hydroxyphenyl)-3- (hexa-2,4-dien-1-yloxy)-6-hydroxy-4H -chromen-4-one, isolated from *T. chebula* fruit was probed for the cytotoxic and protective effects on oxidative DNA damage in two cell lines, HepG2 and Chang liver cell. The results of the MTT assay confirmed that the isolated compound was relatively non-toxic at medium and lower concentrations to the cell lines. In the antigenotoxic activity study, we discovered that the isolated flavonoid had antigenotoxic properties against H_2O_2-induced damage in hepatic cells when administered prior to the genotoxic agents. Ascorbic acid was used as a positive control in this research. The data compiled from this study using comet analysis showed that in the presence of flavonoids, the number of comet-bearing cells was markedly reduced in each cell. At this time, we do not know the precise mechanism(s) underlying the antigenotoxic activity. However, the detected antigenotoxic properties of isolated phenolic molecules may be related to the synergistic action of mechanisms such as restriction of toxin penetration into cells, direct deactivation of toxins by scavenging, stimulation of detoxification, increase or decrease in cytotoxicity, activation of DNA repair enzymes, and structure-activity interaction (27-29). The detected protective effect of the molecule on the cell lines HepG2 and Chang liver may correspond to synergistic participation of the above-mentioned mechanism(s).

Gene expression analysis was carried out on the isolated compound in order to divulge whether this compound exerts DNA protection against oxidative damage either by enhancing DNA repair activity or simply by preventing oxidative damage due to its antioxidant activity. We have selected the best concentration for the isolated compound, which did not induce any toxicity to the cells, and the suitable condition (50 µM for 15 min) for hydrogen peroxide that would induce a significant amount of DNA damage without affecting the viability of the cell. Recognizing the facts mentioned above, we have proceeded to investigate the protective action of an isolated flavonoid compound against H_2O_2-induced oxidative DNA damage. Similar concentrations of H_2O_2 have been used in other studies with HepG2 cells (30).

H_2O_2 predominantly induces single-strand breaks in DNA, which could be repaired by the BER pathway (31). OGG1 and NEIL1 are the two major DNA glycosylases involved in the BER pathway. The potential of the isolated compound to protect DNA from strand breaks was investigated by the RT-PCR method. We

have detected an increase in the mRNA levels of OGG1 and NEIL1 in two cell lines after H_2O_2 treatment. The isolated compound decreased the level of OGG1 and NEIL1. On DNA protection, after a short period of treatment (1 h) with isolated flavonoids, it has exhibited a maximum protective effect against H_2O_2-induced DNA damage in HepG2 and Chang liver cells. Earlier, Kim *et al.* reported that 7,8-dihydroxyflavone induces OGG1 expression *via* the PI3K-Akt pathway and protects cells against oxidative DNA base damage by activating DNA repair systems (31). Kang *et al.* also demonstrated that 7,8-dihydroxyflavone augments the cellular antioxidant defense capacity through activation of the Nrf2/H-1 pathway, which also involves the activation of the PI3K/Akt and ERK pathways, thereby protecting C2C12 myoblasts from H_2O_2-induced oxidative cytotoxicity (32).

The outcome of an isolated compound on recovery from DNA oxidative damage can be explained by two mechanisms, either the capability to enhance the activity of repair enzymes or (ii) absolute and direct protection against oxidation (33). The strong protective effect against oxidative damage for the pre-treated sample suggested that the isolated compound acted through a second mechanism. Protection of DNA from strand breakage together with the increased antioxidant activity exerted by this compound can account for the significant reduction of endogenous oxidative damage.

CONCLUSIONS

Contemplating the empirical evidence, we can culminate that the isolated compound, 7-(but-2-en-1-yloxy)-2-(4(but-2-en-1-yloxy)-3-hydroxyphenyl)-3-(hexa-2,4-dien-1-yloxy)-6-hydroxy-4H-chromen-4-one, has effectively normalized the expression levels of OGG1 and NEIL1 when compared to the untreated cells. The action of the isolated compound seems to be associated with its efficacy on ROS scavenging property, which has major implications for the prevention of H_2O_2-induced strand breakages. This study corroborated the strong hepatoprotective action of a novel flavonoid isolated from *T. chebula*. The active ingredients that trigger these antioxidative activities, however, are currently unknown. Further pharmacological studies must be supplemented by *in vivo* studies to gain a better understanding of the novel compound's mechanism of action, which may pave the way for the invention of an entirely novel therapeutic natural drug.

Acknowledgments

This study was supported by the Council of Scientific and Industrial Research (Sr. No. 1061210077), India. We are also thankful to Mrs. Vidya, Calicut University, Kerala, India for the service provided for cell line studies.

Conflict of interest statement

The authors declared no conflict of interest in this study.

Authors' contributions

K. Soumya performed all the experiments; K.R. Haridas performed structural characterization of the compound; J. James supported conducting experimental parts; S. Sudheesh conceived the original idea, supervised, and funded the project. The final version of the article was read and approved by all authors.

REFERENCES

1. Maynard S, Schurman SH, Harboe C, de Souza-Pinto NC, BohrM VA. Base excision repair of oxidative DNA damage and association with cancer and aging. Carcinogenesis. 2009;30(1):2-10. DOI: 10.1093/carcin/bgn250.
2. Poetsch AR, Boulton SJ, Luscombe NM. Genomic landscape of oxidative DNA damage and repair reveals regioselective protection from mutagenesis. Genome Biol. 2018;19(1):215,1-23. DOI: 0.1186/s13059-018-1582-2.
3. Lee MR, Kim SH, Cho HJ, Lee KY, Moon AR, Jeong HG, *et al*. Transcription factors NF-YA regulate the induction of human OGG1 following DNA-alkylating agent methylmethane sulfonate (MMS) treatment. J Biol Chem. 2004;279(11):9857-9866. DOI: 10.1074/jbc.M311132200.
4. Whitaker AM, Schaich MA, Smith MR, Flynn TS, Freudenthal BD. Base excision repair of oxidative DNA damage: from mechanism to disease. Front Biosci. 2017;22(9):1493-1522. DOI: 10.2741/4555.
5. Aguiar PHN, Furtado C, Repolês BM, Ribeiro GA, Mendes IC, Peloso EF, *et al*. Oxidative stress and

DNA lesions: the role of 8-oxoguanine lesions in *Trypanosoma cruzi* cell viability. PLoS Negl Trop Dis. 2013;7(6):e2279,1-13. DOI: 10.1371/journal.pntd.0002279.
6. Hu J, de Souza-Pinto NC, Haraguchi K, Hogue BA, Jaruga P, Greenberg MM, et al. Repair of formamidopyrimidines in DNA involves different glycosylases: role of the OGG1, NTH1, and NEIL1 enzymes. J Biol Chem. 2005;280(49):40544-40551. DOI: 10.1074/jbc.M508772200.
7. Saleem A, Husheem M, Härkönen P, Pihlaja K. Inhibition of cancer cell growth by crude extract and the phenolics of *Terminalia chebula retz*. fruit. J Ethnopharmacol. 2002;81(3):327-336. DOI: 10.1016/S0378-8741(02)00099-5.
8. Soumya K, Haridas KR, James J, Kumar VBS, Edatt L, Sudheesh S. Study of *in vitro* antioxidant and DNA damage protection activity of a novel luteolin derivative isolated from *Terminalia chebula*. J Taibah Univ Sci. 2019;13:755-763. DOI: 10.1080/16583655.2019.1630892.
9. Soumya K, Jesna J, Sudheesh S. Screening study of three medicinal plants for their antioxidant and cytotoxic activity. Int J Pharm Sci Res. 2018;9(9):3781-3787. DOI: 10.13040/IJPSR.0975-8232.9(9).3781-87.
10. Malekzadeh F, Ehsanifar H, Shahamat M, Levin M, Colwell RR. Antibacterial activity of black myrobalan (*Terminalia chebula Retz*) against helicobacter pylori. Int J Antimicrob Agents. 2001;18(1):85-88. DOI: 10.1016/S0924-8579(01)00352-1.
11. Dutta BK, Rahman I, Das TK. Antifungal activity of Indian plant extracts. Mycoses. 1998;41(11-12):535-536. DOI: 10.1111/j.1439-0507.1998.tb00718x.
12. Shabrina R, Elya B, Noviani A. Antioxidant activities of fractions from ethyl acetate extracts of *Garcinia fruticosa* lauterb leaves. Int J Appl Pharm. 2018;10(1):44-50. DOI: 10.22159/ijap.2018.v10s1.10.
13. Swamy SM, Tan BK. Cytotoxic and immunopotentiating effects of ethanolic extract of *Nigella sativa* L. seeds. J Ethnopharmacol. 2000;70(1):1-7. DOI: 10.1016/S0378-8741(98)00241-4.
14. Auddy B, Ferreira M, Blasina F, Lafon L, Arredondo F, Dajas F, *et al*. Screening of antioxidant activity of three indian medicinal plants, traditionally used for the management of neurodegenerative diseases. J Ethnopharmacol. 2003;84(2-3):131-138. DOI: 10.1016/S0378-8741(02)00322-7.
15. Kang C, Lee H, Yoo YS, Hah DY, Kim CH, Kim E, *et al*. Evaluation of oxidative DNA damage using an alkaline single cell gel electrophoresis (SCGE) comet assay, and the protective effects of N-acetylcysteine amide on zearalenone-induced cytotoxicity in chang liver cells. Toxicol Res. 2013;29(1):43-52. DOI: 10.5487/TR.2013.29.1.043.
16. Leandro LF, Munari CC, Sato VLFL, Alves JM, de Oliveira PF, Mastrocola DFP, *et al*. Assessment of the genotoxicity and antigenotoxicity of (+)-usnic acid in V79 cells and Swiss mice by the micronucleus and comet assays. Mutat Res. 2013;753(2):101-106. DOI: 10.1016/j.mrgentox.2013.03.006.
17. Lei YX, Lu Q, Shao C, He CC, Lei ZN, Lian YY. Expression profiles of DNA repair-related genes in rat target organs under subchronic cadmium exposure. Genet. Mol. Res.2015;14(1):515-524. DOI: 10.4238/2015.January.26.5.
18. Pilařová V, Kuda L, Vlčková HK, Nováková L, Gupta S, Kulkarni M, *et al*. Carbon dioxide expanded liquid: an effective solvent for the extraction of quercetin from South African medicinal plants. Plant Methods. 2022;18(1):87,1-13. DOI: 10.1186/s13007-022-00919-6.
19. Silva JP, Gomes AC, Proença F, Coutinho OP. Novel nitrogen compounds enhance protection and repair of oxidative DNA damage in a neuronal cell model: comparison with quercetin. Chem Biol Interact. 2009;181(3):328-337. DOI: 10.1016/j.cbi.2009.07.024.
20. Ramos AA, Azqueta A, Pereira-Wilson C, Collins AR. Polyphenolic compounds from salvia species protect cellular DNA from oxidation and stimulate DNA repair in cultured human cells. J Agric Food Chem. 2010;58(12):7465-7471. DOI: 10.1021/jf100082p.
21. García-Rodríguez A, Gosálvez J, Agarwal A, Roy R, Johnston S. DNA damage and repair in human reproductive cells. Int J Mol Sci. 2019;20(1): 31,1-22. DOI: 10.3390/ijms20010031.
22. Li S, Tan HY, Wang N, Zhang ZJ, Lao L, Wong CW, *et al*. The role of oxidative stress and antioxidants in liver diseases. Int J Mol Sci. 2015;16(11):26087-26124. DOI: 10.3390/ijms161125942.
23. Madrigal-Santillán E, Madrigal-Bujaidar E, Álvarez-González I, Sumaya-Martinez MT, Gutiierrez-Salinas J, Bautisa M, *et al*. Review of natural products with hepatoprotective effects. World J Gastroenterol. 2014;20(40):14787-14804. DOI: 10.3748/wjg.v20.i40.14787.
24. Srivastava R, Srivastava P. Hepatotoxicity and the role of some herbal hepatoprotective plants in present scenario. Global J Dig Dis. 2018;3:1-4. DOI: 10.4172/2472-1891.100034.
25. Linares V, Alonso V, Albina ML, Bellés M, Sirvent JJ, Domingo JL, *et al*. Lipid peroxidation and antioxidant status in kidney and liver of rats treated with sulfasalazine. J Toxicol. 2009;256(3):152-156. DOI: 10.1016/j.tox.2008.11.010.
26. Kilani-Jaziri S, Bhouri W, Skandrani I, Limem I, Chekir-Ghedira L, Ghedira K. Phytochemical, antimicrobial, antioxidant and antigenotoxic potentials of Cyperus rotundus extracts. S. Afr. J. Bot. 2011;77(3):767-776. DOI: 10.1016/j.sajb.2011.03.015.
27. Prajitha V, Thoppi J.E. Genotoxic and antigenotoxic potential of the aqueous leaf extracts of *Amaranthus spinosus* Linn. using *Allium cepa* assay. S Afr J Bot 2016;102:18-25. DOI: 10.1016/j.sajb.2015.06.018.

28. Prieto AM, dos Santos AG, Oliveira APS, Cavalheiro AJ, Silva DHS, Bolzani VS, *et al*. Assessment of the chemopreventive effect of casearin B, a clerodane diterpene extracted from *Casearia sylvestris* (Salicaceae). Food Chem Toxicol. 2013;53:153-159. DOI: 10.1016/j.fct.2012.11.029.
29. Benhusein GM, Mutch E, Aburawi S, Williams FM. Genotoxic effect induced by hydrogen peroxide in human hepatoma cells using comet assay. Libyan J Med. 2010;5:1-6. DOI: 10.3402/ljm.v5i0.4637.
30. Ismail IH, Nyström S, Nygren J, Hammarsten O. Activation of ataxia telangiectasia mutated by DNA strand break-inducing agents correlates closely with the number of DNA double strand breaks. J Biol Chem. 2005;280(6):4649-4655. DOI: 10.1074/jbc.M411588200.
31. Kim KC, Lee IK, Kang KA, Cha JW, Cho SJ, Na SY, *et al*. 7,8-Dihydroxyflavone suppresses oxidative stress-induced base modification in DNA via induction of the repair enzyme 8-oxoguanine DNA glycosylase-1. Biomed Res Int. 2013;2013:863720,1-10. DOI: 10.1155/2013/863720.
32. Kang JS, Choi IW, Han MH, Kim GY, Hong SH, Park C, *et al*. The cytoprotective effects of 7,8-dihydroxyflavone against oxidative stress are mediated by the upregulation of Nrf2-dependent HO-1 expression through the activation of the PI3K/Akt and ERK pathways in C2C12 myoblasts. Int J Mol Med. 2015;36(2): 501-510. DOI: 10.3892/ijmm.2015.2256.
33. Silva JP, Gomes AC, Coutinho OP. Oxidative DNA damage protection and repair by polyphenolic compounds in PC12 cells. Eur J Pharmacol. 2008;601(1-3):50-60. DOI: 10.1016/j.ejphar.2008.10.046.

Research in Pharmaceutical Sciences, June 2024; 19(3): 319-327
Received: 12-08-2023
Peer Reviewed: 10-09-2023
Revised: 19-09-2023
Accepted: 16-01-2024
Published: 01-07-2024

School of Pharmacy & Pharmaceutical Sciences
Isfahan University of Medical Sciences

Original Article

The effect of *Dracocephalum subcapitatum* hydroalcoholic extract on dexamethasone-induced hyperlipidemic rats

Leila Safaeian[1,*], Zeinab Yazdiniapour[2], Sara Hajibagher[1], Zohreh Bakhtiari[2], and Paridokht Karimian[3]

[1]*Department of Pharmacology and Toxicology and Isfahan Pharmaceutical Sciences Research Center, School of Pharmacy and Pharmaceutical Sciences, Isfahan University of Medical Sciences, Isfahan, Iran.*
[2]*Department of Pharmacognosy, School of Pharmacy and Pharmaceutical Sciences, Isfahan University of Medical Sciences, Isfahan, Iran.*
[3]*Department of Pathology, Medical School, Guilan University of Medical Sciences, Rasht, Iran.*

Abstract

Background and purpose: Recent data show the antihyperlipidemic activities of some plants belonging to the genus *Dracocephalum*. In this study, the effects of hydroalcoholic extract of *D. subcapitatum* (O. Kuntze) Lipsky aerial parts were evaluated in a model of hyperlipidemia induced by dexamethasone.
Experimental approach: The extract was prepared by maceration method and its total phenolic content was determined. Seven groups of 6 Wistar rats were used as follows: group 1 (normal control) received vehicle; group 2 (extract control) treated only with 200 mg/kg *D. subcapitatum*; group 3 (hyperlipidemia control) received dexamethasone (10 mg/kg/day, subcutaneously); group 4 (reference) received dexamethasone and atorvastatin (40 mg/kg, orally), and groups 5-7 (test groups) received dexamethasone and simultaneously treated orally with 50, 100, or 200 mg/kg *D. subcapitatum*. All treatments were done for 1 week. Serum lipid profile, fasting blood glucose, malondialdehyde concentration, and liver histopathology were examined.
Findings/Results: Total phenolic content was 77.34 ± 4.9 mg/g as gallic acid equivalent. Treatment with *D. subcapitatum* (200 mg/kg) meaningfully declined triglycerides, total cholesterol, low-density lipoprotein, very low-density lipoprotein, blood glucose, alanine aminotransferase, aspartate aminotransferase, and malondialdehyde levels, and alleviated hepatic steatosis in dexamethasone-induced dyslipidemic rats.
Conclusion and implications: Findings of the current study suggest that *D. subcapitatum* may be effective in the management of hyperlipidemia. Further studies are necessary to determine the clinical efficacy of this treatment and to understand the underlying mechanisms responsible for its ability to lower lipid levels.

Keywords: Dracocephalum; Hyperlipidemias; Hyperglycemias; Lipid peroxidation; Dexamethasone; Rats.

INTRODUCTION

Hyperlipidemia or disorders of lipid metabolism are generally realized with an increase in the plasma levels of lipids and various lipoproteins (1). Hyperlipidemia is known as an important risk factor for the development and progression of cardiovascular diseases such as atherosclerosis and heart attack (2). Primary hyperlipidemia is rarely caused by genetic abnormalities and usually occurs because of unhealthy diet and inactivity (3). Secondary hyperlipidemia may be caused by diabetes, hormonal changes, excessive alcohol consumption, and adverse effects of medications (4).

Oxidative stress which arises from the high creation of reactive oxygen species (ROS) and diminished efficiency of the antioxidative defense pathway plays a great impact on dyslipidemia and the development of atherogenic particles. Many investigations have documented the significant relationship between plasma levels of oxidative stress markers such as malondialdehyde (MDA) and atherogenic disorders (5).

*Corresponding author: L. Safaeian
Tel: +98-3137927087, Fax: +98-3136680011
Email: leila_safaeian@pharm.mui.ac.ir

Access this article online

Website: http://rps.mui.ac.ir

DOI: 10.4103/RPS.RPS_148_23

Various cholesterol and triglyceride-lowering drugs including statins, fibrates, bile acid sequestrants, and cholesterol absorption inhibitors are currently used for managing hyperlipidemia however there is still no certain cure and the available drugs have many side effects (1).

Medicinal plants have been of interest since ancient times for finding novel effective treatments for many diseases (6). Some medicinal herbs and phytochemicals have been defined for their therapeutic value in hyperlipidemia (7).

The genus *Drcacephalum* is one of the genera in *Lamiaceae* family, with approximately 70 species worldwide, 11 of which are found in Iran. The plants of this genus grow naturally in the temperate areas of the Northern Hemisphere (8,9). There are many phytochemical compounds such as alkaloids, flavonoids, terpenoids, lignans, and coumarins in this genus. Various medicinal uses for the treatment of cardiovascular, respiratory, gastrointestinal, and inflectional diseases have been reported for different *Drcacephalum* plants (10).

D. subcapitatum (O. Kuntze) Lipsky is a local wild plant in Northeastern Khorasan in Iran (11). The phylogenetic examination of *Dracocephalum* species displays that *D. subcapitatum* is more closely related to *D. kotschyi* than other species (12). Several flavonoids and terpenoids have been identified in *D. subcapitatum* (11). Although little information is available about the biological effects of *D. subcapitatum*, many pharmacological properties such as antihyperlipidemic, antidiabetic, and antioxidant effects have been recognized for flavonoids and terpenoids as the bioactive substances that are also present in this plant (13,14). The current study was designed to investigate the possible antihyperlipidemic and antioxidant effects of hydroalcoholic extract of *D. subcapitatum* aerial parts in a rat model of hyperlipidemia induced by dexamethasone.

MATERIALS AND METHODS

Plant material and preparation of extract

Aerial parts of *D. subcapitatum* were collected from mountains in Gifan region (North Khorasan Province) in the northeastern part of Iran. After approval of the plant by a botanist, a voucher specimen (SAM4021) was stored in the Herbarium of the Department of Pharmacognosy, Isfahan University of Medical Sciences. The dried and pulverized aerial parts of *D. subcapitatum* (200 g) were soaked with 70% ethanol for preparation of hydroalcoholic extract by maceration technique for 72 h, 4 times (15). Then plant extract was separated using a vacuum system and ethanol was removed by rotary evaporation at 40 °C. The remaining water was separated with a freeze dryer and the obtained dried extract was kept at 4 °C. The yield of *D. subcapitatum* extraction was 35.5% (w/w). For oral administration in rats, the extract powder was suspended in water and administered using an intra-gastric tube.

Determination of total phenolic content

The amount of phenolic compound in *D. subcapitatum* extract was measured by Folin Ciocalto assay. This method is a colorimetric technique based on the reduction of reagent (a mixture of phosphotungstate and phosphomolybdate) in the reaction with phenolic compounds.

Briefly, the standard or extract samples were mixed with sodium bicarbonate (20%) and then with diluted Folin-Ciocalteu reagent. After 2 h of storage at room temperature, the absorbance was read by a spectrophotometer at 765 nm. Quantitation of total phenolic content in the samples was performed using a standard curve obtained from various concentrations of gallic acid (0-500 mg/L). The results were specified in terms of mg of gallic acid equivalents (GAE)/g of dried extract (16).

Animals

Forty-two male Wistar rats (230-250 g) grown in the animal house of the School of Pharmacy and Pharmaceutical Sciences (Isfahan, Iran) were used in this study. Animals were housed under standard laboratory conditions including room temperature of 20-25 ℃ with a standard diet and water and a daily routine with a 12/12-h light/dark cycle. Rats were acclimatized for one week prior to the experimentation. The research procedures were in accordance with international

guidelines for laboratory animal use and care, and ethical approval was obtained from the Institutional Research Ethics Committee of Isfahan University of Medical Sciences (Ethic No. IR.MUI.AEC.1401.018).

Induction of hyperlipidemia

The glucocorticoid model of hyperlipidemia was established by subcutaneous (s.c.) administration of 10 mg/kg dexamethasone (Darou Pakhsh Pharmaceutical Co., Iran) for 7 days in rats (17). The weight of animals was recorded at the start of the experiment and then every other day. At the end of the trial period, all rats were kept fasting overnight and the blood samples were collected from the retro-orbital sinus under anesthesia with ketamine (70 mg/kg)/xylazine (10 mg/kg). The serum samples were used for biochemical assessments. Liver tissue was also isolated from sacrificed rats and immersed in a 10% neutral-buffered formalin solution after weighing. Tissue samples were examined histologically after further processing.

Experimental protocol

Rats were randomly divided into 7 groups, 6 each, as follows: Group one, as the normal control received a daily injection of normal saline (1 mL/kg, s.c.) and oral administration of the vehicle (water); Group two, as the extract control, animals were treated only with *D. subcapitatum* hydroalcoholic extract orally at the dose of 200 mg/kg; Group 3, as the hyperlipidemic control group received dexamethasone (10 mg/kg/day, s.c.); Group 4, as the reference group, atorvastatin (40 mg/kg, orally; Abidi Pharmaceutical Laboratories Co., Iran) was administered simultaneously with dexamethasone (18); Groups 5-7 as the test groups were treated with dexamethasone and simultaneously with 50, 100, or 200 mg/kg of *D. subcapitatum* extract orally (19). All treatments were completed over 7 days.

Biochemical analysis

The serum content of blood glucose and lipid profile including triglycerides, total cholesterol, low-density lipoprotein (LDL)-cholesterol and high-density lipoprotein (HDL)-cholesterol, and also liver enzymes including alanine aminotransferase (ALT) and aspartate aminotransferase (AST) were determined using biochemical colorimetric kits produced by Pars Azmoon Company (Tehran, Iran). The level of very low-density lipoprotein (VLDL)-cholesterol was calculated by dividing the triglyceride level by 5 (20).

For the determination of lipid peroxidation, the serum content of MDA was assessed using a standard kit based on thiobarbituric acid reactive substances test. The absorbance of the final-colored complex was measured spectrophotometrically at 532 nm. The standard curve was drawn using different concentrations of MDA tetrabutyl ammonium.

Histopathological analysis

After fixation in formalin solution, the liver tissue specimens were processed through sequential stages including dehydrating in ascending grades of alcohol and then clearing using xylene, embedding in paraffin, sectioning at 5-µm thickness, deparaffinization, rehydrating, and finally staining with hematoxylin and eosin (H&E), mounting onto glass slides, and cover-slipping for microscopic observations regarding histopathological changes.

Statistical analysis

Data were reported as mean ± SEM and subjected to one-way analysis of variance (ANOVA) followed by Tukey post-hoc test on SPSS 25.0. The *P*-values < 0.05 were considered statistically significant.

RESULTS

Total phenolic content

The hydroalcoholic extract of *D. subcapitatum* aerial parts was evaluated for the total phenolic content. The calibration curve was drawn by linear regression for various concentrations of gallic acid. The regression equation was $y = 0.0023x + 0.0804$, in which x is the concentration of gallic acid in the sample (mg/L) with the correlation co-factor $R^2 = 0.994$. The total phenolic content of *D. subcapitatum* extract was assessed as 77.34 ± 4.9 mg GAE per gram of the dried plant extract.

Table 1. The effect of hydroalcoholic extract of *Dracocephalum subcapitatum* on serum biochemical parameters in dexamethasone-induced hyperlipidemic rats. Values are mean ± SEM, n = 6. $^{\#}P < 0.05$, $^{\#\#}P < 0.01$ and $^{\#\#\#}P < 0.001$ indicate significant differences compared to the normal control; and $^{*}P < 0.05$, $^{**}P < 0.01$, and $^{***}P < 0.001$ versus DEX control.

Groups	TG (mg/dL)	TC (mg/dL)	LDL (mg/dL)	VLDL (mg/dL)	HDL (mg/dL)	FBS (mg/dL)	AST (IU/L)	ALT (IU/L)
Normal control	80.5 ± 11.3	86.4 ± 7.5	11.2 ± 0.9	16.1 ± 5.2	58.8 ± 5.4	81.2 ± 5.1	143.3 ± 8.2	90.9 ± 9.2
DSE control (200 mg/kg)	94.0 ± 13.2	74.2 ± 5.0	10.0 ± 1.1	18.8 ± 2.1	67.0 ± 3.1	78.3 ± 4.0	168.0 ± 6.3	109.2 ± 10.1
DEX control (10 mg/kg)	271.1 ± 25.3$^{\#\#\#}$	128.1 ± 12.3$^{\#}$	17.2 ± 1.3$^{\#}$	54.2 ± 2.2$^{\#\#\#}$	52.1 ± 1.7$^{\#}$	134.3 ± 3.7$^{\#}$	241.2 ± 21.2$^{\#\#\#}$	216.1 ± 25.0$^{\#\#}$
DEX + ATOR (40 mg/kg)	88.2 ± 15.1***	85.3 ± 3.8*	12.5 ± 1.2	17.6 ± 2.4***	48.5 ± 3.0	86.5 ± 2.1***	173.1 ± 8.0*	78.5 ± 8.2***
DEX + DSE (50 mg/kg)	310.3 ± 8.9	98.1 ± 5.4	12.0 ± 1.4	62.0 ± 3.7	42.1 ± 2.3	91.5 ± 3.0***	240.1 ± 15.5	247.0 ± 24.1
DEX + DSE (100 mg/kg)	189.0 ± 20.4*	95.3 ± 6.9	13.2 ± 1.5	37.8 ± 4.1*	57.2 ± 4.3	90.1 ± 6.2***	159.6 ± 15.4**	160.1 ± 20.2
DEX + DSE (200 mg/kg)	145.5 ± 18.6***	70.4 ± 9.9***	8.1 ± 0.4***	29.1 ± 3.0***	59.5 ± 4.1	94.5 ± 5.1***	163.3 ± 14.1**	143.3 ± 17.3*

ALT, Alanine aminotransferase; AST, aspartate aminotransferase; ATOR, atorvastatin; DEX, dexamethasone; DSE, *Dracocephalum subcapitatum* extract; FBS, fasting blood sugar; HDL, high-density lipoprotein-cholesterol; LDL, low-density lipoprotein-cholesterol; TC, total cholesterol; TG, triglycerides; VLDL, very low-density lipoprotein-cholesterol.

Effect of D. subcapitatum on biochemical parameters

As shown in Table 1, exposure of animals to dexamethasone (10 mg/kg) led to a significant upsurge in blood levels of triglyceride, total cholesterol, LDL, VLDL, and fasting blood sugar, and a notable reduction in HDL in comparison with the normal control group. Dexamethasone also resulted in a large elevation in serum activities of liver enzymes including AST and ALT. Administration of atorvastatin as a standard antihyperlipidemic agent significantly decreased serum content of triglycerides (67.4%), total cholesterol (33.4%), VLDL (67.5%), fasting blood glucose (35.6%), AST (28.2%) and ALT (63.7%) compared to the dyslipidemic control group (dexamethasone-administered control group) without any significant effect on HDL level.

Treatment of rats with hydroalcoholic extract of *D. subcapitatum* at all administered doses significantly decreased fasting blood glucose. The high dose of *D. subcapitatum* extract resulted in a significant reduction of 46.32% in triglycerides, 45.04% in total cholesterol, 52.90% in LDL, 46.31% in VLDL, and 29.63% in fasting blood glucose levels, and 32.29% in AST and 33.69% in ALT activities in hyperlipidemic animals compared to the control group received dexamethasone. Though, no meaningful result was observed on HDL value (Table 1).

Assessment of lipid peroxidation displayed that dexamethasone significantly increased the serum content of MDA compared to the normal control. Treatment with *D. subcapitatum* extract at 200 mg/kg and also with atorvastatin showed an anti-lipid peroxidation effect in hyperlipidemic animals (Fig. 1).

Effect of D. subcapitatum on body and liver weight

Our results exhibited that dexamethasone strictly decreased the rats' body weight during the induction of dyslipidemia. Treatment with atorvastatin and *D. subcapitatum* extract was not able to prevent body weight loss induced by dexamethasone. The relative weight of the liver (liver/body weight ratio) was markedly enlarged in dexamethasone-induced dyslipidemic animals when compared with normal rats. Administration of atorvastatin and *D. subcapitatum* extract at 200 mg/kg prevented liver weight gain induced by dexamethasone (Table 2).

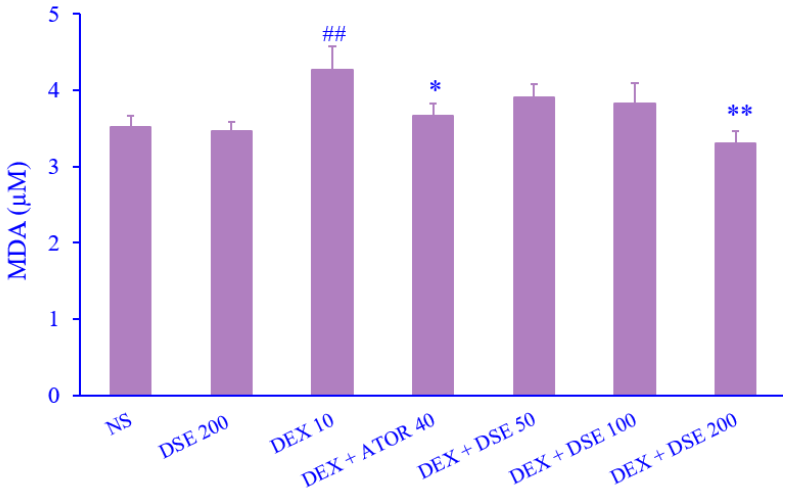

Fig. 1. Effects of *Dracocephalum subcapitatum* extract (50, 100, and 200 mg/kg) and atorvastatin (40 mg/kg) on serum malondialdehyde level in dexamethasone-induced hyperlipidemic rats. Values are mean ± SEM; n = 6. $^{\#\#}P < 01$ indicates a significant difference compared to the normal control; and $^{*}P < 0.05$ and $^{**}P < 0.01$ versus DEX control. ATOR, atorvastatin; DEX, dexamethasone; DSE, *Dracocephalum subcapitatum* extract; MDA, malondialdehyde.

Table 2. The effect of hydroalcoholic extract of *Dracocephalum subcapitatum* on body and liver weight in dexamethasone-induced hyperlipidemic rats. Values are mean ± SEM, n = 6. $^{\#}P < 0.05$, $^{\#\#}P < 0.01$, and $^{\#\#\#}P < 0.001$ indicate significant differences compared to the normal control; $^{*}P < 0.05$ versus DEX control.

Groups	Initial body weight (g)	Final body weight (g)	Body weight changes (%)	Relative liver weight (%)
Normal control	210.4 ± 9.7	216.3 ± 8.5	+2.80 ± 0.13	3.83 ± 0.12
DSE control (200 mg/kg)	190.3 ± 7.5	201.6 ± 5.9	+5.93 ± 0.25$^{\#}$	3.95 ± 0.06
DEX control	230.6 ± 10.2	212.5 ± 6.4	-7.85 ± 0.39$^{\#\#\#}$	5.11 ± 0.18$^{\#\#\#}$
DEX + ATOR (40 mg/kg)	241.5 ± 4.9	223.0 ± 9.5	-7.66 ± 0.94$^{\#\#\#}$	4.10 ± 0.13
DEX + DSE (50 mg/kg)	220.6 ± 9.3	200.7 ± 10.7	-9.02 ± 0.15$^{\#\#\#}$	5.55 ± 0.11$^{\#\#\#}$
DEX + DSE (100 mg/kg)	189.7 ± 10.2	179.9 ± 8.9	-5.16 ± 0.13$^{\#\#\#}$	4.76 ± 0.07$^{\#\#\#}$
DEX + DSE (200 mg/kg)	235.0 ± 9.4	215.6 ± 10.1	-8.25 ± 0.17$^{\#\#\#}$	4.54 ± 0.09$^{\#\#, *}$

ATOR, Atorvastatin; DEX, dexamethasone; DSE, *Dracocephalum subcapitatum* extract.

Effect of D. subcapitatum on liver histopathology

Assessment of liver sections of normal control animals and rats that were treated only with *D. subcapitatum* extract for histopathological alterations showed the typical architecture of the normal hepatocytes (Fig. 2A and B). In dexamethasone-treated animals, there was fatty degeneration, diffused steatosis of hepatic parenchymal cells, and cellular swelling (Fig. 2C). Histopathological examination of liver sections of rats treated with atorvastatin (Fig. 2D) and with *D. subcapitatum* extract at 50, 100, and 200 mg/kg (Fig. 2E-G) showed a great extent of improvement in liver histopathological alterations as decreasing in micro- and macro-vesicular fat accumulation especially at the high dose of extract.

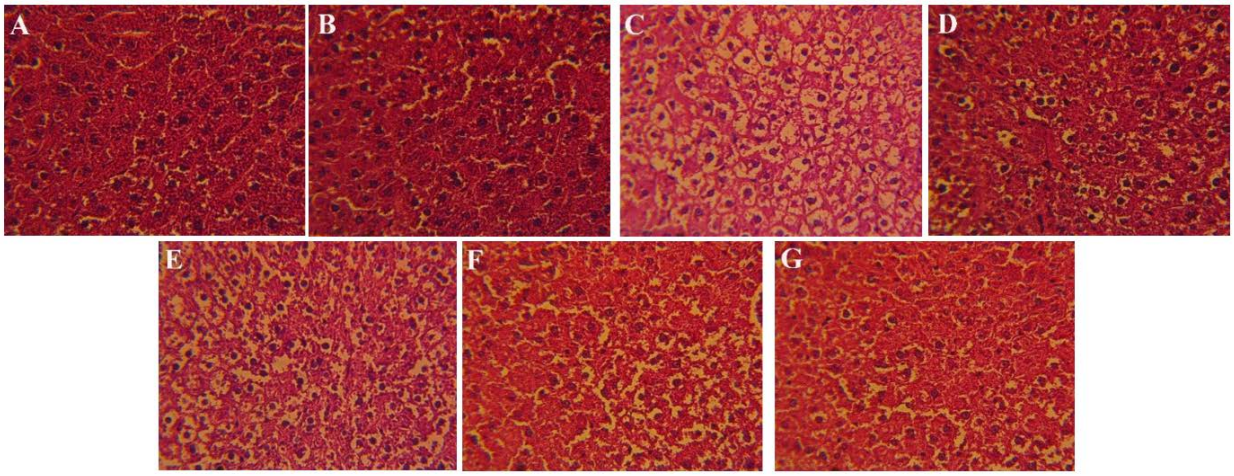

Fig. 2. Representative hematoxylin and eosin histological sections of the liver tissue of (A) normal control group and (B) *Dracocephalum subcapitatum* extract alone-treated group showing normal hepatocytes appearance; (C) dexamethasone-induced hyperlipidemic group indicating diffused steatosis, fatty degeneration, and cellular swelling; (D) atorvastatin-treated group showing mild vesicular steatosis; (E-G) *Dracocephalum subcapitatum* extract-treated groups with doses of 50, 100, and 200 mg/kg showing moderate vesicular steatosis. Magnification: ×400.

DISCUSSION

In this animal model of hyperlipidemia, the effects of hydroalcoholic extract of *D. subcapitatum* aerial parts as a *Drcacephalum* plant with limited pharmacological data were evaluated in rats.

Glucocorticoids-induced dyslipidemia is an animal model in which the administration of dexamethasone as a potent corticosteroid disturbs the fat and glucose metabolism and leads to the metabolic syndrome-like disorder with symptoms of hyperlipidemia and hyperglycemia (21). Dexamethasone augments the serum content of fatty acids and lipids because of the enlarged lipolysis in adipose tissue and more synthesis of fatty acids and VLDL in hepatic tissue. It also declines the clearance of blood lipoproteins by affecting apolipoprotein genes and lipoprotein receptors (22). Decrease in the activity of lecithin cholesterol acetyltransferase and downregulation of LDL receptor contribute to the elevation of total serum cholesterol level during exposure to a high dose of dexamethasone (23,24). Development of fatty liver occurs because of more lipid and fatty acids synthesis and less creation of triacylglycerol *via* the diminished activity of hepatic lipoprotein lipase, activation of adenosine monophosphate-activated protein kinase, and enlarged lipogenesis as a result of upsurges in the activity of crucial lipogenic enzymes including fatty acid synthase, acetyl-coenzyme A carboxylase, and diminution of the fatty acid beta-oxidase activity (25,26). Dexamethasone excess raises liver size with enlarged hepatocytes because of lipid accumulation and motivation of pregnane X receptor/Yes-associated protein (PXR/YAP) without effect on hepatocyte proliferation (27). Moreover, dexamethasone causes liver toxicity due to oxidative damage and enhanced expression of the hepatic enzyme's gene (28).

Insulin resistance and hyperglycemia are other unwanted effects of glucocorticoids due to the hampering uptake of glucose by peripheral tissues and distressing insulin signaling (29).

Oxidative stress also contributes to the pathogenesis of many adverse effects of glucocorticoids during high dosages in long-term use through dysregulation of physiological processes *via* ROS-induced damages (30).

In this investigation, dexamethasone-induced lipid peroxidation, dyslipidemia, and hyperglycemia with significant alterations in the liver architecture and the body and liver weights. Treatment with *D. subcapitatum* aerial parts extract notably improved the serum liver function markers, lipid and glucose profile, and also liver histopathological and weight changes in hyperlipidemic rats at 100 and 200 mg/kg.

There are several reports about the useful effects of some *Drcacephalum* plants in improving hyperglycemia and hyperlipidemia (31-33). *D. kotschyi* is a well-known species in this genus with various therapeutic properties including blood lipid-lowering effect. In a model of high-fat hyperlipidemia, administration of hydroalcoholic extract and polyphenolic fraction of *D. kotschyi* for 14 or 21 days significantly attenuated triglycerides, total cholesterol, and LDL at 80 and 120 mg/kg (30). Aslian *et al.* reported that *D. kotschyi* extract decreased blood levels of triglycerides (54%), total cholesterol (40%), LDL (54%), and blood glucose (25%) and increased HDL (45%) in adipose tissues in diabetic rats (32). In their *in vitro* study, *D. kotschyi* extract augmented expression of some crucial genes involved in lipid metabolism and adipogenesis including peroxisome proliferator-activated receptor gamma (PPARγ), sterol regulatory element-binding type 1 (SREBP-1), forkhead box O-1 (FOXO1), and protein kinase B while suppressed c-Jun N-terminal kinase (JNK) in 3T3-L1 adipocyte cells (32).

In the study conducted by Pouraboli *et al.*, methanol extract of *D. polychaetum* shoot at 300 mg/kg showed hypolipidemic properties through lessening cholesterol and triglycerides levels in diabetic rats. It also diminished blood glucose content (27.1%) at 120 min in the oral glucose tolerance test (33).

Folin Ciocalteu assay revealed total phenolic content as 77.34 ± 4.9 mg GAE in 1 g of the dried extract of *D. subcapitatum* which proposes this plant as a good source of antioxidants. In our study, *D. subcapitatum* extract showed anti-lipid peroxidative activity. Although no previous data is available on the impact of *D. subcapitatum* on oxidative stress, there are many reports of the antioxidant actions of *Drcacephalum* plants through enhancing activities of catalase and superoxide dismutase, scavenging of free radicals, hindering lipid peroxidation, and increasing total antioxidant power due to the various phytochemicals, especially phenolic ingredients (32-34).

The presence of different bioactive constituents in the *D. subcapitatum* extract including flavonoids (as a main group of phenolic compounds) such as luteolin, xanthomicrol, calycopterin, apigenin, and isokaempferide, and some terpenoids like neral, geranial, limonene, ursolic acid, and oleanolic acid may be accountable for the antihyperlipidemic and hypoglycemic actions of this plant (11). The beneficial effects on the serum glucose and lipid profile have been established for many flavonoids and terpenoids. Limonene as a cyclic monoterpene has improved fatty liver, hyperglycemia, and hyperlipidemia profile and reduced the size of white and brown adipocytes in obese mice (35). It has been reported that terpenoids regulate PPARs and subsequently affect lipid and glucose metabolism and energy homeostasis (14). A large number of animal and clinical data support the effectiveness of flavonoids for managing hyperlipidemia, diabetes, and oxidative stress (13). For example, luteolin as a flavonoid which is also found in *D. subcapitatum* can improve hyperglycemia and hyperlipidemia and reduce proinflammatory cytokines and oxidative stress in diabetic rats (36). Apigenin has shown a lipid-lowering effect by reducing triglycerides, total cholesterol, and LDL and increasing HDL in hyperlipidemic mice (37).

CONCLUSION

Regarding our results, hydroalcoholic extract of *D. subcapitatum* aerial parts showed beneficial activities in hyperlipidemia caused by dexamethasone by declining serum lipids, glucose, lipid peroxides and transaminases, and improving liver histopathological changes. Further investigations are required to clarify the mechanisms of antihyperlipidemic action of *D. subcapitatum* and to verify its clinical benefits of using in patients with dyslipidemic disorders.

Acknowledgments

The content of this paper was extracted from a Pharm.D thesis submitted by S. Hajibagher which was financially supported by the Vice-Chancellery for Research and Technology, Isfahan University of Medical Sciences, Isfahan, I.R. Iran through Grant No. 3401367.

Conflict of interest statement

The authors declared no conflict of interest in this study.

Authors' contributions

L. Safaeian was responsible for the research plan, designing the animal study, supervising the investigation, analyzing the data, and editing the manuscript; Z. Yazdiniapour planned the herbal experiments; P. Karimian conducted the histopathological analysis; S. Hajibagher and Z. Bakhtiari performed the experiments, collected the data, and prepared the draft of the manuscript. All authors read and confirmed the finalized article.

REFERENCES

1. Shattat GF. A review article on hyperlipidemia: types, treatments and new drug targets. Biomed Pharmacol J. 2014;7(2):399-409. DOI: 10.13005/bpj/504.
2. Rafieian-Kopaei M, Setorki M, Doudi M, Baradaran A, Nasri H. Atherosclerosis: process, indicators, risk factors and new hopes. Int J Prev Med. 2014;5(8):927-946. PMCID: PMC4258672.
3. Aguilar-Salinas CA, Gómez-Díaz RA, Corral P. New therapies for primary hyperlipidemia. J Clin Endocrinol Metab. 2022;107(5):1216-1224. DOI: 10.1210/clinem/dgab876.
4. Mal GS, Smakhtina AM. Secondary hyperlipidemia: definition, phenotypes, and inducing factors. Int Heart Vasc Dis. 2021;9(32):34-40. DOI: 10.24412/2311-1623-2021-32-34-40.
5. Rizzo M, Kotur-Stevuljevic J, Berneis K, Spinas G, Rini GB, Jelic-Ivanovic Z, *et al*. Atherogenic dyslipidemia and oxidative stress: a new look. Transl Res. 2009;153(5):217-223. DOI: 10.1016/j.trsl.2009.01.008.
6. Mesripour A, Rafieian-Kopaei M, Bahrami B. The effects of *Anethum graveolens* essence on scopolamine-induced memory impairment in mice. Res Pharm Sci. 2016;11(2):145-151. PMCID: PMC4852659.
7. Shaito A, Thuan DTB, Phu HT, Nguyen THD, Hasan H, Halabi S, *et al*. Herbal medicine for cardiovascular diseases: efficacy, mechanisms, and safety. Front Pharmacol. 2020;11:422. DOI: 10.3389/fphar.2020.00422.
8. Lazarević P, Lazarević M, Krivošej Z, Stevanović V. On the distribution of *Dracocephalum ruyschiana* (Lamiaceae) in the Balkan Peninsula. Phytol Balc. 2009;15(2):175-179.
9. Hesami Moghaddam H, Emadi F, Esmaeil-Jamaat E, Kamalinejad M, Alijaniha F. Plants from genus *Dracocephalum* in Iran: pharmacology and phytochemistry overview. Curr Drug Discov Technol. 2022;19(5):e280422204213. DOI: 10.2174/1570163819666220428123059.
10. Zeng Q, Jin H, Qin JJ, Fu JJ, Hu XJ, Liu JH, *et al*. Chemical constituents of plants from the genus *Dracocephalum*. Chem Biodivers. 2010;7(8):1911-1929. DOI: 10.1002/cbdv.200900188.
11. Saeidnia S, Gohari AR, Ito M, Kiuchi F, Honda G. Bioactive constituents from *Dracocephalum Subcapitatum* (O. Kuntze) lipsky. Z Naturforsch C J Biosci. 2005;60(1-2):22-24. DOI: 10.1515/znc-2005-1-204.
12. Saeidnia S, Gohari AR, Ito M, Honda G, Hadjiakhoondi A. Phylogenetic analysis of *Badrashbu* species using DNA polymorphism. J Med Plants. 2005;4(15):66-72.
13. Unnikrishnan MK, Veerapur V, Nayak Y, Mudgal PP, Mathew G. Antidiabetic, antihyperlipidemic and antioxidant effects of the flavonoids. In: Watson RR, Preedy VR, Zibadi S. Polyphenols in human health and disease. Academic Press; 2014. pp. 143-161. DOI: 10.1016/b978-0-12-398456-2.00013-x.
14 Goto T, Takahashi N, Hirai S, Kawada T. Various terpenoids derived from herbal and dietary plants function as PPAR modulators and regulate carbohydrate and lipid metabolism. PPAR Res. 2010;2010:1-9. DOI: 10.1155/2010/483958.
15. Teymuori M, Yegdaneh A, Rabbani M. Effects of *Piper nigrum* fruit and *Cinnamum zeylanicum* bark alcoholic extracts, alone and in combination, on scopolamine-induced memory impairment in mice. Res Pharm Sci. 2021;16(5):474-481. DOI: 10.4103/1735-5362.323914.
16. Feghhi-Najafabadi S, Safaeian L, Zolfaghari B. *In vitro* antioxidant effects of different extracts obtained from the leaves and seeds of *Allium ampeloprasum* subsp. persicum. J HerbMed Pharmacol. 2019;8(3):256-260. DOI: 10.15171/jhp.2019.37.
17. Kumar VRS, Inamdar MN, Nayeemunnisa, Viswanatha GL. Protective effect of lemongrass oil against dexamethasone induced hyperlipidemia in rats: possible role of decreased lecithin cholesterol acetyl transferase activity. Asian Pac J Trop Med. 2011;4(8):658-660. DOI: 10.1016/S1995-7645(11)60167-3.
18. Momi S, Impagnatiello F, Guzzetta M, Caracchini R, Guglielmini G, Olivieri R, *et al*. NCX 6560, a nitric oxide-releasing derivative of atorvastatin, inhibits cholesterol biosynthesis and shows anti-inflammatory and anti-thrombotic properties. Eur J Pharmacol. 2007;570(1-3):115-124. DOI: 10.1016/j.ejphar.2007.05.014.
19. Safary A, Zadhoush F, Yegdaneh A, Hosseini-Sharifabad A, Talebi A, Sadraei H. The Effect of *Dracocephalum kotschyi* hydroalcoholic extract on biochemical and hematological parameters in rat. J Isfahan Med Sch. 2022;40(669):278-287.
20. Pragda SS, Kuppast IJ, Mankani KL, Ramesh L. Evaluation of antihyperlipidemic activity of leaves of *Portulaca oleracea* Linn against dexamethasone induced hyperlipidemia in rats. Int J Pharm Pharm Sci. 2012;4(4):279-283.

21. Ross IL, Marais AD. The influence of glucocorticoids on lipid and lipoprotein metabolism and atherosclerosis. S Afr Med J. 2014;104(10):671-674. DOI: 10.7196/samj.7979.
22. Wang JC, Gray NE, Kuo T, Harris CA. Regulation of triglyceride metabolism by glucocorticoid receptor. Cell Biosci. 2012;2(1):1-9. DOI: 10.1186/2045-3701-2-19.
23. Du WW, Liu F, Shan SW, Ma XC, Gupta S, Jin T, *et al*. Inhibition of dexamethasone-induced fatty liver development by reducing miR-17-5p levels. Mol Ther. 2015;23(7):1222-1233. DOI: 10.1038/mt.2015.64.
24. Wang M. The role of glucocorticoid action in the pathophysiology of the metabolic syndrome. Nutr Meta. 2005;2(1):1-14. DOI: 10.1186/1743-7075-2-3
25. Woods CP, Hazlehurst JM, Tomlinson JW. Glucocorticoids and non-alcoholic fatty liver disease. J Steroid Biochem Mol Biol. 2015;154:94-103. DOI: 10.1016/j.jsbmb.2015.07.020
26. Arnaldi G, Scandali VM, Trementino L, Cardinaletti M, Appolloni G, Boscaro M. Pathophysiology of dyslipidemia in Cushing's syndrome. Neuroendocrinology. 2010;92:86-90. DOI: 10.1159/000314213.
27. Jiao T, Yao X, Zhao Y, Zhou Y, Gao Y, Fan S, *et al*. Dexamethasone-induced liver enlargement is related to PXR/YAP activation and lipid accumulation but not hepatocyte proliferation. Drug Metab Dispos. 2020;48(9):830-839. DOI: 10.1124/dmd.120.000061.
28. Jackson ER, Kilroy C, Joslin DL, Schomaker SJ, Pruimboom-Brees I, Amacher DE. The early effects of short-term dexamethasone administration on hepatic and serum alanine aminotransferase in the rat. Drug Chem Toxicol. 2008;31(4):427-445. DOI: 10.1080/01480540802390247.
29. Geer EB, Islam J, Buettner C. Mechanisms of glucocorticoid-induced insulin resistance: focus on adipose tissue function and lipid metabolism. Endocrinol Metab Clin North Am. 2014;43(1):75-102. DOI: 10.1016/j.ecl.2013.10.005.
30. Bjelaković G, Beninati S, Pavlović D, Kocić G, Jevtović T, Kamenov B, *et al*. Glucocorticoids and oxidative stress. J Basic Clin Physiol Pharmacol. 2007;18(2):115-127. DOI: 10.1515/JBCPP.2007.18.2.115.
31. Sajjadi SE, Movahedian Atar A, Yektaian A. Antihyperlipidemic effect of hydroalcoholic extract, and polyphenolic fraction from *Dracocephalum kotschyi* Boiss. Pharm Acta Helv. 1998;73(3):167-170. DOI: 10.1016/s0031-6865(98)00016-8.
32. Aslian S, Yazdanparast R. Hypolipidemic activity of *Dracocephalum kotschyi* involves FOXO1 mediated modulation of PPARγ expression in adipocytes. Lipids Health Dis. 2018;17(1):1-9. DOI: 10.1186/s12944-018-0893-3.
33. Pouraboli I, Nazari S, Sabet N, Sharififar F, Jafari M. Antidiabetic, antioxidant, and antilipid peroxidative activities of *Dracocephalum polychaetum* shoot extract in streptozotocin-induced diabetic rats: *in vivo* and *in vitro* studies. Pharm Biol. 2016;54(2):272-278. DOI: 10.3109/13880209.2015.1033561.
34. Song E, Choi J, Gwon H, Lee KY, Choi SG, Islam MA, *et al*. Phytochemical profile and antioxidant activity of *Dracocephalum moldavica L*. seed extracts using different extraction methods. Food Chem. 2021;350:128531,1-27. DOI: 10.1016/j.foodchem.2020.128531.
35. Jing L, Zhang Y, Fan S, Gu M, Guan Y, Lu X, *et al*. Preventive and ameliorating effects of citrus D-limonene on dyslipidemia and hyperglycemia in mice with high-fat diet-induced obesity. Eur J Pharmacol. 2013;715(1-3):46-55. DOI: 10.1016/j.ejphar.2013.06.022.
36. Kahksha, Alam O, Al-Keridis LA, Khan J, Naaz S, Alam A, *et al*. Evaluation of antidiabetic effect of luteolin in STZ induced diabetic rats: molecular docking, molecular dynamics, *in vitro* and *in vivo* studies. J Funct Biomater. 2023;14(3):126,1-16. DOI: 10.3390/jfb14030126.
37. Hamed ZS, Altaweel A, Ahmed K KA, Taqa GAA. Evaluation of the antihyperlipidemic effect of apigenin flavonoid in mice. Iraqi J Vet Sci. 2022;36(2):279-283. DOI: 10.33899/IJVS.2021.130008.1718.

ONLINE SUBMISSION

https://review.jow.medknow.com/rps

Research in Pharmaceutical Sciences, June 2024; 19(3): 328-337
Received: 25-08-2023
Peer Reviewed: 19-09-2023
Revised: 18-10-2023
Accepted: 13-11-2023
Published: 01-07-2024

School of Pharmacy & Pharmaceutical Sciences
Isfahan University of Medical Sciences

Original Article

Persianolide-A, an eudesmanolide-type sesquiterpene lactone from *Artemisia kopetdaghensis*, induces apoptosis by regulating ERK signaling pathways

Seyyed Moein Ebrahimi[1,2], Jahanbakhsh Asadi[1,2], Maryam Fattahian[3], Seyyed Mehdi Jafari[1,2,*], and Mustafa Ghanadian[3,*]

[1]*Metabolic Disorders Research Center, Golestan University of Medical Sciences, Gorgan, Iran.*
[2]*Department of Biochemistry and Biophysics, Faculty of Medicine, Golestan University of Medical Sciences, Gorgan, I.R. Iran.*
[3]*Department of Pharmacognosy , Isfahan Pharmaceutical Sciences Research Center, School of Pharmacy and Pharmaceutical Sciences, Isfahan University of Medical Sciences, Isfahan, Iran.*

Abstract

Background and purpose: Herbal components, particularly sesquiterpenes, are progressively recognized as a crucial resource for developing effective therapeutic agents for breast cancer. In this study, the effect of a sesquiterpene lactone known as 8-O-dihydroxy-11α,13-dihydroeudesma-4(15)-en-12,6α-olide (persianolide-A) was examined in breast cancer cell lines.
Experimental approach: MDA-MB-231 and MCF-7 cancer cells were grown in DMEM solution with 10% FBS. Then, an MTT assay was performed to evaluate cell viability. Apoptosis was detected by annexin-PI staining. A caspase 3/7 activity assay kit was used to assess the activity of caspase-3 and caspase-7. Protein expression of Bcl-2, Bax, and p-ERK1/2 was determined by western blotting.
Findings/Results: This study showed that the IC_{50} values of the persianolide-A for MCF-7 and MDA-MB-468 cells are 34.76 and 54.48 µM, respectively. In addition, persianolide-A showed a significant increase in apoptosis in both MDAMB-231 and MCF-7 breast cancer cell lines. Persianolide-A significantly increased the expression of the pro-apoptotic protein Bax and decreased the expression of the anti-apoptotic protein Bcl-2. Also, presinolide-A treatment led to a substantial increase in caspase activity with a ratio of 3/7 in both MCF-7 and MDA-MB-231 cancer cells. In addition, the study showed that persianolide-A decreased the expression of p-ERK1/2 protein.
Conclusion and implications: The results of this study suggest that persianolide-A, sourced from *Artemisia kopetdaghensis*, induces cell apoptosis in breast cancer cell types. The molecular mechanisms could be implicated in the modulation of the ERK1/2 signaling pathway.

Keywords: Apoptosis; Artemisia kopetdaghensis; Breast neoplasms; ERK1/2; Persianolide-A, Sesquiterpene lactone.

INTRODUCTION

Cancer is a major global health problem, causing one in four deaths (1, 2). Among them, breast cancer is common in women (3). According to the World Health Organization, it ranks fifth in cancer-related deaths worldwide and is the second leading cause of cancer deaths in women (4). Standard treatments for breast cancer encompass chemotherapy, radiotherapy, surgery, and hormone therapy; however, the absence of a conclusive therapeutic target poses a challenge in its treatment (5). Furthermore, it should be noted that the mortality rate is significantly elevated in individuals who receive treatment for the condition, which shows the ineffectiveness of these treatments (6). As a result, there is a rising interest in developing and identifying new potential therapeutic agents against breast cancer (7-9).

*Corresponding authors:
S.M. Jafari, Tel: +98-, Fax: +98-1732430319
Email: s.meh.jafari@goums.ac.ir; s.meh.jafari@gmail.com
M. Ghanadian, Tel: +98-3137927131, Fax: +98-3136680011
Email: ghannadian@gmail.com

Access this article online	
	Website: http://rps.mui.ac.ir
	DOI: 10.4103/RPS.RPS_175_23

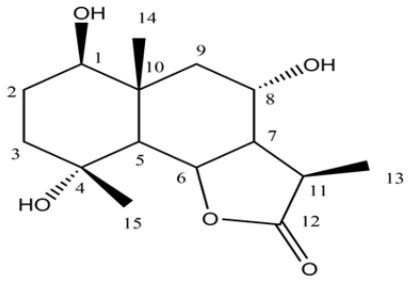

Fig. 1. The structure of persianolide-A (1, 8-O-dihydroxy- 11α,13- dihydroeudesma -4(15)-en-12,6α-olide, isolated from *Artemisia kopetdaghensis* (22).

Herbal components have been recognized recently as a crucial resource for breast cancer therapy (8-10). Flavonoids, phenolic acids, alkaloids, and sesquiterpene lactones (STLs) play an essential role in drug discovery in this field. They work through anticancer signaling pathways, including apoptosis (11-13). Apoptosis is an initial defense mechanism in multicellular organisms to counteract tumor development by eliminating genetically impaired cells (14). STLs encompass a broad and notably varied collection of secondary plant compounds, with their highest prevalence in the Asteraceae family (15). They are categorized into germacranolides, eudesmanolides, eremophilanolides, guaianolides, and pseudoguaianolides (16). Among these compounds, parthenolide (17), artemisinin (18), and thapsigargin (19) have been studied as potential anticancer precursors combating cancer cells. STLs' bioactivities are primarily associated with the stable methylene-lactone ring frequently occurring in their structure (15).

The anti-tumor influence of STLs has been related to regulating different signaling pathways, such as extracellular signal-regulated kinase (ERK) pathways (20). The ERK signaling pathway is a complex network of genes and proteins that transmit signals from the cell's exterior to the nucleus, influencing various cellular processes. Key genes within this pathway include mitogen-activated protein kinase 1 (MAPK1) and MAPK3, which encode the ERK proteins. These genes and their associated proteins are pivotal in controlling cell growth, differentiation, and responses to external stimuli, contributing to the overall regulation of cellular functions. Due to its versatile roles in acquiring malignant phenotypes, obstruction of the ERK pathway in tumor cells is logically expected to cause an anti-proliferative and anti-metastatic (21). A previously conducted phytochemical examination of aerial parts of *Artemisia kopetdaghensis* led to the isolation and identification of eudesmane-type STL, including 11α,13-dihydroeudesman-4(15)-en-olide (Fig. 1) named persianolide-A (22). Few studies to date have focused on the mechanism of action of STLs against breast cancer cells. In our ongoing attempt to discover pharmacologically effective compounds among STLs, persianolide-A was subjected to the 3-(4,5-dimethyl-2-thiazolyl)-2,5-diphenyl-tetrazolium bromide (MTT) assay to examine its cytotoxicity against breast cancer cells. Furthermore, related factors associated with the process of apoptosis, such as Bax, Bcl-2, and p-ERK1/2 expression, were tested by western blotting.

MATERIALS AND METHODS

Dulhocco's modified eagles medium (DMEM) was acquired from Gibco (Rockville, Maryland). Powder of MTT was obtained from Sigma-Aldrich (St. Louis, Missouri, USA). Furthermore, dimethyl sulfoxide (DMSO) was obtained from Merck (Munich, Germany). Serum derived from fetal bovine and trypsin-ethylenediaminetetraacetic acid (EDTA) was graciously provided by Bioidea (Tehran, Iran). The annexin/propidium iodide (PI) apoptosis assay kit was purchased from BioLegend (San Diego, California). The caspase 3/7 colorimetric activity assay kit was secured from Kia Zist (Hamedan, Iran). From Santa Cruz Biotechnology (California, USA), antibodies targeting Bax, Bcl-2, and p-ERK1/2 protein were acquired.

Persianolide-A

Our previous study, including the analysis of chemical components in the upper parts of *A. kopetdaghensis*, led to the discovery and identification of persianolide-A (22). This compound belongs to the sesquiterpene lactone group known as eudesmane. Determining its structure relies on a thorough examination of

various spectral data that includes both 1D and 2D nuclear magnetic resonance (NMR) and HRESIMS. Calculations and experimental evaluations using electronic circular dichroism (ECD) spectral data were used to decide on its exact configuration (22).

Cell culture conditions

The human breast cancer cell lines (MDA-MB-231 and MCF-7) were provided by the Pasteur Institute of Iran. The cells were grown in a DMEM solution with a 10% concentration of fetal bovine serum (FBS) and 1% penicillin G/streptomycin antibiotics. They were subsequently placed in a controlled incubator at 37 °C, containing 5% CO_2 and 95% humidity.

Evaluation of viability assay

The MTT assay was conducted as previously described (23). Ten thousand cells were cultured in each well of a 96-well plate. Following, the cells were treated with different concentrations of persianolide-A (1-200 µM) for over 48 h. An MTT stock solution with a 5 mg/mL concentration was prepared. Next, 20 µL of MTT solution was added to each well. After 4 h, DMSO was introduced. Finally, the number of viable cells was determined by measuring the optical density at 570 nm by the microplate reader.

Evaluation of apoptosis with annexin-PI staining

This research used flow cytometry to evaluate cell apoptosis, using a double staining method with annexin V and fluorescein isothiocyanate (FITC)-labeled PI. This technique was designed to investigate whether the growth-inhibiting effect of persianolide-A was linked to the initiation of apoptotic cell death. In summary, cells were cultured in a 6-well plate at 4×10^5 cells per well. Then, cancer cells were incubated with persianolide-A at concentrations of 34.76 µm for MCF-7 and 54.48 µm for MDA-MB 231 for 48 h. Afterward, the cells were washed twice with a cold phosphate-buffered saline (PBS) solution. Following centrifugation, the cells were suspended in 500 µL of binding buffer at 1×10^6 cells/mL density. Subsequently, 5 µL of annexin V-FITC and PI dye (50 ng/mL, 1 µL) were added and allowed to incubate at room temperature for 10 min. Finally, the stained cells were analyzed by a flow cytometer to ascertain the levels of apoptosis.

Assessment of caspase 3/7 enzymatic activity

The caspase 3/7 colorimetric activity assay kit was employed to evaluate the activity of caspase-3 and caspase-7, following the guidelines provided by the manufacturer. Initially, cells were planted at a concentration of 4×10^5 cells/mL in a 6-well plate and allowed to adhere for 24 h. Then, the cells were exposed to the IC_{50} concentration of persianolide-A (34.76 µM for MCF-7 and 54.48 µM for MDA-MB 231) for 48 h. The cells were then collected and resuspended. Caspase lysis buffer (500 µL) was added and then the cells were incubated at 4 °C for 20 min. For further investigation, the sediment was discarded. Protein levels were assessed using the Bradford method, and consistent protein quantities were utilized for the analysis. Once the protein concentrations were adjusted, 50 µL of each supernatant sample was introduced into a well. Subsequently, 55.5 µL of the working solution (containing 50 µL of caspase buffer, 5 µL of caspase substrate, and 0.5 µL of dithiothreitol) was added to each sample. Afterward, the specimens were placed in an incubator at 37 °C for 90-120 min. After the incubation period, the microplate reader measured absorbance at 405 nm.

Western blotting

The experiment involved seeding 5×10^5 breast cancer cells within every well of six-well plates. Subsequently, the cells were exposed to the STL sample for 48 h, followed by extraction of total protein content using radioimmunoprecipitation assay lysis buffer enhanced with 0.5% protease inhibitor cocktails and 0.5 mM phenylmethylsulfonyl fluoride. For protein quantification, the Bradford assay was employed. Each sample was exposed to 30 µg of proteins and underwent electrophoresis using a 12% sodium dodecyl-sulfate polyacrylamide gel (SDS-PAGE). Following that, the proteins were moved onto a membrane made of polyvinylidene fluoride. Particular mouse monoclonal antibodies

targeting Bcl-2, Bax, and p-ERK1/2 were primarily employed for protein detection. We used a secondary antibody to observe the protein bands; we mainly used a goat secondary antibody against mouse IgG linked with horseradish peroxidase and an ECL chemiluminescent substrate.

Statistical analysis

The statistical examination employed a one-way ANOVA followed by the Tukey post hoc assessment. The data is displayed as the mean ± SD. *P*-values < 0.05 were considered statistically significant. The IC_{50} value was calculated utilizing GraphPad Prism 8.2.1 through analysis of the concentration-response curve.

RESULTS

The effect of persianolide-A on cell viability

Cell cytotoxicity following treatment with persianolide-A was evaluated using the MTT test. Figure 2A and B depicts a concentration-dependent reduction of cell viability of MDA-MB-231 and MCF-7 cells treated with persianolide-A. Additionally, these results demonstrated a more pronounced inhibitory effect on MCF-7 cells than MDA-MB231 cells, starting at 1 µM and reaching its peak at 200 µM. On the other hand, the viability of MDA-MB231 cells treated with persianolide-A at 25-200 µM significantly decreased. The IC_{50} values for inhibiting 50% of cell growth were 34.76 µM in MCF-7 cells and 54.48 µM in MDA-MB-231 cells. This observation underscores the compound's heightened selectivity towards MCF-7 cells.

The effect of persianolide-A on cell apoptosis

Cells apoptosis, exposed to persianolide-A at IC_{50} (34.76 µM for MCF-7 and 54.48 µM for MDA-MB-231) for 48 h, were examined using the flow cytometry. The results demonstrated that persianolide-A effectively induced apoptosis in both MDA-MB-231 (Fig. 3A and B) and MCF-7 (Fig. 3C and D) breast cancer cells. The percentage of apoptosis for the MDA-MB 231 and MCF-7 cells was 52.35% and 49.45%, respectively.

The effect of persianolide-A on activities of caspase 3/7.

To explore the involvement of caspases in initiating apoptosis by persianolide-A, the caspase 3/7 activities in persianolide-A-treated cells were measured using colorimetric assay kits. The outcomes revealed a noteworthy rise in caspase3/7 activity in MDA-MB-231 cells after persianolide-A treatment (Fig. 4A). Similarly, in MCF-7 cells, significant elevation in caspase3/7 activity was observed upon exposure to persianolide-A (Fig. 4B).

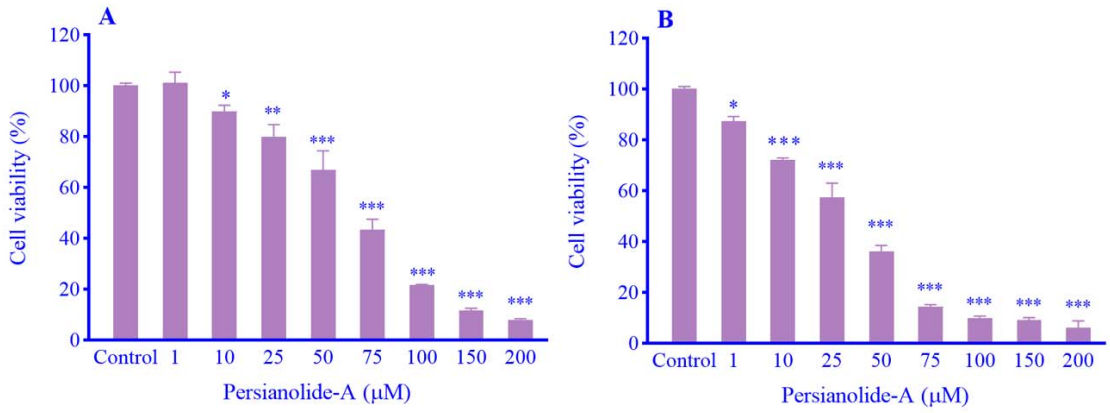

Fig. 2. The effect of persianolide-A on cell viability in breast cancer cells. Various concentrations of persianolide-A were administered to the cells over 48 h, and the viability of the cells was evaluated using the MTT test in (A) MDA-MB-231 and (B) MCF-7 cell lines. As the concentration of persianolide-A increased, there was a notable decrease in the percentage of viable cells. Data are shown as mean ± SD of experiments performed in triplicate. **P* < 0.05, ***P* < 0.01, and ****P* < 0.001 indicate significant differences in comparison with the control group.

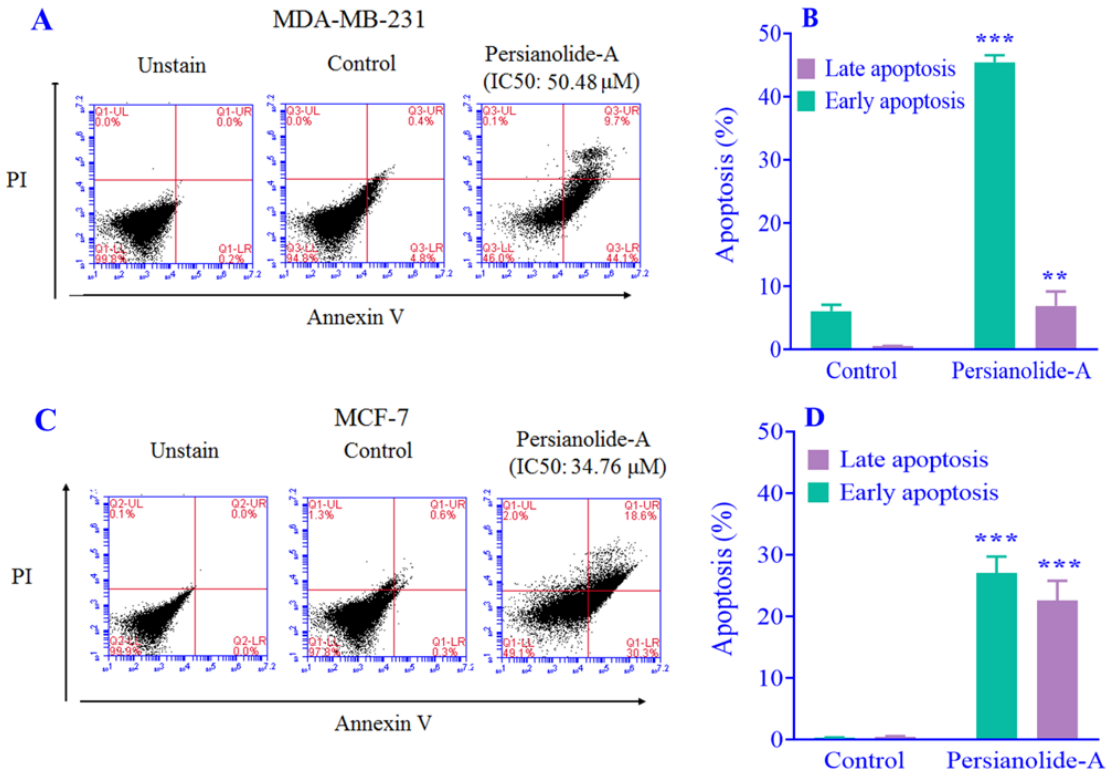

Fig. 3. The effect of persianolide-A on cell apoptosis. MDA-MB-231 and MCF-7 cells were exposed to persianolide-A at IC_{50} values for 48 h (50.48 and 34.76 µM, respectively). Flow cytometry was utilized to evaluate cellular apoptosis. The results demonstrated that persianolide-A induces apoptosis in (A and B) MDA-MB-231 and (C and D) MCF-7 cells. Values represent the mean ± SD, n = 3. $^{**}P < 0.01$ and $^{***}P < 0.001$ indicate significant differences in comparison with the respective control group.

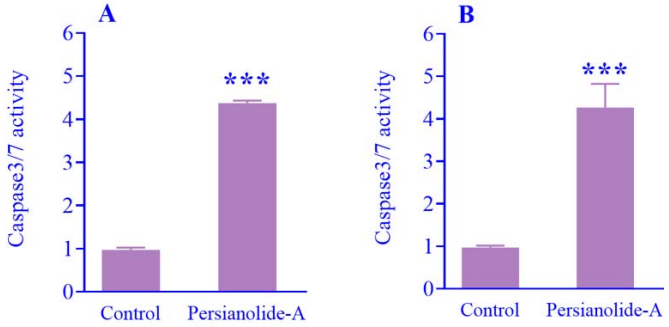

Fig. 4. The effect of persianolide-A on caspase activity 3/7. (A) MDA-MB-231 and (B) MCF-7 cells were treated with persianolide-A at IC_{50} (50.48 and 34.76 µM, respectively). After 48 h, a colorimetric evaluation was performed to ascertain the 3/7 activity ratio. Values represent the mean ± SD, n = 3. $^{***}P < 0.001$ indicates significant differences in comparison with the control group.

The effect of persianolide-A on Bax and Bcl-2 protein expression

To further evidence of cell apoptosis, the presence of Bcl-2 family components, specifically Bax and Bcl-2, in breast cancer cells following exposure to persianolide-A was assessed with the utilization of western blotting. After persianolide-A treatment, a notable decrease in Bcl-2 expression was observed in MDA MB-231 (Fig. 5 A and B) and MCF-7 (Fig. 5 C and D). Additionally, it was observed that the induction of apoptosis by persianolide-A coincided with heightened levels of the proapoptotic Bax expression.

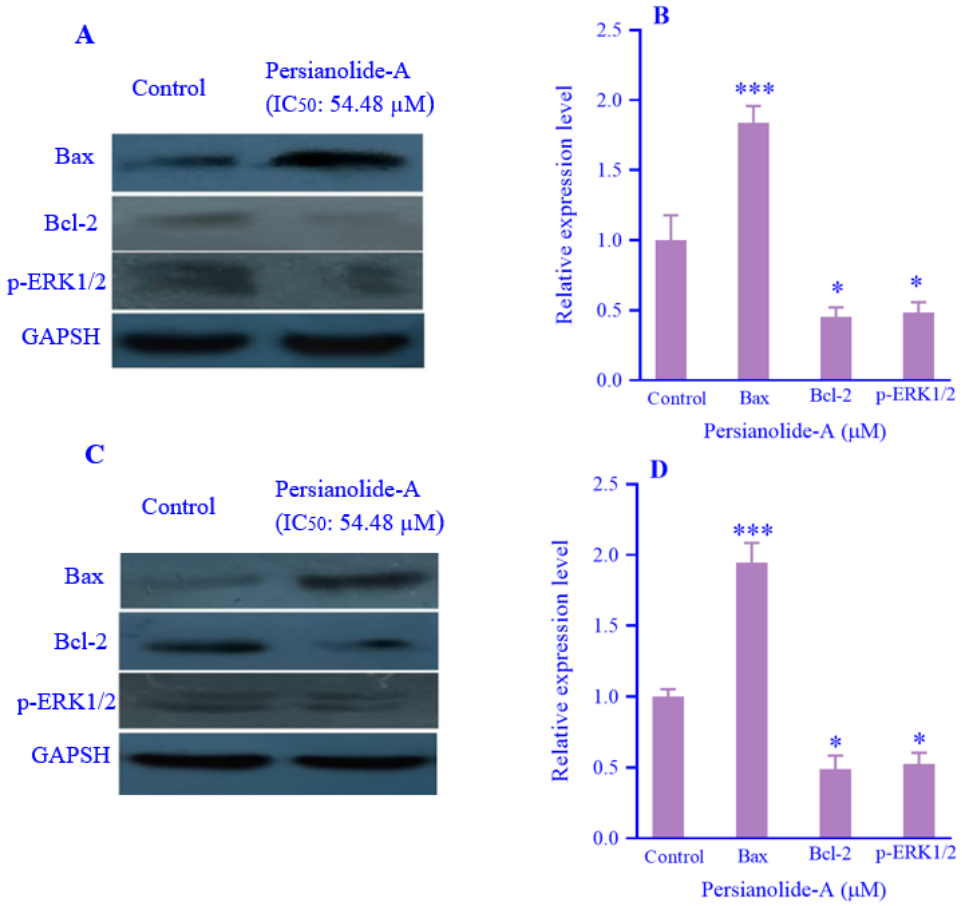

Fig. 5. The effect of persianolide-A on the expression of the proteins Bax, Bcl-2, and p-ERK1/2. (A and B) MDA-MB-231 and (C and D) MCF-7 cells underwent treatment with varying concentrations of persianolide-A for 48 h, following which the protein expressions were evaluated through western blot analysis. Band intensities for Bcl_2, Bax, and ERK1/2 in (B) MDA-MB-231 and (D) MCF-7 were quantified using ImageJ software. To ensure sample equivalency, the loading consistency was verified through comparison with the GAPDH band in untreated cells. Values represent the mean ± SD, n = 3. *$P < 0.05$ and ***$P < 0.001$ indicate significant differences in comparison with the control group.

Involvement of ERK1/2 in persianolide-A-induced apoptosis

ERK1/2 path is one of the most critical pathways that contribute to the growth and sustenance of breast cancer cells (24). Therefore, we explored whether persianolide-A influences the ERK1/2 signaling pathway in breast cancer cells. Our results indicated that persianolide-A reduced levels of pERK1/2 in both MDA MB-231(Fig. 5 A and B) and MCF-7 (Fig. 5 C and D) cancer cells.

DISCUSSION

Despite progress in diagnosis and treatment, the fatality rate resulting from breast cancer remains high. Therefore, developing new drugs or methods for prevention or treatment are much more desirable (25). Today, active ingredients of natural origin (plant, animal, and inorganic) are isolated or semi-synthesized to discover new drugs due to their abundance, side effects, and drug interactions (26,27). A previously conducted phytochemical investigation of aerial parts of *A. kopetdaghensis* resulted in the isolation and characterization of eudesmane-type STLs including 11α,13-dihydroeudesman-4(15)-en-olide named persianolide-A (22). In our ongoing attempt to discover pharmacologically effective compounds among STLs, persianolide-A was subjected to the MTT assay to evaluate its cytotoxicity against MCF-7 and MDA-MB-231 breast cancer cells.

Furthermore, related factors associated with the sequence of apoptosis such as Bcl-2, Bax, and p-ERK1/2 expression were tested by western blotting. The results of our study unveiled a significant decrease in cell growth, which was concentration-dependent, caused by persianolide-A in MDA-MB 231 and MCF-7 cell lines. The IC_{50} values for these cell lines were 54.48 µM and 34.76 µM, respectively. These results align with prior research efforts. Roy *et al*. previously highlighted that costunolide, an STL extract, achieves 50% hindrance of cell growth in MDA-MB-231 and MCF-7 cell lines at a concentration of 40 µM (25). Furthermore, the study by Liu and colleagues revealed that cacalol as an extraordinary STL compound sourced from the exquisite *Cacalia delphiniifolia* is a potent inhibitor of cell proliferation, effectively impeding the growth of breast cancer cell lines (28). Furthermore, deoxyelephantopin and isodeoxyelephantopin have demonstrated anticancer properties in breast cancer cell lines (29). Other studies confirmed alantolactone (27), gaillardin (13), and britannin (19) as inhibitors of MCF-7 cell growth at concentrations of 35.45, 4.93, and 9.56 µM, respectively. Numerous preceding studies also indicated anti-proliferative effects of the STL family, including gaillardin (13), britannin (19), and eupalinolide O (28); concerning the MDA-MB-468 breast cancer cell line, the IC_{50} values were measured 5.54 µM, 6.81 µM, and 1.04 µM, sequentially.

The process of apoptosis entails distinct morphological and biochemical alterations within cells, setting it apart from other forms of cell death. An essential trait signifying apoptotic cell demise is the translocation of phosphatidylserine from the inner cell membrane layer to the outer layer (30). This translocation is detected through annexin/PI dye binding to the negatively charged phosphatidylserines, enabling the quantification of apoptotic cells within sample (31). Our findings indicated that the application of persianolide-A leads to a notable decrease in the ratio of viable cells and an elevation in the initiation of apoptosis. This result showed that persianolide-A significantly initiates cell demise through the apoptotic pathway. This observation aligns with prior studies that demonstrated the strong ability of britannin and gaillardin to the objective is to trigger apoptosis in the breast cancer cell lines, MDA-MB-468 and MCF-7 (13,19). The results indicated that persianolide-A, derived from *A. kopetdaghensis*, inhibited the growth of MDA-MB-231 and MCF-7 cells by inducing apoptosis. To better understand the process of cell apoptosis, we focused on examining the impact of the Bcl-2 family on triggering the apoptotic pathway (32,33). The results revealed that the expression of Bcl-2 as an anti-apoptotic agent was down-regulated; in contrast, the expression of Bax as a pro-apoptotic agent was up-regulated at the same concentrations. Accordingly, in the current study, persianolide-A appeared to function by upregulating the Bax/Bcl-2 ratio in both MDA-MB-468 and MCF-7 cancer cells. The capability of STLs to apoptosis through Bax/Bcl-2 pathways in breast cancer cells has already been widely documented. Studies have demonstrated that STLs including ambrosin, gaillardin, and britannin reduce the Bcl-2 expression while elevating the Bax protein levels, consequently promoting apoptosis in MDA-MB-231 cells (14,23,34). On the other hand, caspases, a class of proteases, with their cleavage and subsequent activation play a crucial role as apoptosis agents (28). To investigate the involvement of caspase family activation in the apoptosis initiated by persianolide-A, the activity of caspases-3/7 was evaluated. The results indicated that treatment of MCF-7 and MDA-MB-231 cells by persianolide-A significantly increases the activity of the caspase-3/7 enzyme. Moreover, persianolide-A triggered apoptosis *via* attenuated survival ERK signaling. The graphical representation (Fig. 6) depicts the hypothesized visual pathway for persianolide A-induced regulated cell death.

Yeo *et al*. showed that the STL β-bisabolene isolated from *Commiphora guidottii*, increases the activity of both caspase-3 and caspase-7 to induce apoptosis in MCF-7 and MDA-MB-231 cancer cells (35).

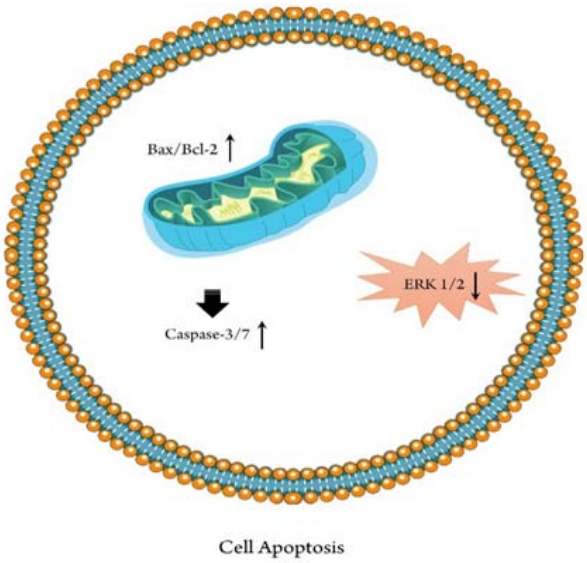

Fig. 6. The graphical representation depicts the hypothesized visual pathway for Persianolide A-induced regulated cell death via intrinsic pathways and attenuated ERK signaling.

ERK is a considerable signaling pathway governing cellular growth, differentiation, and apoptotic processes (36). The results indicated that persianolide-A inhibits the expression of p-ERK protein in MCF-7 and MDA-MB-231 cell lines. In a prior study, the STL dihydroartemisinin, derived from the STL artemisinin, exerts anti-tumor and anti-angiogenic effects by inhibiting the ERK proteins in MDA-MB-231 cells (33). Similarly, the STL costunolide, known for its potential anticancer effects, significantly reduces the p-ERK expression in A431 cells (37).

CONCLUSION

The present study demonstrated that persianolide-A, extracted from *A. kopetdaghensis*, has anticancer effects in human breast cancer cells. The molecular mechanisms could be implicated in the modulation of the ERK1/2 signaling pathway. However, more research is required to determine the molecular mechanism of action of persianolide-A in cancer.

Acknowledgments

This work was an MSc thesis submitted by Seyyed Moein Ebrahimi, which was financially supported by Golestan University of Medical Sciences through Grant No. 112165.

Conflict of interest statement

The authors declared no conflict of interest in this study.

Authors' contributions

S.M. Ebrahimi performed the experimental tests and wrote the manuscript; J. Asadi organized the methods; M. Fattahian contributed to the isolation and identification of persianolide-A; S.M. Jafari and M. Ghanadian designed the study. The finalized article was read and approved by all authors.

REFERENCES

1. Chung TW, Choi H, Lee JM, Ha SH, Kwak CH, Abekura F, *et al*. Corrigendum to "*Oldenlandia diffusa* suppresses metastatic potential through inhibiting matrix metalloproteinase-9 and intercellular adhesion molecule-1 expression *via* p38 and ERK1/2 MAPK pathways and induces apoptosis in human breast cancer MCF-7 cells". J Ethnopharmacol. 2017;204(189):309-317. DOI: 10.1016/j.jep.2017.04.016.
2. Jiang X, Li T, Liu RH. 2α-Hydroxyursolic acid inhibited cell proliferation and induced apoptosis in MDA-MB-231 human breast cancer cells through the p38/MAPK signal transduction pathway. J Agric Food Chem. 2016;64(8):1806-1816. DOI: 10.1021/acs.jafc.5b04852.
3. Ghoncheh M, Pournamdar Z, Salehiniya H. Incidence and mortality and epidemiology of breast cancer in the world. Asian Pac J Cancer Prev. 2016;17(S3): 43-46. DOI: 10.7314/apjcp.2016.17.s3.43.

4. Siegel RL, Miller KD, Fuchs HE, Jemal A. Cancer statistics, 2022. CA Cancer J Clin. 2022;72(1):7-33. DOI: 10.3322/caac.21708.
5. Tan PQ, Zhong YM, Hu ZY, Lou Dm. Size distributions, PAHs and inorganic ions of exhaust particles from a heavy duty diesel engine using B20 biodiesel with different exhaust aftertreatments. Energy. 2017;141:898-906. DOI: 10.1016/j.energy.2017.09.122.
6. Head J, Johnston SRD. New targets for therapy in breast cancer: farnesyltransferase inhibitors. Breast Cancer Res. 2004;6(6):262-268. DOI: 10.1186/bcr947.
7. Yang Y, He PY, Zhang Y, Li N. Natural Products targeting the mitochondria in Cancers. Molecules. 2020;26(1):92,1-27. DOI: 10.3390/molecules26010092.
8. Newman DJ, Cragg GM. Natural products as sources of new drugs over the 30 years from 1981 to 2010. J Nat Prod. 2012;75(3):311-335. DOI: 10.1021/np200906s.
9. Wu T, Geng J, Guo W, Gao J, Zhu X. Asiatic acid inhibits lung cancer cell growth *in vitro* and *in vivo* by destroying mitochondria. Acta Pharm Sin B. 2017;7(1):65-72. DOI: 10.1016/j.apsb.2016.04.003.
10. Abbaspour J, Ehsanpour AA, Aghaei M, Ghanadian M. Sesquiterpene lactones from shoot culture of *Artemisia aucheri* with cytotoxicity against prostate and breast cancer cells. Res Pharm Sci. 2019;14(4):329-334. DOI: 10.4103/1735-5362.263557.
11. Liao YF, Rao YK, Tzeng YM. Aqueous extract of *Anisomeles indica* and its purified compound exerts anti-metastatic activity through inhibition of NF-κB/AP-1-dependent MMP-9 activation in human breast cancer MCF-7 cells. Food Chem Toxicol. 2012;50(8):2930-2936. DOI: 10.1016/j.fct.2012.05.033.
12. Paterson I, Anderson EA. Chemistry. The renaissance of natural products as drug candidates. Science. 2005;310(5747):451-453. DOI: 10.1126/science.1116364.
13. Butler MS. The role of natural product chemistry in drug discovery. J Nat Prod. 2004;67(12):2141-2153. DOI: 10.1021/np040106y.
14. Fallahian F, Aghaei M, Abdolmohammadi MH, Hamzeloo-Moghadam M. Molecular mechanism of apoptosis induction by gaillardin, a sesquiterpene lactone, in breast cancer cell lines: gaillardin-induced apoptosis in breast cancer cell lines. Cell Biol Toxicol. 2015;31(6):295-305. DOI: 10.1007/s10565-016-9312-6.
15. Chadwick M, Trewin H, Gawthrop F, Wagstaff C. Sesquiterpenoids lactones: benefits to plants and people. Int J Mol Sci. 2013;14(6):12780-12805. DOI: 10.3390/ijms140612780.
16. Ghantous A, Gali-Muhtasib H, Vuorela H, Saliba NA, Darwiche N. What made sesquiterpene lactones reach cancer clinical trials? Drug Discov Today. 2010;15(15-16):668-678. DOI: 10.1016/j.drudis.2010.06.002.
17. Ghantous A, Sinjab A, Herceg Z, Darwiche N. Parthenolide: from plant shoots to cancer roots. Drug Discov Today. 2013;18(17-18):894-905. DOI: 10.1016/j.drudis.2013.05.005.
18. Chaturvedi D, Goswami A, Saikia PP, Barua NC, Rao PG. Artemisinin and its derivatives: a novel class of anti-malarial and anti-cancer agents. Chem Soc Rev. 2010;39(2):435-454. DOI: 10.1039/B816679J.
19. Doan NTQ, Christensen SB. Thapsigargin, origin, chemistry, structure-activity relationships and prodrug development. Curr Pharm Des. 2015;21(38):5501-5517. DOI: 10.2174/1381612821666151002112824.
20. Tehrani Fateh ST, Tehrani Fateh ST, Shekari F, Mahdavi M, Aref AR, Salehi-Najafabadi A. The effects of sesquiterpene lactones on the differentiation of human or animal cells cultured *in-vitro*: a critical systematic review. Front Pharmacol. 2022;13:862446,1-15. DOI: 10.3389/fphar.2022.862446.
21. Kohno M, Pouyssegur J. Targeting the ERK signaling pathway in cancer therapy. Ann Med. 2006;38(3):200-211. DOI: 10.1080/07853890600551037.
22. Fattahian M, Ghanadian M, Zolfaghari B, Aghaei M, Zulfiqar F, Khan IA, *et al*. Phytochemical analysis of *Artemisia kopetdaghensis*: sesquiterpene lactones with proapoptotic activity against prostate cancer cells. Phytochemistry. 2022;203:113411. DOI: 10.1016/j.phytochem.2022.113411.
23. Hamzeloo-Moghadam M, Aghaei M, Fallahian F, Jafari SM, Dolati M, Abdolmohammadi MH, *et al*. Britannin, a sesquiterpene lactone, inhibits proliferation and induces apoptosis through the mitochondrial signaling pathway in human breast cancer cells. Tumour Biol. 2015;36(2):1191-1198. DOI: 10.1007/s13277-014-2744-9.
24. Kheraldine H, Gupta I, Alhussain H, Jabeen A, Cyprian FS, Akhtar S, *et al*. Substantial cell apoptosis provoked by naked PAMAM dendrimers in HER2-positive human breast cancer via JNK and ERK1/ERK2 signalling pathways. Comput Struct Biotechnol J. 2021;19:2881-2890. DOI: 10.1016/j.csbj.2021.05.011.
25. Roy A, Manikkam R. Cytotoxic impact of costunolide isolated from costus speciosus on breast cancer *via* differential regulation of cell cycle-an *in-vitro* and *in-silico* approach. Phytother Res. 2015;29(10):1532-1539. DOI: 10.1002/ptr.5408.
26. Deshpande JR, Choudhari AA, Mishra MR, Meghre VS, Wadodkar SG, Dorle AK. Beneficial effects of *Lagenaria siceraria* (Mol.) standley fruit epicarp in animal models. Indian J Exp Biol. 2008;46(4):234-242. PMID: 18512332.
27. Shahali A, Ghanadian M, Jafari SM, Aghaei M. Mitochondrial and caspase pathways are involved in the induction of apoptosis by nardosinen in MCF-7 breast cancer cell line. Res Pharm Sci. 2018;13(1): 12-21. DOI: 10.4103/1735-5362.220963.

28. Liu W, Furuta E, Shindo K, Watabe M, Xing F, Pandey PR, *et al*. Cacalol, a natural sesquiterpene, induces apoptosis in breast cancer cells by modulating Akt-SREBP-FAS signaling pathway. Breast Cancer Res Treat. 2011;128(1):57-68. DOI: 10.1007/s10549-010-1076-8.
29. Verma SS, Rai V, Awasthee N, Dhasmana A, Rajalaksmi DS, Nair MS, *et al*. Isodeoxyelephantopin, a sesquiterpene lactone induces ROS generation, suppresses NF-κB activation, modulates LncRNA expression and exhibit activities against breast cancer. Sci Rep. 2019;9(1):17980,1-16. DOI: 10.1038/s41598-019-52971-3.
30. Furuta Y, Zhou Z. How do necrotic cells expose phosphatidylserine to attract their predators-What's unique and what's in common with apoptotic cells. Front Cell Dev Biol. 2023;11:1170551,1-9. DOI: 10.3389/fcell.2023.1170551.
31. Kim H, Kim HY, Lee EY, Choi BK, Jang H, Choi Y. A quenched annexin V-fluorophore for the real-time fluorescence imaging of apoptotic processes *in vitro* and *in vivo*. Adv Sci (Weinh). 2020;7(24):1-12. DOI: 10.1002/advs.202002988.
32. Brunelle JK, Letai A. Control of mitochondrial apoptosis by the Bcl-2 family. J Cell Sci. 2009;122(4):437-441. DOI: 10.1242/jcs.031682.
33. Juin P, Hunt A, Littlewood T, Griffiths B, Swigart LB, Korsmeyer S, *et al*. c-Myc functionally cooperates with Bax to induce apoptosis. Mol Cell Biol. 2002;22(17):6158-6169. DOI: 10.1128/mcb.22.17.6158-6169.2002.
34. Fan S, Cui Y, Hu Z, Wang W, Jiang W, Xu H. Ambrosin sesquiterpene lactone exerts selective and potent anticancer effects in drug-resistant human breast cancer cells (MDA-MB-231) through mitochondrial mediated apoptosis, ROS generation and targeting Akt/β-catenin signaling pathway. J BUON. 2020;25(5):2221-2227. PMID: 33277839.
35. Yeo SK, Ali AY, Hayward OA, Turnham D, Jackson T, Bowen ID, *et al*. β-Bisabolene, a sesquiterpene from the essential oil extract of opoponax (*Commiphora guidottii*), exhibits cytotoxicity in breast cancer cell lines. Phytother Res. 2016;30(3):418-425. DOI: 10.1002/ptr.5543.
36. Li Q, Chen M, Liu H, Yang L, Yang T, He G. The dual role of ERK signaling in the apoptosis of neurons. Front Biosci (Landmark Ed). 2014;19(8):1411-1417. DOI: 10.2741/4291.
37. Lee SH, Cho YC, Lim JS. Costunolide, a sesquiterpene lactone, suppresses skin cancer *via* induction of apoptosis and blockage of cell proliferation. Int J Mol Sci. 2021;22(4):1-16. DOI: 10.3390/ijms22042075.

Research in Pharmaceutical Sciences, June 2024; 19(3): 338-346
Received: 22-01-2024
Peer Reviewed: 01-03-2024
Revised: 07-04-2024
Accepted: 14-04-2024
Published: 01-07-2024

School of Pharmacy & Pharmaceutical Sciences
Isfahan University of Medical Sciences

Original Article

The enhancement of M13 phage titration by optimizing the origin of replication

Mohammad Hossein Darvishali, Mahmood Fadaie, and Hossein Khanahmad*

Department of Genetics and Molecular Biology, School of Medicine, Isfahan University of Medical Sciences, Isfahan, Iran.

Abstract

Background and purpose: M13KO7, a modified M13 phage variant, carries the p15A replication origin and Tn903 kanamycin resistance gene. This study aimed to optimize M13KO7's replication by substituting the p15A origin with the higher-copy pMB1 origin (500-700 copy numbers).
Experimental approach: A 6431-nucleotide fragment from the M13KO7 plasmid lacking the p15A replication origin and kanamycin resistance gene was amplified using a long polymerase chain reaction (PCR). The modified M13AMB1 plasmid was created by adding adenine to the 3' ends of this fragment and ligating it to the pMB1-containing fragment using T/A cloning. Afterward, to prepare the phage, pM13AMB1 was transformed into *E. coli* TG1 bacteria, and then, using the PEG-NaCl precipitation, the modified phage was propagated. The modified phage titer was determined utilizing the serial dilution and the qPCR methods, compared with the M13KO7 phage.
Findings/Results: The results showed that in the serial dilution method, the titers of modified phage and M13KO7 phage were 4.8×10^{14} and 7×10^{12} pfu/mL, respectively. Besides, the phage titer calculated by the qPCR method for the modified phage was equal to 1.3×10^{9} pfu/mL, whereas it was 4.08×10^{8} pfu/mL for the M13KO7 phage.
Conclusion and implications: This study provides evidence that replication origin replacement led to a significant increase in phage titers. It highlights the importance of replication optimization for molecular biology applications.

Keywords: Bacteriophage; M13 Phage; Phage titer; Replication origin.

INTRODUCTION

Bacteriophages, viruses that exclusively target bacteria, have drawn a lot of attention as invaluable tools in diverse scientific fields. The M13 bacteriophage has long been a cornerstone in molecular biology research, owing to its unique characteristics like excellent safety profile, high stability, manipulability, and non-pathogenic nature. With a filamentous structure and a circular single-stranded DNA (cssDNA) genome, which is approximately 6.4 nucleotides in size, M13 has served as a precious instrument in various endeavors, including phage display, gene cloning, and nanotechnology (1-3). The type n system in phage display offers several advantages over the type n+n system. It is simpler, cost-effective, easier to handle and store, efficient in binder selection, and potentially suitable for polyvalent display. This eliminates the requirement for phagemid and the complications of working with two different genetic components (phage and phagemid), making it a viable tool for many applications in peptide display (4-6).

Phage replication is highly dependent on the replication origin, which also affects the viral load and titration efficiency of the phage.

*Corresponding author: H. Khanahmad
Tel: +98-3137929197, Fax: +98-313668859
Email: h_khanahmad@med.mui.ac.ir

Access this article online	
	Website: http://rps.mui.ac.ir
	DOI: 10.4103/RPS.RPS_14_24

Enhancing the replication kinetics and production process of the M13 phage can be achieved by optimizing its origin of replication. The origin of replication serves as the initiation site for DNA synthesis, allowing for the replication and amplification of the phage genome (7). Traditionally, the p15A ori has been widely used as the replication origin for plasmid vectors due to its compatibility with various host strains. However, its usage in bacteriophage genomes has shown limitations and inefficiencies. It is expected that the introduction of the pMB1 ori, a high (500-700) copy number origin, into the M13 phage genome, will improve the replication efficiency of the phage genome, leading to higher phage titers, which is crucial for the successful development of effective vaccines (8,9). This modification holds great potential for optimizing M13 phage titration, thereby facilitating the development of a reliable and efficient primary vaccination tool (9,10).

In this study, we reported a modified M13KO7-derived phage with an optimized origin of replication, which has a higher titer compared to the wild-type phage. To this end, our research focused on genetically engineering the M13KO7 helper phage to replace its replication origin with a high copy number, pMB1, origin. With this change, our goal was to construct an n-type system that could be used in various scientific applications. This approach combines the well-established features of M13 as a bacterial targeting vehicle with the advantages offered by pMB1 origin-driven replication. By doing so, we anticipate that the modified M13 phage will exhibit increased replication rates, higher production yields, and improved overall efficacy. By optimizing the origin of replication, we aim to unlock the full potential of the M13 bacteriophage, enabling its use as a more efficient and cost-effective tool in various scientific domains.

MATERIALS AND METHODS

Bacterial and bacteriophage strains

In the current study, two widely used strains of *Escherichia coli* bacteria, i.e. Top10 (DH10b) and TG1 strains, were purchased from the Pasteur Institute of Iran. *E. coli* Top10 bacteria, which has a tetracycline resistance gene in its genome, was used for cloning and plasmid storage. Also, *E. coli* K12 TG1 bacteria, which has abundant F-pili, was used in the phage extraction process. The two phage strains used in this research were the wild-type M13KO7 phage carrying the p15A ori, which was bought from the Pasteur Institute of Iran, and the modified M13 phage carrying the pMB1 ori (M13AMB1).

Media and culture preparation

For growing bacteria in a standard manner, cells were cultured in Luria-Bertani (LB). LB Agar plates, which contain 1.5% added agar, were utilized for the solid culture of bacteria. The tetracycline, ampicillin, and kanamycin antibiotics were used at concentrations of 12.5, 100, and 50 μg/mL, respectively, to select antibiotic-resistant genetic markers. The phage extraction process was carried out in a super broth (SB) medium, which contains 20 g/L yeast extract, 35 g/L peptone, and 5 g/L NaCl. Indeed, the extracted phages were diluted in 1× phosphate-buffered saline (PBS) solution containing NaCl, KCl, Na_2HPO_4, and KH_2PO_4. In addition, TBE buffer containing tris, boric acid, and ethylenediaminetetraacetic acid (EDTA) was used to perform gel electrophoresis.

Construction of modified plasmid pM13AMB1

To construct the modified pM13AMB1 plasmid, the helper phage M13KO7 genome was genetically manipulated to amplify a 6431-bp fragment and remove the p15A ori coding sequence and kanamycin antibiotic resistance gene. The 6431-bp fragment was amplified by polymerase chain reaction (PCR) based on the pM13KO7 vector, using Super PCR Master Mix 2X (Yekta Tajhiz, Iran) as well as PFHindIIIM13 and PREcoRIM13 primers (Table 1, Fig. 1A and B). For this purpose, a temperature program of 4 min at 94 ℃, 30 cycles of 30 s at 94 ℃, 30 s at 60 ℃, and 7 min at 72 ℃, followed by 7 min at 72 ℃, was applied to the Thermocycler (Eppendorf, Germany). Subsequently, adenine was added to the 3′ ends of the amplified fragment through the Taq treatment method and then, it was

ligated to the pMB1-containing fragment (the pGetII vector) by the T/A cloning approach. Transformation of the modified M13AMB1 plasmid into competent *E. coli* Top10 cells was carried out using the calcium chloride protocol, as previously described (11,12). The construction of the M13AMB1 plasmid was confirmed using colony PCR on positive clones with PFHindIIIM13 and PREcoRIM13 primers (Table 1) and plasmid digestion with *PstI* restriction endonuclease (Thermo Fisher Scientific, USA), as well as Sanger sequencing.

Preparation of wild-type and modified M13 phages

Plasmids pM13KO7 and pM13AMB1 were separately transformed into *E. coli* K12 TG1 bacteria using calcium chloride protocol. The colony PCR using FRealM13 and REcoRIM13 primers (Table 1) was used to confirm the presence of plasmids in the positive colonies resulting from the transformation, and these clones were then used for phage propagation. TG1 cells containing pM13KO7 were grown in a 1-L Erlenmeyer flask (25% working volume) using SB medium containing 50 µg/mL kanamycin, and in the same way, TG1 cells containing pM13AMB1 were cultured in SB medium containing 100 µg/mL ampicillin. Then, TG1 cells were incubated overnight in a shaker incubator (37 ℃ and 200 rpm). Next, the culture medium containing bacteria and phage was centrifuged for several steps at 5500 rpm and 4 ℃ to precipitate the bacteria. Then, the supernatant was passed through a sterile 0.22 µm syringe filter to obtain pure phage. Finally, by appending PEG-NaCl solution (20% polyethylene glycol 6000 with 2.5 M NaCl) and spinning at 12000 rpm, the modified and wild-type phages were precipitated, and then the pellet was dissolved in sterile PBS.

Table 1. The sequences of used polymerase chain reaction primers.

Primer	Primer sequence
PFHindIIIM13	5'TTTAAGCTTGTCTCGGGCTATTCTTTTGAT3'
PREcoRIM13	5'AAAGAATTCCGAGATAGGGTTGAGTGTTGTT3'
FRealM13	5'GTTCCGATTTAGTGCTTTACG3'

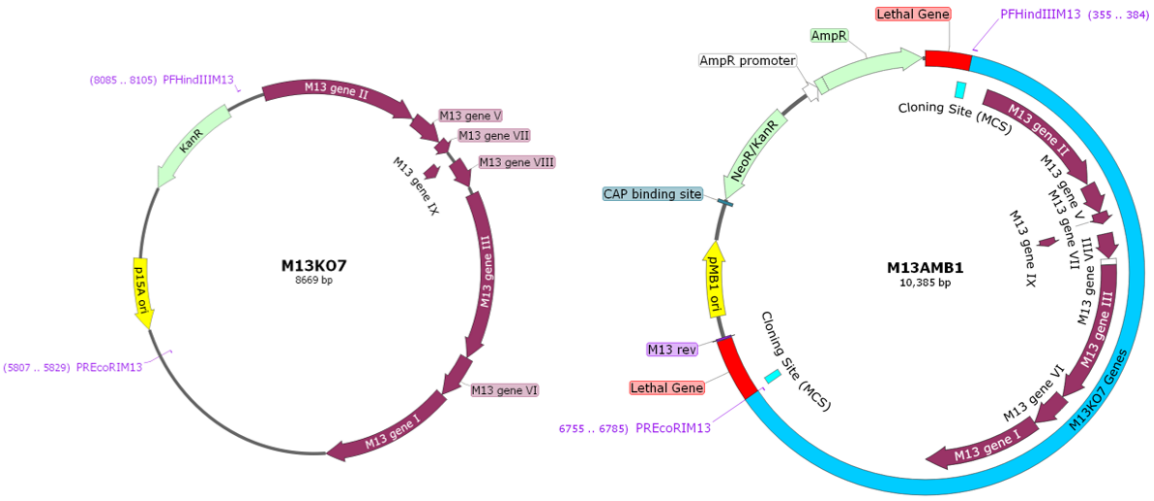

Fig. 1. The M13AMB1 plasmid construction. (A) The M13KO7 vector map; (B) the M13AMB1 vector map. The pM13KO7 derivative, pM13AMB1, was produced through genetic engineering by substituting the origin of replication, p15A, with pMB1.

Enumeration of wild-type and modified phages by serial dilution

The fifteen 1.5-mL vials were filled with 90 µL of sterile PBS to create a dilution series, necessary to calculate the titer of modified and helper phages. A dilution rate of 1:10 was employed, starting with 10 µL of acquired phage added to the first vial to achieve a titer of 0.1. Subsequently, 10 µL from the first vial were put into the second vial for a titer of 0.01, and so forth until the fifteenth vial reached a titer of 10^{15}. Finally, 10 µL of solution from the fifteenth vial was taken out to ensure uniformity across all vials. The resulting phage solutions, with a dilution ratio ranging from 10^{10} to 10^{15}, were then added to bacterial tubes (containing 90 µL of bacteria with an optical density of 0.4-0.6) for transduction. It was placed in an incubator set to 37 ℃ and left for 30 min. Subsequently, each vial's content was cultivated on agar plates that had 100 µg/L of the antibiotic ampicillin on them. The plates were then left to incubate for a whole night at 37 °C. Finally, the grown colonies on each plate were counted and then the titer of phages per milliliter was calculated using the following equation (13,14):

Phages concentration = Colony number × dilution coefficient × volume of bacteria culture per milliliter

Quantification of wild-type and modified phages titer by qPCR

Phages can be enumerated utilizing the quantitative PCR (qPCR) method to calculate the copies of phage genomes, which are equal to the number of phages (*i.e.* a single phage contains a single genome). The 181-bp fragment amplified from the M13KO7 plasmid was used as a standard to prepare serial dilutions from 10^6 to 10^{11} (15). For the samples, ssDNA was prepared for qPCR from the modified and wild-type phages. Primers FRealM13 and REcoRIM13 were designed using GeneRunner software version 6.5.47 (Table 1). A 12 µL PCR reaction mixture was prepared with 6 µL 2× SYBR Green Master Mix, 0.5 µL of each 10 µM primer, 4 µL sterile ddH_2O, and 1 µL ssDNA of phage as a template. PCR cycling conditions were 94 ℃ for 10 min, 40 cycles of 94 ℃ for 20 s, 63 ℃ for 30 s, and 72 ℃ for 20 s. To calculate the phage titer in pfu/mL, the quantity of modified and helper phages in 1 mL had to be ascertained first. The mean counts for both modified and helper phages were then determined by calculating the three qPCR experiment replicates. Considering that the volume of 500 µL of phages was used to extract the genome, and these were then dissolved in 75 µL of water, to convert the number of phages present in 1 µL to 1 mL, the average number of each phage was multiplied by 75 (to obtain the number for the total retrieved genome) and then by 2 (to calculate the number in 1 mL).

Statistical analyses

The statistical analysis was performed using GraphPad Prism version 10 (GraphPad Software, USA). The data are presented as mean ± SD. Statistical significance was determined using an unpaired t-test, and a P-value < 0.05 was considered statistically significant.

RESULTS

Construction and confirmation of modified pM13AMB1

In this work, we attempted to use genetic engineering to produce a modified M13 phage harboring the pMB1 ori and investigate the relationship between the titration of modified bacteriophages and the presence of high copy number origin of replication (Fig. 2). To achieve this, a 6431-bp fragment containing all the genes of the M13KO7 phage except the kanamycin resistance gene and the p15A ori coding sequence was amplified by PCR from the M13KO7 plasmid (Fig. 3A). In the following, adenine base was added to 3′ ends of this fragment, and it was then ligated to the pGetII vector using the T/A cloning method, generating the modified M13AMB1 plasmid. This modified construct was transformed into competent *E. coli* Top10 cells, and the successful construction of the pM13AMB1 plasmid was confirmed using colony PCR (Fig. 3B), which amplified the 6431-bp fragment, and plasmid digestion with *PstI* restriction endonuclease (Fig. 3C), which indicated a linearized plasmid size of ~10 kb.

Also, the presence of the insert (6431-bp) fragment in the pM13AMB1 was confirmed through amplification by PCR (Fig. 3D). Indeed, the Sanger sequencing result confirmed the presence of the M13KO7 phage genome within the modified construct. Ultimately, the existence of pM13AMB1 in *E. coli* TG1 was verified using colony PCR before the phage preparation (Fig. 3E).

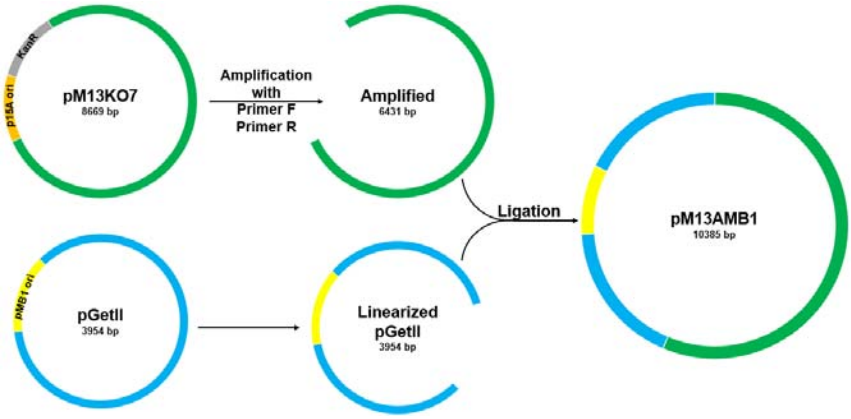

Fig. 2. Construction of M13AMB1 plasmid. Using the T/A cloning technique, a 6431-bp fragment amplified from the M13KO7 plasmid and then ligated to the pGetII vector to create a modified variant of phage M13, known as M13AMB1. The 6431-bp fragment amplified from the M13KO7 plasmid lacks the sequence related to the p15A ori and kanamycin resistance gene (KanR).

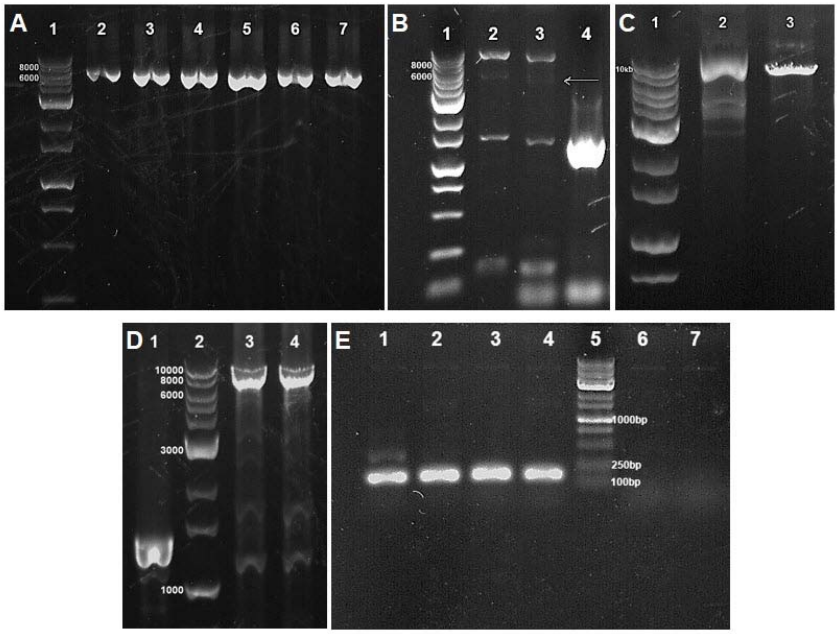

Fig. 3. Gel electrophoresis figures. (A) Using PCR, a 6431-bp fragment was amplified from the M13KO7 plasmid. In this figure, lane 1 represents the 1-kb ladder, and lanes 2 to 7 correspond to the 6431-bp fragment; (B) to confirm the presence of the 6431-bp fragment, a colony PCR reaction was conducted on the positive colonies grown on the plate, the result of which is displayed in lanes 2 to 4 next to the 1-kb ladder in lane 1; (C) the modified M13AMB1 plasmid underwent an enzymatic digestion procedure using the *PstI* restriction enzyme to confirm its approximate size of 10 kb, with related band visible in lane 3 and next to plasmid (lane 2) and 1-kb ladder (lane 1); (D) the 6431-bp fragment from the modified plasmid was amplified using a PCR reaction for additional validation, as demonstrated in lanes 3 and 4 adjacent to the 1-kb ladder in lane 2 and the incorrect-size band in lane 1; (E) prior to the phage preparation process, the presence of the M13AMB1 plasmid in the *E. coli* TG1 bacterium was verified using the colony PCR method by amplification of a 181-bp fragment. The related band is visible in lanes 1 through 4 next to the 1-kb ladder in lane 5; however, it is not present in lanes 6 and 7. PCR, Polymerase chain reaction.

Quantification and comparison of modified and wild-type phage titer

After confirming the process of phage genome manipulation and separately transforming the M13KO7 and the M13AMB1 plasmids into *E. coli* TG1 bacteria, the process of phage preparation and extraction was done. Calculation of live phages was carried out after preparation of a serial dilution for wild-type and modified phages from 10^{10}-10^{15}, and subsequently, transduction of *E. coli* TG1 bacteria with each of these phages. It should be noted that the number of colonies grown on the plate with dilutions 10^{10} and 10^{11} was so high that it was not possible to count the clones. Also, no colonies were grown on plate 10^{14} relating to bacteria transduced with the helper phage M13KO7, while colonies were visible on plates 10^{14} and 10^{15} of bacteria transduced with the modified phage M13AMB1. In general, the modified phage clones were smaller than the wild-type phage clones. Next, by averaging the number of calculated phages present in each plate, the titer of modified and helper phages was obtained, which equals 4.8×10^{14} and 7×10^{12} for the modified and wild-type phages, respectively. In other words, the M13AMB1 phage titer was ~2-log higher than the helper phage titer.

After extracting the genomes of the wild-type and modified phages, the phage titers were also calculated using the qPCR method (Fig. 4). The titer of modified and wild-type phages was calculated as 1.3×10^{9} and 4.08×10^{8}, respectively, which indicates about a 3-fold increase in the titer. Figure 5 represents a comparison of the mean copy numbers of the amplified fragment of the modified M13 phage with those of the wild-type phage, as determined by qPCR analysis. The data indicate a significantly higher titration for the modified phage compared to the wild-type phage.

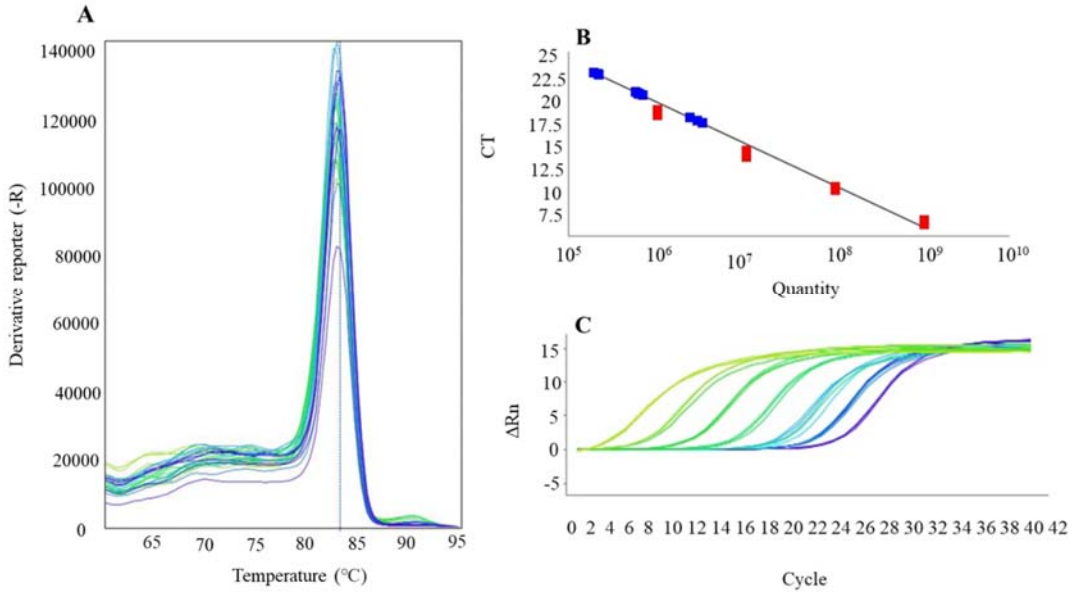

Fig 4. qPCR plots. (A) Melt curve. Melt curves of the amplified fragment from the genomes of M13AMB1 and M13KO7 phages (blue and purple curves) and the standard sample (181-bp fragment) amplified from the M13KO7 plasmid (yellow and green curves) are shown. (B) Standard curve. The graph shows a linear decrease in the average Ct value (the cycle number) with increasing phage quantity (the frequency of phage) in a qPCR reaction. The blue squares represent the 181-bp fragment amplified from the M13AMB1 and M13KO7 phage samples, while the red square represents the 181-bp fragment amplified from the M13KO7 plasmid, which was used as a standard sample to calibrate the qPCR procedure. The Ct value measures PCR cycle requirements for DNA amplification, with lower values indicating higher phage titers. (C) Amplification plot. This graph, plotted as delta-Rn per cycle, illustrates the quantification of the 181-bp fragment amplified from bacteriophages M13AMB1 and M13KO7 (blue and purple curves, respectively) in comparison to the amplification of the same fragment from serial dilutions of a standard sample (yellow to green curves). The plot indicates that the concentration of the target DNA in the M13AMB1 samples is significantly higher than the concentration in the M13KO7 samples.

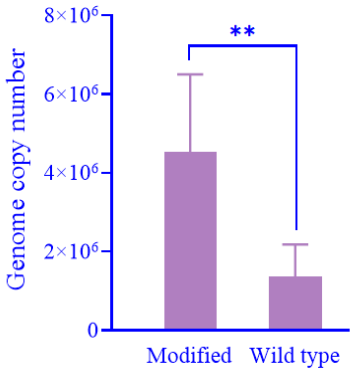

Fig. 5. Comparison of the wild-type and modified M13 phage titration. The column chart, based on qPCR data analysis, showcases the mean copy numbers of the amplified fragment of the modified M13 phage in comparison to the wild-type phage. The chart reveals a significant increase ($P < 0.01$) in the modified phage's titration over the wild-type phage. Data are presented as means ± SD.

DISCUSSION

The M13 phage is a filamentous bacteria-infecting virus that has gained significant attention in recent years for its potential applications in various fields, including biotechnology and medicine. By modifying the wild-type M13 phage, scientists have been attempting to find ways to produce altered strains of M13, which have enhanced capabilities and applications (2). One area of research involves modifying the M13 genome to introduce new functionalities or improve existing ones. For instance, M13 has been successfully engineered to display foreign peptides or proteins on its surface. This modification allows the phage to become a powerful tool for vaccine development, drug delivery, and bioimaging. Researchers have also investigated the potential of using M13 as a scaffold for the assembly of functional materials, such as metallic nanoparticles, quantum dots, or enzymes. These modifications can provide the phage with new properties and enable applications in fields like nanotechnology (1,6).

In this study, we engineered the M13KO7 phage to enhance its yield by modifying its origin of replication. By deleting the origin of replication of p15A in the helper phage M13KO7 and replacing it with the pMB1 origin of replication, which has a higher copy number, the study aimed to increase the phage yield. For evaluating the success of the engineering process, both serial dilution and qPCR methods were utilized. Our results mention that the titer of the modified phage obtained through the serial dilution method was 4.8×10^{14}, while the titer of the helper phage was 7×10^{12}. This indicates a significant increase (~2-log) in phage production for the engineered strain. The qPCR method yielded a titer of 1.3×10^{9} and 4.08×10^{8} for the modified and helper phages, respectively, further confirming the higher abundance (~3-fold) of the engineered phage.

In comparison with other related studies, the research presents some advantages. For example, the genetic modification led to a substantial increase in the phage titer, as evidenced by the significant difference in titer between the modified phage and the helper phage. This demonstrates the potential of genetic engineering to enhance phage yield, which is consistent with the findings of other studies. For instance, Kadiri *et al.* demonstrated the formation of nanonets using genetically modified M13 bacteriophages, highlighting the potential of genetic engineering to create novel phage-based structures with unique properties (16). Additionally, the study by Gosh *et al.* aimed to improve the versatility of the M13 bacteriophage as a platform for multiple peptide display, showcasing the diverse applications of genetic engineering in modifying phage properties (17).

However, the research also presents certain limitations that should be considered. One potential limitation is the impact of genetic modification on phage properties, as highlighted in the study by Wong *et al.* (18). They investigated the possibility of enhancing M13-based phagemids for transgene delivery through the elimination of the bacterial backbone, emphasizing the need to carefully consider the impact of genetic modifications on phage behavior and performance. Furthermore, a genetically engineered recombinant M13 phage containing a series of CRISPR-Cas13a systems has been developed to target antibiotic resistance genes and highlight the complexity and potential challenges associated with phage genetic engineering (19).

Compared to our study attempting to enhance phage yield through genetic engineering, Kok *et al.* took a different approach to achieve the same goal (20). They present a protocol to increase the titers of difficult bacteriophages. The rapid adaptive mutation of phage-up (RAMP-UP) protocol, a liquid infection approach, significantly improved phage titers, allowing the evolution of high-titer bacteriophages within a short timeframe of just four days. The resulting titers were adequate for extracting and sequencing DNA from the bacteriophages, demonstrating the practical implications of the protocol.

The results obtained from the titer determination methods indicated the successful engineering of the M13KO7 phage and validated the effectiveness of replacing the origin of replication. The increased copy number achieved through this modification can have significant implications for large-scale phage production and applications in biotechnology and medicine. Overall, the results demonstrated that small modifications at the genetic level might lead to notable gains in experimental performance, paving the way for innovative research avenues in molecular biology and biotechnology. Notably, ori optimization not only improves phage titration efficiency but also likely has implications for other domains, including gene cloning and nanotechnology.

The strengths of our study include demonstrating the effectiveness of genetic modification in enhancing phage yield, as well as providing a detailed description of the genetic engineering process, which can serve as a valuable reference for similar research endeavors. Also, using both serial dilution and qPCR methods for titer determination enhances the robustness of the findings, providing a comprehensive assessment of the impact of genetic modification on phage yield. While the study presents promising results, it is important to consider the potential effects on phage properties and the need for further validation to fully assess the practical implications of the genetic modification. The detailed methodology and the use of multiple titer determination methods are notable strengths of the study, providing valuable insights into the field of phage genetic engineering.

CONCLUSION

In conclusion, this study highlights the importance of optimizing the origin of replication in the M13 phage to enhance phage titration. Through our exploration of replacing the pMB1 origin with p15A, a significant increase in phage titers was achieved, as validated by both the serial dilution and qPCR methods. The modified M13AMB1 phage exhibited notably higher titers compared to the M13KO7 phage, showcasing the effectiveness of the replication origin replacement approach. These findings underscore the importance of understanding and manipulating phage replication mechanisms for various molecular biology applications, such as phage display and recombinant protein expression. Moreover, this research paves the way for future investigations into further optimizing M13 phage and exploring novel applications of modified phage variants. In essence, this study represents a substantial advancement in leveraging bacteriophages for diverse scientific and technological endeavors.

Acknowledgments

The authors express sincere gratitude to those who contributed to this study, highlighting their collaborative spirit and dedication. They also acknowledge the financial support provided by the Research Department of Isfahan University of Medical Sciences through Grant No. 3401733 and the Behyaar Zist Company.

Conflicts of interest statement

The authors declared no conflict of interest in this study.

Authors' contributions

MH. Darvishali developed the research and helped with the manuscript's drafting, editing, and development; H. Khanahmad supervised the study; and M. Fadaie assisted with editing the article. The finalized article was read and approved by all authors.

REFERENCES

1. Chang C, Guo W, Yu X, Guo C, Zhou N, Guo X, *et al*. Engineered M13 phage as a novel therapeutic bionanomaterial for clinical applications: from tissue regeneration to cancer therapy. Mater Today Bio. 2023;20:1006121,1-16. DOI: 10.1016/j.mtbio.2023.100612.
2. Wang R, Li HD, Cao Y, Wang ZY, Yang T, Wang JH. M13 phage: a versatile building block for a highly specific analysis platform. Anal Bioanal Chem. 2023;415(18):3927-3944. DOI: 10.1007/s00216-023-04606-w.
3. González-Mora A, Hernández-Pérez J, Iqbal HMN, Rito-Palomares M, Benavides J. Bacteriophage-based vaccines: a potent approach for antigen delivery. Vaccines. 2020;8(3):504,1-24. DOI: 10.3390/vaccines8030504.
4. Jaroszewicz W, Morcinek-Orłowska J, Pierzynowska K, Gaffke L, Węgrzyn G. Phage display and other peptide display technologies. FEMS Microbiol Rev. 2022;46(2):1-25. DOI: 10.1093/femsre/fuab052.
5. Bazan J, Całkosiñski I, Gamian A. Phage display a powerful technique for immunotherapy: introduction and potential of therapeutic applications. Hum Vaccines Immunother. 2012;8(12):1817-1828. DOI: 10.4161/hv.21703.
6. Fadaie M, Dianat-Moghadam H, Ghafouri E, Naderi S, Darvishali MH, Ghovvati M, *et al*. Unraveling the potential of M13 phages in biomedicine: advancing drug nanodelivery and gene therapy. Environ Res. 2023;238(P1):117132. DOI: 10.1016/j.envres.2023.117132.
7. Méndez-Scolari JE, Florentín-Pavía MM, Mujica MP, Rojas N, Sotelo PH. A qPCR targeted against the viral replication origin designed to quantify total amount of filamentous phages and phagemids. Indian J Microbiol. 2019;59(3):365-369. DOI: 10.1007/s12088-019-00798-x.
8. Camps M. Modulation of ColE1-like plasmid replication for recombinant gene expression. Recent Pat DNA Gene Seq. 2010;4(1):58-73. DOI: 10.2174/187221510790410822.
9. Kendall Morgan MP. Plasmids 101. In: Plasmid 101. Adgene.2023. Available from: addgene.org.
10. Selzer G, Som T, Itoh T, Tomizawa J. The origin of replication of plasmid p15A and comparative studies on the nucleotide sequences around the origin of related plasmids. Cell. 1983;32(1):119-129. DOI: 10.1016/0092-8674(83)90502-0.
11. Chang A, Chau V, Landas J, Pang Y. Preparation of calcium competent Escherichia coli and heat-shock transformation. J Exp Microbiol Immunol. 2017;1:22-25.
12. Hosseini N, Khanahmad H, Nasr Esfahani B, Bandehpour M, Shariati L, Zahedi N, *et al*. Targeting of cholera toxin A (ctxA) gene by zinc finger nuclease: pitfalls of using gene editing tools in prokaryotes. Res Pharm Sci. 2020;15(2):182-190. DOI: 10.4103/1735-5362.283818.
13. Reddy P, McKenney K. Improved method for the production of M13 phage and single-stranded DNA for DNA sequencing. Biotechniques. 1996;20(5):854-860. DOI: 10.2144/96205st05.
14. Ács N, Gambino M, Brøndsted L. Bacteriophage enumeration and detection methods. Front Microbiol. 2020;11:594868,1-7. DOI: 10.3389/fmicb.2020.594868.
15. Boshtam M, Asgary S, Rahimmanesh I, Kouhpayeh S, Naderi J, Hejazi Z, *et al*. Display of human and rabbit monocyte chemoattractant protein-1 on human embryonic kidney 293T cell surface. Res Pharm Sci. 2018;13(5):430-439. DOI: 10.4103/1735-5362.236836.
16. Kadiri VM, Alarcón-Correa M, Ruppert J, Günther JP, Bill J, Rothenstein D, *et al*. Genetically modified M13 bacteriophage nanonets for enzyme catalysis and recovery. Catalysts. 2019;9(9):1-10. DOI: 10.3390/catal9090723.
17. Ghosh D, Kohli AG, Moser F, Endy D, Belcher AM. Refactored M13 bacteriophage as a platform for tumor cell imaging and drug delivery. ACS Synth Biol. 2012;1(12):576-582. DOI: 10.1021/sb300052u.
18. Wong S, Jimenez S, Slavcev RA. Construction and characterization of a novel miniaturized filamentous phagemid for targeted mammalian gene transfer. Microb Cell Fact. 2023;22(1):124,1-14. DOI: 10.1186/s12934-023-02135-w.
19. Kiga K, Tan XE, Ibarra-Chávez R, Watanabe S, Aiba Y, Sato'o Y, *et al*. Development of CRISPR-Cas13a-based antimicrobials capable of sequence-specific killing of target bacteria. Nat Commun. 2020;11(1):1-11. DOI: 10.1038/s41467-020-16731-6.
20. Kok DN, Turnbull J, Takeuchi N, Tsourkas PK, Hendrickson HL. *In vitro* evolution to increase the titers of difficult bacteriophages: RAMP-UP protocol. Phage. 2023;4(2):68-81. DOI: 10.1089/phage.2023.0005.

ONLINE SUBMISSION

https://review.jow.medknow.com/rps

Research in Pharmaceutical Sciences, June 2024; 19(3): 347-355
Received: 26-04-2022
Peer Reviewed: 13-07-2022
Revised: 13-02-2023
Accepted: 01-06-2024
Published: 01-07-2024

School of Pharmacy & Pharmaceutical Sciences
Isfahan University of Medical Sciences

Original Article

Isolation of two steroidal saponins with antileishmanial activity from *Allium giganteum* L.

Farnaz Chaparian, Zeinab Delazar, and Masoud Sadeghi Dinani*

Department of Pharmacognosy, School of Pharmacy and Pharmaceutical Sciences, Isfahan University of Medical Sciences, Isfahan, Iran.

Abstract

Background and purpose: Alliums are rich sources of steroidal saponins, flavonoids, and sulphoric compounds of which steroidal saponins have recently received more attention due to their important pharmacological activities. *Allium giganteum* (giant onion) which is named locally "Couria" in the Northeast of Iran, is grown widely in "Kouh-Sorkh" mountains in Khorasan province.
Experimental approach: Phytochemical investigation of chloroform-methanol and aqueous extract of the plant resulted in the isolation and identification of two steroidal saponins, using comprehensive spectroscopic methods including 1D and 2D NMR and MS.
Findings/Results: The chemical structures of the isolated saponins were determined as (22S)-cholesta-1b,3b,16b,22b-tetraol 5-en, and 3-O-β-D-glucopyranosyl 26-O-β-D-glucopyranosside and (25R)-26-O-β-D-glucopyranosyl-5α-furostan-1α,3β,22α,26-tetraol3-O-{β-D-galactopyranosyl-(1→2)-O-[β-D-xylopyranosyl-(1→3)]-O-β-D-glucopyranosyl-(1→4)-β-D-galactopyranoside}. Investigation of *in vitro* antileishmanial activity of the isolated compounds at 10, 50, and 100 µg/mL exhibited significant leishmanicidal against the promastigotes of *Leishmania major*.
Conclusion and implications: The results established a valuable basis for further studies about *A. giganteum* and the anti-parasitic activity of steroidal saponins.

Keywords: *Allium giganteum*; Leishmania; Saponins; Structure elucidation.

INTRODUCTION

Amaryllidaceae is a family of plants with 85 genera and approximately 1100 species which are mainly present in tropical and subtropical areas and dry regions (1). Although the origin of these plants is central Asia with a history of 3000 years of use, nowadays they are spread worldwide and among common edible and medicinal plants (2-5).

Allium is a genus that belongs to Amaryllidaceae which has 750 species (4). Iran is known as a main source of *Allium* species which are mainly found in the Zagros mountains and northeast regions of the country (2).

Historically, these plants have been used both for cooking and as raw vegetables, as well as medicinal plants for the treatment of different diseases like diabetes, hypercholesterolemia, blood hypertension, heart disease, insect bites, and tumors (6,7).

Alliums are the main sources of phytonutrients and have important secondary metabolites like steroidal saponins, sapogenins, flavonoids, and sulfur components (2,8), among them, steroidal saponins and sapogenins are some of the most important compounds in these genera (9,10).

Steroidal saponins in nature are found as glycosides which have features like frothing in water, hemolytic effect, being toxic for fishes, and complex formation with cholestrin (11).

*Corresponding author: M. Sadeghi Dinani
Tel: +98-3137927129, Fax: +98-3136680011
Email: m_sadeghi@pharm.mui.ac.ir

Access this article online

Website: http://rps.mui.ac.ir

DOI: 10.4103/RPS.RPS_71_21

There are numerous scientific reports about the various pharmacologic effects of saponins such as anti-tumor effect, anti-fungal effect, inhibitory effect on abnormal bleeding of the uterus, chronotropic effect, and protective effect on gastric ulcers (12). In addition, these compounds have a broad spectrum of biological activities like hemolytic, hypocholesterolemic, immune system modulating, anti-inflammatory, anti-ulcer, and leishmanicidal effects (13,14).

Allium giganteum (giant onion) which is named locally "Couria" in the Northeast of Iran, is grown widely in "Kouh-Sorkh" mountains in Khorasan province. The plant leaves are used locally as a condiment and also as raw vegetables for cooking bread and making dishes (15).

According to the importance of steroidal saponins and their biological effects and in continuous to our previous studies for completing the project of phytochemical investigation of *Allium* species of Iran, extraction, identification, and antileishmanial activity evaluation of steroidal saponins from the aqueous and chloroform-methanol extract of *A. giganteum* flowers was conducted in this study.

MATERIALS AND METHODS

General experimental procedures

Medium-pressure liquid chromatography (MPLC) was performed (Buchi Gradient System C-605 apparatus, Switzerland) using a glass column of LiChroprep® RP-18 (25-40µm). Thin-layer chromatography (TLC) was performed on SiO_2 plates with BuOH: H_2O: CH_3COOH (60:25:15 v/v/v) (BAW) as a mobile phase and cerium sulfate in 2N H_2SO_4 as the reagent for visualizing the spots.

High-performance liquid chromatography (HPLC) was performed using Waters 515 apparatus equipped with a refractive index detector (Waters 2414) and UV detector (Waters 2487) (Waters, USA), using semipreparative C18 column (Novapak® 7.8 × 300 mm) and analytical C18 column (Novapak® 3.9 × 300 mm) in isocratic mode.

H and C nuclear magnetic resonance (NMR) spectra were recorded by Bruker 400 MHz (H at 400 MHz and C at 100 MHz) spectrometer (Bruker, Germany), using the solvent signal for calibration (CD_3OD: δH=3.31, δC=49.0). Distortionless enhancement by polarization transfer (DEPT) experiments was used to determine the multiplicities of CNMR resonances.

2D heteronuclear multiple bond correlation (HMBC), optimized for $^{2,3}JCH$ of 8 Hz, was used for the determination of two and three-bond heteronuclear 1H-13C connectivities, while 2D heteronuclear single-quantum coherence (HSQC), interpulse delay set for ^{1}JCH of 130 Hz, and correlated spectroscopy (COSY) were used for determination of one-bond heteronuclear 1H-13C connectivities and homoneuclear 1H-1H connectivities, respectively. Electrospray ionization mass spectra (ESIMS) were prepared by Shimadzu LCMS 2010 EV (Shimadzu, Japan), using methanol as the solvent.

Plant material

The whole plant of *A. giganteum* was collected from "Kaashmar", 1065 meters high from sea level, Khorasan province, Iran during the Spring of 2019. A voucher specimen (No. 43213) was deposited at the Herbarium of the Department of Pharmacognosy, School of Pharmacy and Pharmaceutical Sciences, Isfahan University of Medical Sciences, Isfahan, Iran.

Isolation and purification

Flowers of *A. giganteum* were separated, air-dried in the shade, and powdered employing a mill. The powder (835 g) was extracted at room temperature in a four-step extraction method with increasing solvent polarity using the solvents consisting of hexane, chloroform, chloroform-methanol (9:1), and methanol. Extraction was done using the maceration method, performing each step four times with 5 L of solvent under occasional stirring. Methanol extract of the sample was concentrated under vacuum, dissolved in water, and then by adding n-butanol, distributed between two solvents. The resulting butanol and aqueous layers were separated and concentrated under a vacuum.

The chloroform-methanol (9:1) extract of the sample was concentrated under vacuum, yielding a crude dried extract (15.32 g) which was fractionated by MPLC on an RP-18 column (36 × 460 mm) using a linear gradient solvent system of H_2O to CH_3OH. Fractions were analyzed by TLC (SiO_2, BAW 60:15:25 v/v/v) and similar fractions were pooled together. Based on TLC and preliminary NMR analysis, 3rd fraction was considered to be richer in steroidal saponins, which was concentrated by rotary evaporator and subjected to HPLC for further purification. The final purification of the fraction was performed by HPLC using a semi-preparative C18 column (Novapak® 7.8 × 300 mm) and H_2O:CH_3OH (80:20) mobile phase in isocratic mode, resulting in 10 mg of compound (1).

The aqueous extract of the sample was concentrated under vacuum, yielding a crude dried extract (12.97 g) which was fractionated by MPLC on an RP-18 column (36 × 460 mm) using a linear gradient solvent system of H_2O to CH_3OH. Fractions were analyzed by TLC (SiO_2, BAW 60:15:25 v/v/v) and similar fractions were pooled together. Based on TLC and preliminary NMR analysis, the 8th fraction was considered to be richer in steroidal saponins, which were concentrated by a rotary evaporator and subjected to HPLC for further purification. The final purification of the fraction was performed by HPLC using a semi-preparative C18 column (Novapak® 7.8 × 300 mm) and H_2O:CH_3OH (80:20) mobile phase in isocratic mode, resulting in 22 mg of compound (2).

Evaluation of antileishmanial activity

Leishmania parasites

Cryopreserved *Leishmania major* (MRHO/IR75/ER) were obtained from the Department of Parasitology & Mycology, Isfahan University of Medical Sciences and were transferred to modified Nicole Novy Neal (N.N.N.) medium supplemented with 4% brain heart infusion (BHI, 0.2 mL), streptomycin (100 µg/mL) and penicillin (100 U/mL). The promastigotes were then passaged in complemented RPMI 1640 with fetal calf serum (FCS, 10% v/v), L- glutamine (2 Mm), penicillin (100 U/mL), and streptomycin (100 µg/mL), and incubated at 25 °C. The antileishmanial activity was evaluated using promastigotes in the logarithmic phase.

Antileishmanial assay

The antileishmanial assay was performed as described by Kazemi Oskuee *et al.* (16). Briefly, *L. major* promastigotes 4×10^5 in 400 µL complemented RPMI were cultured in 24-well plates. The steroidal saponin was dissolved in RPMI 1640 with the aid of 2% DMSO as co-solvent and added to the wells to make the final concentrations of 10, 50, and 100 µg/mL. The plates were incubated at 25 °C for 2 days and the number of viable parasites was counted on the periods of 12, 24, and 48 h. Amphotericin B at 0.5 and 1 µg/well and RPMI medium were used as the positive and negative control groups, respectively.

Statistical analysis

Antileishmanial activities were reported as mean ± SD and statically analyzed by one-way ANOVA followed by the Tukey-Kramer post-hoc test using SPSS Ver. 16. The *P*-values < 0.05 were considered statistically significant.

RESULTS

Based on TLC and preliminary NMR screening, two saponins-rich fractions of the plant extracts were selected for further purification, resulting in the isolation and identification of 2 steroidal saponins (compounds 1 and 2; Fig. 1). The chemical structure of isolated compounds was determined using comprehensive spectroscopic methods and also by comparison of the spectral data with those reported in the literature.

Characterization of compound (1)

Compound (1) was isolated as an amorphous solid and showed in the positive ESIMS spectrum a pseudomolecular ion peak at m/z 781.4 [M+Na]+ which together with CNMR data indicated the molecular formula $C_{39}H_{66}O_{14}$. Diagnostic resonances of the HNMR spectrum were those attributed to two tertiary methyls (2 singlets: δH 0.78 (1H) and 0.95 (1H); CNMR: δC 13.81 and 14.81), two

overlapped secondary methyl (2 doublets: δH 0.77 (1H, d, 6.4) and 0.79 (1H, d, 6); CNMR: δC 23.26 and 12.16), one olefinic δH 5.42 (1H, d, 4.8), and two anomeric protons δH 4.03 (1H, d, 7.23) and 4.22 (1H, d, 7.64). The CNMR spectrum showed 35 resonance lines, supporting the molecular formula deduced from ESIMS, 27 of them were attributed to the aglycone part and 12 to two hexose monosaccharides. Diagnostic resonances regarding the glycone part were anomeric carbon resonances at δC 100.93 and 107.31. Other diagnostic resonances in the CNMR spectrum of compound (1) were δC 70.09 which was attributed to the C-22, δC 83.24 for C1 (C-OH), δC 139.55 for C5 (C=C), δC 126.2 for C6 (C=C), and δC 83.45 for C16 (C-OH) of aglycon part.

Determining the glycon part of the compound (1), using the first anomeric proton position (H1I; δH 4.03) and HSQC and COSY spectral data, especially the characteristic large coupling constant of H4I and H1I, the two sugars were determined as β-D-glucopyranoside. This was confirmed by the glycosylation shifts of C2I and C4I and also by the fragmentation peaks in the ESIMS spectrum due to the loss of sugar units from the pseudomolecular ion.

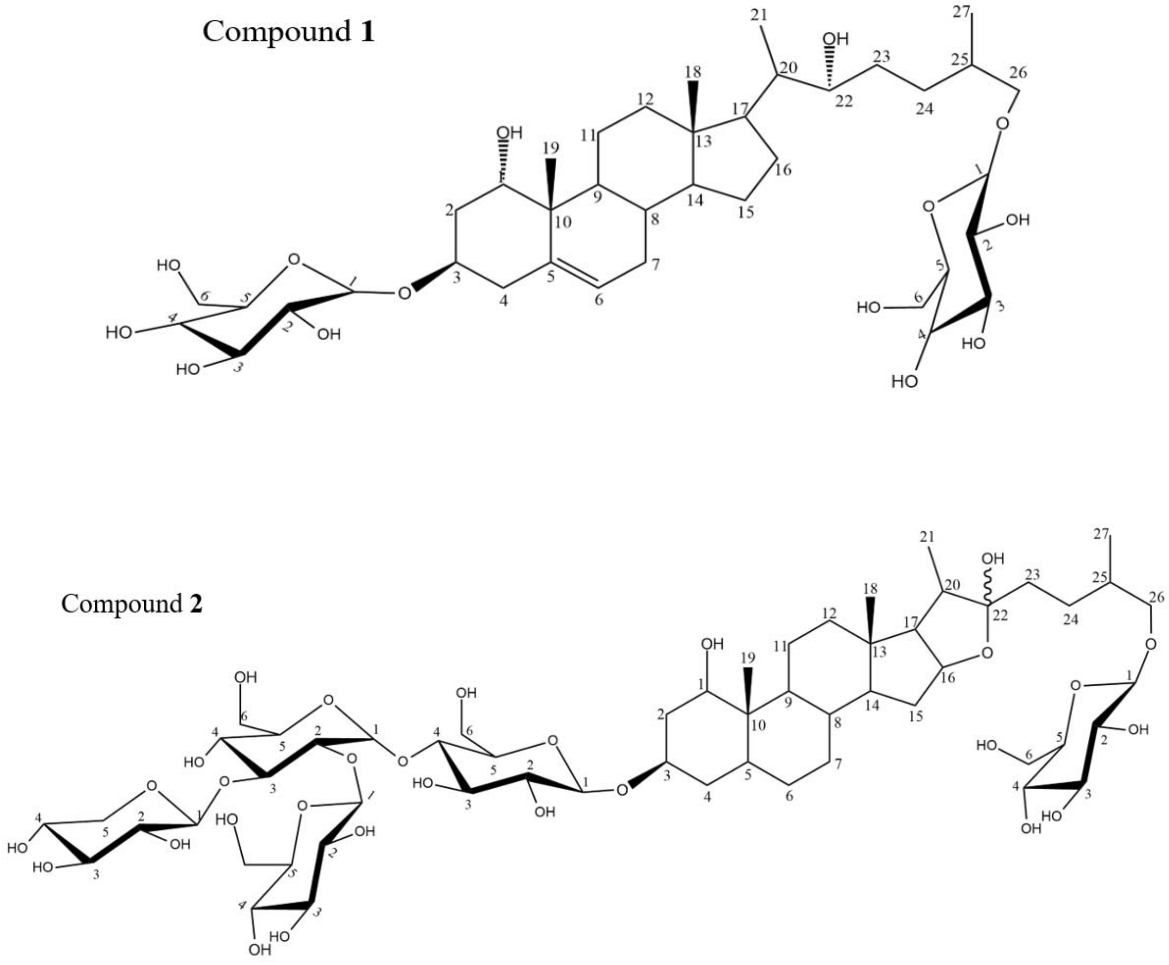

Fig. 1. Chemical structure of compounds **1** and **2.**

Characterization of compound (2)

The saponin nature of compound (2) was confirmed by 1H and 13CNMR spectra of the compound and the existence of diagnostic and characteristic signals of saponins especially two tertiary methyls (2 singlets: δH 0.75 (1H) and 0.94 (1H); CNMR: δC 16.25 and 17.34), two secondary methyls (2 doublets; δH 0.85 (1H,d, 6.8), 0.90 (1H, d, 6.8); CNMR: δC 16.25, 17.08), five anomeric protons (δH 4.15, 4.31, 4.49, 4.51, 4.85) and related anomeric carbon signals (δC 102.60, 104.26, 104.57, 104.72, and 104.93) (Tables 1 and 2). In the ESIMS spectra, compound (2) showed a pseudomolecular ion peak at m/z 1231.33 [M+Na]+ in the positive-ion mode which together with the CNMR data, suggested its molecular formula as $C_{56}H_{94}O_{29}$.

According to H and CNMR spectra of compound 2, two hydroxyl groups were also implied from the molecular formula which were determined to be placed at C1(δC 77.89) and C22 (δC 114.00).

To deduce the glycon part of (2), starting from the first anomeric proton (H1I; δH 4.15) and using the HSQC and COSY spectral data, the sugar chain was determined to be composed of two β-D-glucopyranoside, two β-D-galactopyranoside, and β-D-xylopyranoside monosaccharides, completing the sugar chain structure elucidation (Table 2). This was further confirmed by the fragmentation peaks in the ESIMS spectrum due to the loss of sugar units from the pseudomolecular ion.

Table 1. ^{1}HNMR and ^{13}CNMR data of the aglycon part of compounds **1** and **2** (400 MHz, CD_3OD)

Position	Compound 1		Compound 2	
	δ_C (mult.)	**δ_H (int., mult., *J* in Hz)**	**δ_C (mult.)**	**δ_H (int., mult., J in Hz)**
1a	83.24	3.59	77.89	0.94
1b	-	-	-	1.73
2a	37.10	1.80	30.47	1.32
2b	-	-	-	1.51
3	69.09	3.75	87.88	3.43
4a	41.47	2.50	39.78	2.48
4b	-	2.58	-	2.58
5	139.55	-	34.97	-
6	126.2	5.42	41.18	-
7a	32.51	1.31	32.85	1.73
7b	-	1.73	-	1.87
8	34.18	1.27	27.77	1.54
9	51.21	1.16	55.68	0.86
10	43.27	-	36.86	-
11a	24.69	2.41	21.98	1.46
11b	-	1.47	-	1.39
12a	43.26	2.09	40.78	1.63
12b	-	1.39	-	1.04
13	42.85	-	42.22	-
14	56.21	0.95	57.26	1.04
15a	37.78	1.69	32.75	1.18
15b	-	2.22	-	2.08
16	83.45	4.51	82.46	4.49
17	58.84	1.91	63.09	1.63
18	13.81	0.78	16.25	0.75
19	14.81	0.95	17.34	0.94
20	36.31	2.42	41.22	1.87
21	12.16	0.79	16.25	0.85
22	70.09	-	114.00	-
23a	37.07	1.73	31.38	1.70
23b	-	1.64	-	1.46
24a	34.18	1.78	28.93	1.50
24b	-	1.55	76.00	1.27
25	29.78	1.44	31.37	1.18
26a	73.49	0.78	76.00	3.27
26b	-	-	-	3.21
27	23.26	0.77	17.08	0.90

NMR, Nuclear magnetic resonance.

Table 2. [1]HNMR and [13]CNMR data of sugar part of the compound (**1**) and (**2**) (400 MHz, 100 MHz; CD_3OD)

Position	$2\delta_H$ (int, mult, J in Hz) δ_C (mult)		$1\delta_H$ (int, mult, J in Hz) δ_C (mult)	
I	**Glucopyranoside 1**		**Glucopyranoside 1**	
1	4.15	102.60 (CH)	4.03	100.93
2	3.19-3.79	75.31 (CH)	3.61	74.36
3	3.19-3.79	79.80 (CH)	3.59	77.78
4	3.19-3.79	70.96 (CH)	4.21	72.34
5	3.19-3.79	77,45 (CH)	3.43	75.33
6	3.19-3.79	61.10 (CH_2)	3.23	62.22
II	**Glucopyranoside 2**		**Glucopyranoside 2**	
1	4.31	104.26 (CH)	4.22	107.31
2	3.19-3.79	75.60 (CH)	3.75	75.33
3	3.19-3.79	80.20 (CH)	3.45	78.11
4	3.19-3.79	71.54 (CH)	4.02	72.90
5	3.19-3.79	78.12 (CH)	3.56	76.27
6	3.19-3.79	62.69 (CH_2)	3.35	63.59
III	**β-D-galactopyranoside 1**			
1	4.49	104.72 (CH)		
2	3.19-3.79	75.86 (CH)		
3	3.19-3.79	80.27 (CH)		
4	3.19-3.79	71.69 (CH)		
5	3.19-3.79	77.90 (CH)		
6	3.19-3.79	62.80 (CH_2)		
IV	**β-D-galactopyranoside 2**			
1	4.51	104.93 (CH)		
2	3.19-3.79	76.00 (CH)		
3	3.19-3.79	81.02 (CH)		
4	3.19-3.79	72.45 (CH)		
5	3.19-3.79	78.50 (CH)		
6	3.19-3.79	63.09 (CH_2)		
V	**Xylopyranoside**			
1	4.85	104.57 (CH)		
2	3.19-3.79	73.18 (CH)		
3	3.19-3.79	75.16 (CH)		
4	3.19-3.79	70.40 (CH)		
5	3.19-3.79	67.19 (CH_2)		

NMR, Nuclear magnetic resonance.

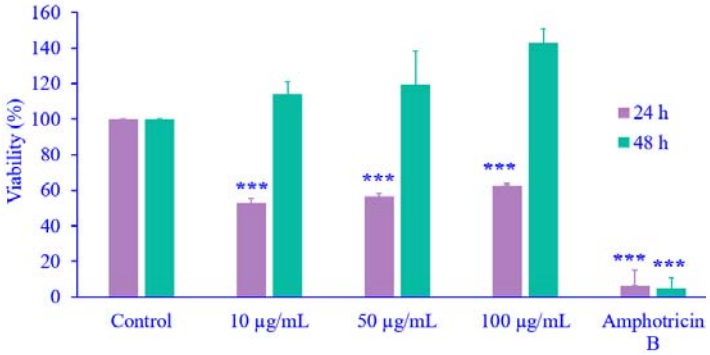

Fig. 2. Antileishmanial activities of different concentrations of compound (**1**). Data are expressed as mean ± SD, n = 3. ***$P \leq 0.001$ indicates significant differences in comparison with the corresponding control group.

Antileishmanial activity of compounds (1) and (2)

The antileishmanial activity of compounds (1) and (2) was assessed against the *L. major* promastigotes using the microplate method. The leishmanicidal activity of the compound (1) was significant in 10, 50, and 100 µg/mL after 24 h as shown in Fig. 2, but after 48 h its leishmanicidal activity decreased. Compound (2) showed a leishmanicidal effect after 24 h only in 10 µg/mL, while in 50 and 100 µg/mL and after 48 h the leishmanicidal activity was not significant (Fig. 3).

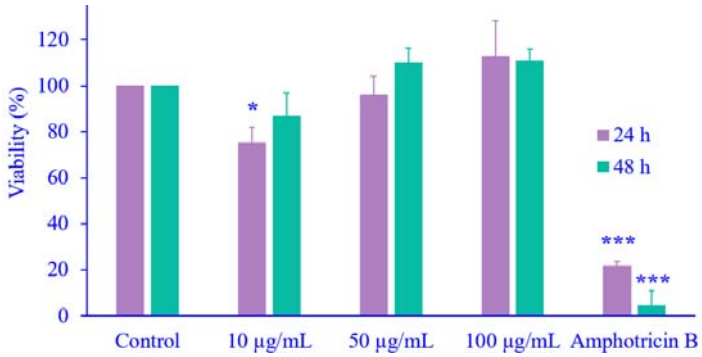

Fig. 3. Antileishmanial activities of different concentrations of compound **2.** Data are expressed as mean ± SD, n = 3. ***$P \leq 0.001$ indicates significant differences in comparison with the corresponding control group.

DISCUSSION

As a member of the Amarillidaceae family, *A. giganteum*, an edible *Allium* species in Khorasan province of Iran, has been shown to possess a variety of pharmacological effects including antioxidant activity, inhibition of cAMP phosphodiesterase activity, *etc.* (17,18).

The phytochemical study of *A. giganteum*, especially the saponin constituents of the plant, resulted in the isolation and identification of two steroidal saponins from the flowers of the plant. Considering previous reports on the antimicrobial and especially antileishmanial activity of some natural steroidal saponins, the leishmanicidal effects of the isolated compound were evaluated, which exhibited its weak leishmanicidal activity on promastigotes of *L. major*. However, the activity has decreased significantly after 48 h which could be the result of metabolization, degradation, or bidesmosidic nature of isolated compounds. The results are in line with few recent reports about the antileishmanial activity of some steroidal saponins such as racemoside A isolated from *Asparagus racemosus* and the steroidal saponin isolated from *A. paradoxum* (8), which could be used as a chemical basis for justification of antimicrobial effects of different *Allium* species and scientific support of future studies of leishmanicidal steroidal saponins. Steroidal saponins in nature are found as glycosides which have features like frothing in water, hemolytic effect, being toxic for fishes, and complex formation with cholestrin (11). There are numerous scientific reports about the various pharmacologic effects of saponins such as anti-tumor effect, anti-fungal effect, inhibitory effect on abnormal bleeding of the uterus, chronotropic effect, and protective effect on gastric ulcers (12). In addition, these compounds have a broad spectrum of biological activities like hemolytic, hypocholesterolemic, immune system modulating, anti-inflammatory, anti-ulcer, and leishmanicidal effects (13,14).

To the best of our knowledge, this is the first time that compound 1 which is a cholestan saponin, isolated from *Allium* species and dioscoreavilloside A, achieved from *Dioscorea villosa* is similar to it with differences in substitution of a hydroxyl group and one of the sugars (19).

Species of the genus *Dioscorea* (family Dioscoreaceae) are widely used as botanical dietary supplements. These plants are well known for containing steroidal saponins, mainly belonging to the spirostanol and furostanol classes, and these have been used as chemical marker compounds for the quality control of botanical products. Wild yam, the rhizomes and roots of *Dioscorea villosa* L., is an important source of diosgenin (20)

Compound 2 is a furostanol saponin and is similar to parivispinoside A, which is achieved from *Tribulus parvispinus*, with a difference in a hydroxyl group substitution (21).

Tribulus parvispinus Presl (Zygophyllaceae) is an annual prostrate herb that grows in the warm regions of Egypt, Iraq, Iran, and Pakistan (22). Tribulus species are rich in furostane- and spirostane-type steroidal saponins that have displayed a wide range of biological activities including cytotoxic (23-26), antiproliferative (27), and antimicrobial effects (28).

CONCLUSION

Phytochemical investigation of *A. giganteum* led to the isolation of two steroidal saponins with weak leishmanicidal activity from the plant for the first time, which established a valuable basis for further studies about steroidal saponins. The results are also of great importance for the explanation of the biological and pharmacological effects of the plant.

Acknowledgments

The content of this paper is extracted from the Pharm. D thesis submitted by F. Chaparian which was financially supported by the Vice-Chancellery of Research of Isfahan University of Medical Sciences, Isfahan, Iran through Grant No. 399191.

Conflict of interest statement

The authors declared no conflict of interest in this study.

Authors' contribution

All the authors contributed equally to this work. The finalized article was read and approved by all authors.

REFERENCES

1. Evans WC. Trease and Evans' pharmacognosy E-book. 16th ed. Elsevier Health Sciences; 2009. pp. 40.
2. Chehri Z, Zolfaghari B, Sadeghi Dinani M. Isolation of cinnamic acid derivatives from the bulbs of *Allium tripedale*. Adv Biomed Res. 2018;7:60,1-5. DOI: 10.4103/abr.abr_34_17.
3. Hosseinzadeh Namin H, Saeidi Mehrvarz S, Zarre S, Fritsch R. Pollen morphology of selected species of *Allium* (Alliaceae) distributed in Iran. Nord J Bot. 2009;27(1):54-60. DOI: 10.1111/j.1756-1051.2009.00319.x.
4. Movafeghi A, Miryeganeh M. Scape anatomy of *Allium* sect. *Allium* (Alliaceae) in Iran. J Sci. 2009;35(1):1-5.
5. Ozturk M, Gucel S, Altay V, Altundag E. Alliums, an underutilized genetic resource in the east Mediterranean. Acta Hort. 2012;969:303-310. DOI: 10.17660/ActaHortic.2012.969.39.
6. Lanzotti V. Bioactive polar natural compounds from garlic and onions. Phytochem Rev. 2012;11(2-3):179-196. DOI: 10.1007/s11101-012-9247-3.
7. Sadeghi M, Safaeian L, Aghaye Ghazvini MR, Ramezani M. Evaluation of fibrinolytic and antioxidant effects of *Allium affine* hydroalcoholic extract. Res Pharm Sci. 2017;12(4):299-306. DOI: 10.4103/1735-5362.212047.
8. Rezaee F, Zolfaghari B, Sadeghi Dinani M. Isolation of dioscin-related steroidal saponin from the bulbs of *Allium paradoxum L.* with leishmanicidal activity. Res Pharm Sci. 2018;13(5):469-475. DOI: 10.4103/1735-5362.236875.
9. Cui M, Song F, Zhou Y, Liu Z, Liu S. Rapid identification of saponins in plant extracts by electrospray ionization multi-stage tandem mass spectrometry and liquid chromatography/tandem mass spectrometry. Rapid Commun Mass Spectrom. 2000;14(14):1280-1286. DOI: 10.1002/1097-0231(20000730)14:14<1280::AID-RCM26>3.0.CO;2-C.
10. Sadeghi M, Zolfaghari B, Senatore M, Lanzotti V. Spirostane, furostane and cholestane saponins from Persian leek with antifungal activity. Food Chem. 2013;141(2):1512-1521. DOI: 10.1016/j.foodchem.2013.04.009.
11. Sang S, Mao S, Lao A, Chen Z, Ho CT. New steroid saponins from the seeds of *Allium tuberosum L.* J Agric Food Chem. 2001;49(3):1475-1478. DOI: 10.1021/jf001062b.
12. Zhang T, Liu H, Liu XT, Xu DR, Chen XQ, Wang Q. Qualitative and quantitative analysis of steroidal saponins in crude extracts from *Paris polyphylla* var. yunnanensis and *P. polyphylla* var. chinensis by high performance liquid chromatography coupled with mass spectrometry. J Pharm Biomed Anal. 2010;51(1):114-124. DOI: 10.1016/j.jpba.2009.08.020.
13. Adão CR, da Silva BP, Tinoco LW, Parente JP. Haemolytic activity and immunological adjuvant effect of a new steroidal saponin from *Allium ampeloprasum* var. porrum. Chem Biodivers. 2012;9(1):58-67. DOI: 10.1002/cbdv.201100005.
14. Adão CR, da Silva BP, Parente JP. A new steroidal saponin with antiinflammatory and antiulcerogenic properties from the bulbs of *Allium ampeloprasum* var. porrum. Fitoterapia. 2011;82(8): 1175-1180. DOI: 10.1016/j.fitote.2011.08.003.
15. Fritsch RM. A preliminary review of *Allium* subg. *Melanocrommyum* in central Asia. Leibniz-Institut für Pflanzengenetik und Kulturpflanzenforschung Gatersleben (IPK), Gatersleben; 2016. pp. 168.
16. Oskuee RK, Jaafari MR, Amani S, Ramezani M. Evaluation of leishmanicidal effect of *Euphorbia erythadenia* extract by *in vitro* leshmanicidal assay using promastigotes of *Leishmania major*. Asian Pac J Trop Biomed. 2014;4(2):S581-S583. DOI: 10.12980/APJTB.4.2014C1018.
17. Štajner D, Milić-Demarino N, Čanadanović-Brunet J, Štajner M, Popović BM. Screening for antioxidant properties of *Allium giganteum*. Fitoterapia. 2006;77(4):268-270. DOI: 10.1016/j.fitote.2006.03.015.

18. Mimaki Y, Nikaido T, Matsomuto K, Sashida Y, Ohmoto T. New steroidal saponins from the bulbs of *Allium giganteum* exhibiting potent inhibition of cAMP phosphodiesterase activity. Chem Pharm Bull. 1994;42(3):710-714. DOI: 10.1248/cpb.42.710.
19. Avula B, Wang YH, Wang M, Ali Z, Smillie TJ, Zweigenbaum J, *et al*. Characterization of steroidal saponins from *Dioscorea villosa* and *D. cayenensis* using ultrahigh performance liquid chromatography/electrospray ionization quadrupole time-of-flight mass spectrometry. Planta Med. 2014;80(4):321-329. DOI: 10.1055/s-0033-1360330.
20. Dong SH, Cai G, Napolitano JG, Nikolić D, Lankin DC, McAlpine JB, *et al.* Lipidated steroid saponins from *Dioscorea villosa* (wild yam). Fitoterapia. 2013;91:113-124. DOI: 10.1016/j.fitote.2013.07.018.
21. Perrone A, Plaza A, Bloise E, Nigro P, Hamed AI, Belisario MA, *et al*. Cytotoxic furostanol saponins and a megastigmane glucoside from *Tribulus p arvispinus*. J Nat Prod. 2005;68(10):1549-1553. DOI: 10.1021/np0502138.
22. Kadria A. Ahmed, Amaal H. Mohamed. A taxonomic study of the genus *Tribulus* L. in Egypt. Arab Univ J Agric Sci. 2005;13(2):197-206.
23. Hu K, Dong A, Yao X, Kobayashi H, Iwasaki S. Antineoplastic agents II: four furostanol glycosides from rhizomes of *Dioscorea collettii var. hypoglauca*. Planta Med. 1997;63(2):161-165. DOI: 10.1055/s-2006-957636.
24. Pan WB, Chang FR, Wei LM, Wu YC. New flavans, spirostanol sapogenins, and a pregnane genin from *Tupistra chinensis* and their cytotoxicity. J Nat Prod. 2003;66(2):161-168. DOI: 10.1021/np0203382.
25. González AG, Hernández JC, León F, Padrón JI, Estévez F, Quintana J, *et al*. Steroidal saponins from the bark of *Dracaena draco* and their cytotoxic activities. J Nat Prod. 2003;66(6):793-798. DOI: 10.1021/np020517j.
26. Dong M, Feng XZ, Wang BX, Wu LG, Ikejima T. Two novel furostanol saponins from the rhizomes of *Dioscorea panthaica* Prain et Burkill and their cytotoxic activity. Tetrahedron. 2001;57(3):501-506. DOI: 10.1016/S0040-4020(00)01024-3.
27. Tran QL, Tezuka Y, Banskota AH, Tran QK, Saiki I, Kadota S. New spirostanol steroids and steroidal saponins from roots and rhizomes of *Dracaena a ngustifolia* and their antiproliferative activity. J Nat Prod. 2001;64(9):1127-1132. DOI: 10.1021/np0100385.
28. Iorizzi M, Lanzotti V, Ranalli G, De Marino S, Zollo F. Antimicrobial furostanol saponins from the seeds of *Capsicum annuum L.* var. acuminatum. J Agric Food Chem. 2002;50(15):4310-4316. DOI: 10.1021/jf0116911.

ONLINE SUBMISSION

https://review.jow.medknow.com/rps

Research in Pharmaceutical Sciences, June 2024; 19(3): 356-365
Received: 05-03-2023
Peer Reviewed: 10-05-2023
Revised: 18-10-2023
Accepted: 01-06-2024
Published: 01-07-2024

School of Pharmacy & Pharmaceutical Sciences
Isfahan University of Medical Sciences

Original Article

Recombinant production of interleukin-1 receptor antagonist in fusion to albumin binding domain with potential affinity to human serum albumin

Fatemeh Shafiee[1,2,*] and Ali Yazdani[1]

[1]*Department of Pharmaceutical Biotechnology, School of Pharmacy and Pharmaceutical Sciences, Isfahan University of Medical Sciences, Isfahan, Iran.*
[2]*Bioinformatics Research Center, School of Pharmacy and Pharmaceutical Sciences, Isfahan University of Medical Sciences, Isfahan, Iran.*

Abstract

Background and purpose: Anakinra must be injected daily due to its short half-life and this leads to lower patient compliance. Therefore, the aim of this study was to produce an interleukin-1 receptor antagonist (IL-1Ra) with albumin binding domain (ABD) as a novel fusion protein and evaluate its binding ability to albumin and its biological effects.

Experimental approach: The three-dimensional structure of IL-1Ra-ABD was predicted by MODELLER software and its interaction with IL-1R was evaluated by the HADDOCK server. The expression of IL-1Ra-ABD was performed in *E. coli* in fusion with intein 1 of pTWIN1 in soluble form and then purified. The affinity of IL-1Ra-ABD to human serum albumin (HSA) was determined on native-PAGE, and its release percent toward time was evaluated. Moreover, an MTT assay was used to determine the antagonizing properties of recombinant IL-1Ra-ABD against IL-1β in A375 and HEK293 cell lines.

Findings/Results: The stable complex of IL-1Ra-ABD with IL-1R established the absence of steric hindrance due to the addition of ABD to IL-1Ra. The expression induction of intein 1-IL-1Ra-ABD using 0.1 mM IPTG at 15 °C, and its cleavage represented bands approximately in 50 and 23 kDa. Furthermore, about 78% of IL-1Ra-ABD was attached to the HSA after 2 h of incubation, and the MTT assay showed no significant differences between the effects of IL-1Ra-ABD and native IL-1Ra in cell survival.

Conclusions and implications: The production of soluble IL-1Ra-ABD with no significant differences in IL-1Ra antagonizing effects was successfully performed. IL-1Ra-ABD showed suitable interaction with HSA and was released over time. However, the half-life of IL-1Ra-ABD *in vivo* must be determined in the subsequent investigations.

Keywords: Albumin binding domain; Human serum albumin; IL-1Ra; Intein.

INTRODUCTION

IL-1Ra (interleukin 1 receptor antagonist), known as anakinra (Kineret®), was produced by Amgen Company for the first time, and the FDA approved it for the treatment of rheumatoid arthritis, as well as the deficiency of IL-1Ra, a rare auto-inflammatory disease with involving skin and bones (1).

This protein has 153 amino acid residues with a molecular weight of 17.3 kDa and is produced in the *Escherichia coli* expression system by recombinant DNA technology. The drug is recommended as the SC (subcutaneous) injection of 100 mg daily with a half-life between 4 to 6 h (2).

*Corresponding author: F. Shafiee
Tel: +98-3137927058, Fax: +98-3136680011
Email: f_shafiee@pharm.mui.ac.ir

Access this article online	
	Website: http://rps.mui.ac.ir
	DOI: 10.4103/RPS.RPS_41_23

The rapid clearance of biomolecules from the bloodstream can limit their clinical effects and lead to frequent administration. As mentioned, anakinra must be administered once a day by the SC injection. Although it is generally safe and well tolerated, the reactions of the injection site are the most concern in anakinra administration, and result in the low acceptance of patients (3). Therefore, trying to produce derivatives with an extended half-life is essential.

Pegylation is one of the most prevalent ways to extend the half-life of drugs and reduce the frequency of administration. However, alternative methods have been considered in recent years due to the complexity of the pegylated formulations and the possibility of polyethylene glycol side effects (4). In this regard, one study showed that anakinra binding to the biodegradable hydroxyethyl starch in comparison to its pegylated form resulted in increasing its thermal stability during the shelf-life (5).

Furthermore, many proteins have been engineered by consensus sequence design methods to enhance drug stability. In evidence, Podust *et al*. used the XTEN sequence to increase the half-life of various recombinant drugs (6). On the other hand, serum albumin is an attractive option to increase the half-life of bio-drugs due to the biological features including the long half-life (19 days in humans), the highest blood concentration compared to the other plasma proteins, and the biological distribution in inflammation or tumor site (7). One study produced a recombinant form of IL-1Ra protein in fusion to human serum albumin (HSA) and showed that this fusion protein is able to bind to the related receptor with no difference to the native protein (8). However, the attachment of a large molecule such as albumin to the target protein may interfere with its receptor binding, in addition to increasing the gene synthesis cost and disrupting the vital processes of the host cell. Thus, the recombinant production of drugs in fusion with the albumin binding domains (ABD) is a suitable approach to overcome these drawbacks (9). Literature has reported several biological drugs such as exenatide (10), hirodin (11), and glucagon-like peptide-1 GLP1 receptor agonist (12) whose half-lives increased *via* the addition of ABD. One study investigated several peptides with G148 ABD of *streptococci* strains as a template. Finally, a 44-amino acid peptide with eukaryotic origin was introduced with the most similarity to the ABD sequence (13).

Accordingly, the aim of the present study was to design an IL-1Ra-ABD fusion protein and produce it by recombinant DNA technology with an intein tag (Ssp intein) from the pTWIN1 plasmid. Furthermore, the current study evaluated the IL-1Ra-ABD antagonizing efficacy of IL-1β compared to the native IL-1Ra and determined its affinity to HSA and release efficacy.

MATERIALS AND METHODS

Protein design and molecular docking

To compare the binding of anakinra and IL1Ra-ABD to IL-1R, the prediction of the three-dimensional structure of IL-1R, IL-1Ra, and ABD was performed by type-1 interleukin-1 receptor complexed with interleukin-1 beta (PDB code: 1TTB), the X-ray structure of interleukin-1 receptor antagonist at 2.0 Å resolution (PDB code: 1ILT), and the crystal structure of the GA module complexed with HSA (PDB code: 1TF0), respectively, using the software of Modeller 9.24 and by multiple homology modeling strategies. In each case, among 1000 predicted models, one with the lowest value of discrete optimized protein energy (DOPE) was considered the best model for protein docking. The analysis of the best model was performed by ProSA, PROCHECK, and Verify3D web servers and finally, the formation of the salt bridge was predicted using the software of visual molecular dynamics. The web server of HADDOCK 2.2 was then used to compare the affinity of two types of IL-1Ra for the interaction with its receptor. The active residues for each molecule were prepared according to the study of Barkestani *et al.* (14).

Expression of IL-1Ra-ABD fusion protein

The coding sequence of IL-1Ra was obtained from DrugBank (https://go.drugbank.com) with accession number DBCAT002727 and fused to the amino acid sequence of ABD obtained from Jacob's study (13). The pTWIN1-IL-1Ra-ABD plasmid

was synthesized by BioMatik Company (Canada) in fusion to intein 1 and a chitin-binding domain (CBD) at the amino end which was used as the affinity tag which can bind to chitin resin to facilitate the purification process (Fig. 1A). This construct was transformed to the *E. coli* BL21 (DE3) (Pasteur Institute, Tehran, Iran) as the host cells, followed by selecting the recombinant colonies on Luria Bertani (LB) agar plates (HiMedia, India) containing 100 µg/mL of ampicillin (Sigma, Germany). The selected colony was then cultivated overnight and used to inoculate fresh culture to reach an optical density at 600 nm (OD_{600}) of 0.4 to 0.6. Next, the expression of intein1-IL-1Ra-ABD was induced by isopropyl β-D-1-thiogalactopyranoside (IPTG) (Sigma, Germany) in various concentrations (0.1, 0.5, and 1 mM) for 4 h at different temperatures (15, 25, and 37 °C). The cells were harvested *via* centrifuging at 7000 *g* at 4 °C for 10 min. For each expression condition, the separation of soluble protein and inclusion bodies was performed by cell lysis via sonicating. The soluble part of the protein in the supernatant and the inclusion body in the cell plate was separated as a precipitate by centrifuging. Finally, the supernatant of various conditions was evaluated by 12% sodium dodecyl sulfate-polyacrylamide gel electrophoresis (SDS-PAGE).

Self-cleavage inducing of Ssp intein

On-column cleavage and the purification of IL-1Ra-ABD were mediated by the intein-mediated purification with an affinity chitin-binding tag (IMPACT™, New England Biolabs, USA) using the CBD at the N-terminal of the intein 1 with affinity to chitin resin. Briefly, the cell pellets related to the most soluble expression and the least auto-cleavage (determined in the previous stage) were re-suspended in B1 buffer (Tris-HCl 20 mM, NaCl 500 mM, and EDTA 1 mM, pH 8.5), and followed by sonicating for the cell lysis. The sample was then centrifuged at 7000 *g* at 10 °C for 15 min and finally, the supernatant was loaded on the chitin column. The flow-through was discarded, and the column washing procedure was repeated five times with B1 buffer and then replaced with B2 buffer (Tris-HCl 20 mM, NaCl 500 mM, and EDTA 1 mM, pH 6.5). The column was incubated for 24 h at 25 °C. Eventually, various elutions were collected and analyzed by 15% SDS-PAGE. All elutions were mixed and subjected to dialysis against phosphate-buffered saline (PBS), pH 7.4 for 24 h at 4 °C. Finally, the protein concentration was determined using the Bradford method against various concentrations of HSA (Octapharma, Sweden).

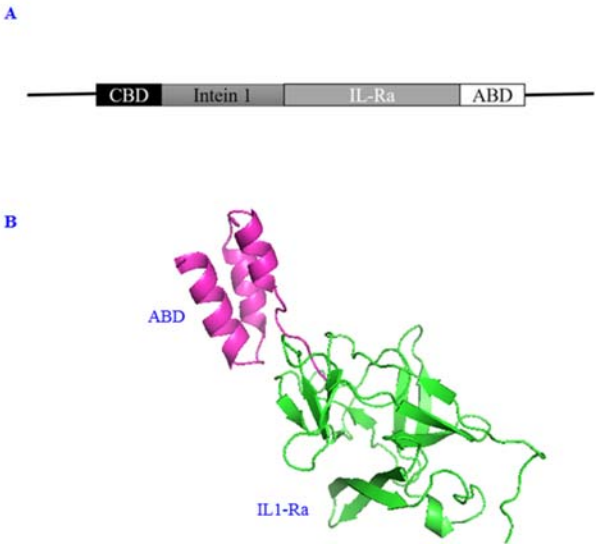

Fig. 1. (A) Schematic structure of the gene encoding the IL-1Ra-ABD in fusion to the intein 1; (B) three-dimensional structure of IL-1Ra-ABD visualized by PyMol. CBD, Chitin-binding domain; IL-1Ra, interleukin-1 receptor antagonist; ABD, albumin binding domain.

Evaluation of the albumin binding ability of IL-1Ra-ABD

To determine the ability of IL-1Ra-ABD fusion protein to attach to the HSA, the equal molar ratios (0.2 µM of the fusion protein and HSA) were shaken in PBS (pH 7.4) in the 10 mL of final volume for 2 h on ice. This content was then transferred to an Amicon filter (Millipore, USA) with a 30 kDa cut-off followed by centrifuging at 7000 *g* at room temperature for 15 min. The supernatant and the flow-through were analyzed by 12% native-PAGE and quantified by the Bradford method. By measuring the amount of IL-1Ra-ABD passed through the Amicon filter after the centrifugation, the relative amount of albumin-bound protein was calculated compared to the total used protein.

Evaluation of the release of IL-1Ra-ABD from the HSA

As mentioned above, the equal molar ratios of the recombinant IL-1Ra-ABD and HSA (0.2 µM of each protein) were added to the 10 mL of PBS as the protein diluent and shaken for 2 h on ice. At various times, the tube content was seeded into the Amicon filter (30 kDa cut-off) and subjected to the centrifuge (7000 *g* for 15 min at room temperature). The flow-through was analyzed by the Bradford method to determine detached protein concentration. Finally, the cumulative release graph of IL-1Ra-ABD was drawn based on the percent of released IL-1Ra-ABD toward the time.

Biological assay

To determine the antagonizing properties of recombinant IL-1Ra-ABD on A375 (as IL-1 receptor-positive cells) and human embryonic kidney 293 cells (HEK293) (as IL-1 receptor-negative cells) 3-(4,5-dimethylthiazol-2-yl)-2,5-diphenyl-2H-tetrazolium bromide (MTT) assay was performed. Briefly, 160 µL of the medium containing 3×10^4 cells/mL of each cell line was poured into each well of 96-well microplates and incubated for 24 h at 37 ºC. Then, 20 µL of the IL-1β (Pepro Tech, Canada) with the final concentration of 2 ng/mL was added to each well except the blank well. After a 1-h incubation, the purified IL-1Ra-ABD or native IL-1Ra at the concentrations of 0.95, 1.9, 3.75, 7.5, and 15 µg/mL produced according to the previous study (15) was added into plates. Next, the plates were incubated in 5% CO2 and at the temperature of 37 °C for 48 h. After that, 20 µL of MTT (5 mg/mL) was added to each well followed by a 3-h incubation period. Then, the content of wells were discarded, and 150 µL of dimethyl sulfoxide (DMSO) was added to each well for dissolving formazan crystals. Finally, the plates were subjected to read the absorbance at 570 nm by a microplate reader (Bio-Rad, USA).

Statistical analysis

To ensure the accuracy and reproducibility of data, the MTT test was performed for each cell line as a triple-independent experiment. Cell culture media, PBS-treated cells, and cells treated with 2 ng/mL of IL-1β were assigned as blank, negative control, and positive control, respectively. The software of SPSS, version 25, was used for statistical analysis. The analysis of variance (ANOVA) followed by Tukey's post hoc test was used to determine the differences among groups. $P < 0.05$ was considered the statistical significance.

RESULTS

Molecular docking

Among 1000 predicted models for IL-1Ra-ABD by multiple homology modeling, one with the lowest molpdf value as 2821.44116, the lowest DOPE score as -16103.19336, and the highest GA341 score as 1 was selected as the best model which was visualized by PyMol software, version 2.3.2 (Fig. 1B). Table 1 shows the interaction between two types of antagonists (native form versus the form with ABD) and the IL-1R. As shown, the attachment of ABD to anakinra molecule had no effects on its ability to interact with its receptor according to the HADDOCK and Z score with no meaningful difference (-1.6 versus -1.4).

Table 1. HADDOCK results of molecular docking.

Parameters	IL-1Ra/IL-1R complex	IL-1Ra-ABD/IL-1R complex
HADDOCK score	-163.6 ± 8.2	-149.6 ± 7.9
Cluster size	138	58
RMSD	0.8 ± 0.4	0.5 ± 0.2
E_{inter}	-332	-466.1
E_{vdw}	-51.1 ± 4.4	-43 ± 2.2
E_{elec}	-300.9 ± 60.5	-403.1 ± 21.7
E_{desolv}	- 68.2 ± 9.4	52.5 ± 7.3
E_{rv}	258.7 ± 31.03	235.4 ± 36.42
Total BSA	1975.1 ± 64.6	13284.7 ± 52.6
Z-Score	-1.6	-1.4

Einter, Intermolecular energy (sum of the van der Waals and electrostatic energies); Evdw, van der Waals energy; Eelec, electrostatic energy; Edesolv, desolvation energy; Erv, restrain violation energy; BSA, buried surface energy; BSA. IL-1Ra, interleukin 1 receptor antagonist; IL-1R, interleukin 1 receptor; ABD, albumin binding domain.

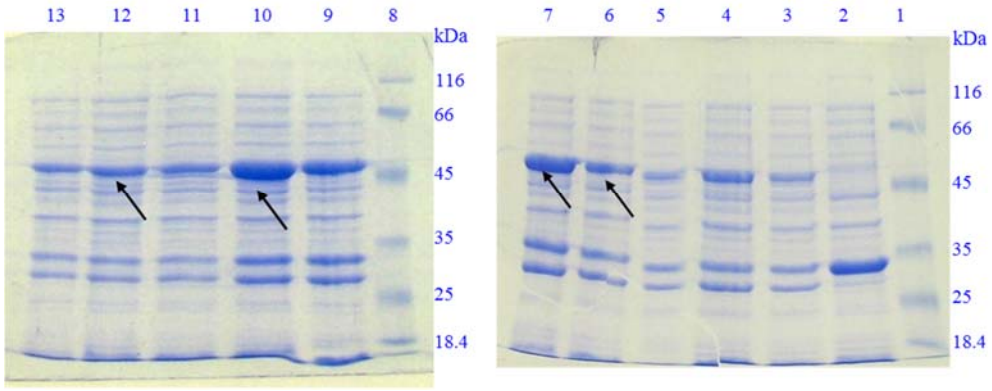

Fig. 2. SDS-PAGE analysis of soluble protein expression induction of IL-1Ra-ABD in various conditions regarding IPTG concentration and temperature of incubation for 4 h of incubation. Lanes 1 and 8, protein marker; lane 2, induced *E. coli* BL21(DE3) cells containing non-recombinant pTWIN1 by 1 mM IPTG at 37 °C; lane 3, induced *E. coli* BL21(DE3) cells containing recombinant pTWIN1-IL1-Ra-ABD; lanes 4-6, induced *E. coli* BL21(DE3) cells containing recombinant pTWIN1-IL1-Ra-ABD by 0.1, 0.5, and 1 mM IPTG at 37 °C, respectively; lanes 7-9, induced *E. coli* BL21(DE3) cells containing recombinant pTWIN1-IL1-Ra-ABD by 0.1, 0.5, and 1 mM IPTG at 25 °C, respectively; lanes 10-12, induced *E. coli* BL21(DE3) cells containing recombinant pTWIN1-IL1-Ra-ABD by 0.1, 0.5, and 1 mM IPTG at 15 °C, respectively. SDS-PAGE, Sodium dodecyl sulfate-polyacrylamide gel electrophoresis; IL-1Ra, interleukin 1 receptor antagonist; ABD, albumin binding domain; IPTG, isopropyl β-D-1-thiogalactopyranoside.

Expression of rIL-1Ra-ABD

The expression of intein 1-IL-1Ra-ABD fusion protein was evaluated by 12% SDS-PAGE. As shown in Fig. 2, the induction of expression using IPTG at the concentration of 1 mM and after 4 h of incubation revealed a band of approximately 54 kDa for cells transformed with non-recombinant pTWIN1 plasmid which corresponds to the molecular weight of inteins 1 and 2 fusion protein. For *E. coli* BL21 (DE3) cells containing recombinant pTWIN1-IL-1Ra-ABD, on the other hand, induction with IPTG at the concentration of 1 mM represented a band approximately 50 kDa which confirmed the expression of IL-1Ra-ABD in fusion to intein 1. Furthermore, the best condition for soluble protein expression and with less auto-cleavage during the bacterial growth and protein expression was determined as 0.1 mM of IPTG at 15 °C used for about 16 h in order to earn the most soluble protein.

Purification of the rIL-1Ra-ABD

In Fig. 3, a band of approximately 23 kDa represented the recombinant IL-1Ra-ABD separated from intein 1 and CBD. The final yield of recombinant protein production was calculated to be 4.3 mg/L of bacterial culture medium.

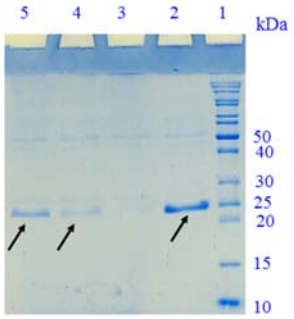

Fig. 3. 15% SDS-PAGE for the evaluation of the IL-1Ra-ABD cleavage. Lane 1, protein marker; lane 2, purified recombinant IL-1Ra after the first elution of the column with B2 buffer; lane 3, the fourth elution of the column; lane 4, the third elution of the column; lane 5, the second elution of the column. SDS-PAGE, Sodium dodecyl sulfate-polyacrylamide gel electrophoresis; IL-1Ra, interleukin 1 receptor antagonist; ABD, albumin binding domain.

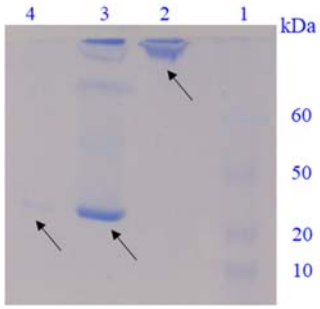

Fig. 4. Native-PAGE for the evaluation of ABD affinity to HSA. Lane 1, protein marker; lane 2, the upper sample of Amicon filter after centrifuging after a 2-h incubation; lane 3, the mixed sample of IL-1Ra-ABD and HSA after a 30-min incubation; lane 4, the flow-through of Amicon filter after centrifuging after a 2-h incubation. PAGE, polyacrylamide gel electrophoresis; ABD, albumin binding domain; HSA, human serum albumin; IL-1Ra, interleukin 1 receptor antagonist.

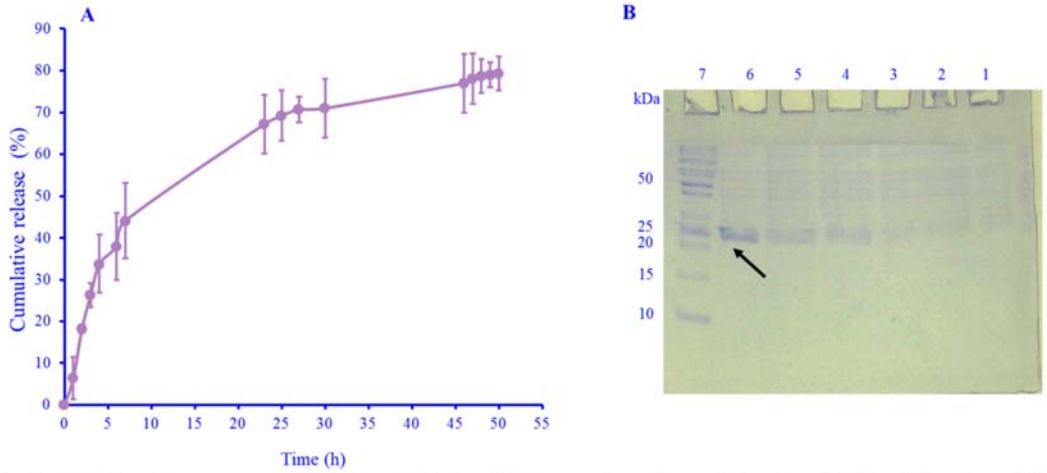

Fig. 5. (A) The release percent of IL-1Ra-ABD from HSA at various times; (B) native-PAGE of the released IL-1Ra-ABD from the HSA from the flow-through of Amicon filter at various times. Lanes 1-6, the flow-through sample after 1-, 3-, 5-, 16-, 18-, and 25-h incubation; lane 7, protein marker. PAGE, polyacrylamide gel electrophoresis; ABD, albumin binding domain; HSA, human serum albumin; IL-1Ra, interleukin 1 receptor antagonist.

Evaluation of the albumin binding ability of IL-1Ra-ABD

With the appearance of a band approximately 90 kDa (equal to the IL-1Ra-ABD and HSA molecular weights) after a 2-h incubation period in the native-PAGE, it was concluded that the binding between two molecules occurred. Actually, from 4.5 mg of IL-1Ra-ABD shaken with HSA, approximately 0.98 mg passed through the Amicon filter, and consequently it was calculated that about 78% of IL-1Ra-ABD in the test solution was attached to the HSA (Fig. 4).

Evaluation of the release of IL-1Ra-ABD from the HSA

The centrifuging of the tube containing IL-1Ra-ABD and HSA via an Amicon filter at room temperature and the determining of passed IL-1Ra-ABD by Bradford method showed that about 80% of the protein was released from HSA during the first 50 h of incubation (Fig. 5).

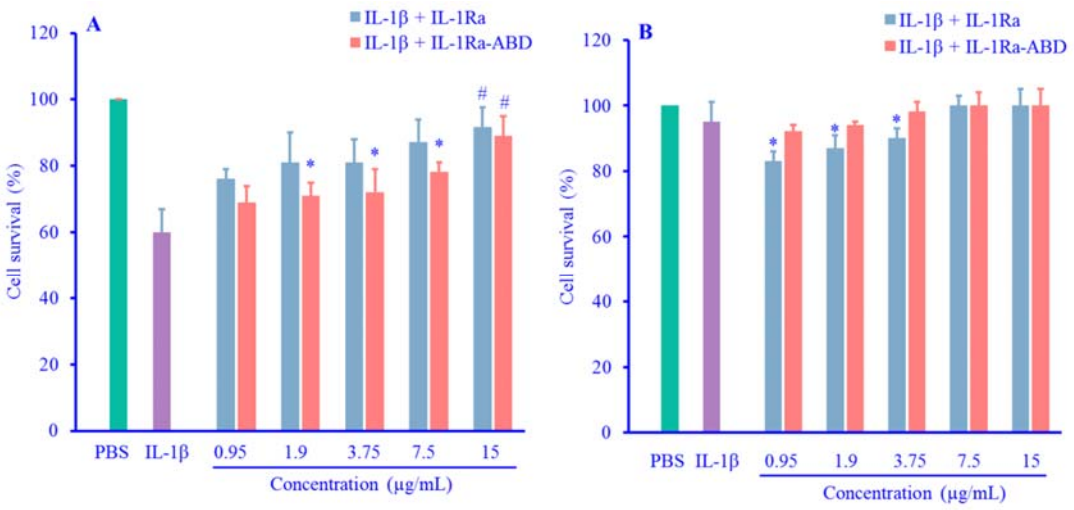

Fig. 6. (A) Comparison of the antagonizing effect of IL-1Ra-ABD and native IL-1Ra on A375 survival percent after the treatment with IL-1β; (B) Comparison of the antagonizing effect of IL-1Ra-ABD and native IL-1Ra on HEK293 survival percent after the treatment with IL-1β. Data were expressed as mean ± SD, n = 3. **P* < 0.05 demonstrates the significant difference in comparison with cells treated with IL-1β + IL-1Ra at the same concentration; #*P* < 0.05 versus IL-1β (2 ng/mL) as the positive control. IL-1Ra, interleukin 1 receptor antagonist; ABD, albumin binding domain; IL-1β, interleukin 1β; HEK293, human embryonic kidney 293.

Comparison of the antagonizing efficacy of IL-1Ra-ABD with IL-1Ra against IL-1β

In the similar concentration of the antagonist (15 µg/mL), there were no significant differences between the effects of IL-1Ra-ABD and native IL-1Ra on A375 cells (*P* = 0.33). Furthermore, IL-1β showed about 60% cell survival on A375 cells which increased significantly after the addition of the antagonists at the final concentration (15 µg/mL; *P* = 0.015) (Fig. 6A). On the other hand, IL-1β led to less cytotoxicity (95% of cell survival) on HEK293, and both types of antagonists (native IL-1Ra and IL-1Ra-ABD) could increase the cell survival; however, this effect was less than A375 cells (Fig. 6B).

DISCUSSION

In the present study, IL-1Ra in fusion to ABD was produced in the *E. coli* expression system as the first stage of introducing a new version of an FDA-approved drug for treating RA and purified using the intein-mediated procedure. The present results indicated that after 2 h, about 78% of this fusion protein could bind to HSA, and about 80% of the bonded protein was released during 50 h until it reached a stationary phase. On the other hand, there was no significant difference between the antagonistic efficacy of IL-1Ra-ABD and native IL-1Ra in this test when A375 and HEK293 cell lines were treated by IL-1β.

Especially during recent years, the usage of the IMPACT system has increased because of the ability of intein tags to produce the soluble form of recombinant proteins as well as the ability of their self-cleavage after protein purification. However, the optimization of conditions for soluble expression and the cleavage of intein play a critical role in earning the most active soluble protein.

Using the intein 1 (Ssp DnaB) of pTWIN1 plasmid is more convenient than intein 2, which induces the ability of its auto-cleavage by adding reducing agents. In other words, intein 1 is induced for self-splicing activity by changing pH, the same as the previous study for purifying the recombinant human granulocyte colony-stimulating factor (G-CSF) (16). However, another problem in this regard is the self-cleavage induction of intein1 during the recombinant production of target protein in the host cell cytosol. To diminish this unwanted reaction, lowering the post-induction temperature and the pH of the cleavage buffer

was used in this study. In general, the auto-cleavage ability of intein 1 can improve by increasing the temperature incubation of the chitin column. In this regard, Jiang *et al*. reported that the best temperature was considered 37 °C among investigated temperatures ranging from 15 to 37 °C for Ssp DnaB mini-intein fused to human GLP-1/7-36 (17). It seems that lowering pH to even 4.5 can increase the time of column incubation and the temperature of incubation leading to the efficient cleavage of intein 1 (18). One study performed on the cleavage of a mutated form of insulin from the intein1 reported that pH 4.5 in comparison to pH 8, and the temperature of 25 °C was more efficient in cleavage ratios (18). The present study used the incubation temperature of 25 °C for 24 h at pH 6.5 according to the IMPACT manual.

Pharmacokinetic assays performed on IL-1Ra fused to HSA showed that native IL-1Ra was completely cleared from the blood circulation after an 8 h-injection period in healthy mice, while for the fusion protein of IL-1Ra-ALB, the data represented that about 30% of the radio-labeled fusion protein could be still observed in the circulation after a 48 h-injection period. In fact, the half-life of IL-1Ra-ALB was calculated as about 10 h in comparison to the native form with a calculated half-life of about 20.5 min (8). In the current study, ABD was used instead of full-length HSA to overcome the probable drawbacks of the expression of target protein in fusion to a large molecule such as albumin with about 66 kDa.

Several studies have used ABD to extend the half-life of biological drugs (10-12). To attempt to increase the half-life of exenatide using ABD, the pharmacokinetics assays showed about a 32-fold increase in the half-life of exenatide-ABD when compared to the native form (16 h vs. 30 min) (10). *In vitro* release tests performed in the present study demonstrated that IL-1Ra fused to ABD could be released from the HSA until 50 h, and native-PAGE revealed the stability of this fusion protein.

For the biological assay, on the other hand, this study used the potent cytotoxic and apoptotic effects of IL-1β against cells with highly expressed IL-1 receptors (19). The biological results showed that an increase in the concentration of IL-1Ra-ABD led to the inhibition of IL-1β cytotoxic effects. Liu *et al*. evaluated the inhibitory effects of the fusion protein of IL-1Ra with an extended half-life and showed that IL-1Ra at the concentration of 32 nM leads to 100% inhibition effects of IL-1β at the concentration of 1 ng/mL (20). In another study, Wang *et al.* produced several mutated forms of IL-1Ra and compared their biological activities to the native IL-1Ra. The results showed that IL-1Ra at the concentration of 25 µg/mL can inhibit the effects of IL-1 (21).

The antagonizing efficacy of IL-1Ra-ABD was not statistically significant compared to native IL-1Ra for highly expressed IL-1 receptor cells, A375. The strength of the produced recombinant protein was about 101% of the native form antagonist.

Liu *et al*. evaluated the antagonizing efficacy of the recombinant IL-1Ra produced in *Pichia pastoris* and presented that this protein could antagonize the cytolytic activity of IL-1β (1 ng/mL) when added only after the treatment of cells by IL-1β (20). However, there was a time interval of 1 h in the present study based on Adelnia *et al*. study (15). The present findings showed that IL-1Ra-ABD could successfully act in antagonizing the cytotoxic effects of IL-1β in a time interval of 1 h without any significant differences from native IL-1Ra.

Finally, Powers *et al*. used the IL-1-responsive A549 cell line to evaluate the competitive antagonizing effects of a PASylated form of IL-1Ra, produced for expanding its half-life (22). In this study, the antagonist was added to cells, and the cells received IL-1α the 1 h later. The efficacy of IL-1α (in the final concentration of 10 ng/mL) was evaluated in the release of IL-6 and found that both anakinra and its PASylated form antagonized the IL-6 secretion (22). The results of the present study also confirmed the anakinra antagonizing effects on IL-1, only before its internalizing to the cells with highly expressed receptors on their surface.

CONCLUSION

This project successfully produced and purified the recombinant IL-1Ra in fusion with

the ABD in soluble form. The antagonizing effects of this protein were statistically equal to the native receptor antagonist produced in the same strategy. On the other hand, this chimeric molecule showed suitable interaction with HSA indicating its correct 3-D structure. Furthermore, *in vitro* release analysis confirmed the 80% cumulative release of the recombinant fusion protein from HSA. However, further *in vivo* pharmacokinetics analysis as well as *in vitro* and *in vivo* biological evaluations are required for this protein to act as a drug candidate for clinical trial phases.

Acknowledgments

This paper was extracted from the Pharm. D thesis submitted by Ali Yazdani financially supported by the Research Deputy of Isfahan University of Medical Sciences, with Grant No. 399095. The authors also would like to appreciate the valuable technical assistance of laboratory experts in molecular biotechnology and cell culture laboratories.

Conflict of interest statement

All authors declared no conflict of interest in this study.

Authors' contributions

F. Shafiee designed the study, wrote the manuscript, and analyzed data; A. Yazdani performed the laboratory tests. All authors approved the finalized article.

REFERENCES

1. Schnellbacher C, Ciocca G, Menendez R, Aksentijevich I, Goldbach-Mansky R, Duarte AM, *et al*. Deficiency of interleukin-1 receptor antagonist responsive to anakinra. Pediatr Dermatol. 2013;30(6):758-760. DOI: 10.1111/j.1525-1470.2012.01725x.
2. Waugh J, Perry CM. Anakinra. BioDrugs. 2005;19(3):189-202. DOI: 10.2165/00063030-200519030-00005.
3. Kaiser C, Knight A, Nordström D, Pettersson T, Fransson J, Florin-Robertsson E, *et al*. Injection-site reactions upon kineret (anakinra) administration: experiences and explanations. Rheumatol Int. 2012;32(2):295-299. DOI: 10.1007/s00296-011-2096-3.
4. Suk JS, Xu Q, Kim N, Hanes J, Ensign LM. PEGylation as a strategy for improving nanoparticle-based drug and gene delivery. Adv Drug Deliv Rev. 2016;99(Pt. A):28-51. DOI: 10.1016/j.addr.2015.09.012.
5. Liebner R, Mathaes R, Meyer M, Hey T, Winter G, Besheer A. Protein HESylation for half-life extension: synthesis, characterization and pharmacokinetics of HESylated anakinra. Eur J Pharma Biopharm. 2014;87(2):378-385. DOI: 10.1016/j.ejpb.2014.03.010.
6. Podust VN, Balan S, Sim BC, Coyle MP, Ernst U, Perers RT, *et al*. Extension of *in vivo* half-life of biologically active molecules by XTEN protein polymers. J Control Release. 2016; 240:52-66. DOI: 10.1016/j.jconrel.2015.10.038.
7. Bern M, Nilsen J, Ferrarese M, Sand KMK, Gjølberg TT, Lode HE, *et al*. An engineered human albumin enhances half-life and transmucosal delivery when fused to protein-based biologics. Sci Transl Med. 2020;12(565):eabb0580,1-13. DOI: 10.1126/scitranslmed.abb0580.
8. Liu M, Huang Y, Lei Hu, Liu G, Hu X, Liu D, *et al*. Selective delivery of interleukine-1 receptor antagonist to inflamed joint by albumin fusion. BMC Biotechnol. 2012;12:68,1-13. DOI: 10.1186/1472-6750-12-68.
9. Mester S, Evers M, Meyer S, Nilsen J, Greiff V, Sandlie I, *et al*. Extended plasma half-life of albumin-binding domain fused human IgA upon pH-dependent albumin engagement of human FcRn *in vitro* and *in vivo*. MAbs. 2021;13(1):e1893888,1-13. DOI: 10.1080/19420862.2021.1893888.
10. Levy OE, Jodka CM, Ren SS, Mamedova L, Sharma A, Samant M, *et al*. Novel exenatide analogs with peptidic albumin binding domains: potent anti-diabetic agents with extended duration of action. PLoS One. 2014;9(2):e87704,1-9. DOI: 10.1371/journal.pone.0087704.
11. Sheffield WP, Smith IJ, Syed S, Bhakta V. Prolonged *in vivo* anticoagulant activity of a hirudin-albumin fusion protein secreted from *Pichia pastoris*. Blood Coagul Fibrinolysis. 2001;12(6):433-443. DOI: 10.1097/00001721-200109000-00003.
12. Lindgren J, Refai E, Zaitsev SV, Abrahmsén L, Berggren PO, Karlström AE. A GLP-1 receptor agonist conjugated to an albumin-binding domain for extended half-life. Biopolymers. 2014;102(3):252-259. DOI: 0.1002/bip.22474.
13. Jacobs SA, Gibbs AC, Conk M, Yi F, Maguire D, Kane C, *et al*. Fusion to a highly stable consensus albumin binding domain allows for tunable pharmacokinetics. Protein Eng Des Sel. 2015;28(10):385-393. DOI: 10.1093/protein/gzv040.
14. Barkestani MN, Naserian S, Khoddam F, Shamdanu S, Bambai B. Optimization of IL-1RA structure to achieve a smaller protein with a higher affinity to its receptor. Sci Rep. 2022;12(1):7483,1-9. DOI: 10.1038/s41598-022-11100-3.
15. Adelnia R, Shafiee F. Recombinant production and one step purification of il-1ra in *Escherichia coli* and evaluation its il-1 antagonizing efficacy. Iran J Immunol. 2021;18(2):141-149. DOI: 10.22034/iji.2021.89103.1929.

16. Sima S, Shafiee F, Jahanian-Najafabadi A. Expression and one step intein-mediated purification of biologically active human G-CSF in *Escherichia coli*. Mol Biol Rep. 2020;47(4):2861-2869. DOI: 10.1007/s11033-020-05404-8.
17. Jiang A, Jin W, Zhao F, Tang Y, Sun Z, Liu JN. Split Ssp DnaB mini-intein-mediated production of recombinant human glucagon-like peptide-1/7-36. Biotechnol Appl Biochem. 2015;62(3):309-315. DOI: 10.1002/bab.1274.
18. Zhang M, Zhang Y, Wu B, Peng Y, Simair AA, Siegel GW, *et al*. Intein-mediated recombinant expression of monomeric B22Asp desB30 insulin. BMC Biotechnol. 2020; 20(1):3, 1-9. DOI: 10.1186/s12896-020-0598-3.
19. Wang C, Wang MW, Tashiro SI, Onodera S, Ikejima T. IL-1β acts in synergy with endogenous IL-1β in A375-S2 human melanoma cell apoptosis through mitochondrial pathway. J Korean Med Sci. 2005;20(4):555-561. DOI: 10.3346/jkms.2005.20.4.555.
20. Liu M, Huang Y, Hu L, Liu G, Hu X, Liu D, *et al*. Selective delivery of interleukine-1 receptor antagonist to inflamed joint by albumin fusion. BMC Biotechnol. 2012;12(1):68,1-13. DOI: 10.1186/1472-6750-12-68.
21. Wang YX, Yang ZX, Zhu HQ, Zhou XW, Huang PT. Construction, expression and preliminary pharmacokinetics of IL-1ra mutants. Chin J Biotechnol. 2006;22(3): 472-476. DOI: 10.1016/S1872-2075(06)60040-X.
22. Powers NE, Swartzwelter B, Marchetti C, de Graaf DM, Lerchner A, Schlapschy M, *et al*. PASylation of IL-1 receptor antagonist (IL-1Ra) retains IL-1 blockade and extends its duration in mouse urate crystal-induced peritonitis. J Biol Chem. 2020;295(3): 868-882. DOI: 10.1074/jbc.RA119.010340.

Instructions to the Authors

About the Journal

Research in Pharmaceutical Sciences (RPS; ISSN: Print -1735-5362, Online - 1735-9414), the journal of School of Pharmacy and Pharmaceutical Sciences, Isfahan University of Medical Sciences, Isfahan, I.R. Iran, published by Wolters Kluwer - Medknow Publications, is a peer-reviewed online journal with bimonthly print on demand compilation of issues published. The journal's full text is available online at rpsjournal.net. The journal allows free access (Open Access) to its contents and permits authors to self-archive final accepted version of the articles on any OAI-compliant institutional/subject-based repository. The editors welcome original contributions that have not been published and are not under consideration elsewhere. Authors are encouraged to submit manuscript by our webpage (https://review.jow.medknow.com/rps).

The journal has a distinguished editorial board with extensive academic qualifications, ensuring that the journal maintains high scientific standards and has a broad international coverage. One key request of researchers across the world is open access to research publications.

Aims and Scope

The journal aims at publishing high quality research papers featuring new findings in all aspects of the pharmaceutical sciences. Criteria for publication in RPS are novelty, quality and current interest. Submission requirements specify that papers should be original, unpublished and not under consideration for publication elsewhere. This restriction does not apply to the results published as abstracts of communications, letters to editors, or as contributions to symposia. The journal publishes research reports, review articles, short communications and scientific commentaries on all aspects of the pharmaceutical sciences including pharmaceutics, novel drug delivery and targeting systems, medicinal and Ppharmaceutical chemistry, pharmaceutical and bilogical analysis, pharmcokinetics, pharmacodynamics, pharmacology, pharmacognosy, pharmacotherapy and clinical pharmacy, pharmacy practice, pharmacoeconomics, pharmacoepidemiology, analytical biochemistry, pharmaceutical biotechnology, and molecular modeling.

Abstracting / Indexing

Thomson Reuters ESCI Web of Science, PubMed and PubMed Central and Elsevier Bibliographic Databases. Databases include Scopus, EMBASE, EMCare, EMBiology and Elsevier BIOBASE. It is also indexed in several specialized databases including Scientific Information Database (SID),

Google Scholar, Iran Medex, Magiran, Index Copernicus (IC), Islamic World Science Citation Center (ISC) and Asian Digital Library.

Editorial Process

A manuscript will be reviewed for possible publication with the understanding that it is being submitted to RPS alone at that point in time and has not been published anywhere, simultaneously submitted, or already accepted for publication elsewhere. The journal expects that authors would authorize one of them to correspond with the Journal for all matters related to the manuscript. All manuscripts received are duly acknowledged. On submission, editors review all submitted manuscripts initially for suitability for formal review. Manuscripts with insufficient originality, serious scientific or technical flaws, or lack of a significant message are rejected before proceeding for formal peer-review. Manuscripts that are unlikely to be of interest to the RPS readers are also liable to be rejected at this stage. Manuscripts received from editorial board members will be screened by the editor-in-chief and sent to external peer reviewers. The editorial board members who are authors will be excluded from publication decisions. Manuscripts that are found suitable for publication in RPS are sent to three or more expert reviewers. During submission, the contributor is requested to provide names of two or three qualified reviewers who have had experience in the subject of the submitted manuscript. The reviewers should not be affiliated with the same institutes as the contributor/s. However, the selection of these reviewers is at the sole discretion of the editor. The journal follows a double-blind review process, wherein the reviewers and authors are unaware of each other's identity. Every manuscript is also assigned to a member of the editorial team, who based on the comments from the reviewers takes a final decision on the manuscript. The comments and suggestions (acceptance/ rejection/ amendments in manuscript) received from reviewers are conveyed to the corresponding author. If required, the author is requested to provide a point by point response to reviewers' comments and submit a revised version of the manuscript. This process is repeated till reviewers and editors are satisfied with the manuscript.

Manuscripts accepted for publication are copy edited for grammar, punctuation, print style, and format. Page proofs are sent to the corresponding author. The corresponding author is expected to return the proofs with corrections (using TRACK CHANGE mode) within five working days (even if he/she has no corrections). It may not be possible to incorporate corrections received after that period. The whole process of submission of the manuscript to final decision and sending and receiving proofs is completed online.

Proposed Time Schedule

- Submission to first editorial decision: 4 weeks
- Submission to acceptance: 4-9 months
- Acceptance to publication: 2-8 weeks

Processes for Appeals

The authors do have the right to appeal if they have a genuine cause to believe that the editorial board has wrongly rejected the paper. If the authors wish to appeal the decision, they should email the editorial office (email: rps@pharm.mui.ac.ir) explaining in detail the reason for the appeal. The appeals will be acknowledged by the editorial office and will be investigated in an unbiased manner.

The processing of appeals will be done within 6-8 weeks. While under appeal, the said manuscript should not be submitted to other journals. The final decision rests with the editor-in-chief of the journal. Second appeals are not considered.

Anti-plagiarism Policy

Plagiarism includes duplicate publication of the author's own work, in whole or in part without proper citation or mispresenting other's ideas, words, and other creative expression as one's own. The Journal follows strict anti-plagiarism policy. All manuscripts submitted to Research in Pharmaceutical Sciences undergoes plagiarism check with commercially available software. Based on the extent of plagiarism, authors may be asked to address any minor duplication, or similarity with the previous published work. If plagiarism is detected after publication, the Journal will investigate. If plagiarism is established, the journal will notify the authors' institution and funding bodies and will retract the plagiarized article. To report plagiarism, contact the journal office (email: rps@pharm.mui.ac.ir).

Multiple, Redundant or Concurrent Publication

An author should not in general publish manuscripts describing essentially the same research in more than one journal or primary publication. RPS does not view the following uses of a work as prior publication: publication in the form of an abstract; publication as an academic thesis; publication as an electronic preprint.

Fundamental Errors in Published Works

When an author discovers a significant error or inaccuracy in his/her own published work, it is the author's obligation to promptly notify the journal editor and cooperate with the editor to retract or correct the paper. This correction will be published as an erratum.

Hazards and Human or Animal Subjects

Statements of compliance are required if the work involves chemicals, procedures or equipment that has any unusual hazards inherent in their use, or if it involves the use of animal or human subjects.

Clinical Trial Registry

Investigations using experimental animals must state in the Methods section that the research followed the Principles of Laboratory Animal Care. The authors must seek approval from the appropriate ethical committee. Investigation with human subjects must state in the Methods section that the research followed the tenets of the last update of Declaration of Helsinki and was approved by the institutional human experimentation committee or equivalent, and that informed consent was obtained. Both human and animal researches conducted in Iran should be approved by Iran National Committee for Ethics in Biomedical Research. Authors are kindly requested to provide the approved ethics ID in Materials and Method section of the manuscript.

Also registration in the following trial registers is acceptable: http://www.ctri.nic.in/; https://www.anzctr.org.au/;http://www.clinicaltrials.gov/; http://isrctn.org/; http://www.trialregister.nl/trialreg/index.asp; http://www.umin.ac.jp/ctr.This is applicable to clinical trials that have begun enrolment of subjects in or after June 2008. Clinical trials that have commenced enrolment of subjects

prior to June 2008 would be considered for publication in Research in Pharmaceutical Sciences only if they have been registered retrospectively with clinical trial registry that allows unhindered online access to public without charging any fees.

Protection of Patients' Rights to Privacy

Identifying information should not be published in written descriptions, photographs, sonograms, CT scans, etc., and pedigrees unless the information is essential for scientific purposes and the patient (or parent or guardian, wherever applicable) gives informed consent for publication. Authors should remove patients' names from figures even if they have obtained informed consent from the patients in order to protect patient privacy. The journal abides by ICMJE guidelines:

1. Authors, not the journals nor the publisher, need to obtain the patient consent form before the publication and have the form properly archived. The consent forms are not to be uploaded with the cover letter or sent through email to editorial or publisher offices.
2. If the manuscript contains patient images that preclude anonymity, or a description that has obvious indication to the identity of the patient, a statement about obtaining informed patient consent should be indicated in the manuscript.
3. In order to protect the patient’s identity, the recognizable facial features not related to the study should be digitally blurred

Written informed consent is the preferred method for obtaining consent. If verbal consent is obtained, the authors must ensure that the verbal consent is recorded in the medical case record of the patient and duly signed by witness.

Authorship Criteria

Authorship credit should be based only on substantial contributions to each of the three components mentioned below:

1. Concept and design of study or acquisition of data or analysis and interpretation of data
2. Drafting the article or revising it critically for important intellectual content
3. Final approval of the version to be published

Participation solely in the acquisition of funding or the collection of data does not justify authorship. General supervision of the research group is not enough for authorship. Each contributor should have participated sufficiently in the work to take public responsibility for appropriate portions of the content of the manuscript. The order of naming the contributors should be based on the relative contribution of the contributor towards the study and writing the manuscript. Once submitted the order cannot be changed without written consent of all the contributors. The journal prescribes a maximum number of authors for manuscripts depending upon the type of manuscript, its scope, and number of institutions involved (vide infra). The authors should provide a justification, if the number of authors exceeds these limits.

Contribution Details

Contributors should provide a description of contributions made by each of them towards the manuscript. Description should be divided in following categories, as applicable: concept, design, definition of intellectual content, literature search, clinical studies, experimental studies, data acquisition, data analysis, statistical analysis, manuscript preparation, manuscript editing and

manuscript review. Authors' contributions will be printed along with the article. If there are no differences between contributors the following statement could be provided: All authors contributed equally in this work. One or more author should take responsibility for the integrity of the work as a whole from inception to published article and should be designated as 'guarantor'.

Conflict of Interest Statement

All authors of article must disclose all conflicts of interest they may have with publication of the manuscript or an institution or product that is mentioned in the manuscript and/or is important to the outcome of the study presented. Authors should also disclose conflict of interest with products that compete with those mentioned in their manuscript.

If there isn't any conflict of interest the following statement should be provided: The authors declare that no conflict of interest for this study.

Changes to the Authorship

Authors are expected to consider carefully the list and order of authors before submitting their manuscript and provide the definitive list of authors at the time of the original submission. Any addition, deletion or rearrangement of author names in the authorship list should be made only before the manuscript has been accepted and only if approved by the journal Editor. To request such a change, the Editor must receive the following from the corresponding author: (a) the reason for the change in author list, (b) written confirmation (e-mail, letter) from all authors that they agree with the addition, removal or rearrangement, and as well as (c) the modified final version of copyright form and first page must be submitted via website or emailed at rps@pharm.mui.ac.ir. In the case of addition or removal of authors, this includes confirmation from the author being added or removed.

Submission of Manuscripts

All manuscripts must be submitted online through the website https://review.jow.medknow.com/rps. First time users will have to register at this site. Registration is free but mandatory. Registered authors can keep track of their articles after logging into the site using their username and password. If you experience any problems, please do not hesitate to contact the journal editorial office by e-mail at: rps@pharm.mui.ac.ir.

The submitted manuscripts that are not prepared based on the "Instructions to Authors" would be returned to the authors for "Technical Modification", before they undergo editorial/peer-review.

Before submitting a manuscript, please make sure you have the following information in hand: The first and last names and e-mail addresses of all authors and full contact information of any preferred peer reviewers (e-mail address, phone number, institution, and her/his specialty and/or academic degree).

The following 4 separate files are required:

1. Title Page / First Page / Covering Letter

This file should contain following information:

- The type of manuscript (review article, original article, brief communication, case report, letter to the editor, etc.), title of the manuscript, running title, names of all authors / contributors (with their highest academic degrees, designation and affiliations), name(s) of department(s) and/or institution(s), the name of schools/ faculties, the name of university, and country to which the

work should be credited. All information which can reveal your institute affiliation should be given here. Use text/rtf/doc files. Do not zip the files.

- Contributors should provide a description of contributions, according to aforementioned categories, made by each of them towards the manuscript.
- Source(s) of support in the form of grants, equipment, drugs, or all of these.
- Acknowledgment(s), if any. One or more statements should specify 1) contributions that need acknowledging but do not justify authorship, such as general support by a departmental chair; 2) acknowledgments of technical help; and 3) acknowledgments of financial and material support, which should specify the nature of the support. This should be included in the title page of the manuscript and not in the main article file.
- A full statement to the editor about all submissions and previous reports that might be regarded as redundant publication of the same or very similar work. Any such work should be referred to specifically, and referenced in the new paper. Copies of such material should be included with the submitted paper, to help the editor decide how to handle the matter.
- Registration number in case of a clinical trial and where it is registered (name of the registry and its URL).
- A statement of financial or other relationships that might lead to a conflict of interest, if that information is not included in the manuscript itself or in an authors' form.
- A statement that the manuscript has been read and approved by all the authors, that the requirements for authorship as stated earlier in this document have been met, and that each author believes that the manuscript represents honest work, if that information is not provided in another form.
- The name, address, academic e-mail, and telephone number of the corresponding author, who is responsible for communicating with the other authors about revisions and final approval of the proofs.

2. Blinded Article File

The main text of the article, beginning from “Abstract” till “References” (all figures, tables, and their corresponding legends could be included at the end of the manuscript file) should be in this file. The file must not contain any mention of the authors' names and affiliation or initials or the institution at which the study was done or acknowledgments. Use doc files. Do not zip the files. Limit the file size to 1 MB. To reduce the size of the file (if file size is large), figures and tables can be submitted as images separately without incorporating them in the article file. The pages should be numbered consecutively, beginning with the first page of the blinded article file.

3. Images

Submit good quality color images of size 4” × 6” and not more than 400 KB size. Images should be uploaded in JPEG, TIFF, BMP, or GIF format. JPEG is most preferred format. Size of the image can be reduced by decreasing the actual height and width of the images. Do not zip the files.

4. The Contributors' / Copyright Transfer Form

This form should be downloaded from authors' area on the website (http://www.journalonweb.com/jrps), Downloads Tab; then submitted in original with the signatures of all the contributors at the time of submission from the authors' area on the abovementioned website.

Manuscript Preparation

Manuscripts must be prepared in accordance with "Uniform requirements for Manuscripts submitted to Biomedical Journals" developed by the International Committee of Medical Journal Editors (October 2008). The uniform requirements and specific requirement of Research in Pharmaceutical Sciences are summarized below. Before submitting a manuscript, contributors are requested to check for the latest instructions available. Instructions are also available from the website of the journal (http://www.rpsjournal.net/) and from the manuscript submission site https://review.jow.medknow.com/rps).

Research in Pharmaceutical Sciences accepts manuscripts written in British English.

Copies of Any Permission(s)

It is the responsibility of authors/contributors to obtain permissions for reproducing any copyrighted material including figures, schemes, etc. A copy of the permission obtained must accompany the manuscript. Copies of any and all published articles or other manuscripts in preparation or submitted elsewhere that are related to the manuscript must also accompany the manuscript. It should be noted that articles cannot be published without providing the required permissions. The material should be submitted via the website (https://review.jow.medknow.com/rps) in the Article Files => the Forms section, or sent to the following e-mail address, rps@pharm.mui.ac.ir.

Types of Manuscripts

1. Original Articles

These include randomized controlled trials, intervention studies, studies of screening and diagnostic test, outcome studies, cost effectiveness analyses, case-control series, and surveys with high response rate. The text of original articles should be divided into sections including Title of the manuscript, Running title, the headings/structured Abstract, Keywords, Introduction, Material and Methods, Results, Discussion, Conclusion, Acknowledgments, Conflict of Interest Statement, Authors Contribution, References, and Tables and Figure legends.

Abstract: The abstract should contain a brief account of the question addressed in the paper, the principal methods and results, followed by the main conclusion(s) and must not exceed 250 words. Abbreviations and symbols should be explained in round brackets ( ) on the first use. References should be avoided in the abstract. Authors are requested to assign 3-6 keywords to the manuscript, preferably taken from the Medical Subject Headings (MESH). These keywords should be typed at the end of the abstract. Also, the abstract must be structured, under the following sub-headings:

***Background and purpose*:** This must indicate why the study was performed and what question it was intended to answer.

***Experimental approach*:** This should state in outline what experimental methods were used. Details on media, buffers, drug concentrations, time points, statistics, etc., should not be given unless they are important in relation to the question that was addressed.

***Findings / Results*:** The main results relevant to the question addressed should be summarized without quantitative elaboration

***Conclusion and implications*:** As well as summarizing the main implications that follow from the results, and mentioning important shortcomings and caveats, this paragraph must clearly state in what ways the work has advanced understanding in the field.

INTRODUCTION

State the purpose and summarize the rationale for the study or observation.

MATERIALS AND METHODS:

It should include and describe the following aspects:

Ethics:

When reporting studies on human beings, indicate whether the procedures followed were in accordance with the ethical standards of the responsible committee on human experimentation (institutional or regional) and with the Helsinki Declaration of 1975, as revised in 2000 (available at https://www.wma.net/policies-post/wma-declaration-of-helsinki-ethical-principles-for-medical-research-involving-human-subjects/). For prospective studies involving human participants, authors are expected to mention about approval of (regional/ national/ institutional or independent Ethics Committee or Review Board, obtaining informed consent from adult research participants and obtaining assent for children aged over 7 years participating in the trial. The age beyond which assent would be required could vary as per regional and/ or national guidelines. Ensure confidentiality of subjects by desisting from mentioning participants' names, initials or hospital numbers, especially in illustrative material. When reporting experiments on animals, indicate whether the institution's or a national research council's guide for, or any national law on the care and use of laboratory animals was followed. Evidence for approval by a local Ethics Committee (for both human as well as animal studies) must be supplied by the authors on demand. Animal experimental procedures should be as humane as possible, and the details of anaesthetics and analgesics used should be clearly stated. The ethical standards of experiments must be in accordance with the guidelines provided by the CPCSEA and World Medical Association Declaration of Helsinki on Ethical Principles for Medical Research Involving Humans for studies involving experimental animals and human beings, respectively). The journal will not consider any paper which is ethically unacceptable. A statement on ethics committee permission and ethical practices must be included in all research articles under the 'Materials and Methods' section.

Study design:

Selection and Description of Participants: Describe your selection of the observational or experimental participants (patients or laboratory animals, including controls) clearly, including eligibility and exclusion criteria and a description of the source population. *Technical information:* Identify the methods, apparatus (give the manufacturer's name and address in

parentheses), and procedures in sufficient details to allow other workers to reproduce the results. Give references to established methods, including statistical methods (see below); provide references and brief descriptions for methods that have been published but are not well known; describe new or substantially modified methods, give reasons for using them, and evaluate their limitations. Identify precisely all drugs and chemicals used, including generic name(s), dose(s), and route(s) of administration.

Reports of randomized clinical trials should present information on all major study elements, including the protocol, assignment of interventions (methods of randomization, concealment of allocation to treatment groups), and the method of masking (blinding), based on the CONSORT Statement (http://www.consort-statement.org).

Choose appropriate guideline from the below table and attach a filled checklist along with the manuscript. Manuscripts with incomplete checklist will be sent back to authors.

Reporting Guidelines for Specific Study Designs:

Guideline	Type of Study	Source
STROBE	Observational studies including cohort, case-control, and cross-sectional studies	https://www.strobe-statement.org/index.php?id=available-checklists
CONSORT	Randomized controlled trials	http://www.consort-statement.org
PRISMA	Systematic reviews and meta-analyses	http://prisma-statement.org/PRISMAStatement/Checklist.aspx
STARD	Studies of diagnostic accuracy	https://pubs.rsna.org/doi/full/10.1148/radiol.2015151516
CARE	Case Reports	https://www.care-statement.org/resources/checklist
AGREE	Clinical Practice Guidelines	https://www.agreetrust.org/wp-content/uploads/2016/02/AGREE-Reporting-Checklist-2016.pdf

The reporting guidelines for other type of studies can be found at https://www.equator-network.org/reporting-guidelines/.

***Statistics*:**

Whenever possible, quantify findings and present them with appropriate indicators of measurement error or uncertainty (such as confidence intervals). Authors should report losses in observation (such as dropouts from a clinical trial). When data are summarized in the Results section, specify the statistical methods used to analyze them. Avoid non-technical uses of technical terms in statistics, such as 'random' (which implies a randomizing device), 'normal', 'significant', 'correlations', and 'sample'. Define statistical terms, abbreviations, and most symbols. Specify the computer software used. Use upper italics *P to indicate* probability values. The given *P* values should be concise (<0.05, 0.01, and 0.001) and in compliance with the presented comparisons. Mean differences in continuous variables, proportions in categorical variables and relative risks including odds ratios and hazard ratios should be accompanied by their confidence intervals.

RESULTS

The results may be presented in tables, figures or schemes, which must be referred to in the accompanying text, using appropriate numbering. Tables should be numbered consecutively with Arabic numerals and the number should be followed by a brief descriptive caption, occupying not

more than two lines, at the head of the table. Each column should have a heading and the units of measurement should be given in brackets (SI units) in the heading. Figures must be presented on separate pages in consecutive order using Arabic numerals. Each figure should be provided with explanatory information. The legend should be typed separately from the figures. Figures, photographs or computer drawn figures should be original, and of high quality, ready for direct reproduction. Figure legends/captions should be consistent with terminology or nomenclature used in the labeling of the Figures. Tables, figures and legends should not have frame around. Statistical analysis of significance should be performed and for significant differences, the *P* values should be provided at the most precise level (0.05, 0.01, or 0.001). Authors may be asked to provide the raw data as well as data analyses in connection with a paper for editorial review.

DISCUSSION

Include summary of key findings (primary outcome measures, secondary outcome measures, results as they relate to a prior hypothesis); Strengths and limitations of the study (study question, study design, data collection, analysis and interpretation); Interpretation and implications in the context of the totality of evidence (is there a systematic review to refer to, if not, could one be reasonably done here and now?, what this study adds to the available evidence, effects on patient care and health policy, possible mechanisms); Controversies raised by this study; and Future research directions (for this particular research collaboration, underlying mechanisms, clinical research).

Do not repeat in detail data or other material given in the Introduction or the Results section. In particular, contributors should avoid making statements on economic benefits and costs unless their manuscript includes economic data and analyses. Avoid claiming priority and alluding to work that has not been completed. New hypotheses may be stated if needed, however they should be clearly labelled as such. About 35 references can be included.

2. ***Review Articles***

It is expected that these articles would be written by individuals who have done substantial work on the subject or are considered experts in the field. A short summary of the work done by the contributor(s) in the field of review should accompany the manuscript.

The prescribed word count is up to 7000 words including tables/figures, references and abstract. The manuscript may have unlimited references. The manuscript should have an unstructured Abstract (250 words) representing an accurate summary of the article. The section titles would depend upon the topic reviewed. Authors submitting review article should include a section describing the methods used for locating, selecting, extracting, and synthesizing data. These methods should also be summarized in the abstract.

The journal expects the contributors to give post-publication updates on the subject of review. The update should be brief, covering the advances in the field after the publication of the article and should be sent as a letter to editor, as and when major development occurs in the field.

3. ***Case Reports***

New, interesting and rare cases can be reported. They should be unique, describing a great diagnostic or therapeutic challenge and providing a learning point for the readers. Cases with clinical significance or implications will be given priority. These communications could be of up to 1000

words (excluding Abstract and references) and should have the following headings: Abstract (unstructured), Key-words, Introduction, Case report, Discussion, Reference, Tables and Legends in that order.

The manuscript could be of up to 1000 words (excluding references and abstract) and could be supported with up to 10 references. Case Reports could be authored by up to four authors.

4. ***Letter to the Editor***

These should be short and decisive observations. They should preferably be related to articles previously published in the Journal or views expressed in the journal. They should not be preliminary observations that need a later paper for validation. The letter could have up to 500 words and 5 references. It could be generally authored by not more than four authors.

5. Short Communications

The short communication should be no more than 1000 words, and could include two figures or tables. It should have at least 15 references. The abstract should not exceed 150 words. Short communications must report completed work, not preliminary findings: they are an alternative format for describing smaller pieces of work.

6. Other

Editorial, Guest Editorial, Commentary and Opinion are solicited by the editorial board.

CONCLUSION

The main conclusions of the study should be presented in a short conclusion section, which should stand alone.

ACKNOWLEDGEMENTS

For non-author contributions, one or more statements should specify 1) contributions that need acknowledging but do not justify authorship, such as general support by a departmental chair; 2) acknowledgments of technical help; and 3) acknowledgments of financial and material support, which should include details about the funding agency/ sponsors, grant number and the role of funders. If the funders have no role to play or the study did not receive funding, a statement declaring the same should be mentioned. Details of the non-author contributors can be cited individually or collectively, and their precise contributions should be specified. The corresponding author is required to obtain written permission to be acknowledged from all acknowledged individuals.

CONFLICT OF INTEREST STATEMENT

All manuscripts for articles, original research reports, editorials, comments, reviews, book reviews, and letters submitted to the journal must include a conflict of interest disclosure statement or a declaration by the authors that they do not have any conflicts of interest to declare.

AUTHORS' CONTRIBUTION

This section should be provided as previously explained.

REFERENCES

The references should be cited according to the "Vancouver *S*tyle". Using this system, references are numbered in consecutive order that they are cited in the text. For in text citation, parenthesis should be used. References are listed in numerical order at the end of the paper. Journal names are to be abbreviated as they are in the *Cumulated Index Medicus*. "In press" references may be used only if the journal that has accepted the manuscript is indicated. Personal communications and other unpublished and non-archival references should not be included in the reference list, in which case the name of the person and date of communication should and the source be cited in parentheses in the text. Examples of references are as follows:

Articles in Journals:

1. **Standard journal article (for up to six authors):** Rezazadeh M, Akbari V, Amuaghae E, Emami J. Preparation and characterization of an injectable thermosensitive hydrogel for simultaneous delivery of paclitaxel and doxorubicin. Res Pharm Sci. 2018;13(3):181-191.
2. **Standard journal article (for more than six authors):** Susidarti RA, Utomo RY, Qodria L, Ramadani RD, Ohta Y, Hattori Y, *et al*. Preparation of pentagamaboronon-0 and its fructose and sorbitol complexes as boron carrier for boron neutron capture therapy (BNCT) application. Res Pharm Sci. 2019;14(4):286-292.

Books:

Lodish H, Baltimore D, Berk A, Zipursky SL, Matsudaira P, Darnell J. Molecular cell biology. 3rd ed. New York: Scientific American; 1995. pp: 151-178.

Chapter citation:

Porter RJ, Meldrum BS. Antiepileptic drugs. In: Katzung BG, editor. Basic and clinical pharmacology. 6th ed. Norwalk, CN: Appleton and Lange; 1995. pp. 361-380.

Patent:

McCormick JB. Apparatus and method for preparing tissue samples for histological examination. United State Patents, 2010. No. US7771992B2.http://www.freepatentsonline.com/7771992.html.

Minyasab SA, Dhamane SP, Hazra P, Iyer H. A method of purifying human growth hormone and purified growth hormone thereof. Google Patents, 2010. Publication No. WO/2010/134084. International application No. PCT/IN2009/000380.
https://www.google.com/patents/WO2010134084A1?cl=en.

Also for getting more information, authors could refer to the guidelines below:
National Library of Medicine (NLM)
http://www.nlm.nih.gov/bsd/uniform_requirements.html.

Electronic Sources as reference

Journal article on the Internet: Parija SC, Khairnar K. Detection of excretory *Entamoeba histolytica* DNA in the urine, and detection of *E. histolytica* DNA and lectin antigen in the liver abscess pus for the diagnosis of amoebic liver abscess .*BMC Microbiology* 2007, **7:**41.doi:10.1186/1471-2180-7-41. http://www.biomedcentral.com/1471-2180/7/41.

Tables

- Tables should be self-explanatory and should not duplicate textual material.

- Tables with more than 10 columns and 25 rows are not acceptable.
- Number tables, in Arabic numerals, consecutively in the order of their first citation in the text and supply a brief and concise title for each.
- Place explanatory matter in footnotes, not in the heading.
- Explain in footnotes all non-standard abbreviations that are used in each table.
- Obtain permission for all fully borrowed, adapted, and modified tables and provide a credit line in the footnote.
- For footnotes use the following symbols, in this sequence: *, †, ‡, §, ‖,¶ , **, ††, ‡‡
- Tables with their legends should be provided at the end of the text after the references. The tables along with their number should be cited at the relevant place in the text

Illustrations (Figures)

- Upload the images in JPEG format. The file size should be within 1024 kb in size while uploading.
- Figures should be numbered consecutively according to the order in which they have been first cited in the text.
- Labels, numbers, and symbols should be clear and of uniform size. The lettering for figures should be large enough to be legible after reduction to fit the width of a printed column.
- Symbols, arrows, or letters used in photomicrographs should contrast with the background and should be marked neatly with transfer type or by tissue overlay and not by pen.
- Titles and detailed explanations belong in the legends for illustrations not on the illustrations themselves.
- When graphs, scatter-grams or histograms are submitted the numerical data on which they are based should also be supplied.
- The photographs and figures should be trimmed to remove all the unwanted areas.
- If photographs of individuals are used, their pictures must be accompanied by written permission to use the photograph.
- If a figure has been published elsewhere, acknowledge the original source and submit written permission from the copyright holder to reproduce the material. A credit line should appear in the legend for such figures.
- Legends for illustrations: Type or print out legends for illustrations using double spacing, with Arabic numerals corresponding to the illustrations. When symbols, arrows, numbers, or letters are used to identify parts of the illustrations, identify and explain each one in the legend. Explain the internal scale (magnification) and identify the method of staining in photomicrographs.
- Final figures for print production: Send sharp, glossy, un-mounted, color photographic prints, with height of 4 inches and width of 6 inches at the time of submitting the revised manuscript. Print outs of digital photographs are not acceptable. If digital images are the only source of images, ensure that the image has minimum resolution of 300 dpi or 1800 x 1600 pixels in TIFF format. Send the images on a CD. Each figure should have a label pasted (avoid use of liquid gum for pasting) on its back indicating the number of the figure, the running title, top of the figure and the legends of the figure. Do not write the contributor/s' name/s. Do not write on the back of figures, scratch, or mark them by using paper clips.

- The Journal reserves the right to crop, rotate, reduce, or enlarge the photographs to an acceptable size.

Also, the authors are highly requested to provide their graphs (either provided using software like Microsoft Excel or GraphPad Prism, or taken from software of an apparatus *e.g.* HPLC, Flowcytometer, …) according to the following comments:

- All characters including words, letters, and digits must be written in Times New Roman, un-bold, non-italic with solid black color.
- An appropriate legend with unit must be defined for both X and Y axes, unit should be provided in parentheses.
- All lines in a graph including X and Y axes, lines around the columns, error bars, …. must be in solid black color with 1 pt thickness.
- If a figure has different parts including different graphs or images, therefore different Capital/UPPERCASE letters in Times New Roman, solid black or white (depends on background color), and bold must be assigned to each part at the inner top left corner.

List of Abbreviations: Include a list of abbreviations along with its description used in the manuscript.

Sending a Revised Manuscript

The revised version of the manuscript should be submitted online in a manner similar to that used for submission of the manuscript for the first time. When submitting a revised manuscript, contributors are requested to include the referees' remarks along with point to point clarification. The authors are strongly requested to show changes and modifications in their manuscript using Track Change mode in Microsoft Word Office, which allows reviewers to find out any changes (additions and deletions) easily. Also the Comments File Template should be downloaded from the website, author's area and then all referees' comment and questions and author's answers and explanation must be included in this table. Eventually both revised manuscript and Table of Comments files should be submitted via website (https://review.jow.medknow.com/rps).

Reprints and Proofs

Journal provides no free printed reprints. Authors can purchase reprints, payment for which should be done at the time of submitting the proofs.

Publication Schedule

The journal publishes articles, six issues per year, 10 in each, on its website.

Article Processing Charge

All manuscripts submitted to the RPS journal are peer-reviewed in the normal way under editorial control. Authors are asked to follow the details of journal charges and word count limits in the table below. Upon acceptance for publication a processing fee will be payable. Payment of this charge allows RPS to recover its processing, editorial, and production costs. Published papers appear electronically and are freely available from our website. Contributors out of Iran can electronically pay through secure Medknow, Wolters Kluwer submission portal.

Authors do not have to pay for submission or processing of their manuscript except for withdrawing their manuscript during processing time. In this case the corresponding author should pay half of manuscript publication fee.

Word Count Limits and Article Processing Charges at One Glance

These numbers show the publication fee according to the word count for Research in Pharmaceutical Sciences (RPS) journal.

Article Type	Abstract	Full text (including references, tables and figures)	Total of illustrations (tables and figures)	Publication fee (for listed word limits)	Extra payment per 600 words
Short Communications	150	850	2	100 USD	50 USD
				3,000,000 IRR	1,000,000 IRR
Case Reports	150	850	5	100 USD	50 USD
				1,500,000 IRR	1,000,000 IRR
Letters to Editor	-	500	1	Free	Free
Original Articles	250	2750	5	500 USD	50 USD
				12,000,000 IRR	2,000,000 IRR
Qualitative Research	250	3250	5	200 USD	50 USD
				3,000,000 IRR	1,000,000 IRR
Review Articles	250	4750	5	500 USD	50 USD
				12,000,000 IRR	2,000,000 IRR

- Additional charges for each extra figure/table are applied as per the occupied space in a page (each full page equals to 600 words).
- The publication fees are considered as IR Rials for Iranian authors and US Dollars for other nationalities.
- Upon request for fast tracking of the submitted manuscript, an additional payment of 5,000,000 IRR /250 USD should be considered, with the journal promising to send the decision letter within eight weeks.
- There are no additional charges for color illustrations.

Copyrights

The entire contents of the Research in Pharmaceutical Sciences Journal are protected under Indian and international copyrights. The Journal, however, grants to all users a free, irrevocable, worldwide, perpetual right of access to, and a license to copy, use, distribute, perform and display the work publicly and to make and distribute derivative works in any digital medium for any reasonable non-commercial purpose, subject to proper attribution of authorship and ownership of the rights. The journal also grants the right to make small numbers of printed copies for their personal non-commercial use under Creative Commons Attribution-Noncommercial-Share Alike 3.0 Unported License.

Checklist

It is strongly recommended to consider the following checklist while preparing the manuscript.

√	**Items**
	First Page/Covering Letter
	Title of the manuscript
	All authors' names and affiliations
	Author for correspondence, with academic e-mail address provided, Tell and Fax numbers.
	Conflicts of interest disclosed
	Source of funding mentioned
	Authors' contribution
	Running title provided (not more than 50 characters)
	Article file
	Double spacing, Margins 2.5 cm from all four sides, and Page numbers included at bottom
	Abstract provided (structured abstract of 250 words for original articles, unstructured abstracts of 250 words for review articles and unstructured abstracts of about 150 words for all other manuscripts excluding letters to the Editor).
	Keywords provided (three to six)
	Headings (UPPERCASE and bold), subheadings (bold, *italic*, and only first letter in capitl form), the lower level of subheading (Capital and *italic*)
	The references cited in the text should be in round brackets
	References according to the journal's instructions, punctuation marks checked
	All figures, schemes, and tables must be cited in a consecutive order in the main text.
	Send the article file without 'Track Changes' and the name and affiliations of authors
	Language and Grammar
	Uniformly British English
	Write the full term for each abbreviation at its first use in the abstract and text separately, unless it is a standard unit of measure. The abbreviations must be assigned to words used more than 5 times in the main text.
	Numerals at the beginning of the sentence spelt out
	Check the manuscript for spelling, grammar and punctuation errors
	If a brand name is cited, supply the manufacturer's name and address (city and state/country).
	Species names should be written in *italics*
	Tables and Figures
	No repetition of data in tables and graphs and in the main text
	Actual numbers from which graphs drawn, provided
	Figures necessary and of good quality
	Table and figure numbers in Arabic letters (not Roman)
	Figure legends provided
	Credit note for borrowed figures / tables provided
	Write the full term for each abbreviation used in the table as a footnote

FARABI
Pharmaceutical Co.

In FARABI Pharmaceutical Company
Quality is Extremely Important

Iran Top Industrial Complex - 2007

Green Industry Trophy Environmental Protection Organization Iran - 1999

Top Brand Name & trademark of iran Iran - 2008 -2010

International Gold Star For Quality

International Gold Star For Quality

Global Quality Management

ISO 9001:2000 2003

OHSAS 18001 2003

ISO 14001-2004 2001

Iran Top Exporter 2002-2007-2008

WWW.FARABIPHARMA.IR
e-mail:farabi@farabipharma.ir